STUDY OF WOLFRAM SYNDROME IN NEURONAL CELL MODELS

BY

SELEY GHARANEI

A Thesis submitted to
The University of Birmingham
for the degree of
DOCTOR OF PHILOSOPHY

College of Medicine & Dentistry
The University of Birmingham
January 2013

Abstract

Wolfram Syndrome (WS) is a rare autosomal recessive disease characterised by insulin-dependent diabetes mellitus, optic nerve atrophy, diabetes insipidus, deafness, and neurological dysfunction leading to premature death. WS is caused by mutations in the *WFS1* gene encoding an Endoplasmic Reticulum (ER) trans-membrane protein (Wolframin) that also localises to secretory granules in pancreatic beta cells. Although its precise functions are unknown, WFS1 protein deficiency affects the unfolded protein response, intracellular ion homeostasis, cell cycle progression, and granular acidification.

The current study demonstrated that neuronal cells (human and mouse neuroblastoma and human NT2 cell lines) stably or transiently depleted of WFS1 protein, showed significantly elevated expression of the ER stress markers BiP, CHOP, spliced XBP1, ATF6 and HRD1, indicating an enhanced ER stress response. This was accompanied by increased apoptosis and impaired cell cycle progression. Cell cycle assays measuring $p21^{cip1}$ showed reduced levels in WFS1 depleted cells, and an inverse association between $p21^{cip1}$ expression and apoptosis. WFS1 depletion also resulted in decreased expression of Na^+/K^+ ATPase beta1 subunit and Vacuolar ATPase (V-ATPase) V1A subunit. The elevated expressions of ER stress markers, but not the decreased expression of pump subunits, were reversed by adenoviral over-expression of BiP/GRP78. Protein degradation assays with cycloheximide showed more rapid degradation of both pump subunits in WFS1 depleted cells compared with controls. Immunofluorescence and electron-microscopy analyses revealed that WFS1 localises not only to ER but also to the secretory

vesicles in human neuroblastoma cells. Most importantly, a novel interaction between WFS1 and the V1A subunit of the vacuolar-type H^+-ATPase (proton pump) was demonstrated by co-immunoprecipitation in transfected HEK293 cells, and with endogenous proteins in human neuroblastoma cells. The interaction was mapped to the WFS1-N terminal, but not the C-terminal domain.

WFS1 depleted human neuronal cells were treated with the therapeutic agents taurodeoxycholic acid (TUDCA) and sodium valproate (VPA) in an attempt to identify effective interventions for WS. VPA treatment significantly induced the expression of WFS1, and increased expression of the neuroprotective protein BCL-2. TUDCA treatment significantly reduced ER stress and apoptosis in WFS1 depleted cells.

In conclusion, this study shows that WFS1 has a specific interaction with the V1A subunit of H^+ V-ATPase; this interaction may be important both for pump assembly in the ER; and for granular acidification. Chemical and molecular chaperones TUDCA, GRP78 and the histone deacetylase inhibitor VPA showed promising results in providing protection against ER stress induced apoptosis in WFS1 depleted neuronal cells.

Dedication

I dedicate this work to my wonderful husband Hewad and my lovely daughter Sana; they have filled my life with love and happiness and motivate me to move on. Also to my loving parents, without their blessings and support, I would have never made it this far.

"I am among those who think that science has great beauty.

A scientist in his laboratory is not only a technician: he is also a child placed before natural phenomena which impress him like a fairy tale."

Marie Curie

Acknowledgments

I would like to thank all the members of the Medical and Molecular Genetics Department at the University of Birmingham, for making the journey of my PhD pleasant and memorable. I would also like to thank the MRC foundation for funding this project. I must admit I was very concerned at the start of my PhD as I was expecting my daughter. I have been very lucky to have such wonderful and caring supervisors, I am very grateful to Prof Tim Barrett and Dr.Malgosia Zatyka for their continuous support and encouragement throughout my PhD. Tim has been an amazing boss; I have not only grown as a scientist under his supervision but also as a person. His hard work, dedication and contribution to the research of Wolfram syndrome are really remarkable. I thank him for such an inspiration. Malgosia has also been very supportive, she told me that she also had her son during the first year of her PhD and explained that it is challenging but possible to do a PhD in science and starting a family, her words encouraged me not to give up. She has taught me a variety of lab and non-lab skills for which am really grateful to her. I must also thank Dr. Dewi Astuti, her support and contribution to my project has been great, she is a very dear friend to whom I could go in any situation. I also would like to thank Dr Nagy and Prof Sik for their contribution to my project.

Finally I have to thank my wonderful family and friends for their support and encouragement throughout this project. My dad has always been my inspiration, from a very young age he encouraged me to do well and achieve something in life. Without my Mum's help and support with my daughter I would have never been able to finish my PhD. I am very fortunate to have her in my life. She puts her life on hold for me to pursue my dreams; I cannot thank her enough. My husband Hewad has been incredibly supportive through my educational journey, encouraging me to follow my dreams and believing in me. I thank him from my heart for being there always for me. My adorable daughter Sana is my world and she puts a smile on my face and inspires me every day. I am truly blessed to have her in my life and after I submit my thesis I will definitely spend more time with her. Last but not least, I have to thank my wonderful brothers and lovely sisters; they mean the world to me. They have supported me a lot throughout my PhD. My brother Mayel deserves special thanks since he played a major part throughout my educational life. He has advised me and supported me since my secondary school, when we were class mates. I must also specially thank my darling sister Hiela for her continuous support in my life and for proof reading my chapters.

Table of Contents

List of Figures

List of Tables

Abbreviations

AC8	Adenylyl cyclase8
AD	Alzheimer disease
AKS1	Apoptosis signalling kinase1
APAF-1	Protease activating factor 1
ATF4	Active transcription factor4
ATF6a	Activating transcription factor 6 alpha
ATP1A1	Alpha subunit of Na+/K+ ATPase
ATP1B1	Beta1 subunit of Na+/K+ ATPase
ATP6V0D2	V1D2 subunit of the proton pump
ATP6V1A	V1A subunit of the proton pump
ATP6V1C1	V1C1 subunit of the proton pump
BAX	Pro-apoptotic protein of BCL-2 family
BCL-2	B-cell lymphoma 2
BIM	Pro-apoptotic protein of BCL-2 family
BiP	Immunoglobulin binding protein, Glucose-regulated protein 78 (GRP78)
BP	Base pair
BSA	Bovine serum albumin
b-Zip	Basic Leucine zipper
CA1	Cornu ammonis 1
cAMP	Cyclic adenosine monophosphate
CDK	Cyclin-dependent kinases
CHOP	Growth arrest and DNA-damage-inducible protein (C/EBP transcription factor)
Cip	CDK interacting protein
CKI	CDK inhibitors
CNS	Central nervous system
CREB	Cyclic AMP responsive element binding protein
CsCl	Caesium Chloride
CX	Cycloheximide
DI	Diabetes insipidus

DIDMOAD	Wolfram syndrome
DM	Diabetes mellitus
DMEM	Dulbecco's Modified Eagle Medium
DMSO	Dimethyl Sulfoxide
DTT	Dithiothreitol
E3	Ubiquitin ligase
ECL	Electrochemiluminescence
EDEM	ER-degradation-enhancing-a-mannidose-like protein
EIF2a	Eukaryotic translation initiation factor 2A
Eif2ak3	Eukaryotic translation initiation factor 2-alpha kinase 3
EM	Electron-microscopy
ER	Endoplasmic Reticulum
ERAD	ER-associated protein degradation
ERSE	ER stress response element
Ess-1	Endometrial stromal sarcomas
FBS	Fetal bovine serum
FCS	Fetal Calf Serum
FDA	Food and Drug Administration
FITC	Fluorescein isothiocyanate
G1 (phase)	Gap1 (cell growth phase)
G2 (phase)	Gap2 (pre-mitotic phase)
GABA	Gamma-aminobutyric acid
GADD34	Growth arrest8 and DNA damage inducible gene 34
GFP	Green Fluorescent Protein
GLP1	Glucagon-like-peptide-1
GRP94	Glucose regulating protein 94
GSK3β	Glycogen synthase kinase 3β
GST	Glutathione S-transferase
HCC	High Content Cytometry
HD	Huntington disease
HDAC	Histone Deacetylase
HEK293	Human Embryonic Kidney cells
HLA	Human leukocyte antigen
HRD1	E3 ubiquitin-protein ligase synoviolin
IF	Immunofluorescence
IFN-γ	γ-interferon
IGF2	Insulin-like growth factor 2

IP	Immunoprecipitation
IPS	Induced Pluripotent Stem
IRE-1	Inositol-requiring enzyme 1alpha
JNK	C-jun N-terminal kinase
KD	Knockdown
LD	Linkage Disequilibrium
M (phase)	Mitosis
MDCK	Made in Darby canine kidney
MG132	proteasome inhibitor
MGB	Minor grove
MIN6	Mouse insulinoma pancreatic beta cell line
MOI	multiplicity of infection
MOMP	mitochondrial outer membrane permeabilisation
NRF2	NF-E2-related factor 2
NS	Not significant
NT2	Human Neuron-committed Teratocarcinoma
OA	Optic Atrophy
OsO_4	Osmium tetroxide
$p21^{cip}$	Cell-cycle regulatory protein
P53	Tumour protein 53
PB	Phosphate Buffer
PBA	4-phenylbutyric acid
PBS	phosphate buffered saline
PBST	PBS with 1% Triton-100x
PCR	Polymerase Chain Reaction
PDI	Protein Disulphide-Isomerase
PDT	Population Doubling Time
PERK	Protein Kinase RNA-like Endoplasmic Reticulum Kinase
PI	Propidium Iodide
PMSF	Phenylmethanesulfonylfluoride
ppRb	Phosphorylated retinoblastoma protein
PTP	Permeability transmembrane pore
QC	Quality control
QPCR	Quantitative Polymerase Chain Reaction (Real time PCR)
RassF1A	RAS association domain family 1A

RIPA	Radio-Immunoprecipitation Assay
ROS	Reactive oxygen species
S (phase)	Synthesis phase (DNA replication)
S1 and 2	Site 1 and 2 proteases
SDS-PAGE	PolyAcrylamide Gel Electrophoresis
SEM	Standard Error of the Mean
shRNA	Short hairpin RNA
siRNA	Small interfering RNA
SK-N-AS	Neuroblastoma cell lines
SNP	Single nucleotide polymorphism
T1D	Type 1 Diabetes
T2D	Type 2 Diabetes
TBS	Tris-buffered saline
Tg	Thapsigargin
Tm	Tunicamycin
TNF	Tumour necrosis factor
TUDCA	Taurine Conjugated Ursodeoxy Colic Acid
UDCA	Ursodeoxycholic acid
UPR	Unfolded protein response
VAMP	Vesicle Associated Membrane Protein
VP	Vasopressin
VPA	Valproate
WB	Western Blotting
WFS1	Wolfram syndrome 1, the gene encoding Wolfram protein
WFS1	Wolfram protein
Wt	Wild type
XBP-1	X-Box binding protein 1

Chapter One: Introduction

1.1 : Neurodegeneration

Neurodegeneration is a universal term for neuronal cell death caused by multifactorial stimuli including genetic predisposition, cellular stresses, environmental factors, neuro-inflammation, disruption of calcium regulating systems, mitochondrial dysfunction and misfolded protein accumulation (Gorman, 2008, Soto, 2003). Several neurodegenerative diseases such as Alzheimer's (AD), Parkinson's (PD), Huntington's (HD) and prion disease occur as a result of one or more neurodegenerative processes (Gao and Hong, 2008). These disorders are characterised by impaired brain functioning caused by progressive but gradual loss of neuronal function and structure in distinct regions of the central nervous systems (CNS) (Gorman, 2008, Stoppini et al., 2004, Stefani, 2004). Progressive research in this area has shown many similarities between these disorders, which could be used as a prerequisite for therapeutic advances, that many disorders could benefit from. One of the hallmarks of many neurodegenerative diseases is endoplasmic reticulum (ER) stress caused by protein aggregation, which plays a key role in their development and pathology (Nieoullon, 2011).

Post mortem and neuro-pathological studies have shown neuritic amyloid plaques and neurofibrillary tangles in the brains of patients with AD. Amyloid Beta protein aggregates are accumulated extracellularly in the brain parenchyma or around the cerebral vessel walls. The tangles containing aggregates of hyper-phosphorylated tau protein are accumulated in the cytoplasm of degenerating neurons (Nieoullon, 2011). In PD patients, protein aggregates called Lewy bodies are deposited in the cytoplasm of neurons from the substantia nigra. Lewy bodies are composed mainly of alpha synuclein protein (Soto, 2003). Furthermore, a typical feature of

the brains from HD patients is the intra-nuclear accumulation of a polyglutamine-rich version of Huntington protein. Therefore, misfolding, aggregation and accumulation of proteins in the brain, resulting in neuronal apoptosis seems to be the pathological mechanism of several neurodegenerative disorders (Nieoullon, 2011). Neuronal cell death involves several mechanisms such as apoptosis, autophagy and necrosis. Apoptosis is the best understood mechanism of neuronal cell death that involves the caspase family of proteins, the BCL-2 family and the adaptor protein Apaf-1. Autophagy involves lysosomal degradation and necrosis involves swelling of intracellular organelles leading to loss of the plasma and nuclear membrane integrity (Yuan et al., 2003).

1.2 Apoptosis in general

Apoptosis, also known as programmed cell death is a tightly regulated energy-dependent process characterised by specific morphological and biochemical features. The morphological features include cell shrinkage, chromatin condensation, and nuclear and cell fragmentation (Cotter, 2009). Apoptosis is a fundamental component of various physiological processes in mammalian cells that occurs during normal development, aging and as a homeostatic mechanism to maintain cell populations in tissues (Elmore, 2007). Examples of these processes are normal cell turnover, proper development and functioning of the immune system, hormone dependent atrophy, embryonic development and chemical induced cell death (Norbury and Hickson, 2001). It has been reported that per day, approximately 60 billion cells are generated by an average adult human body and an equal amount of cells undergo apoptosis to maintain cell homeostasis. Therefore it is not surprising that apoptosis has to be tightly regulated, since imbalance of this

vital process could lead to pathologies such as developmental defects, many types of cancer, ischemic damage auto-immune diseases and neurodegeneration (Cotter, 2009).

Moreover, apoptosis could be triggered by DNA damage caused by irradiation or drugs used for cancer chemotherapy, which leads to cell death through a p53 dependent pathway. P53 determines cells fate to induce growth arrest, DNA repair, or apoptosis. p53 promotes cell death by apoptosis upon exposure to severe DNA damage. The loss of p53 functions and the deregulated activities of p53 are involved in the development of malignant diseases, as well as, cardiovascular, neurodegenerative, infectious and metabolic diseases (Yoshida and Miki, 2010).

1.3 : Endoplasmic Reticulum (ER) stress and the Unfolded Protein Response (UPR)

The ER is a crucial organelle involved in folding, assembly, maturation and processing of newly synthesised secretory and transmembrane proteins, as well as in lipid synthesis and post translational modification (Jonikas et al., 2009, Fonseca et al., 2011, Oslowski et al., 2011). The ER also plays a key role in essential cellular processes such as calcium storage, cell signalling and degradation of misfolded proteins. The ER provides a unique environment with a complement of foldases and chaperones, as well as a high quality control (QC) system for recognition and targeting abnormal proteins for degradation as well as maintaining ER homeostasis. Physiological and pathological insults can perturb this homeostasis leading to accumulation of unfolded and misfolded proteins in the ER lumen resulting in a condition known as ER stress. ER stress is the state where the folding capacity of ER is exceeded due to

mechanisms such as excessive protein synthesis demand (Urano et al., 2000). Examples of the perturbing insults to the ER homeostasis are: reduced calcium levels, overwhelming chaperone capacity, viral infections, environmental toxins, inflammatory cytokines, alteration in redox state, and mutant protein expression. Several drugs are able to pharmacologically induce these perturbations in cells: thapsigargin causes disruption in ER calcium levels; dithiothreitol causes disruption in ER redox, and tunicamycin, inhibits N-linked glycosylation.

When the ER QC is exceeded, a stress response is switched on and prolonged stress leads to apoptosis. The ER stress response, also called the Unfolded Protein Response (UPR) is an adaptive signal transduction system from ER to the nucleus to alleviate ER stress (Harding et al., 2002). The UPR maintains a balance between the load of newly synthesised proteins and the folding capacity of the ER by triggering signalling cascades to prevent the build-up of unproductive and toxic protein products (Rajan et al., 2007, Wei et al., 2008, Rutkowski and Kaufman, 2004). ER stress can be either acute or chronic. Acute stress is any insult that could lead to rapid activation. Examples of acute ER stress are: calcium depletion, glucose deprivation, hypoxia and ischemia. Chronic ER stress brings permanent changes in the function of the cell, especially in the function of the ER and requires a long term adjustment to the cellular function. This type of ER stress is usually caused by genetic mutations in ER chaperones that result in misfolding of the proteins, viral infection, and different neurodegenerative disorders of protein aggregation (Rutkowski and Kaufman, 2007).

The ER stress response pathway consists of four different responses contributing to UPR as shown in (Figure 1.1): (1) transcriptional activation of molecular chaperone genes such as BiP/GRP78 which causes increase in the protein folding capacity and prevents protein aggregation; (2) translational attenuation: reduction of the biosynthetic load and preventing the accumulation of unfolded proteins. (3) Degradation of misfolded proteins by ERAD (ER-associated degradation): misfolded and unfolded proteins in the ER are sent to the cytosol and degraded by proteasomes; (4) apoptosis is the last option to eliminate cells that cannot cope and resolve the ER stress when ER function is extensively impaired (Yoshida, 2004, Rajan et al., 2007).

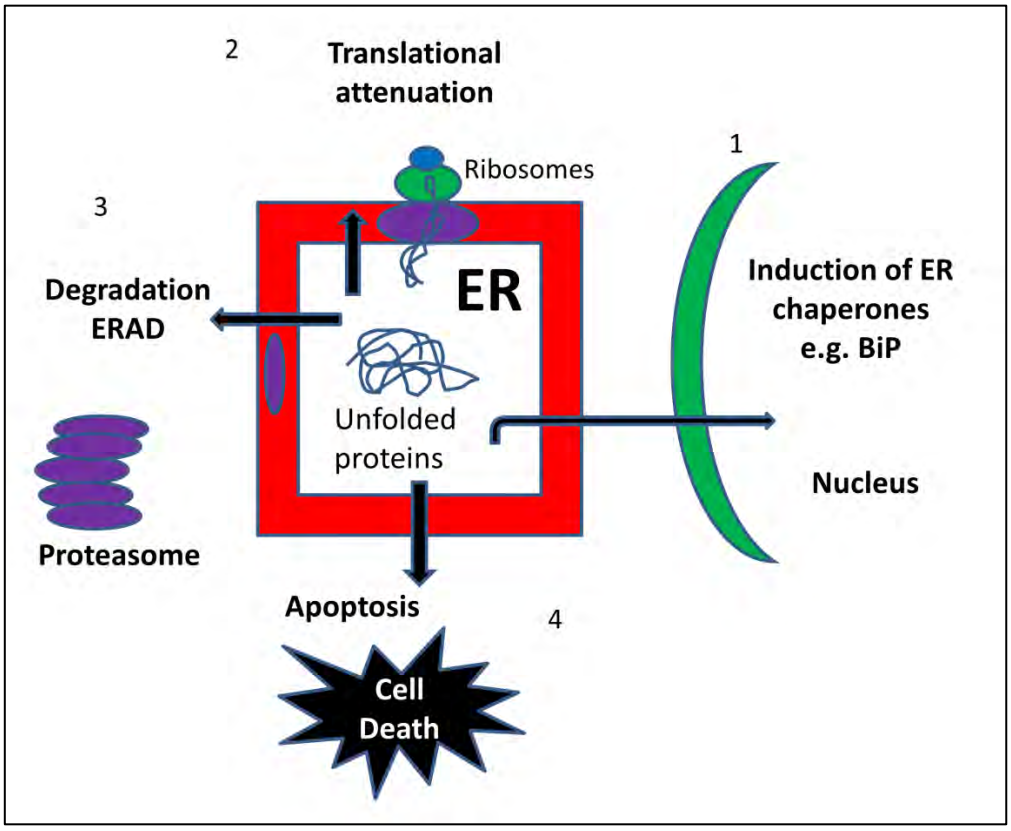

Figure 1.1: UPR pathways induced in presence of unfolded proteins

Four distinct processes are involved in ER stress response to alleviate ER stress: (1) transcriptional induction of ER chaperones such as BiP to enhance ER folding capacity; (2) Translational attenuation to reduce biosynthetic load on the ER; (3) ERAD mediated degradation of unfolded or misfolded proteins by proteasomes; (4) apoptosis to eliminate unrecoverable cells to maintain ER homeostasis. Image adapted from (Rajan et al., 2007).

1.3.1 The UPR pathways

Accumulation of unfolded and misfolded proteins is sensed by three transmembrane master regulators across the ER membrane: the IRE1 (Inositol Requiring 1), PERK (Protein Kinase like ER Kinase) and ATF6 a/b (Activating Transcription Factor 6). These three sensors are bound to immunoglobulin heavy chain-binding protein (BiP) within the ER lumen under normal unstressed conditions to keep them inactivated (Credle et al., 2005, Bertolotti et al., 2000). However, upon the presence of ER stress in the ER lumen this stable complex is broken and each of these sensors dissociates from BiP and becomes activated in response to ER stress (Bertolotti et al., 2000, Urano et al., 2000) (Figure 1.2 and Table 1.1).

1.3.1.1 IRE1

IRE1 is a type1 transmembrane endoribonuclease with a protein kinase activity that regulates chaperone induction and ERAD in response to ER stress. This ER stress sensor exists in two highly conserved forms: alpha and beta. IRE-alpha is expressed ubiquitously with high expression in the pancreas and placenta. IRE-beta is expressed only in epithelial cells of the gastrointestinal tract. The N-terminal luminal domain of IRE1 senses the presence of ER stress, which causes its dissociation from BiP. This dissociation results in dimerisation, auto-phosphorylation and activation of IRE1, leading to unconventional splicing of XBP1 (x-box binding protein1) (Urano et al., 2000). Thus, activated IRE1 splices a 26- nucleotide sequence from XBP-1 mRNA (Lipson et al., 2006). A 376 amino acid basic leucine zipper (b-ZIP) transcription factor is produced by the mRNA of spliced XBP1 that is involved in upregulation of UPR genes. These include genes involved in folding of proteins such as protein disulfide

isomerase (PDI) and genes that function in ERAD such as ER-degradation-enhancing-a-mannosidase-like protein (EDEM) (Yoshida, 2004, Calfon et al., 2002). In the presence of chronic ER stress, the apoptosis signalling kinase1 (ASK1) is activated by tumour necrosis-factor (TNF) receptor-associated factor 2. This TNF2 is recruited by activated IRE1. Activated ASK1 leads to the activation of C-Jun N-terminal kinases (JNK). Activated JNK induces apoptosis by regulating the BCL family of proteins, under extreme ER stress (Fonseca et al., 2005, Urano et al., 2000). Activation of JNK also causes enhancing of autophagy which allow cells to adapt to the stress (Ogata et al., 2006) (Figures 1.2, 1.3 and Table 1.1).

1.3.1.2 PERK

The second sensor of UPR, PERK also belongs to type1 ER transmembrane serine/threonine protein kinase and its N-terminal domain is sensitive to ER stress. PERK plays a crucial role in regulation of protein synthesis in response to ER stress and in selective stress induced gene expression. Similar to IRE1, PERK is activated by unfolded/misfolded proteins in the ER lumen. Upon activation, PERK oligomerises, undergoes trans-auto-phosphorylation and then directly phosphorylates the alpha subunit of EIF2 (eukaryotic translation initiation factor 2) at Ser51. This leads to attenuation of general protein translation, since phosphorylated EIF2a prevents the formation of ribosomal initiation complexes. In this manner the ER work load is reduced and the cells are protected from apoptosis caused by ER stress (Harding et al., 2000b). Phosphorylated EIF2a is also involved in translation of a b-ZIP transcription factor ATF4 through a cap-independent process, which plays a role in upregulation of UPR target genes. Examples of these genes are C/EBP homologous protein (CHOP), growth arrest 8 and DNA damage inducible gene

34 (GADD34) (Marciniak et al., 2006). GADD34 is a phosphatase, which carries out the dephosphorylation of EIF2a and recovery of protein translation (Novoa et al., 2001).

1.3.1.3 ATF6

ATF6 is the third sensor of the UPR and belongs to the type II ER transmembrane transcription factors. It is located with its C terminal domain in the ER lumen and its N-terminal (the DNA binding domain) is facing the cytosol. Two isoforms of ATF6 exist in mammalian cells ATF6-alpha (90kD) and ATF6-beta (110kD). The alpha form has been extensively studied in relation to ER stress. In the presence of ER stress ATF6a dissociates from BiP and translocates from the ER to the Golgi where it is proteolytically cleaved to its active form by site1 and site 2 proteases (Shen et al., 2002, Sommer and Jarosch, 2002). The luminal domain of ATF6 is cleaved by site-1 protease and the N-terminus is cleaved by site-2 proteases. This process generates an activated b-ZIP transcription factor which transits to the nucleus.

Within the nucleus, the processed form of ATF6 binds to the ER stress responsive element ATF/cAMP to activate UPR genes involved in protein folding, processing and degradation, such as BiP, XBP1, glucose regulated protein-94 (GRP94), PDI, and calreticulin (Okada et al., 2002, Adachi et al., 2008). ATF6 is also shown to heterodimerise with XBP1 to upregulate the expression of ERAD genes (Yamamoto et al., 2007). Studies have shown that unprocessed ATF6 is unstable and it is degraded by the ubiquitin-proteasome pathway to prevent hyperactivation of the UPR (Hong et al., 2004a).

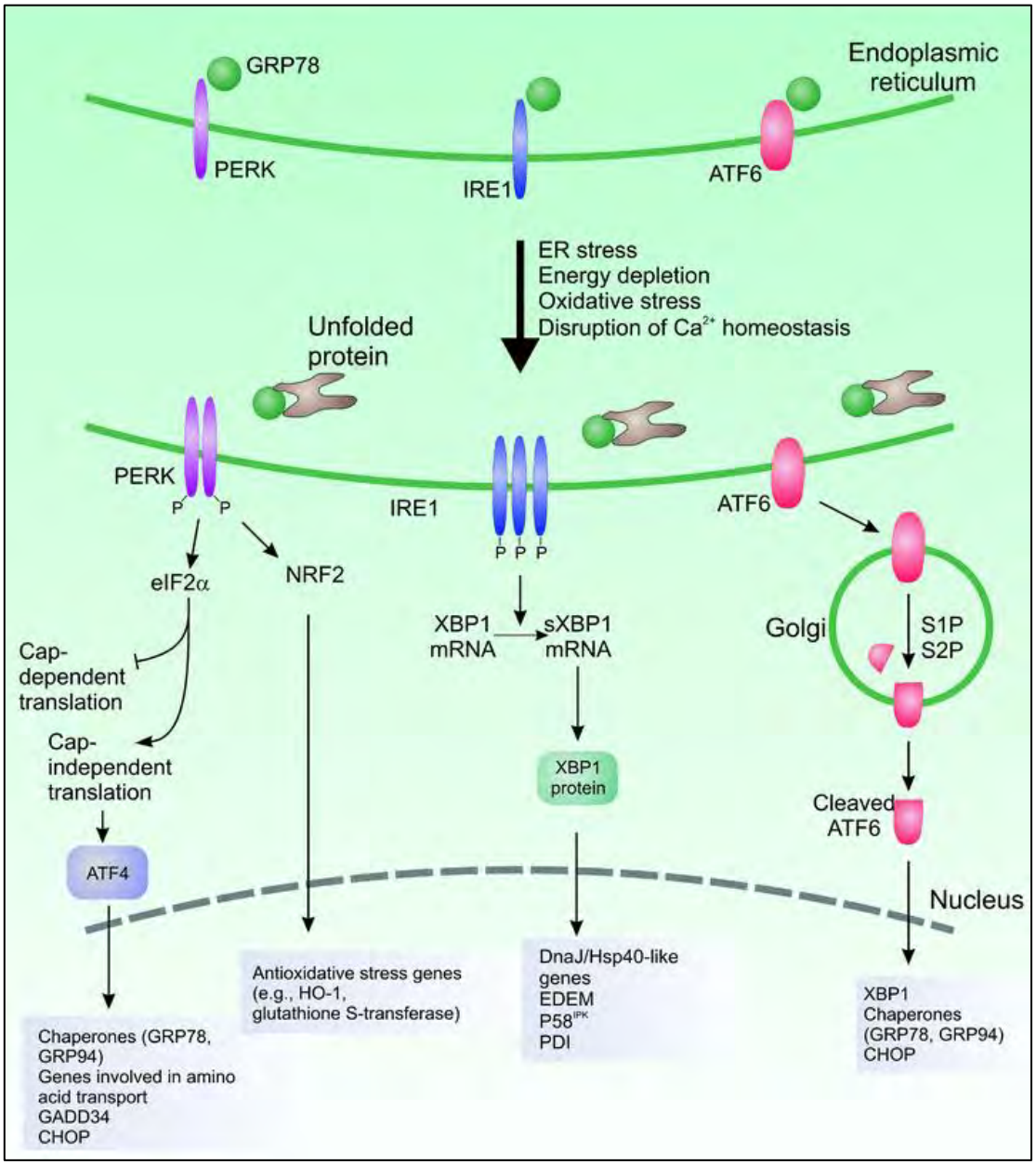

Figure 1.2: Distinct roles of the three arms of UPR: IRE1, PERK and ATF6

The presence of unfolded proteins cause ER stress leading to activation of the UPR sensors IRE1, PERK and ATF6, which function to restore homeostasis. Activation of IRE1 causes non-conventional splicing of XBP1 which results in enhancing the expression of molecular chaperones and the ERAD system. Activation of PERK inhibits cap-dependent translation and robustly enhances the translation of the transcription factor ATF4. ATF4 increases the expression of genes associated with amino acid metabolism. Activated ATF6 translocates to the Golgi where site 1 and 2 proteases perform its cleavage. The cleaved form (ATF6a) is transferred to the nucleus where it activates the transcription of XBP1 and the molecular chaperones GRP78 and GRP94. Image taken from (Doyle et al., 2011).

Protein	Function	Pathway	Reference
BiP	Master regulator of ER stress, Heat shock protein, molecular chaperone	Bound to IRE1, PERK and ATF6 in unstressed conditions	(Munro and Pelham, 1986, Bertolotti et al., 2000, Lee, 2005)
IRE1	Regulates chaperone induction and ERAD in response to ER stress Activated in response to ER stress and dissociates from BiP	When activated: it splices XBP1 and processes HAC1 mRNAs, leading to synthesis of transcription factors. Recruits TNF2, which activates ASK1-leads to activation JNK that promotes apoptosis	(Calfon et al., 2002, Lipson et al., 2006, Oikawa et al., 2009, Urano et al., 2000)
PERK	Regulates translational attenuation and protein synthesis in response to ER stress Activated in response to ER stress and dissociates from BiP	When activated, phosphorylates EIF2a leading to general protein translational inhibition and selective stress induced gene expression: transcription factor ATF4: upregulates **BiP, CHOP** and **GRP94**	(Brewer and Diehl, 2000, Hamanaka et al., 2005, Harding et al., 2000b, Marciniak et al., 2006, Zhang et al., 2006)
ATF6	Transcription factor Activated in response to ER stress and dissociates from BiP	ATF6a translocates to Golgi where it is cleaved by S1P and S2P to its active form which is transferred to the nucleus to upregulate UPR genes: **XBP1, BiP, GRP94**, PDI,	(Adachi et al., 2008, Ceylan-Isik et al., 2011, Okada et al., 2002, Yamamoto et al., 2007, Yamamoto et al., 2008)
CHOP	Transcription factor and pro-apoptotic protein Expression is strongly induced in response to ER stress	Is activated through PERK-ATF4 and ATF6 pathways-induces the production of ROS Induces apoptosis by binding to the promoter of BIM leading to down regulation of BCL-2	(Fradejas et al., 2010, Gow and Wrabetz, 2009, Matsumoto et al., 1996, Mihailidou et al., 2010, Song et al., 2008, Zinszner et al., 1998)
XBP1-(Spliced)	Transcription factor that regulates UPR	Its expression is regulated by unconventional splicing by IRE1. Spliced XBP1 activates the transcription of target genes encoding ER chaperones and ERAD components to protect cells from ER stress induced apoptosis.	(Kakiuchi et al., 2006, Uemura et al., 2009, Yamamoto et al., 2007, Yamamoto et al., 2008, Calfon et al., 2002)
HRD1	E3 ubiquitin ligase is involved in degradation of proteins from the ER	HRD1 supports degradation of all ERAD substrates up on ER stress. Its transcription is regulated by the IRE1-XBP1 pathway	(Fonseca et al., 2010, Kaneko et al., 2002, Kaneko et al., 2007, Yamamoto et al., 2008)

Table 1.1: Proteins involved in ER stress pathways

Main UPR proteins are shown with their functions, pathways and relevant references. The proteins shown in bold are being investigated in this project as they represent the three main UPR branches: IRE1, PERK and ATF6. For example BiP is bound to these three sensors of in absence of ER stress and the presence of ER stress causes their dissociation and activation. Consequently, each pathway upregulates the transcription of BiP to perfume its chaperone functions to reduce ER stress.

1.3.2 ER stress induced apoptosis

When the survival mechanisms of UPR fail to maintain ER homeostasis to rescue the cell, then apoptosis occurs to prevent the production of damaged proteins by stressed cells. Studies have reported that over-activation of UPR generates the apoptotic signals converging on the mitochondria. This leads to the opening of the permeability transmembrane pore (PTP) and loss of mitochondrial membrane potential. Subsequently, pro-apoptotic factors such as cytochrome c are released to the cytoplasm (Figure 1.3). Apoptosis is usually mediated via the activation of initiator-caspases by the protein complex apoptosomes. Examples of apoptosome complexes are apoptotic protease activating factor 1 (Apaf-1), pro-caspase-9 and cytochrome c (Fan et al., 2005). Procaspase-9 is processed by these apoptosomes to its active form, which causes the activation of downstream effector caspases such as caspases 3, 7 and 6 resulting in apoptosis (Bao and Shi, 2007).

The first ER stress induced apoptotic pathway is the caspase 12 cascade, where caspase 12 is activated from procaspase 12. Caspase 12 is localised to the ER and the presence of ER stress induces its expression and cleavage. However, the role of caspase 12 in ER stress induced apoptosis is not fully understood (Fribley et al., 2009). Studies have shown that the cell viability of B16 melanoma cells treated with the ER stress inducing agent thapsigargin, was unaffected by the caspase 12 expression (Morishima et al., 2002, Kalai et al., 2003). Caspase 4 shows similarities with caspase 12: it is activated in response to fluctuations in ER stress homeostasis. Similarly, excessive ER stress cleaves caspase 2; and resistance to ER stress induced apoptosis is conferred by inhibition of caspase 2 (Upton et al., 2008).

The second apoptotic pathway associated with ER stress is the B cell lymphoma 2 (BCL-2) pathway. Accumulating evidence suggests that the BCL-2 family of proteins are the key mediators between the ER and mitochondria in apoptosis (Szegezdi et al., 2009). Some members of this family of proteins function to regulate ER calcium homeostasis. Experimental evidence suggests that over-expression of BCL-2 protects cells from ER stress mediated apoptosis (Gupta et al., 2010). The BCL-2 family consist of anti-apoptotic proteins (BCL-2, BCL-XL and MCL-1), all of them having four BH domains (BCL-2-homology) and pro-apoptotic proteins (BAD, BIM, BIK, BID, PUMA and NOXA), with three BH domains. There are also multi domain pro-apoptotic members BAX and BAK (Szegezdi et al., 2009). Studies suggest that the transition from protective to an apoptotic UPR is regulated by the balance between the pro and anti-apoptotic BCL-2 family members (Gupta et al., 2010, Szegezdi et al., 2009). BAX and BAK are known for their role in permeabilisation of the mitochondrial outer membrane and release of pro-apoptotic molecules including cytochrome c and second mitochondrial-derived activator of caspases (Gupta et al., 2010). ER stress upregulates the expressions of pro-apoptotic proteins such as BAX and suppresses the expression levels of anti-apoptotic proteins such as BCL-2 promoting cell death.

The third pathway involved in ER stress induced apoptosis is the CHOP pathway. CHOP or the growth arrest and DNA damage-inducible gene 153 (GADD153) is a b-ZIP transcription factor, which belongs to the family of C/EBP transcription factors. CHOP expression is strongly induced in response to ER stress; however its expression in unstressed conditions is very low or undetectable (Zinszner et al., 1998). CHOP expression could be induced by all three UPR sensors

as it is activated through the PERK-ATF4 and ATF6 pathways (Gow and Wrabetz, 2009). Experimental evidence has shown that CHOP deletion promotes cell survival in mouse embryonic fibroblasts challenged with an ER stress inducing agent. These cells were significantly less sensitive to ER stress induced apoptosis in comparison to the wild type (Zinszner et al., 1998). CHOP activation induces the production of reactive oxygen species (ROS) (McCullough et al., 2001). One of the downstream effectors of CHOP is caspase 11, which induces apoptosis by activating caspases1 and 3 (Fradejas et al., 2010). In addition, CHOP induces cell death by binding to the promoter of the pro-apoptotic *BIM;* this leads to upregulation of its expression and simultaneously down regulation of the expression of BCL-2. Confirmation that CHOP activation is not the only pathway involved in ER stress induced apoptosis was shown when CHOP was not induced in PERK-/- cells. These cells were shown to undergo ER stress induced apoptosis, indicating a CHOP independent cell death pathway (Harding et al., 2000a).

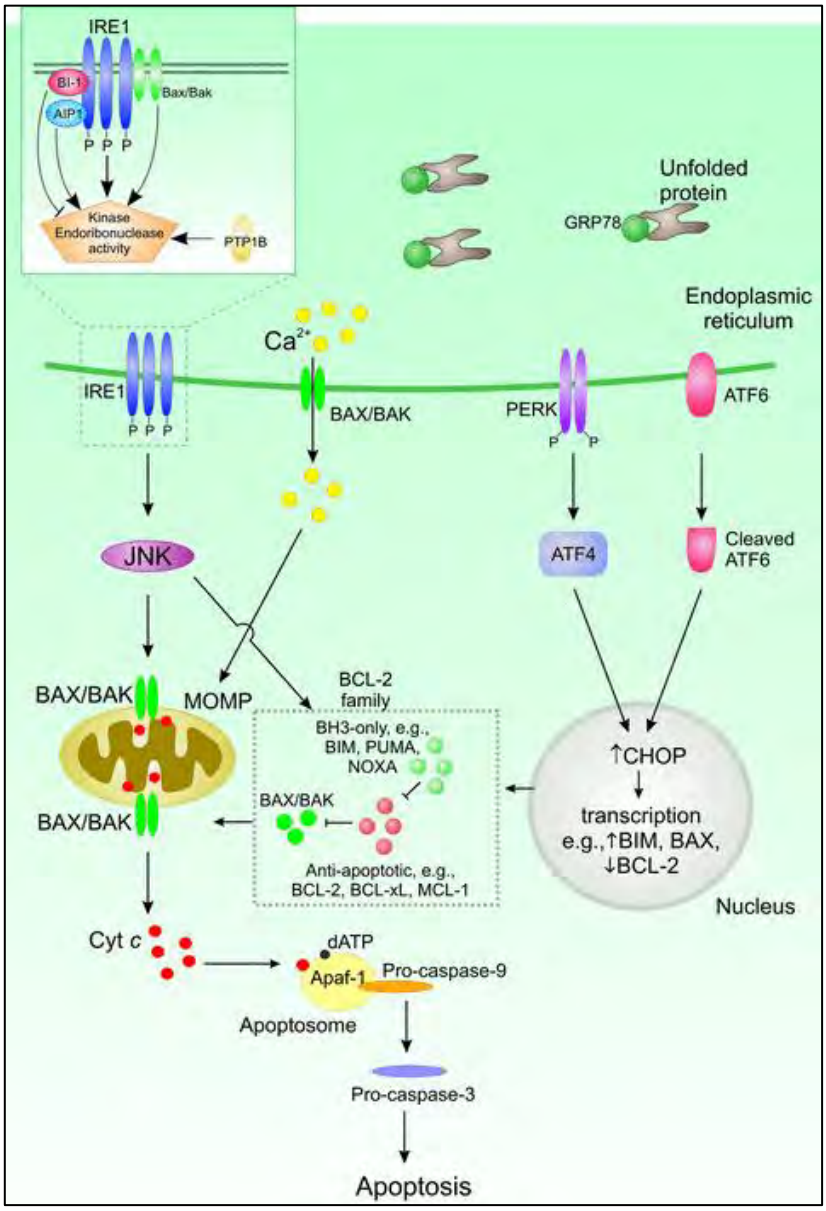

Figure 1.3: Apoptotic pathways induced by ER stress

The pre-apoptotic signalling formed by ER stress is mediated by activation of JNK and activation of CHOP due to increased ER stress. The balance between the pro-apoptotic and anti-apoptotic proteins of the BCL-2 family is disturbed by JNK and CHOP; CHOP down regulates the transcription of BCL-2 and causes upregulation of the transcription of the pro-apoptotic protein BIM. JNK causes phosphorylation and activation of BIM leading to activation of BAK and BAX. This leads to calcium release from the ER, opening of PTP, and loss of mitochondrial membrane potential. Consequently cytochrome c is released which interacts with procaspase-9, apoptosome and Apaf-1 resulting in caspase cascade and causing apoptosis. Mitochondrial outer membrane permeabilisation (MOMP), permeability transmembrane pore (PTP). Image taken from (Doyle et al., 2011)

1.3.3 ER stress and the cell cycle

As mentioned before, the presence of excessive unfolded proteins in the ER lumen induces ER stress. ER stress causes upregulation of ER chaperones and decrease of protein synthesis, resulting in G1 phase arrest (Han et al., 2012, Brewer and Diehl, 2000). The UPR functions as a stress induced checkpoint that gives the cells time to fold proteins properly and to re-establish ER homeostasis (Kaufman, 1999). The activities of several D-type cyclins (D1, D2 or D3) in cooperation with Cyclin Dependant Kinases CDK4 or CDK6 followed by cyclin E and A as well as CDK2 are required for the cell to progress from G1 arrest (Sherr and Roberts, 1995). Cell cycle arrest is induced via several mechanisms such as specific post-translational modifications of the CDK subunits, degradation of cyclin subunits and association of the active cyclin bound CDKs with polypeptide CDK inhibitors (CKI) (Sherr and Roberts, 1995).

The study conducted by Brewer in 1999 suggested that the UPR mediates cells cycle progression by controlling protein translation through PERK activation. This was achieved first by an *in-vitro* study, where they demonstrated that cell cycle arrest in dividing cells occurred through activation of UPR leading to suppression of cyclin D1 expression. The underlying suggested mechanism was inhibition of cyclin D1 translation triggered by increased phosphorylation of eIF2a. These observations suggested that the UPR puts the cell cycle progression on hold until ER homeostasis is restored. These findings suggest that PERK is a critical effector of the UPR that links ER stress to the regulation of cell cycle progression (Brewer and Diehl, 2000).

Neuronal degeneration causes dysregulation of cyclins, cyclin-dependent kinases and their inhibitors in stressed neuronal cells (Hoozemans et al., 2004). There is evidence for dysregulation of these processes in neurones in Alzheimer's disease (AD) (Vincent et al., 1996, Nagy et al., 1997). Induction of neuronal apoptosis is thought to be associated with the re-expression of cell cycle proteins (Copani et al., 1999). This implies that the main mechanism, by which these post mitotic neuronal cells undergo apoptosis, is attributed to the uncoordinated expression of some cell cycle molecules causing a breach in the cell cycle check points (Arendt, 2001). Studies have shown that prior to the appearance of neurological changes in AD patients, cell cycle changes can be detected in their neurons (Yang et al., 2003). These changes include: upregulation of cyclin D1; cyclin E; and phosphorylated retinoblastoma protein (ppRb) observed in non-demented cases showing early signs of AD (Hoozemans et al., 2002, Hoozemans et al., 2004). These findings imply that during the early stages of AD, neurodegenerative responses are leading to neuronal cell cycle changes.

The study conducted by Hoozemans and colleagues investigated the temporal and functional link between UPR activation and the expression of cell cycle proteins in post mitotic neurons in AD pathogenesis. They found the expression of BiP to be negatively correlated with neuronal ppRb expression (Hoozemans et al., 2006). Similarly, differentiated human neuroblastoma cells with induced ER stress were investigated for a potential direct association between UPR activation and cell cycle protein expression. Their findings indicated that cell cycle protein expression was inhibited by activation of UPR and induced a cell cycle arrest in G1 phase. These findings suggest that the UPR activation changes cell cycle protein expression in the pathogenesis of AD.

$p21^{cip1/waf1}$ is one of the cell cycle regulatory proteins that is known to be involved in ER stress dependent regulation of the cell cycle. It is transcriptionally regulated by the p53 tumour suppressor gene and functions as an inhibitor of the cyclin dependent kinases (Seoane et al., 2002, Chang et al., 2000). Human p21 is encoded by the gene CDKN1A located at the short arm of chromosome 6. The expression of p21 is shown to be associated with p53 dependent cell cycle arrest. Although it is well documented that p21 expression inhibits cell cycle progression, this protein is also shown to have anti-apoptotic functions, providing protection from p53 dependent and p53 independent cell death (Coqueret, 2003). The study conducted by Mihailidou et al. (2010) demonstrated that activated UPR causes suppression of p21 protein. They also showed that transient suppression of p21 expression in CHOP deficient cells reduces their sensitivity to apoptosis. The authors speculate that p21 is involved in signalling of ER stress and plays a role in UPR associated apoptosis. This study also indicates that CHOP is involved in the regulation of p21 during ER stress in facilitating pro-apoptotic cell death. Their findings suggest that induction of p21 causes cell cycle arrest and inhibits apoptosis which assists the pro-survival role of UPR during the initial stage of ER stress. Hence, CHOP promotes apoptosis as well as negatively regulates the anti-apoptotic role of p21 (Mihailidou et al., 2010).

1.4 : Diabetes mellitus and ER stress

Diabetes mellitus (DM) is a complex and multifactorial disorder predominantly characterised by glucose intolerance due to defects in the synthesis, secretion or action of insulin. Insulin is a hormone involved in maintaining blood glucose homeostasis. Studies show that the pathogenesis of most forms of diabetes are attributed to beta cell death (Karaskov et al., 2006). Two main

forms of DM are Type1 diabetes (T1D) which results from autoimmune destruction of insulin secreting pancreatic beta cells. This leads to absolute insulin deficiency. T1D accounts for up to 10% of DM cases and usually occurs in childhood or young adulthood. Patients rely on insulin replacement for survival (ADA, 2012). The second common form of DM is Type2 diabetes (T2D), which accounts for about 85% of all diabetic cases. This type usually occurs in adulthood and involves tissue insulin resistance on a background of relative insulin deficiency. The relative insulin deficiency is a result of beta cell dysfunction and death, partly caused by increased circulating blood glucose and saturated fatty acids. The majority of T2D patients are obese or overweight and therefore lifestyle management with dietary restriction and exercise can improve insulin sensitivity (ADA, 2012). T2D is also linked to genetic predispositions in some ethnic groups (Zimmet, 2001).

Several genetic and clinical studies have underlined ER stress as a molecular mechanism involved in the pathology of beta cell dysfunction and death in diabetes. It has been reported that knockout of CHOP improves glycemic control and expansion of the beta cell mass (Song et al., 2008). The link between ER stress and diabetes was first uncovered in a monogenic form of hereditary diabetes called Wolcott–Rallison syndrome. This disease is caused by loss of function mutations in the gene EIF2AK3 that encodes PERK (Mattsson et al., 2002, Zhang et al., 2006). PERK is known for its role in differentiation and survival of beta cells. Knockout models of Eif2ak3 (PERK) show decreased proliferation, preventing expansion of beta cells during neonatal development, and consequently resulting in diabetes. Similarly, key markers of differentiation were shown to be suppressed in Eif2ak3 knockout islets (Zhang et al., 2006).

EIF2 is the primary target of PERK and its phosphorylation plays a crucial role in insulin synthesis and regulation of UPR. This is evidenced in the experiments demonstrating that heterozygous mouse models with mutations in the phosphorylation site of eIF2a (Eif2s1+/tm1Rjk) exposed to high fat diet show severe beta cell deficiency and develop diabetes (Scheuner et al., 2005). These mice also show other abnormalities such as defective insulin trafficking, abnormal beta cell ER morphology and reduced numbers of secretory granules. Therefore, the diabetes in Wolcott–Rallison syndrome is thought to be mainly caused by dysregulation of UPR as a result of vulnerability to ER stress induced apoptosis and loss of beta-cell mass caused by a lack of beta cell proliferation.

Although several *in vitro* and *in vivo* studies have documented the link between ER stress and beta cell dysfunction and death, in humans the role of ER stress induced apoptosis remains debatable. In genetic forms of diabetes, beta cells death is thought to be partly related to the accumulation of misfolded proteins and dysregulation of ER homeostasis. Several studies have shown the presence of ER stress in beta cells of patients with type 2 diabetes (Laybutt et al., 2007).

1.5 : Wolfram Syndrome

Wolfram syndrome (WS) is a rare neurodegenerative disorder characterised by juvenile onset diabetes mellitus (DM) and optic atrophy (OA). This syndrome was originally discovered in 1938 by Wolfram and Wagener who reported Wolfram syndrome in four siblings (Wolfram and Wagener, 1938). The prevalence of Wolfram syndrome in the United Kingdom was estimated to

be 1 in 770 000 and a carrier frequency of 1/354, using a nationwide study conducted in 1995 (Barrett et al., 1995). This prevalence is estimated 1:500,000 worldwide and 1/100,000 in North America with a much higher prevalence in East Asia, Middle East and North Africa, most probably due to consanguineous marriages (Kinsley et al., 1995).

DM and OA are the minimal criteria for diagnosis of this disease; however WS patients also present additional secondary symptoms. Therefore, WS is also known as DIDMOAD (Diabetes Insipidus, Diabetes Mellitus, Optic Atrophy, and Deafness). This acronym describes the predominant symptoms of WS (Barrett et al., 1995). The main feature of this syndrome is young onset diabetes and the average age of onset is reported to be 5.4 years (Rohayem et al., 2011). The cause of the DM is selective non-autoimmune beta cells death. Mutations in the WS gene are the cause of premature death of pancreatic beta cells. This leads to insulin dependent and non HLA linked diabetes (Inoue et al., 1998).

The natural history of WS is shown in figure 1.4A; this figure was first described by Barrett and Bundey in 1997; it shows the presentation of diabetes mellitus in the first decade of life and optic atrophy leading to blindness in the first to the second decades. Deafness, renal complications and diabetes insipidus appear often in 2nd to the 3rd decades. Neurological complications such as ataxia, autonomic nervous system dysfunction, mental retardation and brainstem atrophy occur in 3rd to 4th decade. However, very recent studies based on MRI scans of young patients and more detailed neurological examinations showed that neurological symptoms actually occur in the first decade of life, Figure 1.4B (Chaussenot et al., 2011, Hershey et al., 2012, Pickett et al., 2012).

The median age of death in patients with this syndrome is around 30 years and arises sometimes from respiratory failure as a result of brain stem atrophy (Barrett and Bundey, 1997, Kinsley et al., 1995).

A

B

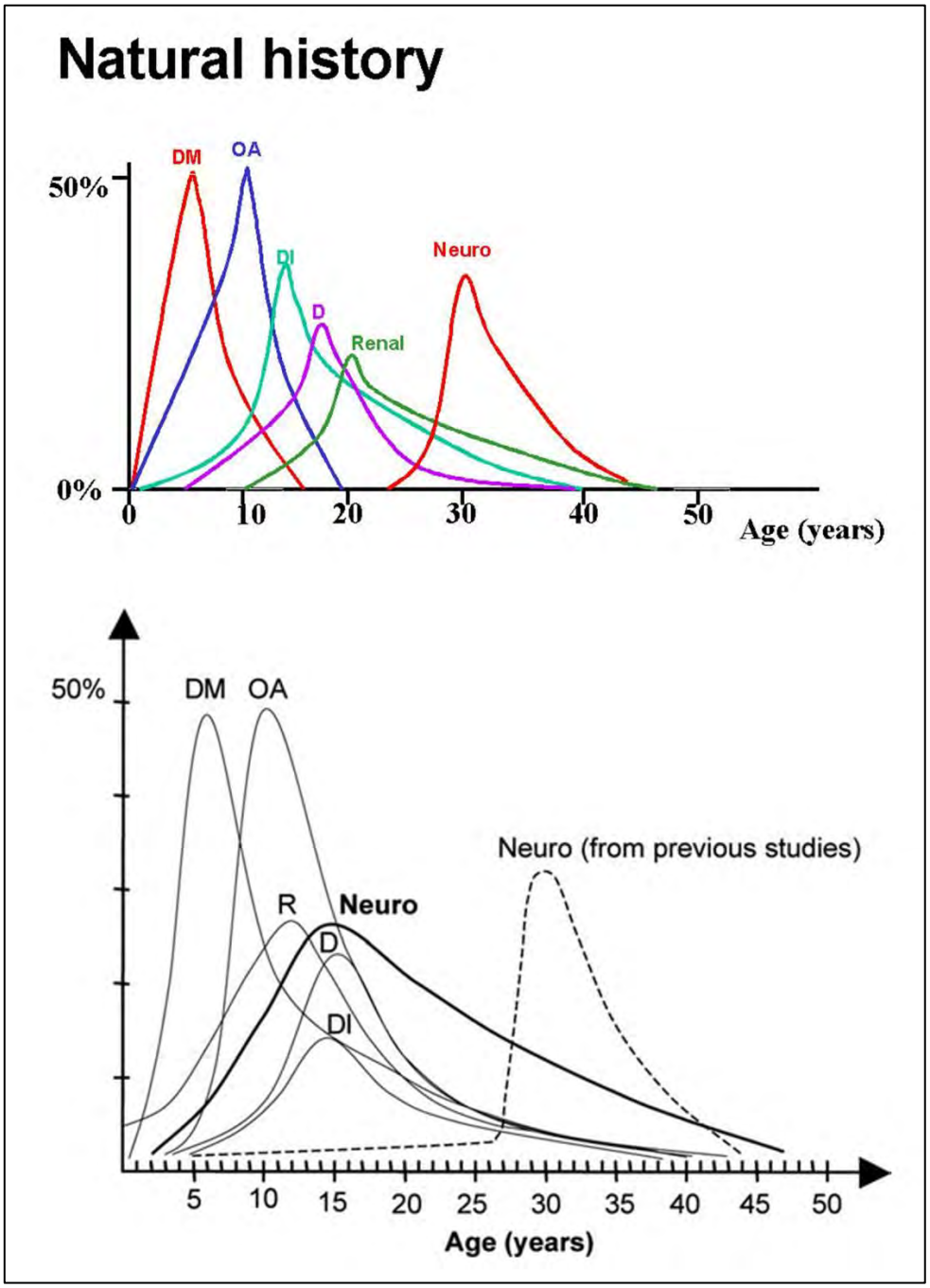

Figure 1.4: Natural history of symptom progression in Wolfram syndrome

A: The median age of onset of the symptoms and complications of Wolfram syndrome are presented with different curves and the intersections with the x-axis. DM: diabetes mellitus; OA: optic atrophy; DI: diabetes insipidus; D: deafness; Renal: renal tract complications; Neuro: neurological complications (Barrett and Bundey, 1997). B) Neurological complication seem to occur earlier in childhood than previously thought (Chaussenot et al., 2011).

1.5.1 Genetics

Wolfram syndrome has an autosomal recessive pattern of inheritance: affected siblings have unaffected parents who are often consanguineous (Fuqua, 2000). The causative gene for this syndrome, *WFS1,* was identified by two different groups in 1998. These researchers cloned *WFS1* and positioned it on the short arm of chromosome 4 (4p16) by linkage analysis and genetic mapping using microsatellite markers such as: D45431 and D45394 (Strom et al., 1998, Inoue et al., 1998). The gene was named *WFS1* by Inoue and colleagues and the protein was named Wolframin by Strom and colleagues. Figure 1.5 shows a schematic representation of *WFS1*. Its genomic structure comprises 8 exons of which exon 1 is non-coding. The majority of mutations found in *WFS1* are in exon 8 as this exon covers half of the coding region of the gene (1,812 nucleotides) (Takeda et al., 2001).

More than 90% of WS patients carry mutations that result in a loss of function of the *WFS1* gene (Khanim et al., 2001, Cryns et al., 2003). Furthermore, a patient mutation survey showed 35% missense, 25% nonsense, 21% frame shift, 13% in-frame deletions/insertions and 3% splice site mutations in the *WFS1* gene (Van den Ouweland et al., 2003). According to the Euro-WABB mutations data base, there are currently about 225 mutations (46% missense, 16%, nonsense, 22.7% frame shift, 8% deletion, 0.2% insertion 1.8% duplication and 3% others) identified in the *WFS1* gene (Euro-WABB-2012, An EU Rare Diseases Registry for Wolfram syndrome, Alström syndrome, Bardet-Biedl syndrome and other rare diabetes syndromes.), from which the majority are loss of function mutations (Chaussenot et al., 2011, Hardy et al., 1999, Cryns et al., 2003, Van den Ouweland et al., 2003, Gomez-Zaera et al., 2001, Hofmann and Bauer, 2006, Noguchi et al., 2004, Zenteno et al., 2008). WS is genetically a very heterogeneous disease and because of

the rarity of the disease and small patient numbers it has been difficult to identify a clear genotype phenotype correlation in this cohort. In a recent report Chaussenot and colleagues conducted a detailed clinical study and genotype-phenotype correlation in 59 patients, so far the largest number of patients. They demonstrated a correlation between neurological manifestation and the location of the mutation within the gene (Chaussenot et al., 2011). This study showed that patient with neurological complications more frequently had a mutation in the C-terminal domain and the presence of mutations in the N-terminal domain was significantly correlated with the absence of neurological symptoms.

Studies have shown that first degree relatives of WS patients have increased frequencies of diabetes and certain psychiatric disorders, suggesting that sequence variants of the WS gene predispose these individuals to these conditions (Ishihara et al., 2004, Zalsman et al., 2009, Sandhu et al., 2007). A review by Wasson and Permutt (2008) described studies which have shown that common gene variants of WS influence the susceptibility to type 2 diabetes. The first study uncovered 5 non-synonymous coding variants, encoding amino acid changes, by DNA sequencing of diabetic patients (Minton et al., 2002). The most important genetic variant changes the amino acid histidine to arginine (H611R) at position 611; this variant is thought to be protective from diabetes (Wasson and Permutt, 2008). Also the study by Sandhu et al. (2007) showed that variations in WFS1 gene are associated with susceptibility to common type 2 diabetes using 1,500 SNPs as markers for 84 beta cell candidate genes in a large number of UK, Europe and Ashkenazi Jewish cases and controls. This study showed four associated SNPs with significant linkage disequilibrium (LD) in a 39 kb LD block including the H611R variant (Sandhu et al., 2007).

A study by Hildebrand et al (2008) showed an association between autosomal dominant cases of the low frequency deafness with *WFS1* mutations. Similarly, a study by Shadrina and Slominsky (2006) showed that *WFS1* polymorphisms are associated with Parkinson disease. This study investigated a cohort of PD patients and controls in Russian population and showed that individuals carrying the c.1645C→T (L459L) SNP in WFS1 were at higher risk of developing PD (Shadrina and Slominsky, 2006).

In recent years, a second form of WS has been reported in Jordanian families. This gene was named *WFS2* and mapped to the locus 4q24 (Amr et al., 2007). In addition to WS clinical features, with the exception of diabetes insipidus, these patients also suffer from bleeding tendencies and defective platelet aggregation.

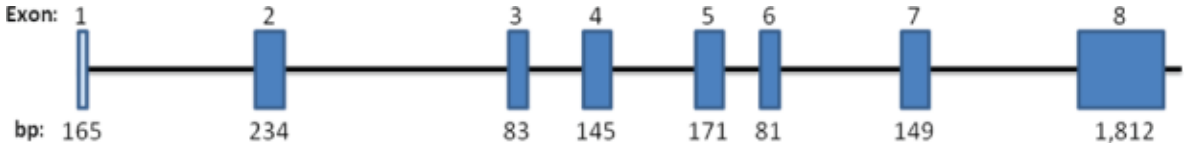

Figure 1.5: Schematic structure of *WFS1*

The *WFS1* consist of eight exons; exon one is non-coding and exon 8 comprises more than 70% of the coding region Figure taken from Rigoli et al. (2010)

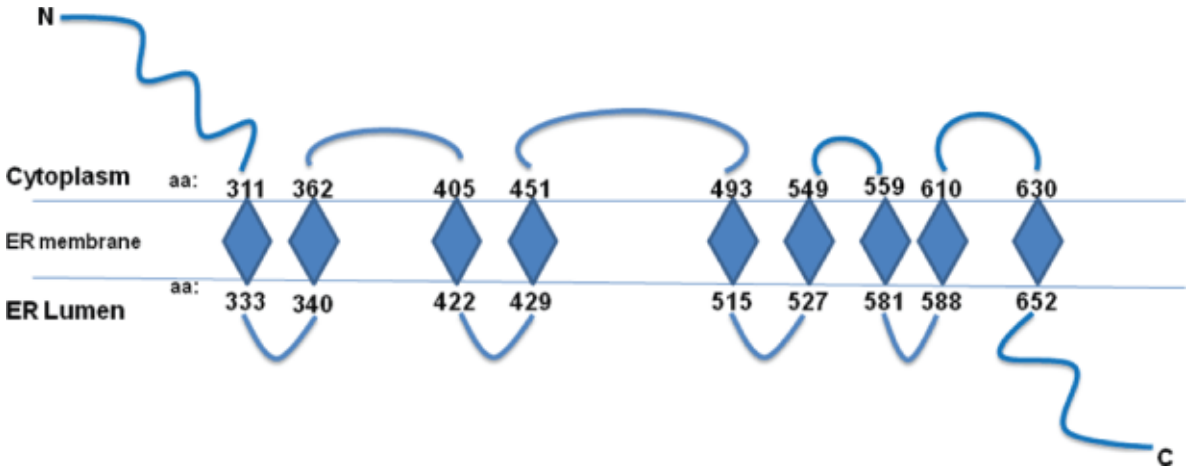

Figure 1.6: Schematic structure of Wolframin protein with transmembrane domains

Wolframin is a glycoprotein, has 9 transmembrane segments. The N-terminus is located in the cytoplasm and the C-terminus in the ER lumen. Figure taken from Rigoli et al. (2010)

1.5.2 WFS1 protein Wolframin

WFS1 encodes a 100 KDa protein called Wolframin which is primarily located to the membrane of the endoplasmic reticulum (ER) (Takeda et al., 2001, Philbrook et al., 2005, Inoue et al., 1998). This is an integral glycoprotein containing 9 transmembrane domains and 890 amino acids. The domains are embedded in the ER membrane with the amino terminus in the cytosol and the carboxyl-terminus in the ER lumen (Hofmann and Bauer, 2006). A schematic diagram of Wolframin is presented in Figure 1.6 (Rigoli et al., 2010). The C-terminal domain is translated from exon 8 of the gene and is associated with a high number of mutations. This region is highly conserved in human, rat and mouse. The mature Wolframin is shown to be fairly stable and the half-life of two days is estimated by pulse-chase experiments (Hofmann et al., 2003). The only post-translational modification reported in Wolframin is N-glycosylation (Yamaguchi et al., 2004, Inoue et al., 1998).

The study by Takeda and colleagues in 2001 reported localisation of WFS1 to endoplasmic reticulum, but not to the mitochondria, by immunofluorescence and cell fractionation studies. Previously, it was thought that WS might be a mitochondrial related disease due to phenotypic similarities between WS and mitochondrial diseases such as Leber's hereditary optic neuropathy, and maternally inherited diabetes and deafness (Rigoli et al., 2010). A more recent study by Hatanaka and colleagues (2011) reported localisation of Wolframin to the secretory granules. This was shown by immunofluorescence and electron microscopy.

Wolframin is ubiquitously expressed; however its expression is high in brain, heart, lungs and pancreas (Inoue et al., 1998, Ishihara et al., 2004). Immuno-histochemical studies on mouse tissue demonstrated that within the pancreas, Wolframin is mainly expressed in the beta cells (Ueda et al., 2005), analogous to the observed dysfunction and selective loss of pancreatic beta cells in WS patient islets.

WFS1 expression within mouse and rat brains has been identified in the hippocampus CA1, amygdaloid areas, olfactory tubercles, cerebellum and superficial layer of the allocortex (Luuk et al., 2008, Philbrook et al., 2005, Takeda et al., 2001). These expression patterns correspond to pathological changes seen in imaging and post mortem studies of WS patients, showing diffuse neurological changes in human brain regions: hypothalamus; pituitary; pons; inferior olivary nucleus; lateral geniculate nucleus; thalamus; optic nerves; optic tract and cerebellum (Genis et al., 1997, Kinsley and Firth, 1992, Galluzzi et al., 1999, Hardy et al., 1999, Barrett et al., 1995, Chaussenot et al., 2011). The observed neurological and pathological changes are most likely to be involved in the neurological and behavioural abnormalities and seen in humans with WS such as: cerebellar ataxia, central sleep apnoea, organic brain syndrome, depression, memory loss, hallucination and anxiety (Barrett et al., 1995, Luuk et al., 2009, Swift et al., 1990, Kõks et al., 2002, Kawano et al., 2009, Raud et al., 2009).

1.5.3 Wolframin function

The precise function of Wolframin is not fully understood; accumulating evidence based on its ER localisation and dimerisation, suggests that this protein plays a role in secretion, processing, folding and assembly of newly synthesised proteins. The presence of 9 transmembrane segments in Wolframin suggests its role in the transport of ions and other small molecules across the ER membrane (Osman et al., 2003). Osman and colleagues (2003) showed that expression of WFS1 in oocytes induced novel-cation-selective channel activity in the ER membranes and resulted in increased cytosolic Ca^{2+}. The authors suggests that Wolframin may function directly as a calcium-sensitive potassium channel that maintains ER membrane potential during calcium release or as a regulator of ER calcium channel (Osman et al., 2003).

The pathophysiology of WS suggests that Wolframin is involved in the survival pathways of neurons and pancreatic beta cells. Furthermore, studies have demonstrated crucial functions of Wolframin in the regulation of ER stress, ER stress induced apoptotic pathways, insulin biosynthesis, acidification of the secretory granules and regulation of ER calcium homeostasis (Fonseca et al., 2005, Fonseca et al., 2010, Hatanaka et al., 2011, Hofmann et al., 2003, Philbrook et al., 2005, Riggs et al., 2005, Yamada et al., 2006).

Mouse model studies of WFS1 have greatly advanced the knowledge of WS pathophysiology over the last two decades. WFS1 deficient knockout mice demonstrated glucose intolerance, high blood glucose levels, defective insulin secretion and reduced Ca^{2+} flux across the ER membrane (Yoshida, 2004, Ishihara et al., 2004, Riggs et al., 2005). A strong correlation was shown

between impaired insulin secretion and both reduction in stimulus-secretion coupling and overall beta cell mass and insulin content. *In vitro* studies of adenoviral re-expression of WFS1 have revealed that insulin secretion could be restored and ER calcium concentrations could be normalised (Takei et al., 2006, Fonseca et al., 2005, Fonseca et al., 2010). The study by Takei et al. (2006) demonstrated that Wolframin plays a crucial role in maintaining the correct levels of calcium ions by modifying ER calcium stores.

Diabetes insipidus (DI) in Wolfram syndrome arises at the hypothalamo-pituitary level and is usually vasopressin (VP) sensitive. The study by Gabreel et al. (1998) reported disturbances in VP precursor processing in the supraoptic and paraventricular nuclei of WS patients. This study demonstrated a complete absence of processed VP but substantial presence of VP precursors in WS patients with DI, suggesting that these patients have a defect in VP precursor processing and exhibit VP neuron loss (Gabreëls et al., 1998). More recently, the study conducted by Kawano et al. (2009) demonstrated that the WFS1 protein plays a major role in the survival of neurons in vasopressin precursor processing from birth to early adulthood.

Raud et al. (2009) showed that WFS1 deficiency in mice results in reduced levels of alpha and beta subunits of the GABA receptors in the temporal lobe and frontal cortex. As a consequence these mice displayed increased anxiety in a stressful environment. The study by Koks et al. (2002) showed that Wolframin plays a role in regulation of emotional behaviour by demonstrating increased expression of Wolframin in amygdaloid area of rats exposed to cat odour. In this study, the activation of WFS1 was found in parallel with the activation of carboxy-

peptidase E suggesting that Wolframin is involved in the synthesis of bioactive peptides and neuropeptides (Kõks et al., 2002).

1.5.4 WFS1 and UPR

A body of evidence showed that WFS1 is involved in ER stress pathways and is associated with the three ER stress sensors. A study by Fonseca and colleagues (2005) showed that WFS1 is a component of IRE1 and PERK signalling pathway and its expression is regulated by these two proteins. These authors demonstrated attenuation of ER stress by induction of WFS1 expression in *IRE1α*-/- and *PERK*-/- cells. This study suggests that WFS1 protects the cells against ER stress (Fonseca et al., 2005). Similarly, another study by Fonseca and colleagues in 2010 demonstrated that WFS1 plays a key role in the negative regulation of a feedback loop in the ER stress signalling network through the ubiquitin proteasome pathway. The authors suggested that WFS1 prevents secretory cells from death caused by dysregulation of this signalling pathway (Fonseca et al., 2010). This study showed that HRD1 (ER-resident E3 ligase) forms a complex with ATF6a and that WFS1 plays a role in the stabilisation of HRD1. The authors imply that under non-stress conditions, the WFS1-HRD1 complex causes suppression of UPR by recruiting ATF6 to the proteasome and enhancing its ubiquitination and proteasome-mediated degradation. In the presence of ER stress, ATF6 is released from WFS1 and activates the UPR to mitigate ER stress. However, contrary reports have shown increased levels of HRD1 in WFS1 deficient cells (Yamada et al., 2006, Yamamoto et al., 2008).

Accumulating evidence shows that WS pathogenesis is associated with chronic ER stress resulting in apoptosis caused by the loss of WFS1 function. Studies have shown that the diabetes mellitus phenotype in mice could be generated by silencing of *WFS1* only. Riggs and colleagues (2005) suggested that during ER stress conditions, WFS1 was necessary for cell survival in MIN6 cells. A study by Yamada et al. (2006) investigated the UPR in WFS1-deficient islets and MIN6 beta cells from mutant mice. They found that the levels of various ER stress markers including BiP, CHOP, XBP1 and GRP94 were markedly increased in these cells. Their results indicated that WFS1 deficiency activates the ER stress response in beta cells (Yamada et al., 2006). A study by Kakiuchi and colleagues in 2006 showed that XBP1 induces the expression of WFS1 through the UPR pathway. They investigated the target genes of XBP1 in neuroblastoma cells (SH-SY5Y) to clarify the role of XBP1 in neuronal cells and identified *WFS1* as the most upregulated gene by XBP1. They found an ER stress response element (ERSE)-like sequence in the promoter region of *WFS1* which is critical for the regulation of *WFS1* by *XBP1* (Kakiuchi et al., 2006). All these studies suggest that WFS1 is involved in the ER stress pathway and protects cells from ER stress induced apoptosis.

1.5.5 Interacting partners

Over the last years several interacting partners have been identified for Wolframin, which have greatly enhanced the current knowledge about its subcellular localisation and function. Zatyka and colleagues in 2008 identified an interaction between the Na^+/K^+ ATPase beta1 subunit with C-terminal domain of Wolframin. The sodium pump plays a crucial role in neuronal functions such as electrical excitation and signal transduction. The authors suggested that Wolframin could

play a role in folding of the subunit and therefore in proper functioning of the sodium pump (Zatyka et al., 2008). Moreover, the N-terminal domain of Wolframin was identified to be an interacting partner of calmodulin (CaM) (Yurimoto et al., 2009). CaM is a ubiquitously expressed protein that is known as an important second messenger of intracellular calcium signalling. Previous studies have suggested that Wolframin may serve as an ER calcium channel or, as a regulator of ER calcium channel activity. These interactions of WFS1 with the ion pumps or related proteins, are confirming this notion that, similar to other ER membrane associated proteins, Wolframin may also form an ion channel. More studies are needed to clarify whether Wolframin acts directly as a channel or functions only in a regulatory capacity.

Furthermore the master regulator of UPR, ATF6 was recently shown to interact with WFS1 (Fonseca et al., 2010). This study showed protein interaction between WFS1 and ATF6a in non-stressed pancreatic beta cells. The proteins dissociated following a time-dependent treatment with the ER stress inducing agents thapsigargin and dithiothreitol (Fonseca et al., 2010). Similarly, the study by Kakiuchi and colleagues (2009) showed an association between WFS1 and the molecular chaperone, GRP94, in rodent neuronal cells. These interactions with the UPR regulator confirm the role of WFS1 in ER stress pathways. More recently, Fonseca and colleagues (2012) identified an interaction between WFS1 and adenylyl cyclase8 (AC8) at the cytoplasmic membrane. This interaction seems to be important for the regulation of insulin production and secretion. AC8 is an essential cAMP generating enzyme that plays a role in glucose and glucagon-like-peptide-1(GLP1) signalling within the pancreatic beta cells. This study demonstrates a function for Wolframin outside the ER and shows that WFS1 is also localised to

the plasma membrane. The authors showed that *WFS1* mutations and ER stress cause inhibition of the WFS1-AC8 complex formation, which results in reduction of cAMP synthesis and insulin secretion (Fonseca et al., 2012).

1.5.6 Treatment of Wolfram syndrome/ ER stress

Currently there is no treatment for WS. Agents that are able to treat ER stress-mediated apoptosis are the attractive candidates. A study by Kakiuchi et al. (2009) used the histone deacetylase inhibitor, sodium valproate (VPA) to treat WFS1 depleted cells. They showed that VPA modulates the unfolded protein response (UPR) through the regulation of WFS1. This study demonstrated induction of WFS1 protein and mRNA in Neuro2a cells with VPA treatment. These authors also showed that under normal conditions WFS1 forms a complex with GRP94 and VPA treatment enhances its dissociation from GRP94. A recent study by Terasmaa et al. (2011) used VPA in a *WFS1* knockout mouse model and streptozotocin induced diabetic mice. They showed that VPA normalised the glucose intolerance in *WFS1* knockout mice. The authors also showed that acute VPA administration lowered blood glucose levels in the diabetic mouse model (Terasmaa et al., 2011).

Resolving ER stress is one of the main therapeutic strategies for many neurodegenerative disorders. Therefore, the first step in treatment of WS would be to consider resolving ER stress, which is the major cause of neuronal and pancreatic beta cell death contributing to the pathogenesis of this disease. As mentioned before, one of the UPR defence mechanisms is to upregulate the cells' chaperone capacity. Chaperones play crucial roles in maintaining cellular

homeostasis by improving the ER's folding capacity, facilitating the trafficking of mutant proteins and stabilising protein conformation (Ozcan et al., 2009). In unstressed cells the chaperones are expressed at low levels but are highly upregulated in the presence of stress. Dysregulated chaperone activity leads to accumulation of unfolded proteins causing impairment of cellular function and contributing to ER stress related diseases. Chaperones are also involved in histone-mediated chromatin remodelling, the transition between the active and inactive state of signalling molecules and protein-protein interactions (Ransom et al., 2010). For all these reasons, modulating chaperones, or identifying chemical chaperones that can enhance or modulate endogenous chaperone activity, could be potential therapeutic approaches for treatment of many ER stress related disorders. There are three types of molecules with chaperone like activity: small chemical chaperones; molecular chaperones and pharmacological agents (Figure 1.7, (Engin and Hotamisligil, 2010)).

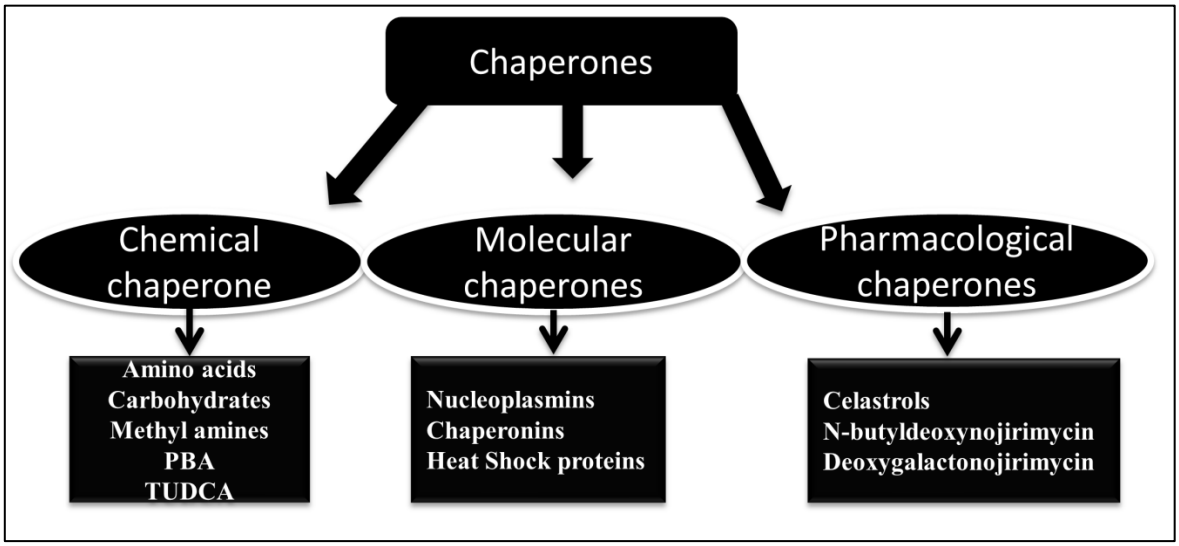

Figure 1.7: Molecules with chaperone like activity

There are three groups of chaperones that are able to enhance proper folding of the proteins: molecular, pharmacological and chemical chaperones. Examples of each group are listed. Figure adapted from (Engin and Hotamisligil, 2010)

1.5.6.1 Chemical chaperones

Chaperones are proteins that enhance the proper folding and assembly of macromolecules; their function is to prevent the formation of protein aggregates. Chemical chaperones belongs to two groups of osmolytes including carbohydrate osmolytes (glycerol, sorbitol, inositol) and aminoacids (glycine, taurine, alanine, proline) (Welch and Brown, 1996). Many of these chemical chaperones are required in high concentration to perform effectively, which can cause toxic effects. Currently there are two chemical chaperones approved by The US Food and Drug Administration (FDA) for use in humans. These are 4-phenylbutyric acid (PBA) and Tauroursodeoxycholic acid (TUDCA) (Welch and Brown, 1996). PBA is mainly used for treatment of urea cycle disorders and TUDCA is used as a liver protecting agent in humans. Currently TUDCA is under clinical testing for treatment of many ER stress related disorders (Engin and Hotamisligil, 2010).

A study by Ozcan et al. (2006) investigated whether these chaperones could alleviate the increased ER stress in type 2 diabetes *in vitro* and *in vivo*. They used PBA and TUDCA and found that these two chaperones were capable of alleviating ER stress in cells and in whole animals. They showed that the treatment of ER stress in mice with these two active chemical chaperones resulted in normalisation of hyperglycemia and restoration of systemic insulin sensitivity. Moreover these chaperones were beneficial in resolution of fatty liver disease, and enhancement of insulin action in liver, muscle, and adipose tissues. Their results showed that chemical chaperones enhance the adaptive capacity of the ER and act as anti-diabetic agents with potential application in the treatment of type 2 diabetes (Ozcan et al., 2006). Another study by

Wei et al. (2008) investigated the effects of TUDCA on cells under ER stress. Their results suggested that treatment with chemical chaperones not only suppresses the expression of ER stress markers, it is also very effective in reducing the levels of cell death by apoptosis (Wei et al., 2008).

1.5.6.2 Molecular chaperones

These chaperones provide the cell with a quality control system for recognising, retaining, and targeting misfolded proteins for degradation (Welch and Brown, 1996). When an unfolded protein enters the ER lumen, it interacts with molecular chaperones such as GRP78/94 or calnexin. This interaction stabilises the protein and allows it to complete its folding or assembly. This newly synthesised protein exits the ER and moves further along the secretory pathway. Proteins that are unable to fold properly e.g. due to mutations are prevented from further movement out of the ER by the action of these molecular chaperones (Schroder and Kaufman, 2005).

Molecular chaperones recognise unfolded proteins by the presence of the hydrophobic residues within the polypeptides. These chaperones enhance protein folding through substrate binding and release cycles, which are regulated by their ATPase activity (Bando et al., 2004). Recent studies suggest that over-expression or upregulation of molecular chaperones can suppress the neurotoxicity of protein folding diseases such as neurodegenerative diseases including Alzheimers diseases, Parkinsons disease and Huntingtons disease (Barral et al., 2004). Similarly, the study conducted by Yamada et al. (2006) showed that the elevated levels of ER stress in WFS1 depleted cells were reversed by over-expression of the molecular chaperone BiP/GRP78.

Another study by Bando et al. (2004) showed that the expression of the molecular chaperone GRP94 reduces cell death in neuroblastoma cell lines and stabilises their calcium homeostasis.

1.5.6.3 Pharmacological Chaperones

These chaperones are small molecules such as ligands or inhibitors of mutant proteins that stabilise these proteins by reversibly binding to them. Pharmacological chaperones play a major role in restoring the function or folding ability of mutant proteins that partially lose their biological activity due to deletions or missense mutations. These chaperones are also improving the stability and lysosomal trafficking of mutated enzymes. An example is the co-application of proteasome inhibitor MG-132 and a pharmacological chaperone for restoration of mutant enzymes in patient-derived fibroblasts from lysosomal storage disorders such as Gaucher and Tay-Sachs-disease (Mu et al., 2008). Pharmacological chaperone therapy (PCT) is translated into clinical trial applications for Gaucher, Fabry, and Pompe diseases after initial proof of concept studies (Parenti, 2009).

1.6 Aims and hypothesis

The main focus of this thesis has been to study the neurodegenerative aspects of Wolfram syndrome. Until the start of this project, the majority of research in Wolfram syndrome has been focused on diabetes in animal models. The disease characteristics and protein functions have been mainly discovered in mice pancreatic beta cells (Hofmann et al., 2003, Osman et al., 2003, Philbrook et al., 2005). Since diabetes is the first manifestation of the disease and pancreatic beta cell loss is the underling mechanism, more attention has been dedicated to this area (Fonseca et al., 2005, Riggs et al., 2005). Nevertheless in the recent years, it has become more evident that neurodegeneration is the main area in WS that needs urgent attention. Death in WS arises from neurological complications and recent studies on MRI scans have shown that neurological changes occur in early childhood in WS patients' brains. Therefore it is believed that neurodegeneration could be one of the first manifestations of WS and other complications could be arising as a result of neurodegeneration.

In order to understand the neurodegenerative mechanisms in Wolfram syndrome and relate this rare monogenic disease to more common forms of neurodegenerative disorders, it was attempted to generate and characterise cell models of human and rodent neuronal cells with WFS1 depletion; and to investigate whether human neuronal cells with WFS1 depletion show disease phenotypes of WS previously described in mice pancreatic beta cells. The functions of WFS1 in neuronal cells were investigated by assessing its role in apoptotic pathways, in cell cycle regulation and in the regulation of the sodium pump subunits expression. To elaborate the functions of WFS1, the existence of novel interacting partners were investigated. Since there is

no current treatment for this devastating disorder, in this body of work, chemical and molecular chaperones were used to rescue the cells from ER stress and ER stress induced apoptosis. To induce the expression of WFS1 in cultured cells and investigate therapeutic efficacy, treatment with the histone deacetylase inhibitor sodium valproate was undertaken.

Several hypotheses were developed in this study: a) WFS1 depleted neuronal cells are a valid cell model of the disease and exhibit enhanced ER stress leading to apoptosis and cell cycle impairment; b) these cell models show reduced levels of the Beta1 subunit of the sodium pump and might play a role in its stability and regulation of its expression; c) WFS1 might have a role outside the ER, therefore this protein might also have cytoplasmic interacting partners; d) molecular and chemical chaperone treatment in WFS1 depleted neuronal cells would rescue the cells from ER stress, apoptosis and cell cycle disturbances.

Chapter Two: Materials and Methods

2.1 Reagents

Taqman assays and QPCR reagents were acquired from Applied Biosystems and the majority of antibodies were purchased from Abcam and general chemicals were purchased from Sigma-Aldrich. Specific reagents were acquired from the following list of companies and the relevant company is cited with the relevant method:

Abgent

Amersham

Bio-Rad laboratories ltd

Cell Signalling

Invitrogen

Promega Ltd

Protein tech

Roche Diagnostics

Santa Cruz Biotechnology, Inc

Thermo Scientific

2.2 Cells and cell culture

2.2.1 Cell lines

SK-N-AS cell line was kindly donated by Dr Carmel McConville and NT2 cell line was kindly donated by Dr Shiao Chan. Neuro2a mouse neuroblastoma cell lines was purchased from ECACC (European Collection of Cell Cultures). These cell lines were grown under the standard tissue culture conditions as described in section 2.2.3

2.2.2 Tissue culture

Tissue culture (TC) experiments were performed in class 2 tissue culture hoods (Holten LaminaAir) under sterile conditions; wearing lab coat and gloves. All solutions and equipment's used for cell maintenance were either obtained sterile or autoclaved, where appropriate, before use. The TC hood was switched on15 min before use and cleaned thoroughly with 10% Trigene. The media, PBS and trypsin were warmed in water bath (37 °C). Before placing in the hood all items (flasks, dishes, pipettes, waste pot, flasks, pipettes, universals, media, PBS bottles and trypsin tubes and all other plastic ware) were wiped with either 10% Trigene or 70% ethanol.

2.2.3 Cell Growth and maintenance

Cells were maintained in an incubator at 37°C, 5% CO_2, in air MCO-15AC, Sanyo). Human neuroblastoma SK-N-AS cell lines were grown in the Dulbecco's Eagle Medium (DMEM) supplemented with 10% Fetal bovine serum (FBS), 1% L-glutamine (GIBCO), 1% Pen/Strep (penicillin 10.000units/mL, streptomycin 10.000µg/mL from GIBCO) and 1% non-essential amino acids (GIBCO). Puromycin (Sigma) was added into the media at a final concentration of 2.5µg/mL to select for resistance in stably WFS1 depleted clones. Human NT2 cell lines were grown in DMEM: F12 HAM media (SIGMA) supplemented with 10% FCS, 1% penicillin-streptomycin and 1% glutamine and mouse Neuro2a cell line was grown in Minimum Essential Eagle Medium (ATCC) supplemented with 10% FCS, 1% penicillin-streptomycin and 1% glutamine. The growing cells were fed approximately twice a week by replacing the media. When cells reached about 90% confluency in the flask, they were passaged or harvested. The

neuro2A cells were very sensitive, the medium was changed every day and they were passaged at lower confluency.

2.2.4 Trypsinisation of confluent cells

Trypsin was used to detach the cells for passaging. Upon reaching confluency of the cells the media was aspirated from the flask using a sterile pipette. Cells were washed with 10 mL PBS (2.7mM KCl, 137mM NaCl, 10mM phosphate buffer, pH 7.4). PBS was aspirated, 2 mL of trypsin solution was added and the flask was placed in the incubator for approximately 3 minutes until the cells were detached; sometimes a gentle agitation was required. When the cells were floating in the flask, 8mL of supplemented media was added and mixed thoroughly. The suspension was subsequently transferred into a 20mL universal tube (Lab ware) and centrifuged at 250 RCF for 3 minutes at 20 °C. The supernatant was carefully aspirated without disturbing the pellet. The pellet was resuspended in the medium and the cells were reseeded (section 2.2.5) either for transfection (section 2.2.10), RNA (section 2.4) or protein extraction 2.3 or frozen (section 2.2.7).

2.2.5 Cell Reseeding

For routine cells maintenance, the trypsinised cell pellets were resuspended in 10mL of supplemented media: 2mL of this mix was added into a new 75cm^2 flask. 8mL of fresh media was added and pipetted up and down to ensure even distribution of the cells. The flask was then placed in an incubator and cells were grown to the required confluency.

2.2.6 Reviving cells

The frozen cells were taken from liquid nitrogen and placed in the float in the 37 ^{o}C water bath. When defrosted, the cells were added into a universal tube containing 9 mL of media and the falcon was centrifuged at 250 RCF for 3 minutes at 20^{o}C. The centrifugation was carried out to remove the freezing medium containing Dimethyl Sulfoxide (DMSO), which is important to keep cells alive when frozen, however it is toxic for living cells. The supernatant was removed and 5 mL of media was added into the falcon. The cells were mixed with the media by pipetting, then transferred into a 25 cm^2 flask and another 2mL of media was added. The flask was placed in the incubator to allow the cells to grow. NT2 and Neuro 2a cell lines were put straight into the media after defrosting as these cell lines could not tolerate centrifugation before reviving.

2.2.7 Cell Cryopreservation

When sufficient amount of cells was grown, it was necessary to produce frozen aliquots of cells. The cells were frozen in DMEM with 10% (v/v) DMSO as a cryoprotectant. The trypsinised cell pellets were resuspended in 1.5 mL of the prepared freezing medium, mixed well and transferred to a 2mL cryovial (Corning). The cryovial was labelled and placed in a cryogenic vessel (Mr. Frosty filled with iso-propanol) and placed at -80 ^{o}C for at least 4 hours. The cryovials were later transferred to liquid nitrogen for long term storage.

2.2.8 Cell count

Cell count was performed using the haemocytometer. The haemocytometer was cleaned with 70% ethanol and a cover slip was placed in the centre. About 25µL of the trypsinised cells in

DMEM were pipetted beneath the cover slip. The cells were observed through a light microscope, and counted in the central square of the haemocytometer taking two counts every time. The number of cells per mL was calculated by multiplying the average of cell counts, by the conversion factor ($1x10^4$) of the haemocytometer and by the dilution factor used.

2.2.9 Adenoviral transduction of BiP/GRP78

The amplification and purification of the viruses were performed by Dr. Zatyka in the following manner. *The adenoviruses were amplified first on a small scale by infecting HEK293 cells in 25cm tissue culture flasks. The cells were grown for several days until signs of infection were visible. About 3mL of these cells were used to infect HEK293 cells for large scale amplification. The adenovirus was harvested by scraping and spinning down the cells at 1000xg, 10min, at 4°C and 1/100 volume of N-butanol was added. The samples were incubated on ice for 1 hour before being spun down at 1000g, for 10min at 4°C.The supernatant was harvested and loaded onto a CsCl gradient. The virus was purified by CsCl banding. The titre of the virus was established using Adeno-X rapid titer kit.*

Cells were seeded with a density of $4x10^5$ cells/well in a 6 well plate. After 24 hours the cells were about 50% confluent and ready for infection. Initially, the cells were infected with 2µL virus per well to obtain an MOI (multiplicity of infection) 85; this was subsequently optimised to MOI 8.5. Both adenoviruses ad-GRP78 and ad-GFP had similar titre: $1.7\ x10^{10}$ ifu/mL (infection units). Approximately 16 hours after the infection, the cells were washed once with PBS and fresh media was added. The cells infected with ad-GFP were monitored under the fluorescence

microscope for GFP (Green Fluorescent Protein) expression, emitting green light. The cells were harvested 48 hours after the infection either in TRIzol for RNA measurements (section 2.4) or in RIPA buffer for protein measurements (section 2.3). The untreated cells were cultured similarly without adding the adenovirus. The adenoviral infected cells were also assessed by High Content Cytometry (section 2.5); 16 hours after the infection the cells were washed with PBS, trypsinised, counted and reseeded in a 96 well plate. The cells were grown, fixed and stained as described in section 2.5.

2.2.10 Transient Gene Silencing

SK-N-AS neuroblastoma or NT2 cells were transfected using small interfering RNA (siRNA, Ambion) with two oligonucleotides (WFS1-57 and WFS1-58) targeting different regions of *WFS1* gene, at final concentration of 8nM (Table 2.1). Trypsinised cell pellets were resuspended in 10mL media; cells were counted and seeded in 6 well plates. 3mL of $6x10^4$ cells/mL were plated per well to achieve 50-60% confluency the next day. The transfection was carried out after 24 hours using interferin, an siRNA transfection reagent (Source Biosiences). 100µM siRNA solution was made by adding 50µL dH2O to 5nmol lyophilised siRNA. The working solution was prepared by diluting this stock solution 40x to 2.5 µM. The transfection procedure: for each transfected well, 300µL OPTI-MEM (GIBCO) was aliquoted in a sterile 1.5mL microcentrifuge tube. 8µL of the siRNA working solution was added to a final concentration of 8 nM and the tube was vortexed gently. Accordingly, 10µL of the transfection reagent interferin (Polyplus Transfection) was added into each tube and vortexed immediately for 10 seconds. The microcentrifuge tubes were left at room temperature for 20 minutes. While waiting, the media of

the cells was changed to 2.2mL of fresh media. After drop wise adding the 300µL tube content to the cells the final volume of media in the cells was 2.5mL. Alongside targeted knockdowns, a negative control siRNA was used (Ambion). The cells were harvested 72 hours after transfection either in RIPA (Section 2.3) or in TRIzol (section 2.4.1).

Table 2.1: Si RNA Sequences

Si-RNA	Sequence	Cat-No
S14857 (WFS1-57)	5'CCAUCGACUUCGCCUUtt3' 5'AAGGCGAAGAAGUCGAUGGtg3'	ASO0KP9Q
S14858 (WFS1-58)	5'GUCAUGUACUGGAAGCUCAtt3' 5'UGAGCUUAGUACAUGACca3'	ASO0KP9P
Negative control	Sequence unknown	4390843

2.2.11 Stably Transfected Cell Line Generation

Stable knockdowns in human neuroblastoma cell lines SK-N-AS were prepared by Dr. Zatyka using shRNA (Open Biosystems). Stable knockdowns in mouse neuroblastoma cell lines Neuro2a were prepared by Dr. Astuti using lentivirus system. Lentiviral particles were prepared by Dr. Zatyka from lentiviral DNA purchased from Genecopoeia and concentrated by Dr Astuti. Puromycin resistance selection was used for both types of knockdowns.

2.2.12 Protein degradation assay

Protein degradation assays are used to assess the degradation rate of a protein based on its half-life. Cycloheximide (CX) is a protein synthesis inhibitor in Eukaryotes that is produced by Streptomyces Griseus. The stability of the beta1 subunit of the sodium pump and theV1A subunit of proton pump were assessed in WFS1 depleted stable clones in comparison to the control. Cells were counted and plated at a density of $8x10^5$ cells/well in a 6 well plate. After 24 hours they were treated with 50µg/mL of CX (Sigma). The cells were harvested in RIPA buffer at 0, 2, 4 and 6 hours after treatment and prepared as described for Western blotting (Section 2.3). The samples were resolved on SDS-PAGE gel. 20µg of protein extract was loaded per lane. CX toxicity was assessed by High Content Cytometry (section 2.5) using concentration in the range 10 to 90µg/mL.

2.2.13 Thapsigargin treatment

SK-N-AS cells were grown in $10cm^2$ dishes for 24 hours to reach 80-90% confluency. The cells were starved for approximately 14 hours in serum free medium. Afterwards 10µL of thapsigargin

stock in DMSO was added to final concentration of 1µM. An equal volume of DMSO was added as a negative control. The cells were then harvested after 24 hours of treatment in RIPA buffer (section 2.3).

2.2.14 Drug treatment

Stably depleted human neuroblastoma (SK-N-AS) cells were treated with Tauroursodeoxycholic acid (TUDCA) and Valproate (VPA). $4x10^5$ cells/well were plated in 6 well plates and grown for 24 hours. For valproate treatment, the cells were treated with 4 different concentrations of Valproate: 50, 100, 200 and 600 µg/mL (in duplicates). A stock solution of 100µg/µL valproate in water was prepared and working solution was made by diluting the stock solution 10x in culture medium. For example for a final concentration of 50µg/mL in cultured cell containing 2mL media, 10µL of the valproate solution was added. The cells were grown for 24 hours with the drug and harvested in TRIzol for RNA and in RIPA buffer for protein extractions.

TUDCA was dissolved in DMSO and two concentrations were used in the experiments: 100µM and 500µM. First of all 1M solution was prepared in DMSO, which was again diluted in DMSO to get stock solutions of 100mM and 500mM. For achieving a final concentration of 100µM TUDCA in cells, the stock of 100mM was diluted 10x in DMSO to get 10mM and 20µL of this was added to the cells in 2mL media; the final concentration of DMSO in the cells was 1%. 500mM stock was used to prepare samples of final concentration 500uM.The cells were grown

over night, and harvested the following day in TRIzol for RNA and in RIPA buffer for protein extractions.

2.3 Protein Harvesting and Quantification

2.3.1 Protein extraction

For protein extraction cells were either harvested in RIPA buffer (50mM Tris pH8, 150mM NaCl, 0.1% sodium dodecyl sulfate (SDS), 1mM EDTA, 0.5% deoxycholate, 1% Igepal and protease inhibitor cocktail, Roche), Laemmli buffer (62.5mM Tris pH 6.8, 2% SDS, 25% Glycerol, 5% β-mercapto-ethanol, 0.01% bromo-phenol blue and protease inhibitor) or ice cold TNE buffer (50mM Tris HCl, pH7.5; 150mM NaCl; 1mM EDTA; 1% NP-40 and protease inhibitor cocktail).

To harvesting cells in RIPA or Laemmli buffer: the media was aspirated and cells were washed with PBS. The lysis buffer (RIPA/Laemmli, 100µL to a 6 well plate and 500 µL to a 10cm^2 dish) was added to the cells and left for five minutes to allow lysis of the cells. Afterwards, the cell lysates were collected using a scraper and transferred to a labeled 1.5mL sterile tube and placed on ice for 20 minutes, sonicated 2x 10s and centrifuged at 14,000 rpm for 30 minutes at 4 °C. The supernatant was carefully removed and placed into a fresh 1.5mL microcentrifuge tube and stored at -80 ^{o}C, ready for western blotting. For detection of ATF6, cells were harvested in ice cold TNE buffer and lysed for 15 minutes on ice. The lysates were cleared by centrifugation at 12 000g for 20 minutes at 4 °C.

2.3.2 Protein quantification

Before starting the experiments, the concentration of the proteins was measured using the protein concentration determination kit (Bio-Rad). The concentration was calculated by comparing the absorbance of samples at 690nm wavelength against standard BSA (Bovine Serum Albumin) known concentrations. To prepare BSA standards: 2mg/mL BSA (Pierce) was diluted to obtain the following concentrations (0, 0.2. 0.4, 0.6, 0.8, 1.0, 1.2 and 1.4 µg/µL). The protein samples were usually 5x diluted and 5µL was plated in sterile 96 well flat bottom plates. The samples and the standards both were plated in duplicates. The Bio-Rad kit consists of 3 types of solutions A, B and S. Solution C was prepared by adding 1mL of solution A to 20µL of solution S. 25 µL of this solution was pipetted per well with protein sample or standard and mixed by passing it through the tip. Accordingly, 200µL of solution B was added gently to the wells without any mixing. The plate was incubated for 20 minutes at room temperature and measured by protein plate reader (Perkin Elmer). The absorbance data was transferred to an Excel spreadsheet and a scatter graph was plotted from the standards (R square values lower than 0.9 were not accepted). The unknown concentrations were calculated using absorbance and the equation from the graph.

2.3.3 Sodium dodecyl sulphate polyacrylamide gel electrophoresis

The presence of proteins in the extracts was detected by western blotting with specific antibodies. SDS-polyacrylamide gels (SDS-PAGE) for immunoblotting were prepared with a resolving gel segment and overlaying stacking gel segment. The percentage of the resolving gel segment was 10%, 12% or 15% dependent on the molecular weight of the proteins to be resolved. The resolving gel was made up by adding the relevant volume of 30% acrylamide Protogel (National

Diagnostics), 375mM Tris pH8.8 and 0.1% SDS. The gels were polymerised with 10% APS (Ammonium Persulphate) and TEMED (Tetramethyl Ethylene Diamine, Sigma). The gel was poured up to 4/5 of the gel plate and the rest was filled with water while the gel was set. The water was removed and replaced with stacking gel (3% acrylamide 50mM Tris pH6.8, 0.1% SDS and polymerised with 10% APS and TEMED). The combs were immediately placed after the stacking gel was poured and left to set. Once set, the gels were placed into an electrophoresis tank (BIORAD Mini), filled with 1x SDS running buffer (10x running buffer was prepared: 0.25M Tris, 1.92M glycine, 0.1% SDS Gene flow) and the combs removed.

Before loading, the protein samples, typically 20µg were mixed with loading buffer. Samples harvested in RIPA buffer were mixed with 5x loading buffer (0.313 M Tris HCl- pH 6.8, 10% SDS, 0.05% bromophenol blue, 50% glycerol, Fermentas). Protein samples harvested in Laemmli buffer were mixed with 1% BB (Bromophenol Blue) dye only. The samples were denatured at 100°C for 5min and placed immediately on ice. The samples were loaded into the wells of the gel along with 5µL of a protein marker (Page Ruler, Fermentas). The gel was resolved at 150V for approximately 60 minutes until the loading dye approached the bottom of the gel.

2.3.4 Protein transfer from SDS-PAGE to PVDF Membrane

When the gel was run to the appropriate level, the plates were carefully split, the stacking gel was removed and the gel was transferred to a PVDF transfer membrane (Polyvinylidene Fluoride, GE Healthcare). The transferring cassette was prepared by dipping a thin piece of sponge in 1x cold transfer buffer (10x: 0.25M Tris and 1.92M Glycine, Geneflow) containing 20% methanol and

placing it on the cassette. This was followed by 3 pieces of Whatman 3MM paper wet in transfer buffer; the gel was carefully placed on the top. The membrane was activated by brief immersion in methanol and placed on the top of the gel, followed by 3 pieces of wet Whatman 3MM papers and another wet sponge. The cassette was closed, making sure there were no bubbles between the gel and the membrane. The cassettes were placed in the transfer device which was placed into a transfer unit (Amersham) with the gels facing the cathode and oriented in a way to make transfer in the electric field possible; an ice block was positioned in the transfer unit. This was filled with cold 1x transfer buffer and run at 100 volt for 90 minutes. Once the transfer was completed the membrane was removed and marked to identify the side where the proteins had transferred. The membranes were blocked using 5% milk in PBS +0.1% Tween (PBS/Tween) for either 1 hour at room temperature or overnight at 4 °C.

2.3.5 Western blotting

The blocked membrane was first probed with a specific primary antibody to the protein to be studied. The primary antibody was diluted in 5mL of blocking solution in a 50mL centrifuge tube volume to the concentration required with blocking solution in a 50mL centrifuge tube. The membrane was placed in this solution with the protein side of the membrane facing inwards and incubated overnight at $4^{o}C$ on a tube rotator. Different dilutions of the primary antibody were used depending on the antibody. A list of primary antibodies with the dilution factors are shown in Table 2.2. The next day, the membrane was placed in a tray containing PBS-Tween buffer on an orbital shaker for 3x5 minutes to wash off the primary antibody. The membrane was placed inside another 50mL centrifuge tube containing secondary antibody in 5mL of 5% milk in

PBS/Tween and incubated at room temperature for 1 hour on a tube rotator. See Table 2.3 for dilutions of secondary antibodies. This membrane was subjected to further 3x10 minutes washes in PBS/Tween. Subsequently, the washed membrane was placed on a piece of flat saran wrap with protein side up. The membrane was developed to detect secondary antibody using the ECL kit (ECL or ECL Plus, GE Health care). The membrane was covered with ECL solution and left to incubate for 5 minutes at room temperature. The membrane was wrapped in saran and the excess ECL was drained off. The membrane was then placed in a developing cassette and exposed to medical X-ray film (Kodak, Sigma) for the appropriate amount of time depending on the strength of the signal. The autoradiography films were then developed in an X-ray film developer (Konica Minolta).

2.3.6 Immunoprecipitation (IP)

$3x10^6$ HEK293 cells were seeded in a $10cm^2$ dish, incubated overnight and co-transfected with pCMV-Myc-WFS1 (full length, N-ter, or C-ter)/ pFLAG-CMV-ATP6V1A using Turbofect transfection reagent (Fermentas) according to manufacturer's instructions. Control cells were co-transfected with pCMV-Myc empty vector/ pFLAG-CMV-ATP6V1A and pCMV-Myc-WFS1 (full length, N-ter or C-ter)/pFLAG-CMV-4 empty vector. The cells were harvested in IP buffer (20mMTris-HCl, pH 7.4; 100mM NaCl; 1% Triton X-100; 1mM DTT; 1mM PMSF; 1x Protease Inhibitors cocktail), incubated at 4°C for 30 min with end-to-end rotation and sonicated on ice for 30 seconds (10s pulses with 3 intervals), and centrifuged at 9000g for 20 minutes at 4°C to remove cell debris. For co-immunoprecipitation in an overexpression system, 500µg of protein lysate was incubated with either WFS1 rabbit polyclonal antibody (Proteintech) or rabbit

polyclonal c-Myc antibody (Sigma) or mouse monoclonal FLAG antibody overnight at 4 °C with end-to-end rotation. Protein G sepharose beads (Sigma) were washed in IP buffer then added to the lysate-antibody complex and further incubated for 4 hours. Beads were collected, washed twice in IP buffer with 150mM NaCl, once in IP buffer with 500mM NaCl and again in IP buffer with 150mM NaCl. Bound proteins were then eluted in sample buffer. To detect endogenous interaction, human neuroblastoma cells were harvested in IP buffer as described above. The lysate (containing about 1mg of protein) was precipitated with rabbit polyclonal WFS1 antibody (Abcam). Mouse monoclonal FLAG antibody (Sigma) was used as negative control. This experiment was performed in collaboration with Dr Astuti.

Table 2.2 List of primary antibodies

Primary Antibodies	Company	Cat-nr	Source	Dilution	Application
Anti-WFS1	Proteintech Group, INC	11558-1-AP	Rabbit	WB:1/500 IF:1/100 HCC: 1/800	WB, IF, HCC
Anti-BIP	Abcam	Ab21685	Rabbit	WB:1/1000 HCC:1/500	WB, HCC
Anti-CHOP	Abcam/Santa Cruze	Ab11419 Sc-7351	Mouse	1/200 1/500	WB
Anti-ATF-6a	Santa Cruze	SC-22799	Rabbit	1/100	WB
Anti-HRD1	Abgent/Abcam	AP2184a Ab38456	Rabbit	1/200 1/500	WB

Anti-ATP1B1	Sigma	A278	Mouse	1/5000	WB
Anti-ATP1A1	Cell signaling	05-369	Mouse	1/500	WB
anti-ATP6V1A	Abcam	Ab103445	Rabbit	WB:1/200 IF:1/100	WB, IF,IP
anti-ATP6V1C1	Abcam	ab87163	Rabbit	1/2000	WB
anti-ATP6V0D2	Abcam	ab87059	Rabbit	1/500	WB
anti-cleaved caspase-3	Cell Signalling	ASP175	Rabbit	1/100	WB
anti-beta actin	Sigma	A544	mouse	1/14 000	WB
c-Myc	Sigma	M4439	Mouse	1/2000	WB, IP
FLAG	Sigma	A1080	mouse	1/2000	WB,IP
Anti-WFS1	The Binding Site, custom made	N-terminal	Sheep	1/50	IF
Anti-VAMP	Abcam	Ab3346	Rabbit	1/100	IF
Anti-PDI	Stressgene	SPA-891	Mouse	1/50	IF
Anti-ERAB-5F3	Abcam	Ab10260	Mouse	1/100	IF

(WB= Western blotting, IF=Immunofluorescence, IP=immunoprecipitation, HCC= High Content Cytometry)

Table 2.3 List of secondary antibodies used for W.B, IF, IP and HCC

Secondary Antibodies	Company	Cat-nr	Source	Concentrations	Application
Anti-Mouse	Dako	P0161	Rabbit	1/20 000	W.B
Anti-Rabbit	Dako	P0448	Goat	1/20 000	W.B
Anti-sheep	Invitrogen	Alexa-488-green	Donkey	1/500	IF
Anti-mouse	Invitrogen	Alexa-633-Red	Goat	1/1000	IF
Ani-Rabbit	Invitrogen	Alexa-488-Green	Goat	1/1000	IF
Ms IgG FITC	Abcam	AB6785-1	Goat	1/1000	HCC
RB IgG FITC	Abcam	AB6717-1	Goat	1/1000	HCC

(WB= Western blotting, IF=Immunofluorescence, HCC= High Content Cytometry)

2.3.7 Stripping and reprobing

For re-probing the membrane antibody complex was stripped off either by incubation in sodium hydroxide (NaOH) or boiling in water and reprobed with a different primary antibody. For the NaOH procedure: the membrane was first washed in distilled water for 5 minutes on the orbital shaker. Afterwards, the membrane was transferred into a tray containing 0.2M sodium hydroxide and placed on the orbital shaker for 2 x 15 minutes. Then the membrane was washed again in distilled water for 5 minutes. For boiling, the membrane was removed from the saran and put in a glass beaker with boiling water on the hot plate. Boiling of the membrane was timed accurately to make sure the membrane was out of the boiling water within less than 5 minutes. The membrane was then ready for blocking and subsequent reprobing.

2.3.8 Quantification of the western blots

The signals on the film, (black bands indicating the position of protein of interest) were labelled and their size was established by comparison with the protein weight marker. The film was scanned and further used for quantitative analysis of the band intensities. The intensity of the bands was proportional to the amount of proteins, as long as the film was not overexposed. The quantification was performed using the computer program Gene Tools. The data was analysed using Excel.

2.4 RNA extraction and quantification

2.4.1 RNA extraction by TRIzol reagent

A confluent 75 cm^2 flask was trypsinised and centrifuged at 250 RCF for 3 minutes. The pellet was re-suspended in 10 mL media and cell count was performed. $2x10^6$ cells were plated in each well of the 6 well plate in total volume of 2 mL media. The next day, the cells were fully confluent. The media was aspirated and the cells were washed twice with PBS. The last PBS was removed in the fume hood and 1mLof TRIzol was added to each well to lyse the cells. These were then incubated for 5 minutes at room temperature to allow complete dissociation of nucleoprotein complexes. The lysate was transferred into a sterile eppendorf tube using a scraper and a pipette and 200µL chloroform was added per 1mL TRIzol used. The tubes were shaken vigorously by hand for 15 seconds and incubated for 3-4 minutes at room temperature. Afterwards, the samples were centrifuged at 12000xg for 20 min at 4°C. Following centrifugation the mixture was separated into three phases: aqueous upper phase containing RNA, a white interphase and a lower red phenol-chloroform phase.

The upper phase was carefully transferred to a clean eppendorf with a 200 µL pipette and the RNA was precipitated by adding 500µL isopropyl alcohol and mixing. The samples were incubated for 30 minutes at room temperature or incubated overnight at -20 °C. Afterwards the samples were centrifuged at 12000xg for 20 minutes at 4 °C and the supernatant was removed. The pellet was washed once by adding 1mL of 75% ethanol, mixed by vortexing and centrifuged at 8000xg for 20 minutes at 4°C. The RNA pellet was briefly air dried for 30 minutes (but not

dried completely as this would decrease the solubility). The pellet was dissolved in 30-50 µL RNase free water and the solution was passed a few times through a pipette, incubated for 10 minutes at room temperature and the RNA frozen in a -80 ^{o}C freezer.

2.4.2 RNA extraction and purification by Qiagen RNeasy spin columns

The RNA was extracted from cells grown in 10cm^2 dishes or a 75cm^2 flask using the Qiagen RNeasy extraction and purification kit (Qiagen). Cell lysates were produced when the cells in a 75cm^2 flask reached an approximate confluency of 90%. The cells were trypsinised; 8 mL of media was added into floating cells and centrifuged at 250 RCF for 3 minutes at 20 ^{o}C. The pellet was washed twice with cold PBS. 600 µL of RNA lysis buffer was added to the pellet, mixed thoroughly and stored at -80 ^{o}C for RNA experiments. This RNA was purified according to the manufacturer's recommendation: briefly, samples were first homogenised by passing the lysate 5 to 10 times through a syringe and 20-guage needle. Afterwards, the lysate was also homogenised by QIA-shredder (Qiagen) homogeniser by pipetting the lysate directly into a QIA-shredder spin column. This column was placed in a 2mL collection tube and centrifuged for 2 minutes at full speed (13000 rpm) in a micro-centrifuge. For RNA extraction 600µL of 70 % ethanol was added to the homogenised lysate and mixed well by pipetting. This mixture was passed through an RNeasy spin column by centrifuging it for 1 minute at 10 000 rpm and the flow through was discarded. Afterwards 700µL of RW1 buffer was added to the columns and centrifuged for 1 minute at 10 000 rpm and the flow through was discarded. 500µL of RPE buffer was added followed by a centrifugation at 10 000 rpm for 1 minute and the flow through was again discarded. This step was repeated with a centrifugation step for 2 minutes. The column was

placed in a 1.5mL centrifuge tube and 50µL of RNase-free water was added to the column and centrifuged at 10 000 rpm for 1 minute to elute the RNA. This step was also repeated by using the eluate instead of RNase-free water to concentrate the sample. The resulting RNA was stored at -80 ^{o}C.

2.4.3 Quantification of RNA

To ensure equal loading of RNA in the experiments, it was important to measure the concentration of the samples. The quantifications were carried out using Nanodrop. The samples were mixed thoroughly and each sample was measured twice and the mean measurement was taken. RNase free water was used as blank and 2µL of the samples was loaded. The concentration was automatically displayed in ng/µL. For measuring expression at RNA level, the RNA samples were DNase treated and converted to cDNA. The obtained cDNA was used mainly for Quantitative PCR (Real-Time PCR) or Reverse Transcription (RT) PCR.

2.4.4 DNase digestion

The RNA extracts were treated with DNase to eliminate DNA contamination of the RNA preparation. For these experiments either the RNase-Free DNase set (Qiagen) or the DNA- free kit (Ambion) was used. When using the kit from Qiagen; DNase I stock solution was prepared by dissolving the lyophilized DNase 1(1500 Kuntz units) in 550 µL of RNase-free water. The RNA (100µg or less) extract was mixed with 2.5µL DNase I stock solution and 10µL of RDD buffer (Qiagen), and the volume was adjusted to 100µL with RNase free water. This mixture was

incubated on the bench for 10 minute to allow DNase digestion. Afterwards, the RNA was cleaned as described above to remove the DNase (RNeasy mini kit, Qiagen).

When using the Ambion kit, 2µg RNA was added to a mixture of 1µL of DNase1 and 10% of 10x DNase buffer. The content was mixed well and incubated for 20 minutes at 37 ºC. After that, 5 µL of inactivating reagent was added, mixed and left at room temperature for 2 minutes. At this stage, if the volume was between 5 and 10µL, more nuclease free water was added to make the collecting of samples from the above inactivating reagent easier. Afterwards this mixture was centrifuged at maximum speed for 20 minutes and the supernatant was harvested.

2.4.5 cDNA synthesis

The cDNA synthesis was performed with either High-Capacity cDNA Reverse Transcription Kit from Applied Biosystems or the Reverse Transcription System (Promega). When the high capacity cDNA reverse transcription kit from Applied Biosystems was used, a volume of DNase treated RNA corresponding to either 350ng or 400ng of RNA was added per reaction and the volume was adjusted to 10µL with RNase free water.

A master mix was prepared using the protocol provided with this kit. The master mix contained (per reaction); 2 µL of 10x RT Buffer, 0.8 µL of 100mM dNTP, 2 µL of 10x random primers, 1µL of MultiScribe Reverse Transcriptase, 1µL of RNase inhibitor and 3.2 µL of nuclease-free water. The RT negative mix was prepared without the RT enzyme MultiScribe, and the volume was compensated by nuclease free water. 10µL of the RNA (400ng) was added into 10µL of this master mix in a 96 well PCR plate. The reaction was run for 2 hours in the PCR machine using

the following program: 25ºC for 10 min, 37 ºC for 2 hours and 85 ºC for 5 min. Afterwards, the sample was diluted 2x, by adding 20 µL of RNase free water making the final concentration 10ng/µL and stored at -20 ºC.

When the Promega kit was used the reaction was set up with 2µL of RNA at 1µg/µL RNA. A master mix was prepared with 4 µL of 25mM $MgCl_2$, 2 µL of RT-10x Buffer, 2µL of 10mM dNTP, 1µL of random primers, 1µL AMV-RTase (Avian Myeloblastosis Virus Reverse Transcriptase) enzyme and 0.5 µL of RRRI (Recombinant RNase in Ribonuclease Inhibitor). The RNA was denatured at 70 ºC for 10 minutes and spun. Then the master mix was added and the volume was adjusted to 20 µL with nuclease free water. This reaction was first incubated at room temperature for 10 minutes, and then heated at 42 ^{o}C for 30 minutes. After that the sample was denatured at 95 ^{o}C for a 5 minutes followed by a 5 minute incubation on ice. The obtained cDNA was then diluted to 100µL with nuclease free water and tested by running 10µL on agarose gel for the presence of cDNA. The cDNA was stored at -20^{o}C for further experiments.

2.4.6 RT-PCR (Reverse Transcription Polymerase Chain Reaction)

The cDNA template was amplified by PCR to measure the gene expression on RNA level. These reactions were performed using PCR kit from Invitrogen in a final volume of 100 µL. The reaction was set up with 20 µL of cDNA (1µg/ µL), 10 µL of 10x PCR buffer, 4 µL of 50mM $MgCl_2$, 1.8 µL of 10mM dNTP's, 0.6µL of *Taq* DNA polymerase and 3 µL of each forward and reverse primers (20pmoles/ µL). The final volume was adjusted with RNase free water. The PCR program is shown in Table 2.4. The primers were designed by the program Primer3 and obtained

from Alta Biosciences. The annealing temperature was chosen depending on the melting temperature of the primers. The primer pairs used in these reactions are shown in Table 2.5. The reaction was first optimised to avoid primer dimers and it was decided to take 61 ^{o}C as the annealing temperature for RT4, 65 ^{o}C for RT3 and 60^{o}C for β-actin primers. The PCR reactions were performed on a GeneAmp 9700 thermocycler (Perkin Elmer).

Table 2.4: RT-PCR programme

Temperature	Time		purpose
95 ^{o}C	5 minutes		Melting
95 ^{o}C	30 seconds		Denaturing
T_A ^{o}C	30 seconds	30 Cycles	Annealing
72 ^{o}C	45 seconds		Elongation
72 ^{o}C	10 minutes		Extension

Table 2.5: Primers used for RT-PCR

Gene	Forward primer	Reverse primer	Product length	Annealing-temperature
WFS1-RT3	5'CTC-AAC-AGC-TGC-ACC-GCT-GT-3'	5'CCA-TCG-TGC-TCG-TTG-ACC-TG-3'	275 bp	65˚C
WFS1-RT4	5'GGA-AGC-TCA-ACC-CCA-AGA-AG- 3'	5' CCA-GCT-CGT-CAT-CAT-CTT-CG- 3'	270 bp	61 ˚C
Beta-actin	5'GAG-CGG-GAA-ATC-GTG-CGT-GAC-ATT-3'	5' GAT-GGA-GTT-GAA-GGT-AGT-TTC-GTG-3'	234 bp	60 ˚C

Table 2.6: Sequencing PCR programme

Temperature	Time		purpose
94 ^{o}C	25 seconds		Denaturing
50 ^{o}C	25 seconds	28 Cycles	Annealing
60 ^{o}C	4 minutes		Elongation

2.4.7 Agarose Gel Electrophoresis

The PCR products (which are a mixture of DNA fragments) were separated according to the size by agarose gel electrophoresis. The negatively charged DNA migrated through the gel and its position was visualised under UV light due to the presence of ethidium bromide. Gels of different percentages were needed depending on the size of the DNA fragments. In these experiments either 1.5% or 2% gels were used. For 2% agarose gel: 4g agarose was dissolved in 200 mL 1x TBE buffer (10x; 0.89M Tris Borate pH 8.3 and 20mM Na_2EDTA, Geneflow) The gel mixture was melted in a bottle in a microwave and left to cool to about 50 to 40 ^{o}C. Ethidium bromide was added to a final concentration of 0.5µg/mL: this dye interacts with DNA and makes it fluoresce and therefore visible under UV light.

The gel was poured into a gel casting tray, combs were placed and it was left to set for approximately 10 minutes. When the gel was set, it was placed in an electrophoresis tank, the combs were removed and the samples containing DNA loading buffer (10x loading buffer: 50% glycerol, 0.05% bromophenol blue) were loaded. To determine the size of the fragments, 5µL of a 100bp DNA ladder (Invitrogen) was also loaded to the gel. The products were resolved by running the electrophoresis at 180 volts for approximately 20 minutes, or until the products had migrated about 10 cm from the well. An UV trans-illuminator was used to visualise the products and a picture of the gels was taken using the programme Gene Snap. The pictures were used to quantify the intensity of the bands using the programme Gene Tools.

2.4.8 ExoSAP (Exonuclease I and Shrimp Alkaline Phosphatase) reaction

The DNA/cDNA was further purified by Exo-SAP (New England Biolabs) from PCR mixture. This reaction was carried out to clean up the PCR product for downstream applications such as DNA sequencing. The Exo-SAP reaction removes any contaminants such as unwanted dNTPs and primers from the PCR mixture. The enzyme Exonuclease I removes residual single-stranded primers and any extraneous single-stranded DNA produced in the PCR. Shrimp Alkaline Phosphatase dephosphorylates the remaining dNTPs in the PCR mixture. The reaction was set up in 10µL of PCR product with 3µL of a master mix containing 1µL antaractic phosphatase, 1µL antaractic phosphatase buffer, 0.25µL exo-nuclease and 0.75µL nuclease free water. This reaction was incubated at 37^{o}C for 30 minutes and at 85^{o}C for another 20 minutes. The samples were ready for sequencing.

2.4.9 DNA Sequencing

DNA sequencing was carried out to analyse the sequence of the DNA or cDNA obtained in the PCR reaction, to compare to the sequence of interest in the database and to confirm its identity. The sequencing reaction was set up in 20µL reaction volume, consisting of 5µL of the PCR product after Exo-Sap treatment with 2µL sequencing buffer, 1µL Big Dye (Invitrogen), 1 µL of primer (10pmol/ µL, Table 2.5) and 1µL distilled water. The sequencing PCR cycle is shown in Table 2.6.

2.4.10 Ethanol precipitation

Ethanol precipitation was carried out to purify the DNA from the sequencing reaction. 3.5µL of 0.5M EDTA (Ethylene Diamine Tetraacetic Acid) and 100 µL of 100% ethanol was added to the 10µL of PCR reaction and allowed to stand at room temperature in the dark for 20 minutes. The plate was centrifuged at 4000 rpm at 4^{o}C for 30 minutes to pellet DNA. Then ethanol was removed by inversion of the plate onto the tissue paper and centrifugation for 1 minute at 400 rpm. After that, 200 µL of 70% ethanol was added and centrifuged for 30 minutes at 4^{o}C and the supernatant was removed by inversion. This last step was repeated twice, followed by drying the samples at 60^{o}C for 10 minutes.

2.4.11 Sample preparation for Sequencing Analysis

The DNA pellet was resuspended in 10µL of Hi-Di formamide loading buffer (Applied Biosystems). The DNA was denatured for five minutes and the plate was immediately transferred onto ice to stop re-annealing of the products. The plate was then screened on the Sequence Analyser version 5.2. The sequencing results were then analysed using Bio-Edit Sequencing Alignment Editor.

2.4.12 Real time PCR

Real time PCR was used to get quantitative differences in gene expression. The experiments were carried out using either the Taqman or the SYBR green methods. For the Taqman method, the Taqman universal master-mixII and Taqman gene expression assays were purchased from Applied Biosystems. The probes were labelled with 6-carboxy fluorescein (FAM) dye at the 5'

end and quenched by minor groove binder (MGB) at the 3′ end of the probe. MGBs increase the melting temperature (Tm) without increasing probe length and allow for the design of shorter probes. Beta actin was used as endogenous control. The Taqman expression assays used in this study are presented in Table 2.7. The real time PCR reaction was set up by adding 10µL of the master mix, 1 µL gene assay, 4µL RNase free water and 5µL of cDNA containing 10 ng cDNA, making a total reaction volume of 20 µL. The real-time PCR machine '7500' from Applied Biosystems or the Icycler from BIO-RAD were used for these reactions and the program is shown in Table 2.8.The delta delta CT methods was used to calculate the expression levels.

2.4.13 Description of the calculation method for QPCR

To understand the quantitative PCR data and to be able to analyse it, it is very important to know the basics of this technique. In QPCR, the initial amount or the concentration of cDNA is doubled with each cycle. Changes to the initial concentration will shift the QPCR curve to the left (less cycle needed to reach the threshold), or right (more cycles needed). Increase of the initial amount of cDNA by a factor 10 will shift the curve around 3.33 cycles to the left and a decrease by factor 10 with shift the curve around 3.33 cycles the right. During the exponential growth of product in QPCR, the number of cycles it takes to reach a threshold value is counted; this cycle number is called Ct. In QPCR reaction a Ct difference of 3.33 equals to a copy rate 2. The copy rate refers to the multiplication factor from one cycle to the next. A factor of 2 would mean that all the input DNA is copied to a perfect or 100% efficiency. When using the delta-delta-Ct method the CT values are normalised assuming the efficiency was 100%, taking the copy rate 2. The Ct values for a target gene are normalised against a housekeeping gene such as beta actin, which is

expressed at constant levels. The equation $2^{\Delta\Delta CT}$ is used in delta delta CT methods; the ΔCT is calculated by subtracting the Ct values of the house keeping gene (reference) from the Ct values of the gene under investigation (ΔCt= Ct target gene-Ct reference gene). This is done for both: experiment and control e.g. for drug treated samples and untreated (ΔCt exp and ΔCt ctrl). In the next step ΔΔCt is calculated by subtracting the ΔCT exp from the ΔCTctrl (ΔΔCt=ΔCt ctrl-ΔCt exp). This value is then used in the equation $2^{\Delta\Delta CT}$ to calculate the fold change of gene expression (how much more or less the target gene is expressed in the experiment in comparison to the control). Up regulation of the gene was shown by $2^{\Delta\Delta ct}>1$ and down regulation; when $2^{\Delta\Delta ct}<1$(Livak and Schmittgen, 2001).

Table 2.7: Taqman assays for QPCR from ABI

Assay name	Source	Cat-number
WFS1	Human	Hs00903605_m1
BiP	Human	Hs99999174_m1
CHOP	Human	Hs99999172_m1
spliced XBP1	Human	Hs03929085_g1
BCL-2	Human	Hs00608023-m1
BAX	Human	Hs00180269-m1
GRP94	Human	Hs00427665_g1
Beta-actin	Human	4352935E
WFS1	Mouse	Mm00495979_m1
BiP	Mouse	Mm00517691_m1
CHOP	Mouse	Mm00492097_m1
Beta-actin	Mouse	Mm00607939_s1

Table 2.8: Programme used for QPCR reactions for Taqman assays

Thermal Cycler Profile			
Stage	Repetitions	Temperature	Time
1	1	50.0 °C	02:00
2	1	95.0 °C	10:00
3	40	95.0 °C	00:15
		60.0 °C	01:00
9600 Mode Emulation			
Data Collection : Stage 3 Step 1			
PCR Volume: 20 µL			

2.4.14 The SYBR Green

The primers used in the QPCR reactions using the SYBR green method were designed using the programme Primer3. The primers were purified by HPLC (High Performance Liquid Chromatography) and purchased from Thermo Scientific, presented in Table 2.9. The stock concentration of these primers was 100pmol/µL and was 5x – 20x diluted for different experiments and optimised for the real time PCR reaction. Accordingly, the real time PCR reaction was set up in a total volume of 25 µL containing 20µL of a mastermix, which was prepared by adding 1.5µL of F/R primers (ranging from 20pmol/µL to 5pmol/µL), 12.5µL of Power SYBR Green (Applied Biosciences) and 4.5 µL of RNase free water. The cDNA was 5 times diluted, 5µL (10ng) of this dilution was added to the master mix in 96 well PCR optical plates (Bio-Rad). The PCR plate was then sealed and spun for 2 minutes at 4000 rpm. The plate was then placed in the real time PCR machine to run the reaction. During analysis a melting curve was checked to ensure that there was only one product of the reaction. The protocol for the QPCR reactions is presented in Table 2.10. The Bio-Rad IQ5 program was used for this reaction using the IQ5 ICycler machine from Bio-Rad.

Table 2.9 Primers used for QPCR reactions using SYBR Green

Gene	Forward primer	Reverse primer
HW1-RT3	5CTCAACAGCTGCACCGCTGT3	5CCATCGTGCTCGTTGACCTG3
HW1-RT4	5GGAAGCTCAACCCCAAGAAG3	5CCAGCTCGTCATCATCTTCG3
HB-actin-3	5GGACTTCGAGCAAGAGATGG3	5AGCACTGTGTTGGCGTACAG3
HB-actin-AN	5GGGGACGAGGCCCAGA3	5CGATTTCCCGCTCGGC3
CHOP	5TGGAAGCCTGGTATGAGGAC3	5TGTGACCTCTGCTGGTTCTG3
BIP	5TGAAACTGTGGGAGGTGTCA3	5TTTGTCAGGGGTCTTTCACC3
Hamster-BIP	5GGCCGCGTGGAGATCATA3	5CACATACGACGGCGTGAT3

Table 2.10: Protocol for QPCR cycles for SYBR green assays

Protocol:

Cycle 1: (1X)		
Step 1:	50.0 °C	for 02:00.
Cycle 2: (1X)		
Step 1:	95.0 °C	for 10:00.
Cycle 3: (40X)		
Step 1:	95.0 °C	for 00:15.
Step 2:	60.0 °C	for 01:00.
Data collection and real-time analysis enabled.		
Cycle 4: (81X)		
Step 1:	55.0 °C-95.0 °C	for 00:30.
Increase set point temperature after cycle 2 by 0.5 °C		
Melt curve data collection and analysis enabled.		

2.5 High Content Cytometry

5,000 cells were seeded per well of a 96 well plate and incubated overnight. The next day, they were fixed with ice cold 85% ethanol and stained with 10µL propidium iodide staining solution per well. The cells were incubated with the staining solution for 25 minutes at 37 °C, and then DNA content based on total fluorescence was measured with a High Content Cytometer (ex3 Acumen). This allows rapid analysis of whole 96 well plates with resolution equivalent to a 20x microscope objective.

2.5.1 Drug treatment

TUDCA, Valproate and Cycloheximide were used in these experiments. TUDCA and Cycloheximide were dissolved and diluted in DMSO and Valproate was dissolved in water. When the drugs were dissolved in DMSO it was important to keep the final concentration of DMSO in the cells at 1%. A dose toxicity curve experiment was carried out for each drug with a range of concentrations to find out whether the drug is toxic for cells at any concentration.

The principle of preparation of TUDCA dilutions was as follows:

First of all the final concentration range in cells for the toxicity experiment was decided: For TUDCA the following concentrations were chosen (100µM to 1000µM). 1M stock of TUDCA was prepared in DMSO; this was further diluted in relevant volumes of DMSO to prepare 1000x stocks (red stocks) for each final concentration of TUDCA; 100mM to 1000mM. Accordingly, each of these1000x stocks (called 'red stocks') was diluted 10x to prepare 100x stocks (called 'black stocks'). Preparation of "black stocks": in the TC hood, 40 µL of DMSO was aliquoted in 15mL falcons followed by adding 4 µL of the drug dilution (from 'red stock'); mixed and 4 µL

was removed. One falcon was prepared with no drugs as a control containing just DMSO. These black stocks were further diluted 50x in medium to obtain 2x drug solutions (called 'green stocks'); 1960µL of medium was added to the 40µL of each black stock. Finally, 100µL of this 2x drug solution was gently dispensed into the cultured 96 well plate containing cells in 100µL media using a multi-channel pipette and the plate was incubated for 24 hours. The final volume of media in the cells was 200 µL and the final concentration of DMSO in cells was 1%. Cycloheximide was diluted in a similar fashion: the stock solution of 100mg/mL was prepared in DMSO. The ranges of concentrations used for the toxicity experiment (10 to 90µg/mL) were tested in a time dependent manner. 5 identical plates were prepared; the plates were fixed during a 6 hours time-course with 2 hours intervals.

The principle of preparation of sodium valproate (VPA) dilutions was as follows:

The desired final concentrations of VPA in the cells were 50, 100, 200, 400 and 600µg/mL. First of all 100mg/mL stock of valproate was prepared in water. This stock was then 10x diluted in media to get a stock solution of 10µg/µL. The final volume of media in the cells was 200 µL, and it was convenient to pipette the drugs in 100 µL volumes into the cells in the 96 well plates. Therefore a 2x working solution was prepared for each final concentration of VPA. For example; for a final concentration of 50µg/mL in 200 µL media: the working solution was prepared by adding 20µL of the drug stock solution (10µg/µL) to 1980 µL of media. Thus this stock contained 20x10 µg=200 µg VPA in 2mL media, which equalled 100µg/mL. 100µL of this solution was then dispensed gently into the cells containing 100 µL of media, making the final VPA concentration 50µg/mL in 200µL volume, and the plate was incubated for 24 hour

2.5.2 Fixation and Staining

The cells were fixed by adding 100 µL Glyo-Fixx (Thermo) per well and incubated for at least two hours at room temperature. This was then followed by removing the Glyo-Fixx, adding 100µL of cold 85% ethanol and incubating the plate at 4^{o}C for 30 minutes (the plate can be incubated up to two days when 200 µL of 85% ethanol is added). After fixation, the cells were first stained with antibodies and then with propidium iodide. Firstly, the ethanol was removed (as much as possible) and the plate was incubated with blocking solution (5% BSA in PBST (0.1% Triton-X-100, in 10x PBS)) for 30 minutes at room temperature. After aspirating the blocking solution 50 µL/well of primary AB solution was added, PBST was used as a negative control and the plate was incubated overnight at 4^{o}C (the antibodies were diluted in PBST, Table 2.2). The next day, the cells were washed twice with cold PBST by adding 200µL/well. After aspirating the PBST 50µL/well of secondary antibody (anti-mouse or anti rabbit-FITC, Table 2.3) solution was added, protecting the solutions and plate from light. The plate was incubated overnight at 4^{o}C or two hours at room temperature. Subsequently the cells were washed twice with cold PBST. The PBST was gently aspirated and 100µL/well of propidium iodide staining solution (0.1% Triton-X-100, 100µg/mL RNase A (Sigma), 10µg/mL propidium iodide (Invitrogen)) was added. The plate was then incubated at 37 ^{o}C for 20 minutes, protected from light. Afterwards, any bubbles were removed using a needle and the plates were ready for screening by the High Content Cytometry System (Acumen). The Acumen machine was operated by Dr Nagy's lab staff.

2.6 Immunofluorescence microscopy

2.6.1 Fixation of cells

Wild type SK-N-AS human neuroblastoma cell lines were grown in 6-well dishes containing 22mm x 22mm cover slips. The cover slips were first washed with 80% ethanol, air dried and placed in 6 well or 24 well plates. The plate with the cover slips was sterilised under UV light in the tissue culture hood for 30 minutes. $3x10^4$ cells were plated in each well of a 6 well plate containing 2-3 cover slips. The cells were grown over night to form a monolayer on the cover slips. The cells were washed three times with PBS for 10 minutes and fixed in 4% paraformaldehyde for 10 minutes. Afterwards the cells were washed three times and permeabilised by adding 0.2% Triton-X-100 in PBS to the cells and incubating for up to 4 minutes. This was followed by further three washes of 10 minutes with PBS to remove the Triton-X.

2.6.2 Immuno-probing

The blocking of non-specific proteins was performed by adding 1% BSA in PBS into the cells and incubating for 1 hour at room temperature on a rocking platform. The blocking solution was removed and the cells were washed again three times with PBS followed by overnight incubation of the primary antibody (Table 2.2) at 4°C. The antibodies were diluted in PBS and 200 to 300 µL of the antibody solution was pipetted on the cover slips in a 24 well plate and incubated at 4°C. The next day, the cover slips were washed for 3x10 min in PBS in the 24 well plate. The secondary antibody (Table 2.3) was added in the dark and incubated for one hour in the dark. This was followed by another three washes of 10 minutes with PBS.

2.6.3 Mounting and Visualisation

The slides were mounted with Vectashield (Vector Laboratories, USA) mounting medium, containing 4', 6-Diamidino-2Phenylindole (DAPI). The cover slip was carefully picked with a thin forceps and positioned on microscopic slides (VWR) containing a drop of mounting medium. The slides were left to dry in the dark, and the coverslips were sealed with clear nail vanish and left overnight at 4°C before analysis. When the slides were dry, the cells were visualised and photographed with AXI-overt 100M confocal image collection apparatus (Zeiss), using 100x oil lens or 65x water lens. The images from the confocal microscope were taken by Janine Fenton.

2.6.4 Paraformaldehyde preparation

4% Paraformaldehyde was prepared with precautions as it is toxic. Eye protections, lab-coat and gloves were worn; 4g paraformaldehyde was weighed in a measuring scoop inside the hood and added to 100mL of warm PBS to dissolve. This suspension was placed in a water bath at 65 °C to dissolve completely; after dissolving this solution was aliquoted and stored in a -20 °C freezer.

2.7 Electron microscopy using pre-embedding immunostaining

Wild type SK-N-AS human neuroblastoma cells were grown on plastic coverslips for 24 hours. This experiment was performed by and in collaboration with Prof Attila Sik: *To reveal the subcellular distribution of Wolframin, cell cultures were cryoprotected in 30% sucrose (0.1M PB), freeze-thawed over liquid nitrogen, and incubated in polyclonal rabbit anti WFS1 (1:100) in Tris-buffer saline (0.05M, TBS). After intensive washing with TBS, cell cultures were incubated*

with goat anti-rabbit IgG coupled to 1nm gold particles (Amersham, UK) diluted 1:50 overnight at 4°C. Then, cultures were washed and fixed for 10 min in 4% v/v formaldehyde solution (made up in PBS), washed three times in 10 min in Enhancement Conditioning Solution (Aurion Immunoresearch, Wageningen, The Netherlands) and the gold particles were intensified with R-Gent silver intensification solution (Aurion). At the end of the immunogold reactions, cultures were treated with 1% OsO4 for 15 min, dehydrated in graded ethanol (70% v/v ethanol containing 1% w/v uranyl acetate) and in propyleneoxide and embedded in Durcupan (Fluka Sigma-Aldrich). Regions of interest were re-embedded, sectioned serially in 50nm sections, collected on formvar-coated single slit copper grids, and counterstained with lead citrate. Electron micrographs were taken using a Tecnai Krios electron microscope equipped with digital camera.

2.8 Cloning

The PCR product was gel extracted, purified and cloned into a pGEM and/or pCMV vectors followed by sequencing. This process consists of a number of experiments: gel extraction-purification, ligation, transformation, DNA isolation using mini prep or maxi prep, restriction enzyme digestion and sequencing.

2.8.1 Gel extraction and purification

The QIAquick Gel Extraction Kit Protocol was used for this experiment. DNA fragments were separated on 2 to 1.5 % agarose gel and DNA bands were cut off using a clean sharp scalpel in UV light. The gel slices were transferred into an eppendorf and then weighed. Three volumes of

QG buffer was added into 1 volume of the gel (it was assumed that 100mg of the gel had the volume of 100µL) and incubated at 50 ˚C for 10 minutes to completely dissolve the agarose gel. One gel volume of iso-propanol was added to the sample and mixed by pipetting. A QIAquick spin column was placed in a 2mL collection tube, the sample was applied to the QIAquick column and centrifuged for 1 min at 13000rpm to bind the DNA. The flow through was discarded and 0.5 mL of QG buffer was added and centrifuged for 1 minute at 17000rpm to remove all traces of agarose. To wash the DNA 0.75mL of PE buffer was added to the QIAquick column and centrifuged for 1 min at 17000rpm; the flow through was discarded and another round of centrifugation was carried out at 17000rpm for 1 min. Afterwards, the QIAquick column was placed in a 1.5 mL micro centrifuge tube. To elute the DNA, 50µL water was added to the centre of the QIAquick membrane. The column was left to stand for 1 minute and then centrifuged for 1 minute at the same speed.

2.8.2 Ligation reaction

The ligation reaction was set up according the protocol provided with the T4 DNA ligase kit (Promega). Positive and negative control reactions were included: the positive reaction contained control insert DNA and negative reaction contained no DNA. The standard reaction was set up by adding 5µL 2x ligation buffer, 1µL pGEM vector (50ng), volume of insert dependent on the concentration of PCR product, 1 µL LT4 DNA ligase and the reaction volume was adjusted with nuclease free water to 10µL. The reaction was mixed by pipetting and incubated over night at 4ºC.

2.8.3 Transformation

For transformation α-Select Silver Efficiency Competent Cells were used from Bioline. These are high-efficiency (>1x10^8cfu/µg pUC19) cells containing a lacZ marker which provides α-complementation of the ß-galactosidase gene for blue/white colour colony screening. The cells were removed from -70ºC, thawed on ice, and mixed gently by flicking the tube. 100 µL of cells were aliquoted into a chilled 1.5mL tube. 10µL of DNA solution was added into the cell suspension and gently mixed by swirling. 2µL of control DNA were added to a control tube. The reaction was incubated for 30 minutes on ice followed by placing the cells in a 42 ºC water bath for 45 seconds without shaking. The tubes were replaced on ice for 2 minutes and 900 µL of SOC medium (Invitrogen) were added to the transformation mixture. Then the tubes were shaken at 200 rpm for 60 minutes at 37ºC. Afterwards 50-200µL of transformation mixture was spread on previously prepared LB agar (Sigma) plates containing 100µg/mL ampicillin and supplemented with 80µg/mL X-GAL (Sigma) and 0.5mM IPTG (Sigma) followed by incubating the plates overnight at 37 ºC.

2.8.4 Blue/White colony selection

After growing the bacteria for 16-24 hours in the 37 ºC incubator, the plates were checked for blue and white colonies. The white colonies, formed from successful ligation reactions were selected and grown in LB-broth medium (Sigma). The LB-broth medium was prepared by dissolving 8g LB-broth in 400mL water and autoclaving. After cooling to 50ºC, this medium was supplemented with 100µg/mL ampicillin. 5mL of LB-broth medium was poured into a 50mL

falcon tube and one white bacterial colony was added with a tip. The tubes were securely tightened and placed in the shaker for overnight incubation (>16 hours) at 37 ºC vigorously shaking at 200 rpm. The next day, the bacterial cells were centrifuged at 5400 x g for 10 minutes at 4 ºC, and all traces of supernatant were removed. The pellet was harvested for DNA isolation.

2.8.5 Small scale plasmid DNA extractions

The bacterial cell pellets from 20mL culture was resuspended in 250 µL buffer P1 and transferred to a micro centrifuge tube. In addition 250 µL of P2 buffer was added to the tube and mixed thoroughly by inverting the tube 4-6 times. 350 µL of N3 buffer was added into the tube and mixed thoroughly by inverting the tube 4-6 times. The tube was centrifuged for 10 minutes at 13,000 rpm and the supernatant was applied to a QIAprep spin column by pipetting. After centrifugation for 30-60 seconds the flow-through was discarded. The column was washed by adding 0.5mL PB buffer and centrifuged for 30-60 seconds and the flow through was again discarded. The spin column was washed again by adding 0.75mL PE buffer and centrifuged for 30–60 seconds. The flow through was discarded and the spin column was centrifuged for 1 minute-to remove residual wash buffer. Finally the QIAprep column was placed in a clean tube, to elute DNA. 50µL EB buffer was added to the centre of each spin column. The column was left for 1 minute and centrifuged for 1 minute at 13,000 rpm. The sample was stored at -20 ^{O}C before further use.

2.8.6 Large scale Plasmid DNA extractions

The pCMV plasmid was extracted and purified using Endofree Plasmid Maxi kit (Qiagen). Briefly, 200mL of culture was centrifuged at 6000rpm for 10mins. The pellet was resuspended in 10mL of buffer P1.10mL of lysis buffer (P2) was added to the cell solution and mixed thoroughly; this was then left for 5 minutes incubation at room temperature. 10mL of neutralisation buffer (P3) was added to the cell lysate and was decanted into the QIAfilter cartridge and incubated at room temperature for 10 minutes. During this time the Qiagen-tips were equilibrated by applying 10mL of equilibration buffer (QBT) and allowing the column to empty by gravity flow. The nozzle cap from the QIA filter cartridge was removed and the plunger was inserted into the cartridge, filtering the cell lysate into a 50mL tube. The cell lysate was applied to the equilibrated Qiagen-tip and was left to enter by gravity flow. Thirty mL of wash buffer (QC) was applied twice to the Qiagen-tip. The DNA was eluted in 15mL of elution buffer. 10mL of isopropanol was added to precipitate the DNA; this was centrifuged at 6000xg for 15 minutes at 4^{o}C. The DNA pellet was washed using 70% ethanol and centrifuging for 10 minutes at 11,000rpm. The pellet was left to dry and then resuspended in 500µL dH_2O.

Chapter Three: WFS1 depletion results in enhanced ER stress, apoptosis and cell cycle disturbances in neuronal cell models

3.1 Introduction

Wolfram syndrome (WS) is a rare neurodegenerative disorder involving the central nervous system (CNS), the peripheral nerves and the neuro-endocrine tissues (Wolfram and Wagener, 1938, Barrett et al., 1995). The prognosis of this syndrome is poor due to premature death of the patients with severe neurological disabilities such as bulbar dysfunction and organic brain syndrome (Barrett et al., 1995). Neurological studies have shown diffuse neurodegenerative changes in the brain (Genis et al., 1997, Shannon et al., 1999). The acronym DIDMOAD (Diabetes Insipidus, Diabetes Mellitus, Optic Atrophy, and Deafness) describes the predominant symptoms of this disorder (Barrett et al., 1995, Barrett and Bundey, 1997).

The main features include young onset diabetes which is insulin dependent, non-autoimmune and non-HLA linked. Mutations in the gene causing WS (*WFS1*) are associated with premature death of pancreatic beta cells, which results in insulin dependent diabetes (Inoue et al., 1998). The *WFS1* gene was cloned in 1998 and is positioned on the short arm of chromosome 4 (4p16) (Strom et al., 1998, Inoue et al., 1998). *WFS1* encodes a 100 KDa protein called Wolframin which is located across the membrane of the Endoplasmic Reticulum (ER) (Takeda et al., 2001). The precise function of Wolframin is not fully understood; however studies have shown that Wolframin is involved in protein biosynthesis, modification/folding, secretion, processing, membrane trafficking and regulation of ER calcium homeostasis (Yamada et al., 2006, Fonseca et al., 2005, Riggs et al., 2005, Hofmann and Bauer, 2006, Yamaguchi et al., 2004).

As mentioned in the main introduction, ER stress is sensed by 3 transmembrane proteins across the ER membrane: IRE1 (Inositol Requiring 1), PERK (Protein Kinase like ER Kinase) and ATF 6a/b (Activating Transcription Factor 6). These three sensors are bound to BiP (Binding Protein/HSPA5) within the ER lumen under normal unstressed conditions; however, they get activated in the presence of ER stress and dissociate from BiP to perform their activities. The role of WFS1 in the ER stress pathways has been investigated by many studies suggesting that β-cell death and neuronal cell dysfunction in WS are attributed to high levels of ER stress in the affected cells (Yamada et al., 2006). Fonseca and colleagues (2005) reported that WFS1 is a component of the UPR and its deficiency leads to apoptosis especially in neuronal and pancreatic beta cells due to chronic ER stress. This suggested that WFS1 protects cells against ER stress. Another study by the same group showed that WFS1 has a key role in the negative regulation of a feedback loop of the ER stress network (Fonseca et al., 2010). This study showed that WFS1 prevents secretory cells from apoptosis caused by dysregulation of ER stress signalling pathways by negatively regulating ATF6a through the ubiquitin proteasome pathway.

Apoptosis of the neuronal and pancreatic beta cells has been reported to be the main reason for progression of WS due to the presence of irresolvable ER stress (Oslowski et al., 2011). Apoptosis is one of the important cellular mechanisms critical for development and tissue homeostasis. The apoptotic pathway is regulated by several genes such as p53. This gene is able to upregulate the expression of genes involved in apoptosis such as the members of the BCL-2 family (Lassus et al., 2002). The BCL family consists of pro-apoptotic and anti-apoptotic proteins, which function in regulating the permeability of the mitochondrial membrane (Szegezdi

et al., 2006, Chipuk et al., 2010). The pro-apoptotic proteins, Bak and BAX are required for induction of apoptosis by a variety of stimuli, including ER stress, and regulate both the release of pro-apoptotic factors from mitochondria and the release of calcium from the ER. BAX and BID function in permeabilising the mitochondrial membrane, which leads to the release of cytochrome c from the mitochondria to the cytoplasm (Szegezdi et al., 2006). In the cytoplasm cytochrome c is able to activate Caspase 9 (Szegezdi et al., 2006). Bcl-2 is a neuroprotective protein that is released in response to neuronal cell death (Rasheva and Domingos, 2009). The caspase family are specific proteases which are responsible for the destruction of the cells in a controlled manner. Caspases consist of cysteine proteases that remain in an inactive form within a cell. On induction of apoptosis, caspases are cleaved and form active enzymes. Caspase 9 is able to activate other caspases causing a caspase cascade (Fan et al., 2005).

Many studies have been focusing on apoptosis in WFS1 deficient pancreatic beta cells; the study by Philbrook et al. (2005), showed that WFS1 negative cells were more sensitive to ER stress induced apoptosis by measuring the activity of caspase-3. The study conducted by Riggs and colleagues (2005) assessed apoptosis in βWfs−/−mice by immunohistochemistry for the active subunit of cleaved caspase-3. They found significant increases in caspase-3 positive nuclei in βWfs−/−animals compared with control animals. Similarly Yamada and colleagues (2006) found increased expressions of CHOP and cleaved caspase-3 in WFS1 deficient MIN6 cells.

Cell cycle impairment has been previously reported in WS, where WFS1 deficiency was associated with increased expression of the cell cycle regulatory protein p21 in MIN6 cells

(Yamada et al., 2006). The cell cycle consists of events that lead to cell division and DNA replication. It is divided into two main periods: interphase (consisting of G1, S and G2 phase), which are concerned with cell growth and duplication of DNA; and mitosis, which is the cell division period ending with cytokinesis. Figure 3.1 shows a schematic diagram of the cell cycle phases and regulation. During the G1 phase the cells increase in size and the G1 check-points prepare the cells for DNA synthesis. During the G2 phase, the checkpoints prepare the cells to enter mitosis (Hannon and Beach, 1994).

The cell cycle events are regulated by two main classes of molecules: the cyclins and the cyclin-dependent kinases (CDKs). Cyclin and CDKs form a heterodimer which permits the activation or inactivation of target proteins to enter the next phase of the cell cycle. Cyclins are the regulatory subunits and are synthesised during specific stages of the cell cycle. The CDKs are the catalytic subunits which are constitutively expressed in cells and remain inactive in the absence of a cyclin partner (Sherr, 1993). The main cyclins involved in cell cycle regulation are A, B, D and E, each of these have different roles in the different check points of the cell cycle.

Cyclin D is induced at the G0/G1 transition by growth factors and its expression is associated with apoptosis of post mitotic neurons. Cyclin E plays a role in G1/S transition and it is degraded at the start of S-phase. Activation of cyclin E-CDK2 complex is necessary for G1/S transition and deactivation of this complex leads to cell cycle arrest in the G1 phase. Cyclin A plays a role in G2/M transition and its inhibition leads to G2 arrest. The activation of cyclin B is also necessary for the G2/M transition. At the beginning of mitosis cyclin B enters the nucleus and it is degraded

at the end of mitosis to allow cells to leave mitosis. Activation of cyclin B is inhibited by DNA damage and lack of DNA replication leading to G2 arrest (Dehay and Kennedy, 2007, Nagy et al., 1997).

The progression of the cell cycle is prevented by tumour suppressor genes also known as cell cycle inhibitors. These inhibitors consist of the cip (CDK interacting protein) family of genes that include p21, p27 and p57. P21 (CIP1/WAF1) is also known as cyclin dependent kinase inhibitor 1(CK1) and functions as a regulator of cell cycle progression at the G1 phase by binding to and deactivating cyclin-CDK heterodimers. P21 expression is controlled by p53 (a tumour suppressor gene) that enables this protein to mediate p53 dependent G1 arrest (Coqueret, 2003). P21 therefore negatively regulates cyclin-CDK-dependent progression of the cell cycle. This protein also plays a role in cellular differentiation, senescence, inhibition of apoptosis and activation of cyclin D-CDK4. The subcellular localisation of p21 plays a role in its ability to regulate cell cycle. When present in the nucleus, it can perform the cell cycle inhibitory activities and its cytoplasmic retention causes loss of cell cycle inhibition and gain of apoptosis inhibitory activity (Dash and El-Deiry, 2005).

Cell cycle studies are usually performed using flowcytometry based assays, where specific nuclear DNA profiles are generated using DNA dyes such as propidium iodide. Other methods traditionally used in cell cycle studies are based on the measurements of the expression patterns of cell cycle checkpoint markers such as proliferating cell nuclear antigen (PCNA) and cyclin B1 by immunofluorescence or flowcytometry. PCNA is a marker for the G1/S progression and

cyclin B1 is a marker for the G2/M transition. More recently High Content Cytometry (HCC) using the acumen eX3 cytometer from TTP Labtech has been applied to study the effects of therapeutic agents on the cell cycle at the single cell level. This is a fast laser scanning imaging system that is able to collect and analyse over 40 images/second. The acumen cytometer is applied to study several features at single cell level such as size, shape, number and intensity of subcellular compartments. These features are used for quantitative analysis of a broad range of biological processes including: toxicity testing, cell cycle status, colony formation, protein kinase activity, alterations in cell morphology, and ongoing apoptosis in cell culture. The acumen operates by passing a laser through a wide field objective across the bottom of a microplate or slide, allowing rapid analysis of whole wells (TTPlabtech, 2012).

Human Neuroblastoma cell lines were used in this project as a neuronal cell models. Neuroblastoma cell lines were originally used by Murry and Stout in 1947 in an *in vitro* study; these investigators found that these cells readily elaborated axons (Murray and Stout, 1947). Later, the study by Goldstein (1968) revealed the differentiating properties of neuroblastoma cell lines *in vivo* and *in vitro*. SK-N-AS cell lines were shown to adapt in serum-free conditions because of their property to constitutively express Insulin-like Growth Factor 2 (IGF-2) (El-Badry et al., 1991, Goldstein, 1968). Neuroblastomas are thought to arise from post ganglionic sympathetic neuroblasts of the embryonic neural crest. Several studies have shown that neuroblastoma cell lines express neuronal properties such as induced elaboration of neuritic processes; the synthesis of neurotransmitter biosynthetic enzymes; expression of neurofilaments; opioid, muscarinic and neurotrophin receptor expression. Neuroblastomas also contain dense core

granules which are presumed sites for catecholamine storage and show immunoreactivity to neuron specific enolase (Thiele et al., 1987).

This chapter will focus on the choice and characterisation of the cell models in terms of ER stress, apoptosis and cell cycle impairment.

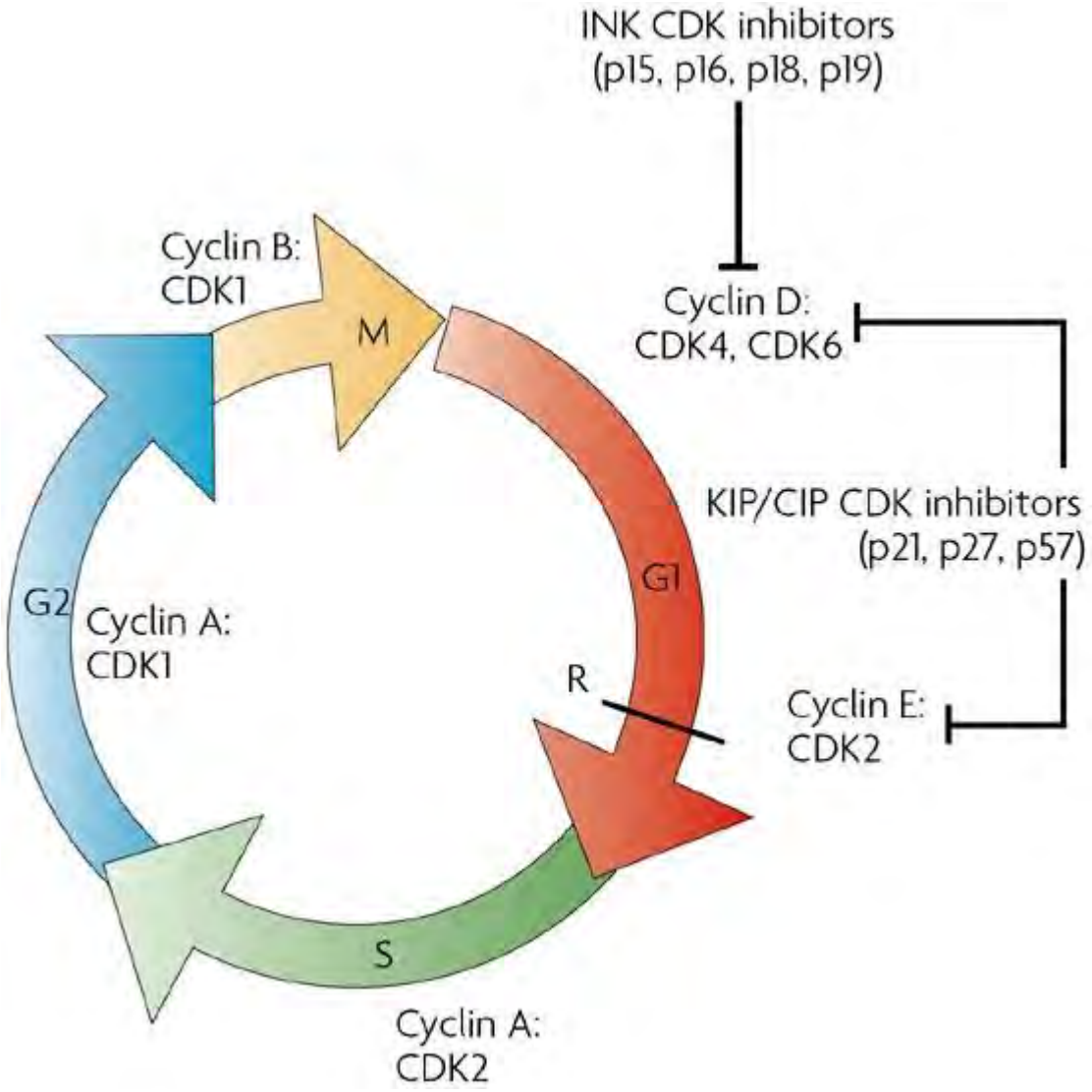

Figure 3.1: Eukaryotic cell cycle regulation

There are four events in eukaryotic cell cycle: M phase (mitosis), S phase (DNA synthesis), and two gap phases (G1 and G2). The G1phase allows responses to extracellular signals to induce cell division or withdrawal from cell cycle and enter the quiescent state (G0). During the G2 phase the cell checks whether the DNA replication is completed before the start of cell division. R is the major cell cycle restriction point at the end of the G1 phase. The cell cycle checkpoints are regulated by the cyclin-CDK complexes that are in charge of the correct progression of cell cycle phases (Dehay and Kennedy, 2007).

3.2 Aims

The aims of this study were as follows:

1. To investigate the expression of WFS1 on mRNA and protein levels by real time PCR and immunoblotting in WFS1 stably depleted human and mouse neuroblastoma cell models.
2. To prepare and characterise two WFS1 transiently depleted cell models in human SK-N-AS and NT2 cell lines.
3. To test the validity of the obtained cell models by investigating the levels of ER stress markers on protein and RNA levels.
4. To investigate the levels of apoptosis in WFS1 stably depleted cells.
5. To investigate the role of WFS1 in cell cycle regulation

3.3 Results

3.3.1 Characterisation of the cell models on mRNA and protein levels

3.3.1.1 The cell models

The aim of this project was to study the neurodegenerative aspects of Wolfram Syndrome since this is the main cause of death in WS patients (Genis et al., 1997). Human neuroblastoma (SK-N-AS), human NT2 and mouse neuroblastoma (neuro2A) cell lines were used to investigate the function of Wolframin. The reason for choosing SK-N-AS cells lines was because of their neuronal properties; these neuroblastoma cells are human cells derived from childhood neuroblastoma tumours and have many features in common with neuronal cells that express Wolframin (Thiele, 1998).

Three candidates WFS1 depleted stable clones (KD1-3) and one control were prepared in human neuroblastoma SK-N-AS cell lines by sh-RNA transfection. To reproduce the main findings obtained in the stable clones and to avoid the possibility of clonal effects, SK-N-AS cell line was used to construct a set of transiently WFS1 depleted cells using si RNA. The transiently WFS1 depleted cells were named KDA and KDB with their negative control (CL). To confirm the findings in another cell type, human neuronal progenitor (NT2) cells derived from a human teratocarcinoma cell line were used to construct a second set of transient knockdowns. These knockdowns were named KDC and KDD. Additionally, to reproduce the findings in another species, mouse neuroblastoma cell line (Neuro-2A) was used to prepare a set of WFS1 depleted stable clones: KDX, KDY and CTRL as empty vector treated control.

The levels of *WFS1* depletion were measured on mRNA level by quantitative real time PCR (QPCR) or on protein level by immunoblotting. QPCR is a very sensitive method to quantitate differences in mRNA expression using very small amounts of cDNA. In the first sets of experiments, SYBR Green was used in the reaction. Later on, to avoid the optimisation and validation of the primers, the SYBR green method was replaced with the Taqman method. The predesigned primer and probe combinations available from Applied Biosystems as 'Taqman gene expression assays' make it easier to run multiple reactions simultaneously. The QPCR data was analysed using the delta-delta CT method ($2^{\Delta\Delta\ Ct}$), a commonly used method to express relative changes between two parameters such as normal and diseased expression levels. This methods is explained in great details in (Materials and Methods Chapter, section 2.4.13)

For the SYBR Green method, HPLC purified primers (WFS1 and β-actin) were used for the real time PCR reaction. The primers were first optimised by analysis of the PCR product on the gel and validated by producing a standard curve presented in Figure 3.2. These results show that the PCR products were free of primer dimers and the reaction was linear over a wide range of cDNA concentrations (from 100ng to 3.1ng). The linearity graphs show that both graphs have a R^2 value of about 0.99 and the efficiency value is between -3.1 and -3.6. These are the essential factors to establish whether the efficiency of both primers are similar, which is the important condition for applying the ΔΔCT method (Livak and Schmittgen, 2001).

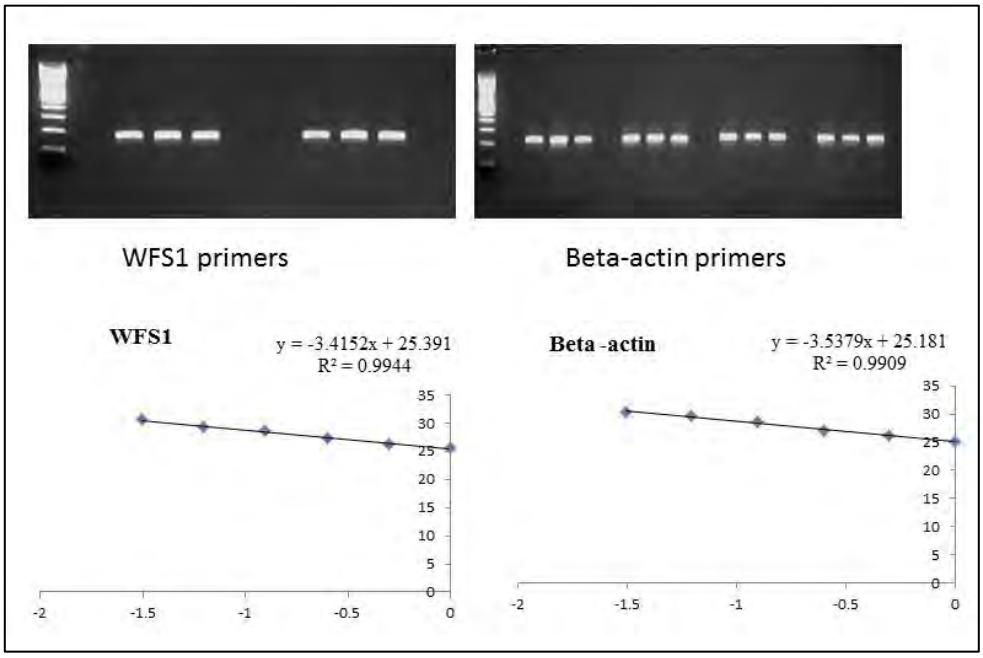

Figure 3.2: Optimisation and validation of SYBR Green primers

The QPCR reaction was performed with 20pmoles of the primers, the PCR product was run on a 2% agarose gel. For the standard curves the following range of concentrations of the cDNA was used. (100ng, 50ng, 25ng, 12.5ng, 6.25ng and 3.1ng). Each concentration was tested in triplicate.

3.3.1.2 Determination of WFS1 depletion levels in the cell models

The expression of *WFS1* was first measured by the SYBR Green method in WFS1 depleted and control stable SK-N-AS clones (KD1, KD2 and CL). The experiments were repeated 7 times with different sets of cDNAs. The data presented in Figure 3.3 shows that the expression of *WFS1* was significantly reduced in the two knockdowns in comparison to the control. The levels of *WFS1* depletion observed in KD1 was 80.5±1.5% with $p=4.6x10^{-07}$ and in KD2, the level of *WFS1* mRNA depletion was 68±4.9% with p=0.014.

The expression of *WFS1* mRNA was also measured by QPCR using the Taqman method. As Taqman offers optimised and validated probe and primer combinations, these do not require further optimisation. One more WFS1 depleted clone was added to the experiments (KD3); the three WFS1 stably depleted neuroblastoma clones (KD1-3) showed WFS1 expression reduced by 60-80% in comparison to the control (CL). *WFS1* expression on RNA level was reduced by 71±2%, 61±3% and 60±4% (mean±SEM) in KD1, KD2 and KD3 respectively vs control (n=6, $p<0.001$) Figure 3.4A.

Furthermore, the expression of WFS1 in these stable knockdowns was also measured by immunoblotting using rabbit polyclonal anti-WFS1 antibodies from Proteintech and the blots were developed using the ECL kit. The data showed significant reduction in the expression of WFS1 protein in the three knockdowns in comparison to the control. Protein depletions were measured by densitometry using the Gene Tools software, which showed: 76±7%, 78±4% and 63±7% WFS1 depletion in KD1-3 vs control respectively (n=6, $p<0.05$, Figure 3.4B).

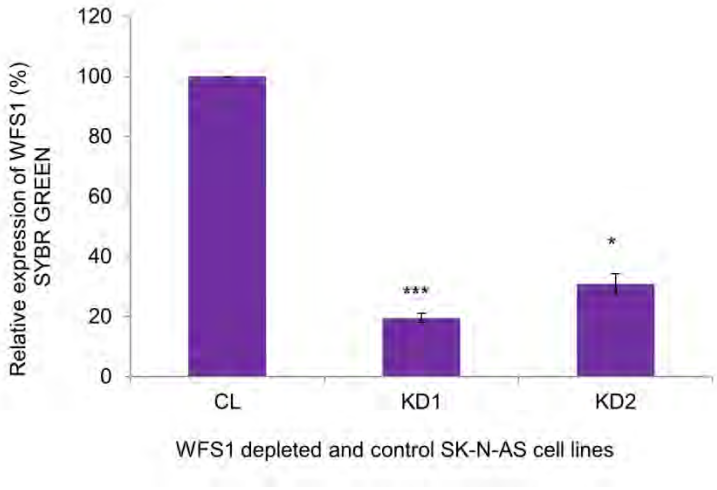

Figure 3.3: *WFS1* mRNA expression by SYBR Green

Quantitative real-time PCR analysis of *WFS1* in stable clones with WFS1 depletion in comparison to control by SYBR Green, CL=control, KD1, KD2= WFS1 depleted stable clones in human SK-N-AS cell line.. *p<0.05, **p<0.01, and ***p<0.001, T-test: KD1 $p=4.6x10^{-07}$, KD2 p=0.014, n=7. n = number of independent runs using at least 3 RNA preparations from independently cultured stable clones

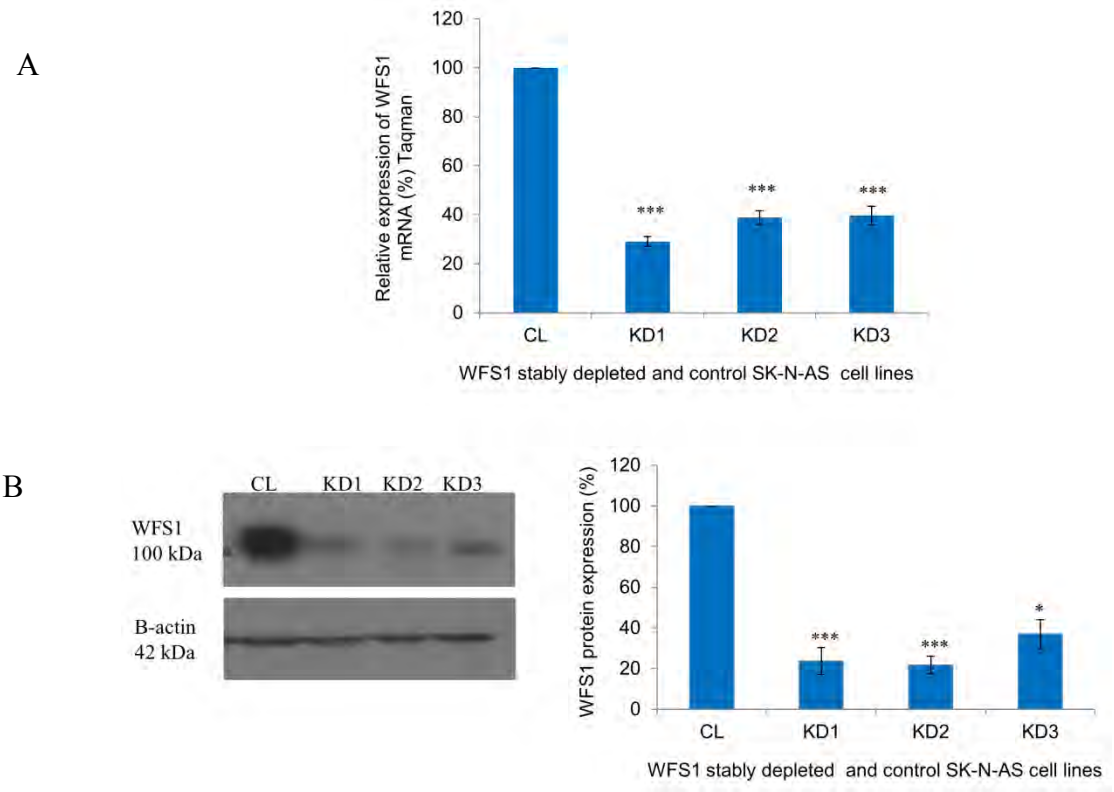

Figure 3.4: *WFS1* mRNA and protein expression in SK-N-AS stable clones

A: Quantitative real-time PCR analysis of *WFS1* in WFS1 depleted cells in comparison to control by Taqman. CL=control, KD1, KD2, KD3=WFS1 depleted stable clones in human SK-N-AS cell line. *p<0.05, **p<0.01, and ***p<0.001**,** n=7. n=number of independent runs using at least 3 RNA preparations from independently cultured stable clones. B: Western blots analysis of WFS1 in WFS1 depleted cells in comparison to control - representative experiment. (Beta actin = reference). Bar chart - quantification of WB, T-test: WFS1: p<0.001 for KD1 and KD2, p< 0.05 for KD3, n=6, n= number of independent runs using at least 3 independently prepared protein extracts.

In addition, transiently depleted WFS1 knockdowns were prepared in SK-N-AS human neuroblastoma cells (KDA and KDB) using siRNA (Ambion). The expression of *WFS1* in these cells was measured by real-time PCR using the Taqman method and by immunoblotting. The data presented in Figure 3.5A showed significant reduction in the levels of *WFS1* in the two knockdowns in comparison to the control. The levels of *WFS1* mRNA showed 79±2% reduction in KDA and 61±9% in KDB ($n=6$, $p<0.001$). On protein level the results were similar: 76±6% WFS1 depletion in KDA and 72±3% in KDB ($n=5$, $p<0.05$).

To verify the findings in another cell line, it was decided to prepare WFS1 transiently depleted human NT2 cells (KDC and KDD) using siRNA (Ambion). In both cases, the expression of WFS1 was significantly decreased at both RNA and protein levels. The results of QPCR (Figure 3.6A) showed WFS1 depletion 83±1% in KDC and 83±1% in KDD ($n=5$ and $p<0.001$). The WFS1 depletion on protein level (Figure 3.6B) was 63±8% and 61±6% in KDC and in KDD, ($n=3$ and $p<0.05$).

A

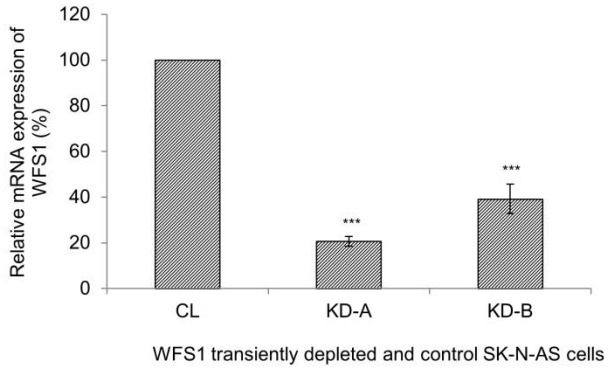

B

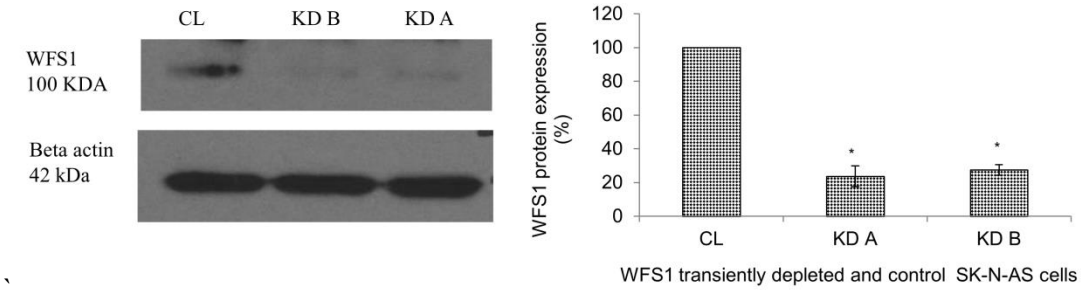

Figure 3.5: WFS1 expression in transiently depleted SK-N-AS cells

A: Quantitative real-time PCR analysis of *WFS1* in WFS1 transiently depleted cells in comparison to control in human SK-N-AS cell. *p<0.05, **p<0.01, and ***p<0.001**,** n=6. n = number of independent runs using at least 3 RNA preparations from independently transfected cells. T-test WFS1: $p<10^{-05}$ for KDA and KDB, n=6.B: Western blots analysis of WFS1 in WFS1 transiently depleted cells in comparison to control - representative experiment. (Beta actin = reference). Bar chart -quantification of WB, T-test: WFS1: p<0.05. T-test: p<0.05 for KDA and KD2 v control. N= number of independent runs using at least 3 protein extracts from independently silenced neuroblastoma cells.

A

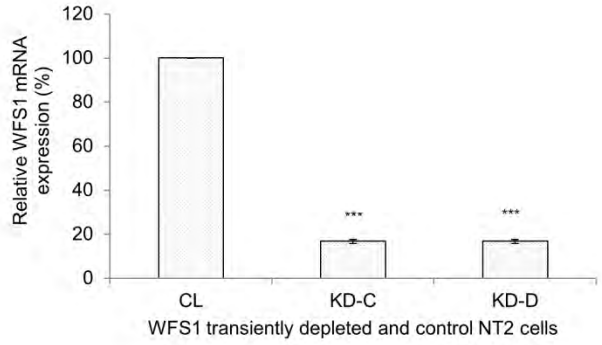

B

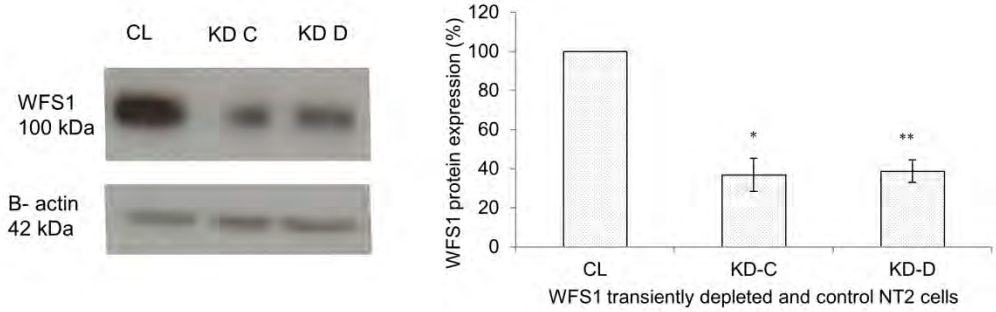

Figure 3.6: Levels of WFS1 expression in transiently depleted NT2 cells

A: Quantitative real-time PCR analysis of *WFS1* in WFS1 transiently depleted human NT2 cells in comparison to control. *p<0.05, **p<0.01, and ***p<0.001**,** n=6. n = number of independent runs using at least 3 RNA preparations from independently cultured transient cells. T-test WFS1 depletion: $p<10^{-05}$ for KDC and KDD respectively, n=5. B: Western blot analysis of WFS1 in WFS1 transiently depleted human NT2 cells in comparison to control. Representative experiment (Beta actin = reference). Bar chart - quantification of WB, T-test WFS1: p<0.05 and p<0.015 for KDC and KDD respectively (n=3)

Finally, it was decided to confirm the findings in cells from another species to find out whether the data is species dependent. A mouse neuroblastoma (Neuro2a cell line) was chosen to prepare stably depleted WFS1 knockdowns using the lentivirus system. The knockdowns were prepared by Dr Astuti. Two knockdowns and one control clones were chosen for the experiments (KDX, KDY and CTRL). Similarly, the levels of WFS1 expression were measured in these cells by QPCR and immunoblotting. The results presented in Figure 3.7 showed significant reductions in the expression of WFS1 both on protein and mRNA levels. The levels of *WFS1* depletion in these cell lines on mRNA level was 83±5% in KDX and 67±6% in KDY with p-values 0.025 and 0.0069 respectively, n=6 (Figure 3.7A). On the protein level the data showed 85±12% decrease in KDX and 57±11 decreased expression in KDY (n=4 $p<0.05$, Figure 3.7B).

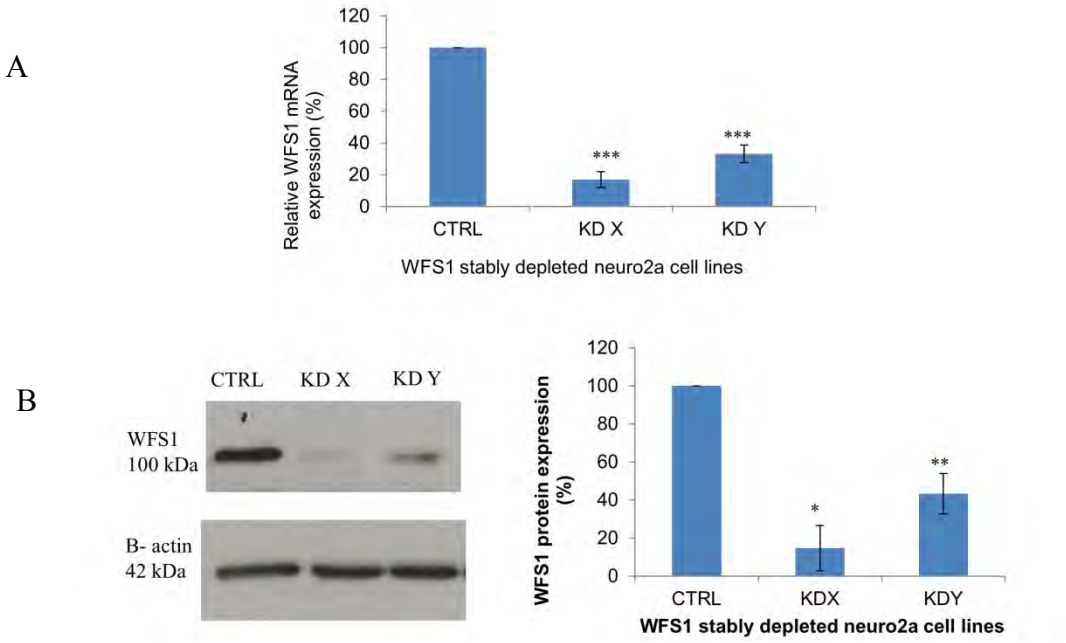

Figure 3.7: WFS1 expression in Neuro2A stable clones

A: Quantitative real-time PCR analysis of *WFS1* in WFS1 stably depleted clones in comparison to control in mouse neuro2a cell line. *p<0.05, **p<0.01, and ***p<0.001**,** n=6. n = number of independent runs using at least 3 RNA preparations from independently cultured stable clones. T-test WFS1 depletion: $p=9.5x10^{-06}$ and $8x10^{-04}$ for KDX and KDY respectively. B: Western blots analysis of WFS1 in WFS1 stably depleted clones in comparison to control - representative experiment. (Beta actin = reference). Bar chart -quantification of WB, T-test: WFS1: p<0.05. T-test WFS1: 0.025 and 0.0069 for KDX and KDY respectively (n=4)

3.3.2 Expression of ER stress markers in WFS1 depleted neuronal cells

WFS1 depleted cells have been shown to present enormous ER stress in different animal and human cell models. To characterise the cell models, it was decided to measure the expression of various ER stress markers (BiP, CHOP, spliced XBP1, GRP94, ATF6 and HRD1) on protein and/ or mRNA levels by real time PCR and immunoblotting. The reason for choosing these particular markers was based on their involvement in the three main branches of the ER stress pathways as described in the main introduction (Table 1.1). The levels of the three ER stress markers CHOP, BiP and spliced XBP1 were significantly increased in WFS1 stably depleted clones in comparison to the control (Figure 3.8). CHOP expression was increased by 146±7% (Mean±SEM) in KD1, 56±9% in KD2 and 54±14% in KD3 ($n=3$, $p<0.05$). The expression of BiP was increased by 70±17%, 83±28% and 59±13% in KD1-3 ($n=5$, $p<0.05$) and the expression of spliced XBP1 was increased by 107±28%, 110±27% and 94±33% in KD1-3 respectively ($n=7$, $p<0.01$).

At protein level the expressions of BiP, GRP94, ATF6a and HRD1 were measured in WFS1 stably depleted clones. All four markers showed significant elevation in WFS1 depleted cells in comparison to the control. The expression of BiP protein shown in Figure 3.9A was significantly increased in the WFS1 depleted cells in comparison to the control: 407±71%, 255±94% and 129±49% increase in KD1-3, respectively ($n=6$, $p<0.05$). The expression of GRP94 was measured in KD2 and KD3 in comparison to the control Figure 3.9B; in KD2 the expression of GRP94 was increased by 211±36% and in KD3 by 182±70% ($n=3$, $p<0.05$). The protein expression of ATF6 and HRD1 were measured in KD1 and KD2 clones and is presented in

Figure 3.9C. Significant increases were observed in the expression of ATF6 and HRD1 in WFS1 depleted cells: ATF6 expression was increased by 377±119% and 280±149% in KD1 and KD2 respectively (n=4, $p<0.05$). Also, the expression of HRD1 was increased by 375±121% in KD1 and in KD2 by 424±120% (n=4, $p<0.05$).

Similarly, the WFS1 transiently depleted cells (SK-N-AS and NT2) showed also significant elevations in the levels of ER stress markers BiP, CHOP and spliced XBP1 on mRNA level by real time PCR Figure 3.10. CHOP expression was increased by 70±6% and 38±7% in KDA and KDB respectively. The expression of BiP was increased by 133±2% and 25±6% in KDA and KDB and the expression of spliced XBP1 was increased by 89±8% and 53±6% in KDA and KDB respectively (for all experiments n=3, $p<0.05$, Figure 3.10A). In WFS1 transiently depleted human NT2 cells the expression of CHOP was elevated by 52±31% and 52±5% in KDC and KDD respectively, (n=3, $p<0.05$) and the expression of BiP was increased by 23±8% and 49±13% (n=3. $p<0.05$, Figure 3.10B). In addition, the expression of BiP was measured in the mouse neuro2a cell line with stable WFS1 depletion and presented in Figure 3.10C. In KDX BiP expression was elevated by 169.7±16 and in KDY BiP expression was increased by 179.5±4 (n=4, $p<0.05$, Figure 3.10C)

In summary, WFS1 depletion in both stably and transiently depleted human and mouse neuroblastoma and transiently depleted human NT2 neuronal cells resulted in enhanced ER stress.

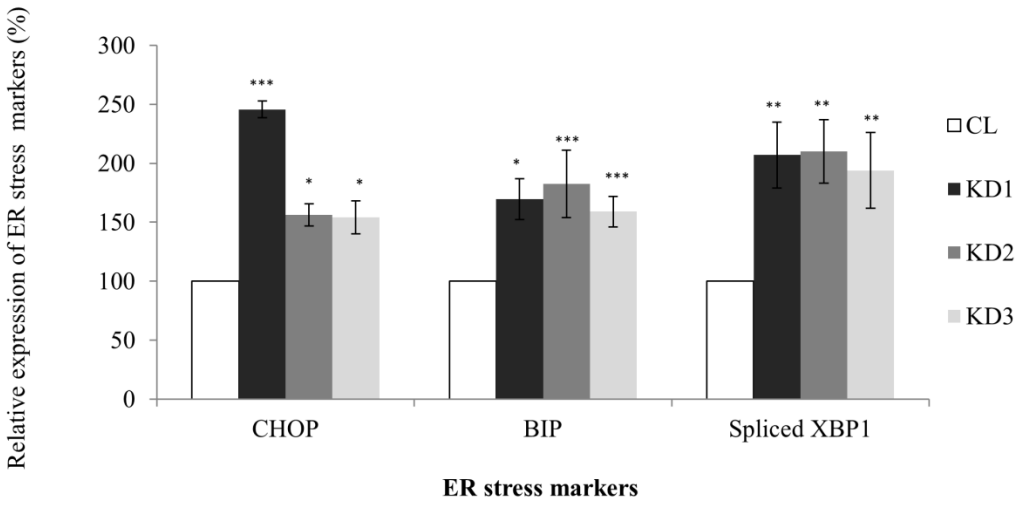

Figure 3.8: Expression of ER stress markers in WFS1 depleted stable clones

Quantitative real-time PCR analysis of BiP, CHOP and spliced XBP1 in stable clones with WFS1 depletion in comparison to the control in human neuroblastoma cell line, *p<0.05,**p<0.01, and ***p<0.001**,** T-test CHOP: $p<10^{-05}$ for KD1 and p<0.05 for KD2 and KD3, n=3. T-test BiP: p<0.05 for KD1 and p<0.001 for KD2 and KD3, n=5.T-test Spliced XBP1: p<0.01 for KD1-KD3, n=7. n=number of independent runs using at least 3 RNA preparations from independently cultured stable clones.

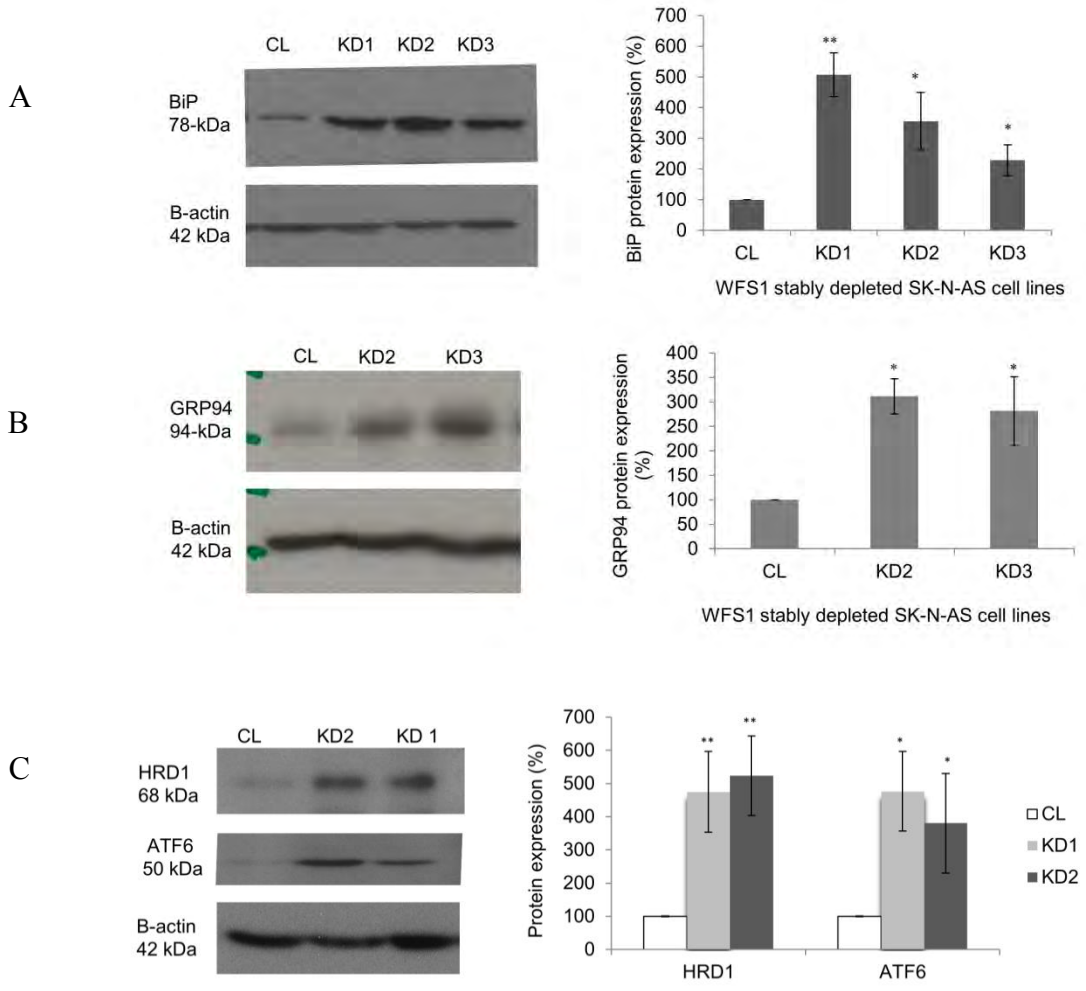

Figure 3.9 Expression of ER stress proteins in WFS1 depleted stable SK-N-AS cell lines

Western blot analysis of BiP, GRP94, HRD1 and ATF6 in WFS1 stably depleted clones in comparison to the control- representative immunoblot (beta actin = reference). Bar chart-quantification of western blot A: *p<0.05,**p<0.01, and ***p<0.001, T-test: BiP: p< 0.01 for KD1 and p<0.05 for KD2 and KD3, n=6, B: GRP94: p<0.05, n=3 for KD 2 and 3; C: HRD1: p<0.01 for KD1 and KD2, n=4. C: ATF6: p<0.05 for KD1 and KD2 respectively, n=4. N=number of independent runs using 3 independently prepared protein extracts.

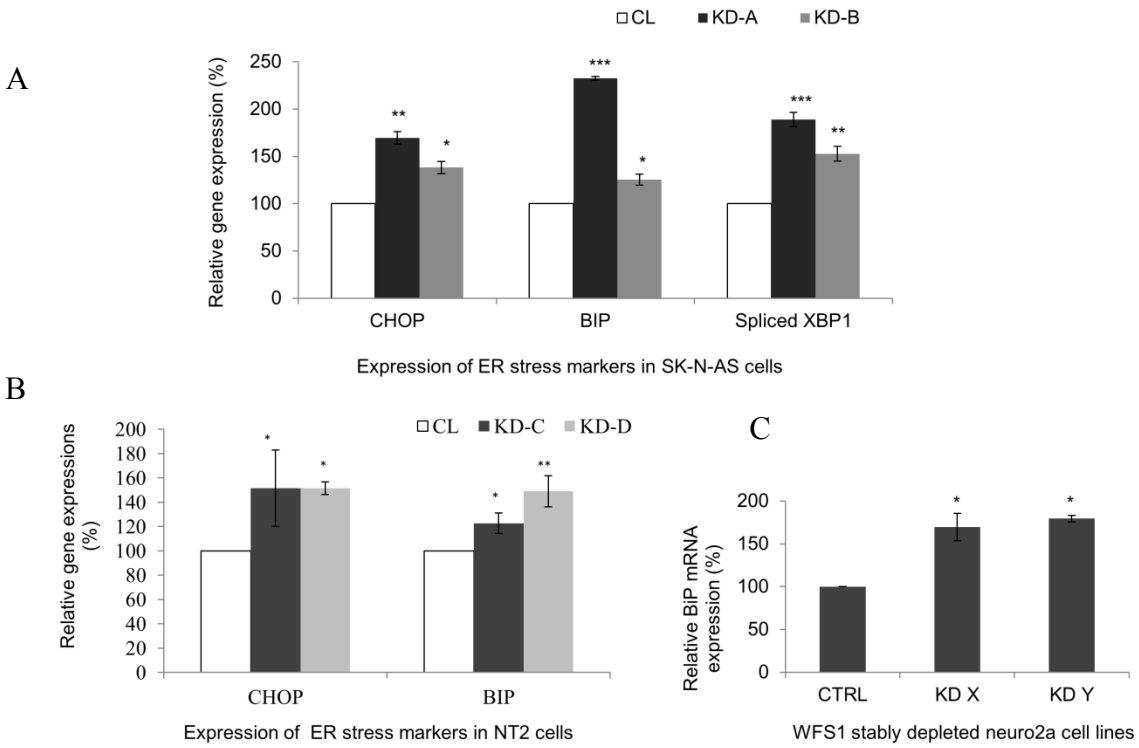

Figure 3.10: mRNA expression of ER stress markers in WFS1 depleted cells

A: Quantitative real-time PCR analysis of BiP, CHOP and spliced XBP1 expression in WFS1transiently depleted SK-N-AS cells in comparison to the control. *p<0.05,**p<0.01, and ***p<0.001, T-test CHOP: p<0.01 and p<0.05 for KDA and KDB respectively n=3, BiP $p<10^{-05}$ and p<0.05 respectively, n=3 and spliced XBP1 p<0.001and p<0.01, n=3, B: QPCR analysis of ER stress markers BiP and CHOP expression in WFS1 transiently depleted NT2 cells in comparison to the control. T-test CHOP p<0.05 for KDC and KDD, n=3. BiP: p<0.05 and p<0.01 for KDC and KDD respectively, n=3. C: Quantitative real-time PCR analysis of BiP in WFS1 stably depleted neuro2a cells in comparison to the control. T-test BiP elevation p= 0.038 and 0.018 for KDX and KDY respectively, n=3. N= number of independent runs using at least 3 RNA preparations.

3.3.3 Levels of apoptosis in WFS1 depleted human neuroblastoma cells

Many studies have reported that WFS1 depleted cells exhibit high levels of apoptosis caused by irresolvable ER stress (Philbrook et al., 2005, Riggs et al., 2005, Ishihara et al., 2004, Yamada et al., 2006). Therefore, the levels of apoptosis were measured in WFS1 stably depleted SK-N-AS cells with a variety of methods: immunoblotting, QPCR and HCC. The levels of cleaved caspase-3 and pro-apoptotic protein CHOP were both significantly increased in the three WFS1 stably depleted clones in comparison to the control (Figure 3.11A). The expression of CHOP was increased by 95±15%, 96±62% and 67±17% in KD1-3 respectively, ($n=3$ and $p<0.05$). The expression of cleaved caspase-3 was increased by 73±18%, 100±41%, 47±6% in KD1-3 respectively ($n=5$, $p<0.05$). At mRNA level, the expression of the two members of the BCL-2 family were measured in one WFS1 depleted cell line (KD2) and one control cell line. The data presented in Figure 3.11B shows the expressions of the pro-apoptotic protein BAX and anti-apoptotic protein BCL-2 in the WFS1 stably depleted and control cell lines. The expression of BAX was significantly elevated in the WFS1 depleted cell line by 169±19, $n=4$ and $p<0.01$. The expression of BCL-2 in the WFS1 depleted cells was significantly decreased by 62±6% in comparison to the control ($p<0.001$, $n=4$).

HCC measures ongoing or early apoptosis by measuring total fluorescence from DNA fragmentation (Payne, 2005). The results are expressed as percentage of apoptotic cells in the whole population. On average there were 4±0.37% apoptotic cells in control samples. This was increased to 7±0.40% in KD1, 11±0.8% in KD2 and 14±2.8% in KD3 ($n=5$, $p<0.05$, Figure 3.11C). Overall, this data suggests that WFS1 depleted cells display high levels of apoptosis which is most probably triggered by irresolvable ER stress.

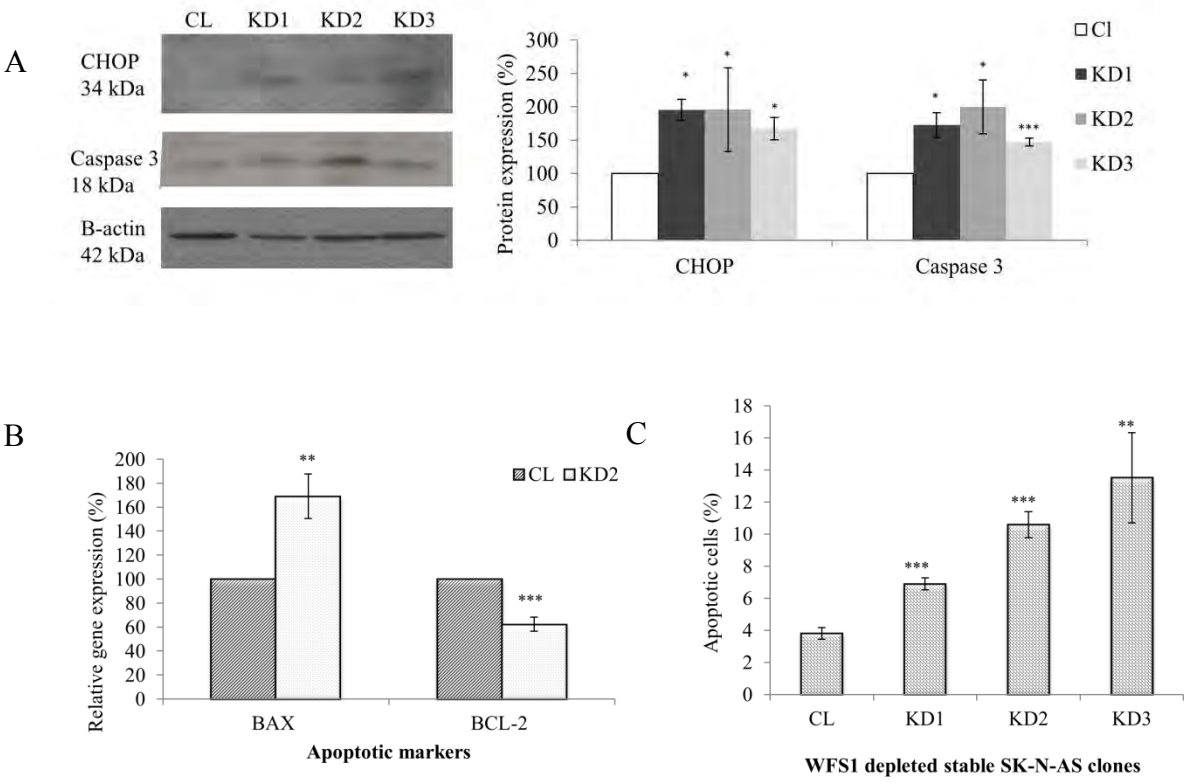

Figure 3.11: Levels of apoptosis in WFS1 stably depleted SK-N-AS clones

A: Western blot analysis of CHOP and cleaved caspase-3 in WFS1 stably depleted cells in comparison to the control- representative immunoblot. (Beta-actin = reference). Bar chart-quantification of western blot, *p<0.05,**p<0.01, and ***p<0.001, T-test: CHOP: p<0.05 for KD1, KD2 and KD3, n=3. Caspase-3 p<0.05 for KD1 and KD2, p<0.001 for KD3, n=5. N= number of independent runs using 4 independently prepared protein extracts. B: QPCR analysis of apoptosis markers BAX and BCL-2 in WFS1 stably depleted cells in comparison to the control. T-test: BAX p=0.006, n=4; T-test: BCL-2: $p=6.4x10^{-04}$, n=4. C: Increase in the percentage of early apoptotic cells in the WFS1 depleted stable clones in comparison to the control – by High Content Cytometry. T-test: $p<10^{-05}$ for KD1 and KD2, p<0.01 for KD3 versus control, n=5. N= number of technical replicates (independent cultures of stable clones).

3.3.4 Role of WFS1 in cell cycle regulation by High Content Cytometry

WFS1 was previously shown to be associated with cell cycle regulation (Yamada et al., 2006, McBain and Morgan, 2003). In this chapter, the role of WFS1 in cell cycle was further investigated by assessing cell cycle kinetics and cell proliferation using HCC in the WFS1 depleted neuroblastoma cells. Measured parameters indicated the percentage of cells in each phase of the cell cycle, population doubling time (PDT) and the length of each phase of the cell cycle. In addition, the expression and effect of the cell cycle regulatory protein $p21^{cip1}$ was measured in WFS1 depleted and control cells. The cytometry was performed at 24 and 48 hour time points, following an initial 24 hour incubation (which allowed the cells to attach) and the results are presented in Figures 3.12-3.14 and Table 3.1. Figure 3.12 represents a cytometry histogram of the cells cycle events. This figure shows that KD1 is a tetraploid cell line; the DNA content of the cells is double that seen in the control and the other two cell lines (showing right shift in cytometry histogram).

Cell cycle kinetics data showed that in KD1 there were more cells in G1 and fewer in G2; in KD2 there were fewer cells in G1 and more in G2 in comparison to control cells (Figure 3.13 and Table 3.1). The percentages of cells in KD3 after 24 hours of cell growth were significantly different from control (fewer cells in G1 and more cells in G2 phase). However at 48h cell growth this difference was not statistically significant. At 24h the differences between the control and KD1 in G1 and G2 phase were statistically significant ($p<0.001$), KD2 vs CL; p=NS and KD3 vs CL, ($p<0.001$, Figure3.13A). At 48 hours of cell growth the differences between control

versus KD1 and KD2 were significant ($p<0.001$) but the differences between CL and KD3 were not statistically significant (p=NS, Figure 3.13B).

The cell proliferation data presented in Figure 3.14 and Table 3.1 show that the population doubling time (PDT) was lower for KD2 in comparison to the other cell lines (Figure 3.14C). The time spent in G1 phase was longer for KD1 (39h) and shorter for KD2 (14h) in comparison to the control (25h, Figure 3.14A). The differences between control versus KD1 and KD2 were significant ($p<0.001$) but the differences between CL and KD3 were not statistically significant (p=NS). The time spent in G2 phase was significantly shorter in KD1 (16h) in comparison to the control. However, the G2 phase was longer for KD2 (31h) but the difference was not significant in comparison to the control (Figure 3.14B, Table 3.1). Overall these results show that the KD1 cell line has a longer G1 phase while the KD2 cell line has an elongated G2 phase and a shorter population doubling time in comparison to the control but no significant differences were observed between CL and KD3.

To evaluate whether the cell cycle effects of WFS1 observed in this study were associated with alterations in $p21^{cip1}$ levels, the expression of $p21^{cip1}$ was measured by HCC as fluorescence units per cell and is presented in Figure 3.15. The data showed that significant $p21^{cip1}$ down-regulation was present in all three WFS1 depleted cell lines (Figure 3.15A). Furthermore, the expression of $p21^{cip1}$ was associated with the inhibition of progression through the G2 phase of the cell cycle and inhibition of apoptosis in all four cell lines, a representative finding of one cell line are presented in Figure 3.15B and C and all four clones follow the same trend.

Overall, these data suggest that WFS1 depleted cells that retain their p21 expression are protected from apoptosis and cell cycle impairment. These are preliminary data which needs to be confirmed further.

Table 3.1: Cell cycle and apoptosis data of WFS1 depleted neuroblastoma cells

Measured parameters	CL	KD1	KD2	KD3
G1 cells (%) at 24h	56±0.3	77±1.3	55±0.4	44±0.4
G2 cells (%) at 24h	29±0.3	12±0.4	30±0.5	35±0.5
G1 cells (%) at 48h	47±0.3	68±0.4	32±0.5	47±0.3
G2 cells (%) at 48h	36±0.4	18±0.4	48±0.8	32±0.6
PDT (h)	65±2h	65±3h	54±3h	65±2h
G1 time (h)	25±0.8h	39±1.5h	14±0.7h	25±0.8h
G2 time (h)	29±1h	16±1h	31±2h	26±1h
P21-protein-per-cell (FLU)	303±43	226±42	243±18	89±12
P21-pos-G2 cells	44±2.6	34±3.8	67±4.5	65±10.7
P21-neg-G2 cells	13±1.9	6±1.2	8±2.3	29±3.9
P21-pos-apop cells	1±0.3	1±0.4	0±0.3	1±0.4
P21-neg-apop cells	19±3	20±3	23±0.3	9±3.1

PDT=population doubling time, apop=apoptosis, h=hours, %=cells in cell cycle phase.
p21-pos-G2 cells: Cells expressing $p21^{cip1}$ in G2 phase. The data is presented as mean±sem

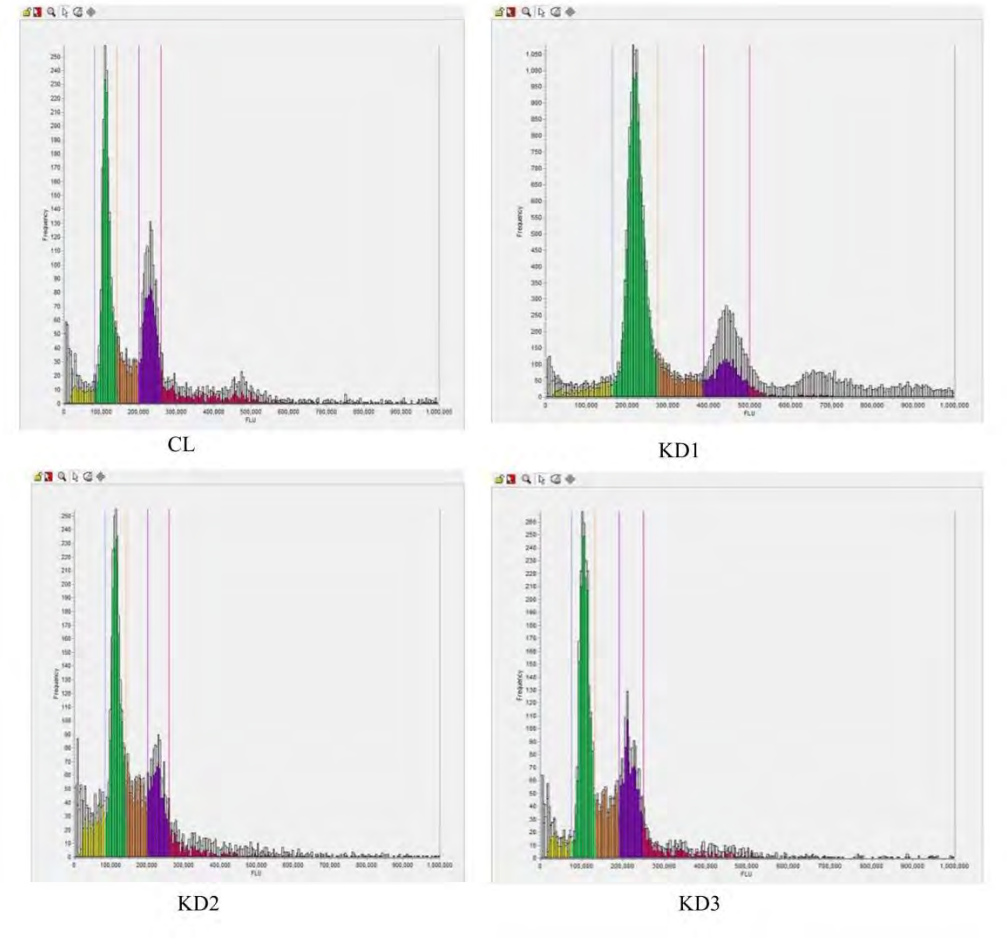

Figure 3.12: Cytometric histogram of number of cells in different phases of the cell cycle

WFS1 stably depleted and control SK-N-AS cells were grown for 24h, fixed with ethanol, stained with PI and scanned by Acumen eX3 cytometer as indicated in Methods chapter. The **c**ytometric histogram shows the number of cells (y axis) with different DNA content (x axis) The KD1 line is clearly tetraploid, showing a shift in the DNA content. The control, KD2 and KD3 cell line have similar histogram representing diploid cells. The colours represent cell cycle phases: (yellow=G0, green=G1, brown=S, purple=G2)

A

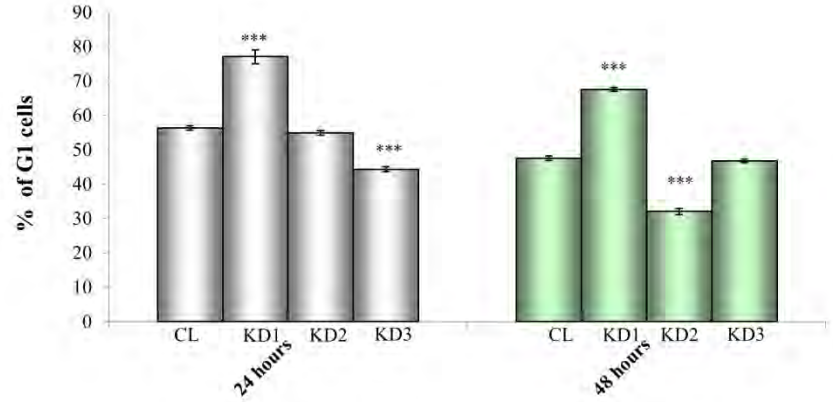

B

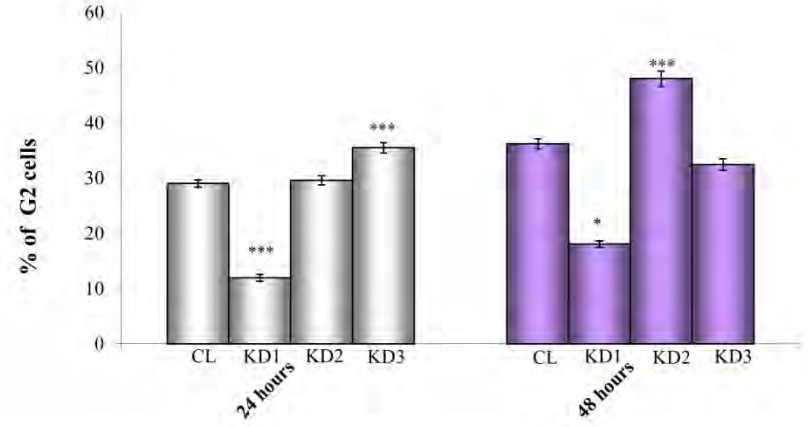

Figure 3.13: Cell cycle kinetics in WFS1 stably depleted SK-N-AS cell lines

WFS1 stably depleted and control SK-N-AS cells were grown for 24h, fixed with ethanol, stained with PI and scanned by Acumen eX3 cytometer as indicated in Methods chapter. A) Percentage of cells in G1 phases of the cell cycle after 24 and 48 hour cell growth. *p<0.05,**p<0.01, and ***p<0.001, p values calculated by Stat Calc using the comparison of means between independent groups (different cell lines versus control). After 24 hours cell growth the p-values for G1 (KD1 v Cl: p<0.001, KD2 v Cl: p=NS, KD3 v Cl: p<0.001). After 48 hours cell growth, G1 cells: (KD1 v Cl: p<0.001, KD2 v Cl: p<0.001, KD3 v Cl: p=NS). B) Percentage of cells in G2 phases of the cell cycle after 24 and 48 hour cell growth. After 24 hours cell growth the p-values for G2 (KD1 v Cl: p<0.001, KD2 v Cl: p=NS, KD3 v Cl: p<0.001). After 48 hours cell growth, G2 cells: (KD1 v Cl: p<0.05, KD2 v Cl: p<0.001, KD3 v Cl: p=NS).

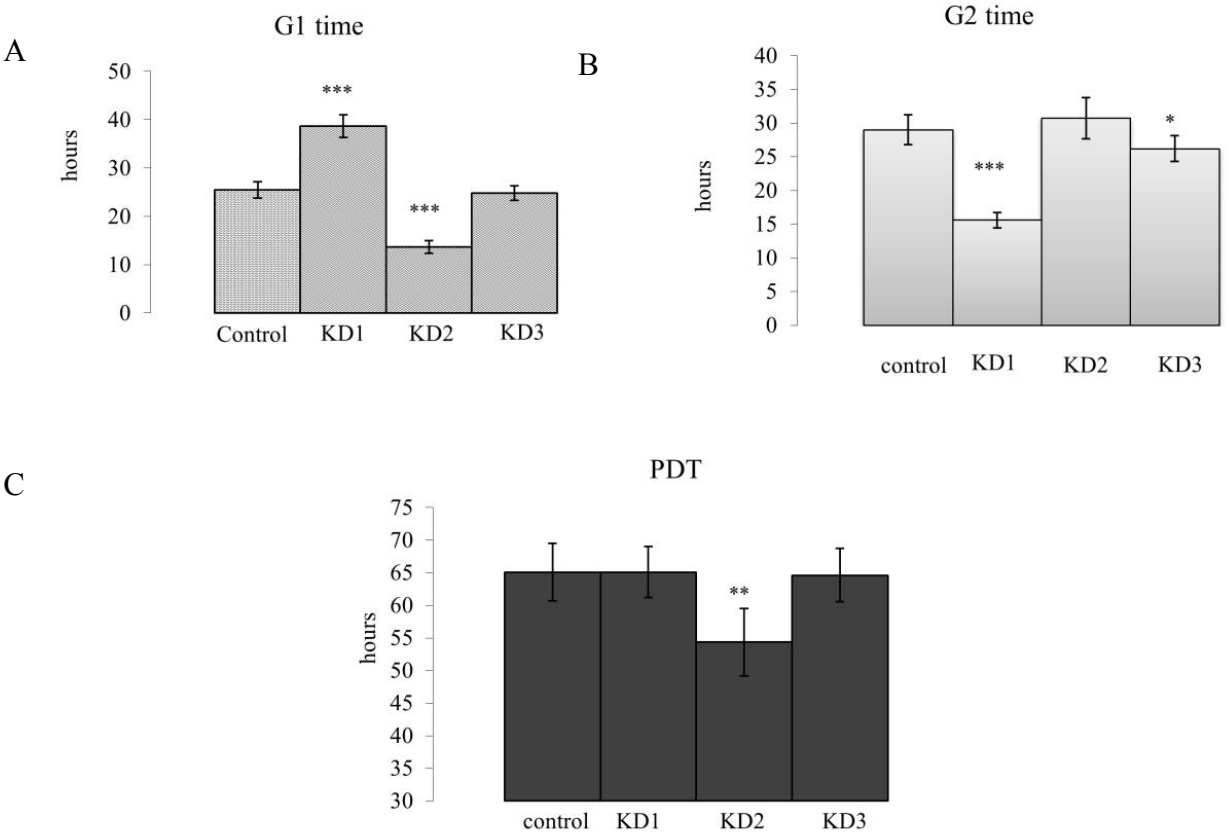

Figure 3.14: Cell proliferation of WFS1 stably depleted SK-N-AS cell lines

WFS1 stably depleted and control SK-N-AS cells were grown for 24h, fixed with ethanol, stained with PI and scanned by Acumen eX3 cytometer as indicated in Methods chapter A: Length of the G1 phase ; p-value (KD1 v Cl and KD2 v Cl: $p<0.001$, KD3 v Cl: p=NS). B: Length of the G2 phase: p-value (KD1 v Cl: $p<0.001$, KD2 v Cl: p=NS, KD3 v Cl: $p<0.05$), C: population doubling time (PDT): p value (KD1 v Cl and KD3 v Cl: p=NS, KD2 v Cl: $p<0.01$). *$p<0.05$,**$p<0.01$, and ***$p<0.001$, p values calculated by Stat Calc using the comparison of means between independent groups (different cell lines versus control).

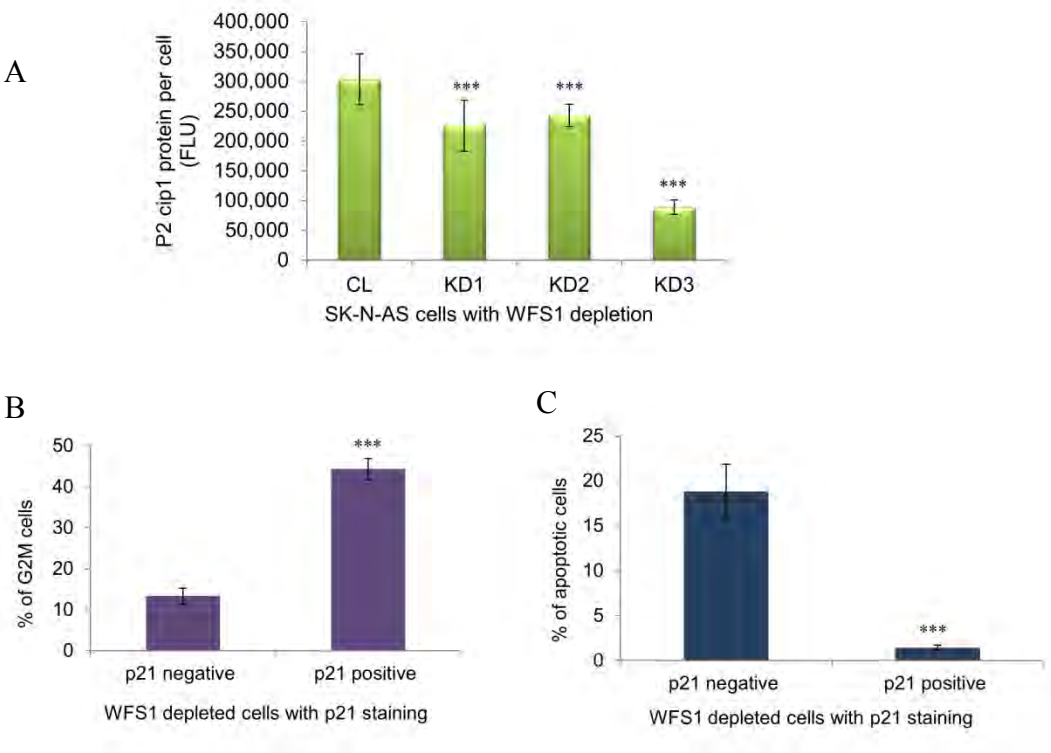

Figure 3.15: p21^{cip1} levels in WFS1 stably depleted SK-N-AS cell line by HCC

WFS1 stably depleted and control SK-N-AS cells were grown for 24h, overnight incubated with the p21 antibody, fixed with ethanol, stained with PI and scanned by Acumen eX3 cytometer as indicated in Methods chapter. *p<0.05,**p<0.01, and ***p<0.001, p values calculated by Stat Calc using the comparison of means between independent groups (different cell lines versus control). A: Expression of p21^{cip1} protein per cell, measured as fluorescence units in WFS1 depleted cells in comparison to the control, p<0.001, n=8. B: Representative data showing percentage of cells in G2 phase of cell cycle with and without p21^{cip1} expression, p<0.001, n=8. C: Representative data showing percentage of apoptotic cells with and without p21^{cip1} expression, p<0.001, n=8. .

3.4 Discussion

The data presented in this chapter demonstrates four cell models of Wolfram syndrome in neuronal cells with similar characteristics previously described to be associated with rodent disease models of WS. The four cell models: WFS1 stably depleted human SK-N-AS, WFS1 transiently depleted SK-N-AS, WFS1 transiently depleted human NT2 cells and WFS1 stably depleted mouse Neuro2A cell lines, all showed significant depletion of WFS1 on protein and mRNA levels. In the four cell models, WFS1 depletion resulted in significant elevation of ER stress markers: BiP, CHOP, spliced XBP1, GRP94, ATF6a and HRD1 on protein and/or mRNA levels. These findings suggest that the neurodegeneration in WS is likely caused by increased ER stress in neuronal cells, analogous to the ER stress related diabetes previously described (Fonseca et al., 2011, Laybutt et al., 2007, Ozcan et al., 2006).

Furthermore, the enhanced ER stress was shown to be associated with activation of several apoptotic pathways: by showing increased levels of cleaved caspase-3, CHOP and BAX as well as significantly reduced levels of BCL-2 in WFS1 depleted cells in comparison to the control. The data also showed high levels of pro-apoptotic cells measured as DNA fragmentation by HCC in WFS1 stably depleted SK-N-AS cells. Moreover, the obtained data indicated that WFS1 depletion was associated with impaired cell cycle progression in neuroblastoma cells with significantly reduced levels of the cell cycle regulatory protein $p21^{cip1}$ in WFS1 depleted cells in comparison to the control.

This is the first study of WS in human neuronal cell lines; previously studies were conducted mainly on mouse or rat brain tissues (Takeda et al., 2001, Kato et al., 2008, Luuk et al., 2008, Kawano et al., 2009) and the WFS1-ATF6a complex formation was demonstrated in mouse Neuro2A cells (Fonseca et al., 2010). The WFS1 depleted neuronal cells showed similar abnormalities to those described in pancreatic beta cells with WFS1 depletion (Fonseca et al., 2005, Riggs et al., 2005, Yamada et al., 2006). The data suggest that enhanced ER stress is a common mechanism underlying both the neurodegeneration and pancreatic beta cell loss in WS. WFS1 was shown to play a role in regulating ATF6a transcriptional activity through HRD1-mediated ubiquitination and proteasome–mediated degradation of ATF6a protein (Fonseca et al., 2010). In agreement with these observations, the present study indicates a 3 to 4 fold increase in nuclear ATF6a levels in human neuroblastoma cell lines with reduced WFS1 expression (Figure 3.9C).

However, in contrast to their findings of suppressed HRD1 with absent WFS1, the present study shows that the expression of HRD1 was significantly increased in WFS1 depleted neuroblastoma (by 4 fold in comparison to the control, Figure 3.9C). The observations were consistent with the study conducted by Yamada and colleagues (2006) who observed increased levels of HRD1 in WFS1 depleted MIN6 cells. In addition, the study conducted by Yamamoto et al. (2008) showed that HRD1 is regulated by the IRE1-XBP1 pathway and activated in the presence of ER stress.

Previously, it has been shown that WFS1 deficient pancreatic beta cells are susceptible to ER stress mediated apoptosis (Fonseca et al., 2005, Riggs et al., 2005, Yamada et al., 2006). Apoptosis is an important mechanism to induce cell death that requires the activation of caspases and Bcl-2 family members to eliminate cells that cannot cope with ER stress.

The present study demonstrated increased levels of cleaved caspase-3 and the pro-apoptotic protein CHOP by immunoblotting in WFS1 depleted neuroblastoma cells, indicating that the caspase pathway of apoptosis was activated. Similarly, the study by Yamada and colleagues (2006) showed increased apoptosis in WFS1 depleted MIN6 cells by demonstrating increased expression of CHOP and cleaved caspase-3 by immunoblotting. In addition, the obtained data showed that the expression of the pro-apoptotic protein BAX was significantly enhanced and the expression of the anti-apoptotic protein Bcl-2 was significantly suppressed in WFS1 depleted neuroblastoma cell lines. These findings suggest that WFS1 plays a role in regulation of the Bcl-2 family of the apoptotic proteins. The role or the expression of the Bcl-2 family of the proteins has not been previously studied in Wolfram syndrome. Furthermore, HCC data showed significantly increased numbers of apoptotic cells in WFS1 depleted cells in comparison to the control; this technique measures early apoptotic cells rather than late apoptotic or dead cells. Overall, these findings suggest that decreased WFS1 expression leads to a final common pathway of apoptosis in these cells, presumably mediated by irresolvable ER stress.

Yamada et al. (2006) reported cell cycle arrest and impaired cell cycle progression in WFS1 deficient islets. The data presented in this chapter revealed that the KD1 cell line became tetraploid after WFS1 depletion with a marked accumulation of cells in the G1 phase of the cell cycle and elongation of the G1 phase at the expense of the G2 phase. The observed cell cycle disturbances and the development of the tetraploidy are thought to be associated with WFS1 depletion. These results also suggest that the tetraploidy induced a G1 phase arrest associated with the high level of ER stress and apoptosis in these cells. The QPCR results showed that the expression of CHOP was increased by 150% in this cell line, and only 50% in KD2 and KD3; this could clearly influence the cell cycle behaviour in comparison to KD2 and KD3. Studies suggest that adaptation via endopolyploidy can provide protection from stress and thus increase cell survival (Lee et al., 2009). Therefore, it was supposed that the development of tetraploidy in KD1 was a result of the increased ER stress. However, it is also possible that this tetraploidy was caused by chance; for instance random integration of plasmid to the cell genome, which impaired in KD1 a region/gene involved in the control of ploidy. In contrast to the KD1 cell line, the KD2 cell line showed an accumulation of cells in G2 and an elongated G2 time (31 hours, table 3.1). The population doubling time of the cells in this knockdown was significantly lower than the control.

The data presented in this study showed that WFS1 depleted cells displayed significantly reduced expression of $p21^{cip1}$ in comparison to the control cells. Furthermore, $p21^{cip1}$ expression appeared to be inversely associated with apoptosis and cell cycle impairment; suggesting that cells retaining their $p21^{cip1}$ expression were protected against apoptosis and cell cycle disturbances.

However these are preliminary findings that need to be expanded and confirmed in different cell models. These findings are in contrast to the findings by Yamada et al. (2006) who reported p53-independent increase of $p21^{cip1}$ in WFS1 depleted cells associated with the inhibition of the G2 phase of the cell cycle. However, the current findings are supported by other studies showing that chronic or severe UPR results in down-regulation of $p21^{cip1}$ and increased levels of CHOP (Mihailidou et al., 2010).

Studies have shown that p21 expression protects cells from apoptosis in response to DNA damage or stress stimuli by inducing cell cycle arrest. Similarly, overexpression of p21 has shown protective effects in colorectal cancer cells in response to gamma radiation induced apoptosis. This protein has been shown to shift the balance between survival and apoptosis by regulating apoptosis proteins such as JNK and caspase-3. Therefore, p21 expression is thought to play a vital role in determining a cell's fate to adapt or to undergo apoptosis in response to cellular insults, due to its downstream role in many signal transduction pathways. Similarly, the role of $p21^{cip1}$ is well established in regulation of the G1 checkpoint (Warfel et al., 2013) and its implications in the G2/M checkpoint have also been reported (Dulić et al., 1998). P21 is suggested to play a role in the G2/M checkpoint by promoting a transient pause late in G2 phase, where it has been shown to co-localise with cyclin B1 (Dulić et al., 1998). The study by Dash (2005) reported that phosphorylation of p21 specifically at the G2/M checkpoint has a role in the assembly and activation of the cyclin B1-Cdc2 kinase, a crucial process for cell cycle progression (Dash and El-Deiry, 2005). The preliminary data presented in this study implies that induction of p21 may provide protection against apoptosis induced by WFS1 depletion. In addition, increased

p21 expression may inhibit or delay G2M progression of the cell cycle, perhaps allowing cells to repair before mitosis.

To summarise, four cell models of Wolfram syndrome were developed in human and mouse neuronal cells. The experimental approach used was immunoblotting, real time PCR and High Content Cytometry which provide very sensitive and reproducible data. The cell models showed enhanced ER stress associated with increased apoptosis and impaired cell cycle progression. The following chapters will focus on treatment of WS by addressing ER stress, apoptosis and cell cycle kinetics by molecular and chemical chaperones as well as therapeutic agents such as sodium valproate.

Chapter Four: WFS1 stabilises the beta1 subunit of the sodium pump and the V1A subunit of the proton pump

The data presented in this chapter is published in Human Molecular Genetics:

(Gharanei et al., 2012)

4.1 Introduction

The sodium-potassium ATPase beta1 subunit (ATP1B1) was previously shown to be a molecular partner of Wolframin and WFS1 deficiency was shown to result in reduced expression of ATP1B1 (Zatyka et al., 2008). The authors used Yeast Two-Hybrid analysis to demonstrate that the C-terminal domain of WFS1 binds to the C-terminal domain of ATP1B1(Zatyka et al., 2008). On the other hand, a recent study by Hatanaka and colleagues (2011) showed that WFS1 is located to the insulin secretory granule membranes and lack of functional WFS1 results in disruption of intra-granular acidification. The secretory granules are acidified through a proton gradient established and maintained by coordination between H^+ vacuolar type ATPase (V-ATPase), ion channels and transporters. To understand the possible role of WFS1 in regulation of the sodium and the vacuolar H^+ proton pump, it is necessary to review the structure and functions of these two ion pumps.

The vacuolar system in the eukaryotic cell serves as a communication system between the various compartments and between the interior and exterior of the cell. The vacuolar system therefore plays a crucial role in the brain where intracellular communication is complex. One such example is the cycle of neurotransmitter release, storage, re-uptake and accumulation in specific vesicles. Two ATP-dependent ion pumps: the Na^+/K^+-ATPase and the vacuolar H^+ ATPase (V-ATPase) are the main energy providers for these cellular processes (Toei et al., 2010, Hinton et al., 2009, Forgac, 2007). These ion pumps belong to two very distinct families of ATPases and have different structures and functions. The Na^+/K^+-ATPase generates an ionic and osmotic gradient to drive the processes at the plasma membrane, whereas the vacuolar H^+-V-

ATPase energises the vacuolar system by generating proton motive force. The sodium pump generates Na^+ and K^+ electrochemical gradients by using energy from ATP hydrolysis. The concentration of sodium ions (Na^+) inside the cell is lower than outside and the majority of uptake systems are driven by the Na^+ concentration gradient across the plasma membrane (Scheiner-Bobis, 2002, Horisberger, 2004). The main example of this system is the re-uptake of the neurotransmitters as well as glucose and amino-acid transporters. The V-ATPase also utilises energy from ATP hydrolysis to generate an electrochemical gradient that is used for various secondary processes including accumulation of neurotransmitters in synaptic vesicles (Beyenbach and Wieczorek, 2006, Nelson, 1991). The sodium potassium and the vacuolar H^+ ATPases therefore generate ion, pH and electrochemical gradients to energise the presynaptic neurotransmitter cycle of release, re-uptake and accumulation inside the internal vesicles of cells.

4.1.1 The sodium potassium ATPase

The sodium potassium pump is a heterodimer consisting of a catalytic alpha-subunit which has three isoforms and a regulatory beta subunit (Nishi and Forgac, 2002a, Tokhtaeva et al., 2009, Nishi and Forgac, 2002b). It is responsible for maintaining the Na^+ and K^+ gradients across the plasma membrane. A well-functioning sodium pump therefore regulates the membrane potential, nutrition uptake, intracellular volume and pH. The membrane potential is maintained by the active transport of the ions against the concentration gradient by the pump, with three sodium ions pumped out of the cell for every two potassium ions pumped in at the cost of energy expense from ATP hydrolysis. Excitable cells such as neurons depend on this pump for responding to

transmitting impulses and generating action potentials. In neurons, the Na^+/K^+ ATPases are responsible for about two thirds of the total energy expenditure (Köksoy, 2002).

The Na^+/K^+ ATPase was discovered by the Danish scientist Skou in 1957, earning him a Nobel Prize in 1997. The sodium pump belongs to the family of the P-ATPases. The name is attributed to the mechanism whereby energy from ATP hydrolysis changes the conformation of the enzyme in order to transport ions. P-ATPases are structurally and functionally different from the V-ATPases and F-ATPases. The P-ATPase family consists of two groups of enzymes: the single subunit enzymes (alpha) such as the sarco-endoplasmic Ca^{2+}-ATPase and the two subunit enzymes (alpha and beta) such as the Na^+/K^+ ATPases and the gastric H^+/ K^+ ATPases.

Figure 4.1 shows a schematic structure of the sodium pump; the alpha and the beta subunits of this enzyme are required for its enzymatic activity. The alpha subunit is composed of 1018 residues (110kDA) and the beta subunit is about 300 residues (33kDA that migrate to 55kDA). Alpha is the catalytic subunit containing binding sites for ions, ATP and transient phosphorylation sites. This protein consists of 10 transmembrane domains and 2 large intracellular loops. There are four defined alpha isoforms (alpha 1-4). Alpha1 is expressed ubiquitously; Alpha 2 is expressed in skeletal muscle, adipocytes and brain cells. Alpha 3 is mainly expressed in nerves and brain cells and isoform 4 is found only in the testis.

The beta subunits of the sodium pump consist of one transmembrane domain, a short cytoplasmic tail and a large extracellular glycosylated segment. The precise function of these glycoproteins is

not fully understood, although their presence and heterodimerisation with the alpha subunit are crucial for the proper expression and functioning of the enzyme (Tokhtaeva et al., 2009, Köksoy, 2002). There are three known isoforms of the beta subunit of the sodium pump. Beta1 is ubiquitously expressed, Beta 2 is expressed in glia and brain cells and Beta 3 is expressed only in the skeletal muscles. The beta subunits play an important role in the formation of the binding sites for ligands and modulation of the ion transport function of the pump (Jaunin et al., 1993, Jaisser et al., 1994).

According to studies, the alpha and the beta subunits are present in equimolar amounts in the isolated Na^+/K^+ ATPase. The mature sodium pump is located in the plasma membrane. During maturation however, it is transiently present in the ER. Studies have shown that the beta subunit makes a direct contact with the alpha subunit resulting in stabilisation of the alpha subunit and assisting in the transport of the sodium pump from the ER to the plasma membrane. Unassembled subunits are retained in the ER and degraded rapidly (Tokhtaeva et al., 2009, Beggah et al., 1996). The majority of mutations in WS have been found in the C-terminal domain of WFS1. Since the interaction of the ATP1B1 was also shown with the C-terminus of WFS1, it is possible that mutations in this region cause disruption of this interaction. This disruption may contribute to the hearing loss seen in WS and LFSNHL families with *WFS1* mutations due alterations of potassium transport in the inner ear (Rigoli et al., 2010).

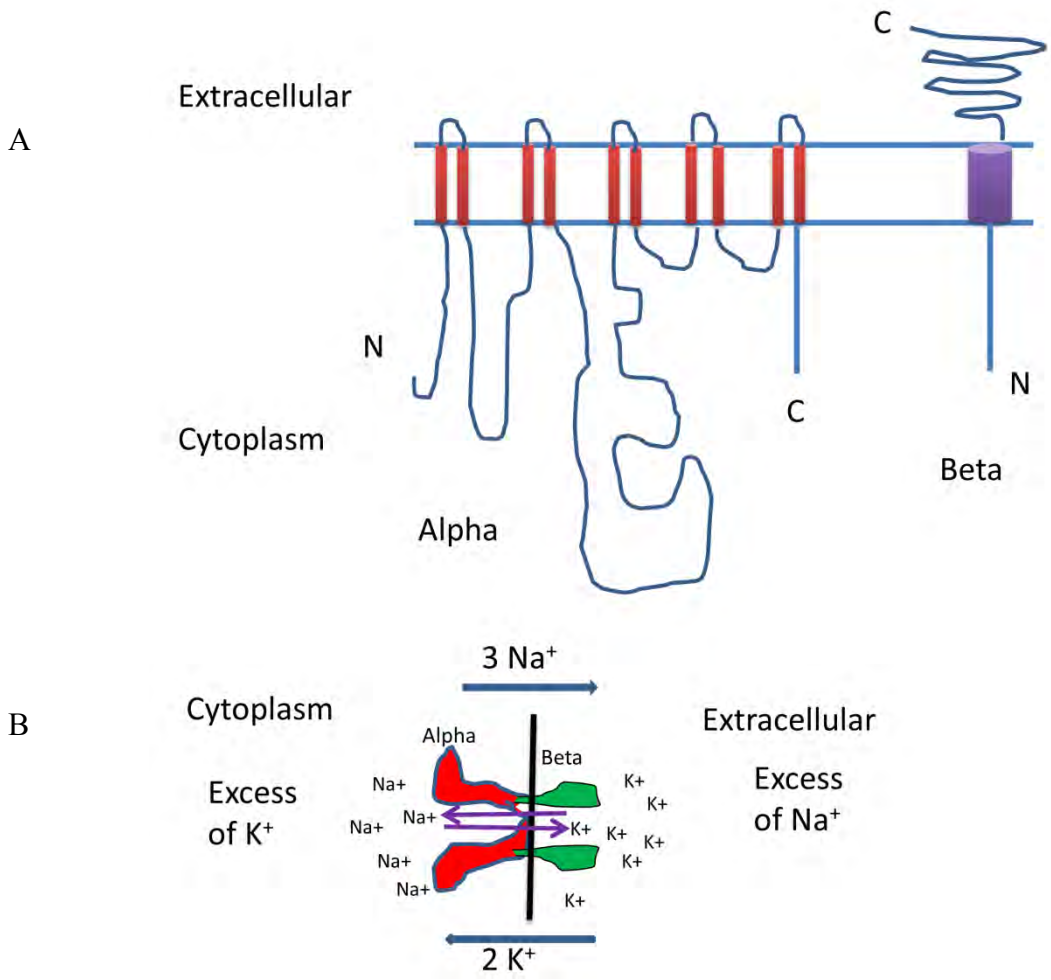

Figure 4.1: Structure and function of the sodium potassium ATPase

A: The sodium pump consists of a catalytic Alpha and a regulatory Beta subunit in 1:1 ratio. B: Mechanism of action of the sodium pump; active transport of the Na^+ and K^+ ions in opposite direction against the concentration gradient on the expense of ATP hydrolysis. 3 Na^+ ions from the intracellular space are exchanged with $2K^+$ ions from the extracellular medium. Adapted from (Köksoy, 2002)

4.1.2 The Vacuolar H^+ ATPase

The vacuolar (H^+)-ATPases (V-ATPases) are a family of ATP-dependent proton pumps located at the cellular membranes of a variety of eukaryotic cells. They function in generating electrochemical potential differences of protons across biological membranes through transport of H^+. The V-ATPases are large multi-subunit enzymes consisting of a hydrophobic membrane channel sector (V0) and a peripheral hydrophilic catalytic complex (V1). Figure 4.2 represents a schematic diagram of V-ATPase (Toei et al., 2010). The V1 domain contains 8 different subunits (A-H) from which the A and the B subunits are present in triplicates per complex forming a hexameric ring. The integral V0 domain contains 6 different subunits (a,c,c″,d,e and Ac45) in humans (Nishi and Forgac, 2002a, Tokhtaeva et al., 2009, Forgac, 2007, Nishi and Forgac, 2002b). The V1 subunits are mainly involved in ATP hydrolysis whereas the V0 subunits are responsible for translocation of protons. In mammalian cells, the V-ATPase subunits exist in several isoforms which have tissue specific expression. The catalytic site of the V-ATPase is located at the interface of A and B subunits where ATP hydrolysis takes place.

The two domains of the V-ATPases are connected by one central and three peripheral stalks. The central stalk is composed of subunits D, F and d which extend from the proteo-lipid ring up through the centre of the A3B3 hexameric head. The three peripheral stalks are composed of subunits C, E, G and H of the V1 domain and the ATP6V0a of the V0 domain. This proton pump functions by a rotary mechanism where the rotation of the central stalk and the proteo-lipid subunits relative to subunit V0a are driven by the ATP hydrolysis at the catalytic site of the V1 domain (Forgac, 2007, Toei et al., 2010).

Fully functioning vacuolar proton pumps are crucial for every eukaryotic cell since they are involved in basic cellular mechanisms. V-ATPases function in several organelles including endosomes, lysosomes, Golgi membranes, several types of secretory granules and clathrin-coated vesicles (Nishi and Forgac, 2002b). The V-ATPases establish an acidic luminal proton gradient within these compartments, which is used to drive coupled transport of small molecules and ions, receptor mediated endocytosis and fusion of certain organelles with the plasma membrane (Nelson, 2003). For example, the role of V-ATPases in receptor mediated endocytosis is to activate the release of internalised ligands from their receptors by providing the necessary acidic endosomal pH. The acidic pH generated by the V-ATPases is also required in the formation of endosomal carrier vesicles which are essential for endocytotic processes. Similarly, the intracellular traffic of newly synthesised lysosomal enzymes from Golgi to lysosomes is performed by the acidification of late endosomes by the V-ATPases. Thus the V-ATPases function to generate a pH gradient across the membrane of vesicles and organelles involved in the secretory pathway as an interior acidifier. They carry out ATP-dependent proton transport from cytoplasm to the extracellular compartment (Sun-Wada et al., 2006, Hinton et al., 2009).

The V-ATPases within the secretory vesicles promote the activity of acid proteases that are involved in the processing of prohormones to their mature forms. For example, the processing of proinsulin to insulin in the pancreatic beta cells is regulated by the acidification of secretory vesicles. The V-ATPases of the secretory vesicles also drive the transport of small molecules such as neurotransmitters by providing the required membrane potential or the pH gradient. For instance, the luminal positive membrane potential in the synaptic vesicles of the glutamatergic

neurons is generated by the V-ATPases to drive the uptake of negatively charged glutamate into the vesicles. In contrast, the uptake of neurotransmitters in the synaptic vesicles containing norepinephrine utilises a pH gradient via a proton coupled antiporter (norepinephrine/H^+). In short, the V-ATPases directly energise all neurotransmitters uptake by providing the required pH gradient. Therefore, acidification of secretory vesicles is very important for neuronal and endocrine functions (Sun-Wada et al., 2006, Hinton et al., 2009).

The activity of V-ATPases is regulated by the reversible dissociation of the complexes into the V1 and V0 domains. This process was first characterised in yeast cells and later confirmed in mammalian cells. In both yeast and in mammalian cells this dissociation occurs in response to glucose deprivation (Kane, 2006, Beyenbach and Wieczorek, 2006). ATP hydrolysis and proton translocation are silenced in the separated V1 and V0 domains following dissociation. Dissociation and reassembly of the two V-ATPase domains are independently regulated processes. The 90 amino acid non-homologous region of the V1A subunit is shown to be important for the reversible dissociation of the complex. EM images of the V1 complex reveal that this non-homologous region is located as an insert approximately one third away from the N-terminal end of the V1A subunit. It appears to be sticking out like an "ear" from the V1A subunit in the A3B3 hexameric head (Wilkens et al., 1999). Mutations in this region of the V1A subunit have been shown to block the dissociation of the complex upon glucose depletion without affecting the catalytic activity (Shao et al., 2003).

This chapter will focus on the role of WFS1 in expression and stability of these two ion pumps subunits in Wolfram syndrome. The hypothesis was that Wolframin depletion results in reduced expression of beta1 subunit of sodium pump in neuronal cells, similarly to WFS1 depleted pancreatic cells and fibroblasts from Wolfram patients. Moreover, Wolframin is expressed on neurosecretory granules analogous to insulin secretory granules; it interacts with subunits of a proton pump and affects their expression. This may affect the acidification of secretory granules in neurons in similar way as it accounts for the reported defects in acidification in insulin secretory granules.

.

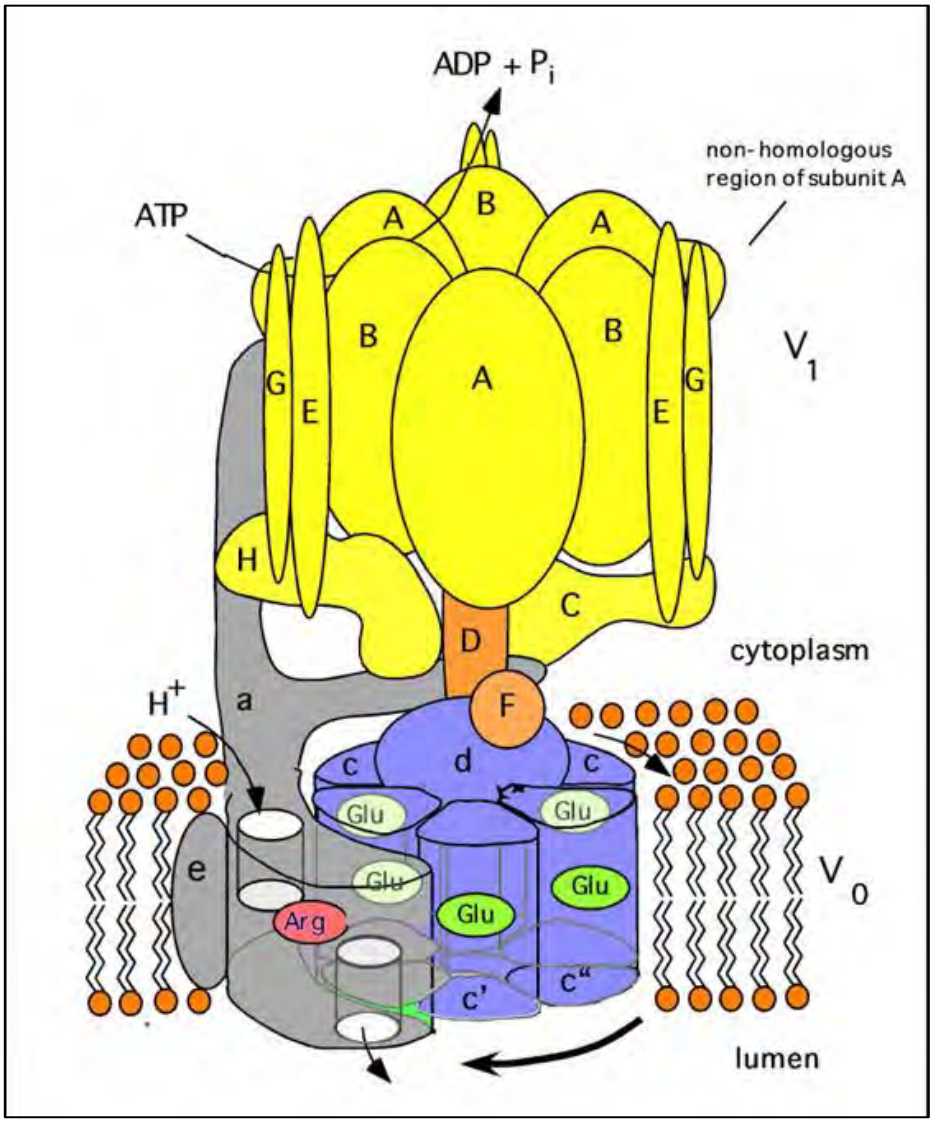

Figure 4.2: Schematic structural model of mammalian H^+ V- ATPase

The V-ATPase complex consists 14 subunits organised into two structurally and functionally distinct domains: a peripherally oriented ATP hydrolysing V_1 domain (A-H subunits) and a membrane-associated proton translocating V0 domain (*a*, *c*, *c″*, *d*, *e,* and Ac45). The V_1 and V_0 domains are joined by a central rotor (subunits D, F, *d*) and three peripheral stators composed of (subunits C, E, G, H, and *a*). The V_1 A_3B_3 hexameric ring contains the ATP hydrolytic sites. The proton translocation is made possible by the two hemi-channels and an arginine residue at the V0a subunit (Toei et al., 2010).

4.2 Aims

The aims of this study were as follows:

1. To investigate the expression of the beta1 subunit of the sodium pump and the V1A subunit of the proton pump in WFS1 depleted neuronal cells.
2. To investigate the role of WFS1 in degradation of ATP1B1 and ATP6V1A
3. To investigate possible co-localisation between V1A and WFS1 in wild type neuroblastoma cell lines by immunofluorescence and electron-microscopy
4. To investigate possible interaction between V1A and WFS1 proteins in both over-expression and endogenous systems.

4.3 Results

4.3.1 Expression of ATP1B1 and ATP6V1A in human neuronal cell lines

The study conducted by Zatyka and colleagues in 2008 showed that the Na^+/K^+ ATPase beta1 subunit (ATP1B1) is a molecular partner of Wolframin and WFS1 deficiency results in reduced expression of ATP1B1 (Zatyka et al., 2008). More recently, the study conducted by Hatanaka and colleagues (2011) reported that WFS1 is additionally located in the secretory granules of pancreatic beta cells and plays a role in granule acidification. Secretory granules are acidified through a proton gradient established and maintained by H^+ vacuolar type ATPase (V-ATPase). In the light of these studies, it was decided to measure the expression of the beta1 subunit of sodium pump (ATP1B1) and V1A subunit of the proton pump (ATP6V1A) in WFS1 stably depleted SK-N-AS, WFS1 transiently depleted NT2 and SK-N-AS cells as well as in WFS1 stably depleted mouse neuro2A cell lines. The reason for choosing the V1A subunit was based on the literature as this subunit is the catalytic subunit of the proton pump and plays a central role in its expression and function (Toei et al., 2010).

The data presented in this chapter showed that the levels of ATP1B1 were significantly decreased in WFS1 depleted human neuronal cells. The results presented in Figure 4.3 (top panel) show that the expression of ATP1B1 in WFS1 stably depleted neuroblastoma cells was decreased by 54±4%, 64±8% and 51±7% in KD1-3 respectively ($n=6$, $p<0.05$, Mean±SEM). In WFS1 transiently depleted neuroblastoma cells the levels of ATP1B1 were decreased by 68±10% in KDA and by 41±8% in KDB ($n=4$, $p<0.05$, Figure 4.4A) while in WFS1 transiently depleted neuronal NT2 cells the level of ATP1B1 was decreased by 36±5% and 50±14% in KDC and in

KDD (n=4, $p<0.05$, Figure 4.4B). To verify the findings in animal cell model, the expression of ATP1B1 was also measured in WFS1 stably depleted mouse neuro2A cell lines by immunoblotting. The data presented in Figure 4.5 showed that there was a significant decrease in the levels of ATP1B1 by 78±18% and 73±8% in KDX and KDY respectively (n=4 and $p<0.05$).

Similarly, the levels of the V1A subunit of the proton pump (ATP6V1A) were also significantly decreased in WFS1 depleted neuronal cells. Figure 4.3, (2nd panel) shows that the levels of ATP6V1A protein were decreased in WFS1 stably depleted neuroblastoma clones KD1-3 by 66±12%, 57±18% and 67±1% respectively (n=3, $p<0.05$). These findings were confirmed in both transiently WFS1 depleted models. In WFS1 transiently depleted neuroblastoma cells the ATP6V1A protein levels were decreased by 38±7% and 42±6% in KDA and KDB (n=3 and $p<0.05$, Figure 4.4A). In WFS1 transiently depleted NT2 cells the expression of ATP6V1A protein was decreased by 45±14% and 41±5% in KDC and in KDD (n=3, $p<0.05$, Figure 4.4B). Overall, these results suggest that WFS1 plays a role in the expression of both ion pump subunits.

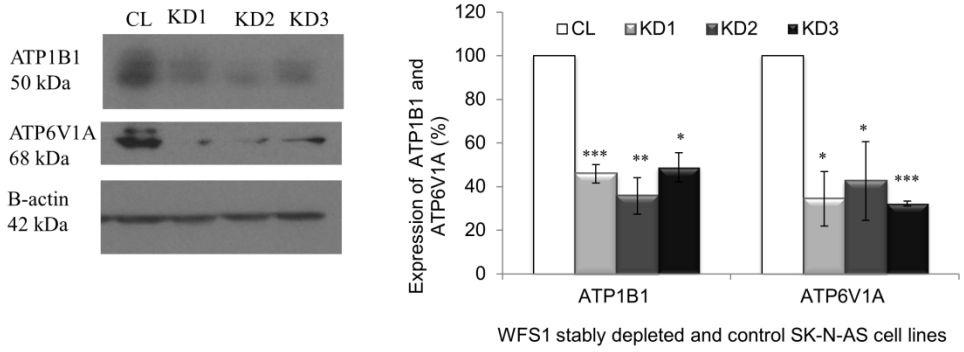

Figure 4.3: Protein expression of ATP1B1 and ATP6V1A in WFS1 stably depleted SK-N-AS cell lines

Immunoblot analysis of ATP1B1 and ATP6V1A proteins using lysates from WFS1 stably depleted human SK-N-AS cells in comparison to control. Bar chart -quantification of WB, T-test: *$p<0.05$, **$p<0.01$, and ***$p<0.001$, ATP1B1 $p<0.001$, $p<0.01$ and $p<0.05$ for KD1-KD3 respectively, n=6 ATP6V1A: $p<0.05$ for KD1 and 2, $p<0.001$ for KD3, n=3. n= number of independent runs using at least 3 independently prepared protein extracts.

A

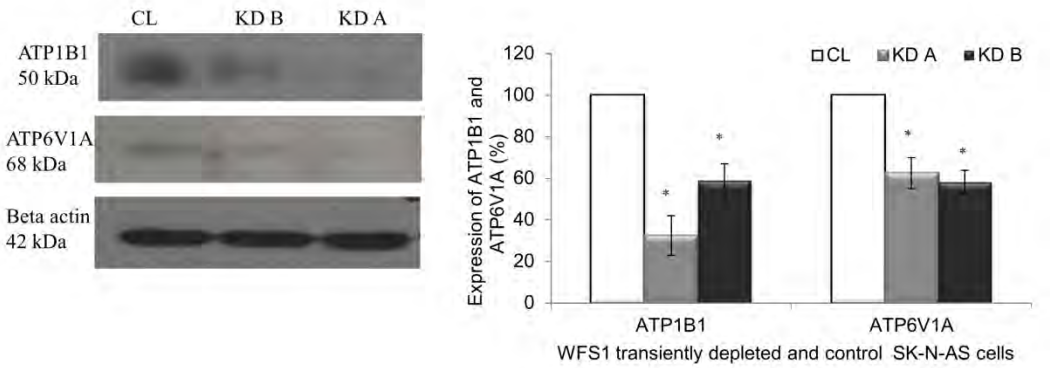

B

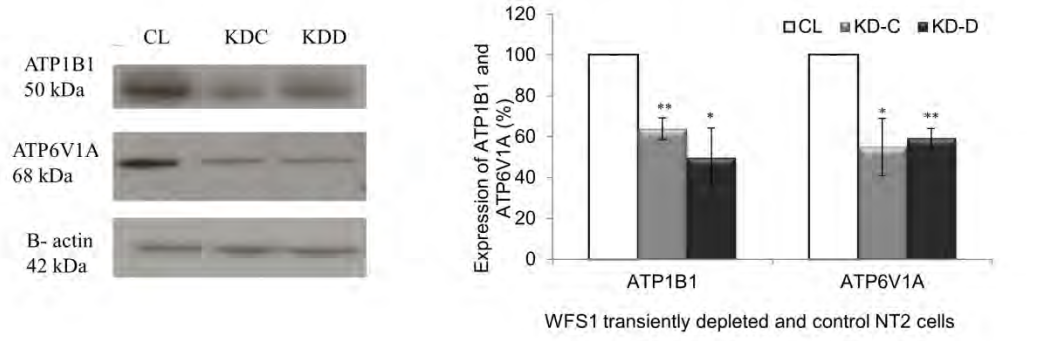

Figure 4.4: Protein expression of ATP1B1 and ATP6V1A in WFS1 transiently depleted neuronal cells

A: Immunoblot analysis of ATP1B1 and ATP6V1A proteins using lysates from WFS1 transiently depleted human SK-N-AS cells in comparison to control. Bar chart -quantification of WB, T-test: *p<0.05, **p<0.01, and ***p<0.001, p<0.05 for both proteins for both KDA and KDB v control. B: immunoblot analysis of ATP1B1 and ATP6V1A proteins using lysates from WFS1 transiently depleted human NT2 cells. Bar chart -quantification of WB, T-test: ATP1B: p<0.01 and p<0.05 for KDC and KDD respectively (n=4). ATP6V1A: p<0.05 and p<0.01 for KDC and KDD (n=3). n= number of independent runs using at least 3 protein extracts from independently silenced cells.

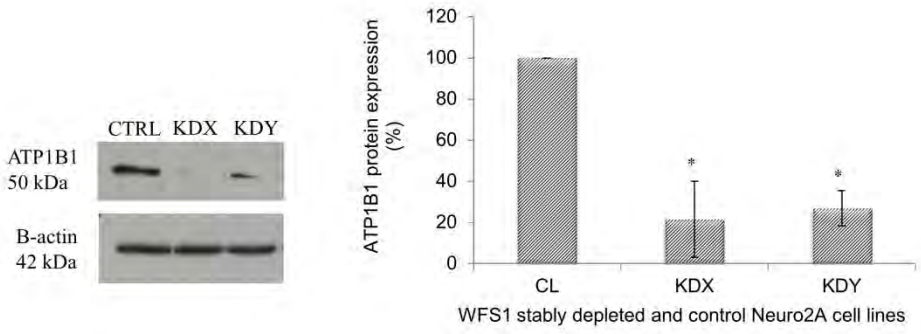

Figure 4.5: Protein expression of ATP1B1 in WFS1 stably depleted mouse neuro2A cell lines

Immunoblot analysis of ATP1B1 using lysates from WFS1 stably depleted mouse neuro2A cells in comparison to control. Bar chart -quantification of WB, T-test: *$p<0.05$, **$p<0.01$, and ***$p<0.001$, $p<0.05$ for KDX and KDY respectively (n=4).

4.3.2 Specificity of the effect of WFS1 depletion on the sodium and proton pump subunits

After observing reduced levels of beta1 subunit of the sodium pump and V1A subunit of the proton pump in WFS1 depleted cells in different cell models, it was decided to assess whether WFS1 is necessary for the expression of other subunits of these pumps. Therefore, the expression of the alpha subunit of the sodium (ATP1A1) was investigated in WFS1 stably depleted neuroblastoma cell lines in comparison to the control. The data presented in Figure 4.6 showed no significant difference in the levels of the alpha subunit of sodium pump in WFS1 depleted cells in comparison to the control. ATP1A1 levels were measured as 98±17% and 91±9% in KD2 and KD3, respectively (n=3 and p=NS).

Moreover, the expression of two more H^+ proton pump (VATPase) subunits: the ATP6V1C1 and the ATP6V0D2 subunits were measured in WFS1 stably depleted SK-N-AS cells by Dr Astuti. The data presented in Figure 4.6 showed that expression of ATP6V1C1 was slightly increased by 12.24%±3.3 in KD2 and 16.49%±2.9 in KD3 (n=3 and $p<0.05$) and no significant differences were observed in the expression of ATP6V0D2 subunit in both KD2 and KD3 cell lines in comparison to control.

Taken together these data suggest that the effects of WFS1 depletion could be specific for the beta1 subunit of sodium pump and V1A subunit of the H^+ proton pump since no significant decreases were observed in the expressions of ATP1A1, ATP6V1C1 and ATP6V0D2.

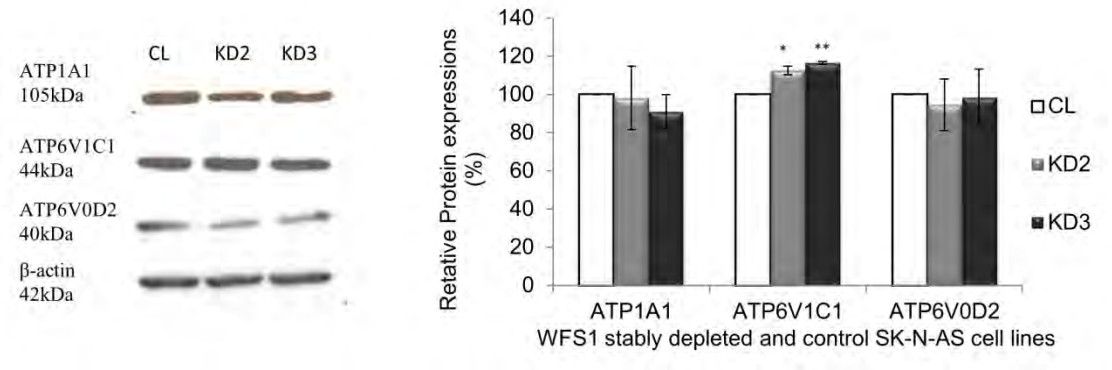

Figure 4.6: Protein expression of ATP1A1, ATP6V1C1 and ATP6V0D2 in WFS1 stably depleted SK-N-AS cells

Immunoblot analysis of ATP1A1, ATP6V1C1 and ATP6V0D2 proteins using lysates from WFS1 depleted human SK-N-AS cells in comparison to control. Bar chart -quantification of WB, T-test: ATP1A1 p=0.89, p=0.33 in KD2 and KD3 respectively, n=4. T-test: ATP6V1C1 p=0.022 and p=0.007 in KD2 and KD3 respectively. T-test: ATP6V0D2, p = 0.673 and 0.908 in KD2 and KD3 respectively. n= number of independent runs using at least 3 independently prepared protein extracts. In collaboration with Dr Astuti.

4.3.3 Role of WFS1 in stability of ATP1B1 and ATP6V1A

After observing specific effect of WFS1 on the expression of beta1 subunit of the sodium pump and V1A subunit of the proton pump, it was hypothesised that WFS1 may be necessary for the stability and maturation of these two subunits during their assembly in the ER. To investigate this hypothesis, a protein stability assay was performed in which the degradation rate of ATP1B1 or ATP6V1A subunits in WFS1 depleted cells was compared to WFS1 positive control cells. The protein translation inhibitor (Cycloheximide, CX) was used to investigate the stability of ATP1B1 and ATP6V1A in WFS1 stably depleted and control neuroblastoma cells. First of all, the toxicity of CX (10-90µg/mL) was assessed in human neuroblastoma cell line by HCC. The data presented in Figure 4.7 showed that treatment with up to 90µg/mL CX for 6 hours was not toxic to neuroblastoma cells. This figure shows that the number of cells and the percentage of pro-apoptotic cells did not change significantly with CX treatment within these concentrations.

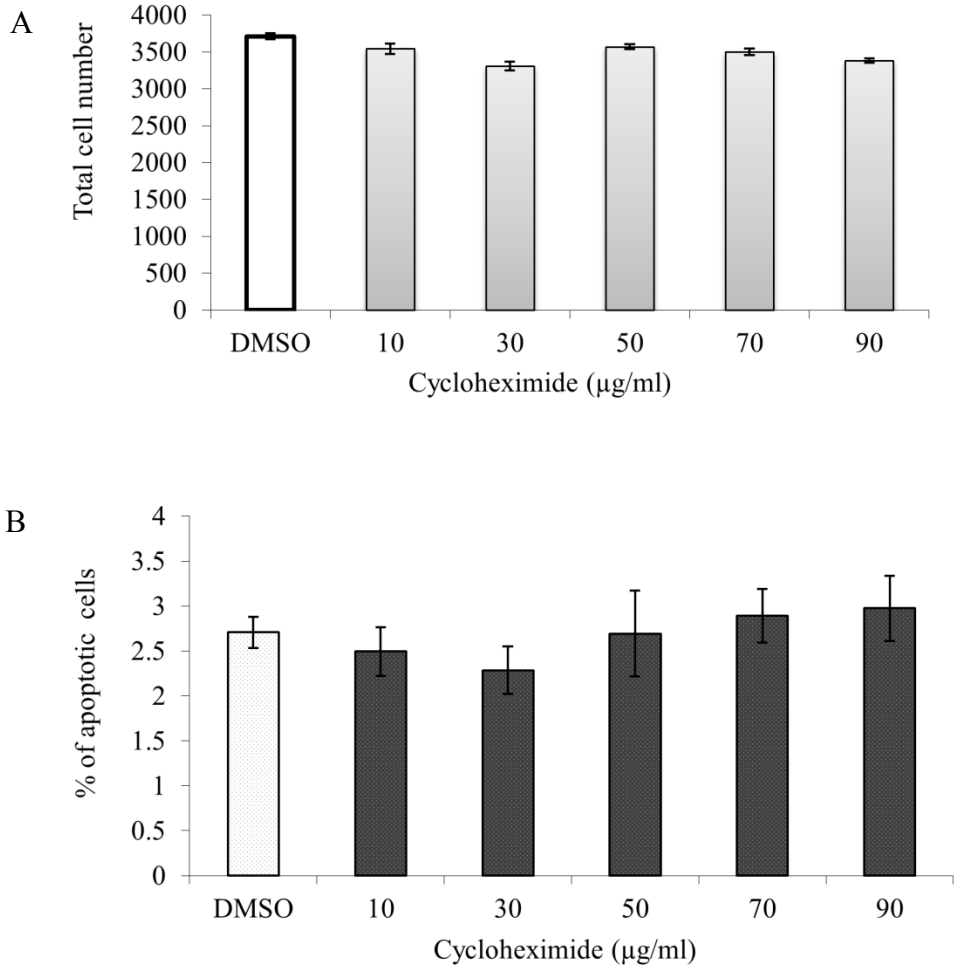

Figure 4.7: Toxicity assessment of cycloheximide to human neuroblastoma cell lines

SK-N-AS cells were grown for 24h and incubated with various concentrations of CX for 6 hours. At the end of incubation, cells were fixed and stained with PI as indicated in Materials and Methods before being scanned with the Acumen eX3 cytometer. (A) Total cell number at different concentrations of cycloheximide. (B) The percentage of apoptotic cells with CX treatment.

Accordingly, the cells were treated with 50μg/mL CX and harvested in RIPA buffer for immunoblotting at two hour intervals over 6 hours. The data presented in Figure 4.8A and B show that both proteins (ATP1B1 and ATP6V1A) were degraded much more rapidly in the WFS1 depleted cells in comparison to the control cells. For each clone the expression after CX treatment at each time point was compared to time zero. In WFS1 depleted cells, ATP1B1 was more rapidly degraded in comparison to the control where ATP1B1 seemed to be stable over a 6 hours time course (the 15% decrease after 6h was not statistically significant, Fig 4.8A). Two hours after CX treatment, there was only 70±9% (Mean±SEM, p=0.0019) ATP1B1 remaining in KD1, 83±8% (p=0.018) in KD2 and 93±2% (p=0.016) in KD3 in comparison to time 0. Four hours post CX treatment, there was only 56±9% (p=0.0035) ATP1B1 remaining in KD1, 47±13% (p=0.018) in KD2 and 71±4% (p=0.016) in KD3. Finally, after six hours of CX treatment there was only 55±6% (p=0.0035) ATP1B1 expression remaining in KD1, 45±6% (p=0.0021) in KD2 and 44±22% (p=0.0023) in KD3 in comparison to time 0 (n>3). These results show that the degradation rate is significantly different between WFS1 wt and depleted clones.

Similarly, the degradation rate of ATP6V1A in WFS1 depleted neuroblastoma cells was also more rapid in comparison to the control, in which expression was stable over a 6 hour time course and showed 101±22% after 6h in comparison to time 0, (n=3, p=NS, Figure 4.8B). Two hours after CX treatment, there was 75±2% ($p=9.8x10^{-04}$) of ATP6V1A remaining in KD1, 57±9% (p=0.013) in KD2 and 67±13% (p=0.032) in KD3 in comparison to time 0. At four hours, there was 42±3% ($p=2.4x10^{-04}$) ATP6V1A remaining in KD1, 43±13% (p=0.005) in KD2, and 63±12% (p=0.035) in KD3, whereas after 6 hours treatment, there was only 18±2% ($p<4x10^{-05}$)

in KD1, 30±11% ($p=0.005$) in KD2 and 49±3% ($p=2.0x10^{-04}$) in KD3 in comparison to time 0 ($n = 4$). Overall, this data suggests that WFS1 may be necessary for the stability of both ATP1B1 and ATP6V1A during their maturation in the ER.

A

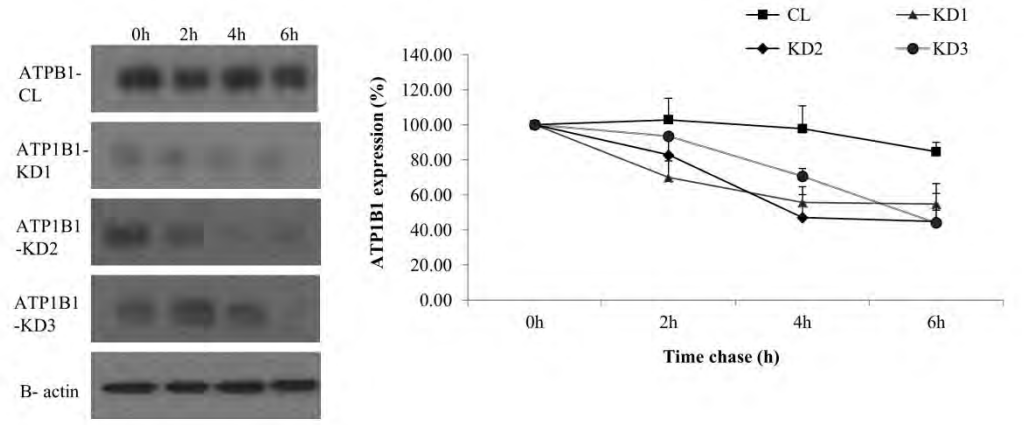

B

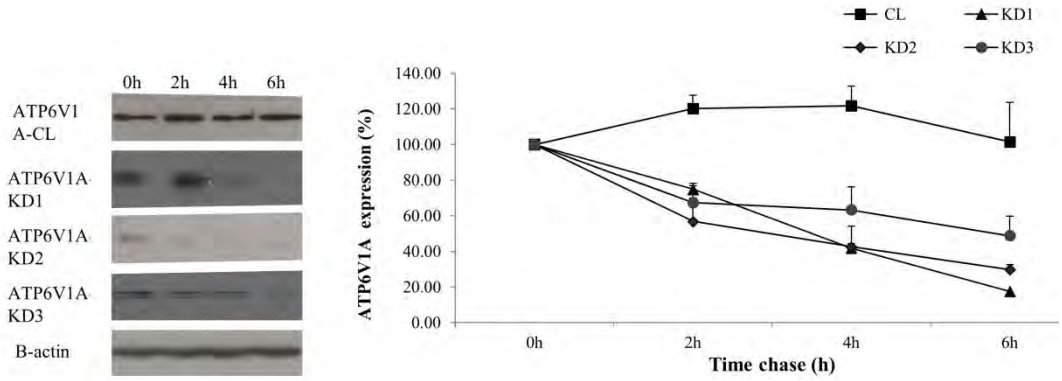

Figure 4.8: Degradation rate of ATP1B1 and ATP6V1A

A: Immunoblot analysis of beta1 subunit of sodium pump and beta actin showing expression of ATP1B1 at 0, 2, 4 and 6 hours after treatment with 50µg/mL of cycloheximide - representative experiment in WFS1 depleted stable clones. Each time point is compared to time zero. Immunoblot quantification: T-test ATP1B1 levels at 2, 4, 6 hours after treatment versus time 0: CL p=NS, n=4; KD1 $p<0.01$, n=4; KD2 $p<0.05$, n=4; KD3 $p<0.05$, n=3.
B: Immunoblot analysis of V1A subunit of vesicular proton pump and beta actin showing expression of ATP6V1A at 0, 2, 4 and 6 hours after treatment with 50µg/mL cycloheximide-representative experiment. Quantitative comparison of ATP6V1A degradation rate in WFS1 depleted stable clones. Each time point is compared to time zero. T-test: V1A levels at 2, 4, 6 hours after treatment versus time 0. CL: p= NS, n=3; KD1: $p<0.001$, n=4; KD2: $p<0.05$, n=4; KD3: $p<0.05$, n=4.

4.3.4 Co-localisation and interaction of WFS1 and ATP6V1A

The study by Zatyka (2008) showed an interaction between the WFS1 and the beta1 subunit of the sodium pump. Since the expression of both B1 and V1A subunits depend on the presence of WFS1 and both proteins are rapidly degraded in absence of WFS1, it was hypothesised that V1A subunit of V-ATPase may interact with WFS1 in a similar manner to beta1 subunit for sodium pump. First of all, the co-localisation of WFS1 with ATP6V1A, and with the vesicular associated membrane protein (VAMP) was investigated by immunofluorescence microscopy. The co-localisation with the ER marker PDI was used as a positive control since this was shown by several studies (Philbrook et al., 2005, Inoue et al., 1998, Takeda et al., 2001) and the mitochondrial marker ERAB was used as a negative control as no colocalisation was shown between WFS1 and mitochondrial markers (Takeda et al., 2001). The data presented in Figure 4.9 showed co-localisation between WFS1 and VAMP (Figure 4.9A), and WFS1 and ATP6V1A (vesicular proton pump, Figure 4.9B) by confocal microscopy. Additionally, the co-localisation of WFS1 was confirmed with the ER protein PDI (Figure 4.9C) and no co-localisation was observed between WFS1 and the mitochondrial marker ERAB (Figure 4.9D).

Moreover, the subcellular distribution of WFS1 was investigated in human neuroblastoma cells by electron microscopy (Figure 4.10) in collaboration with Prof Sik. Silver intensified immunogold particles were absent in the nucleus, and abundant in the cytoplasm. Detailed examination revealed an association of WFS1 protein with the secretory vesicles. No association of the WFS1 protein was observed with the mitochondria by EM, Figure 4.10E.

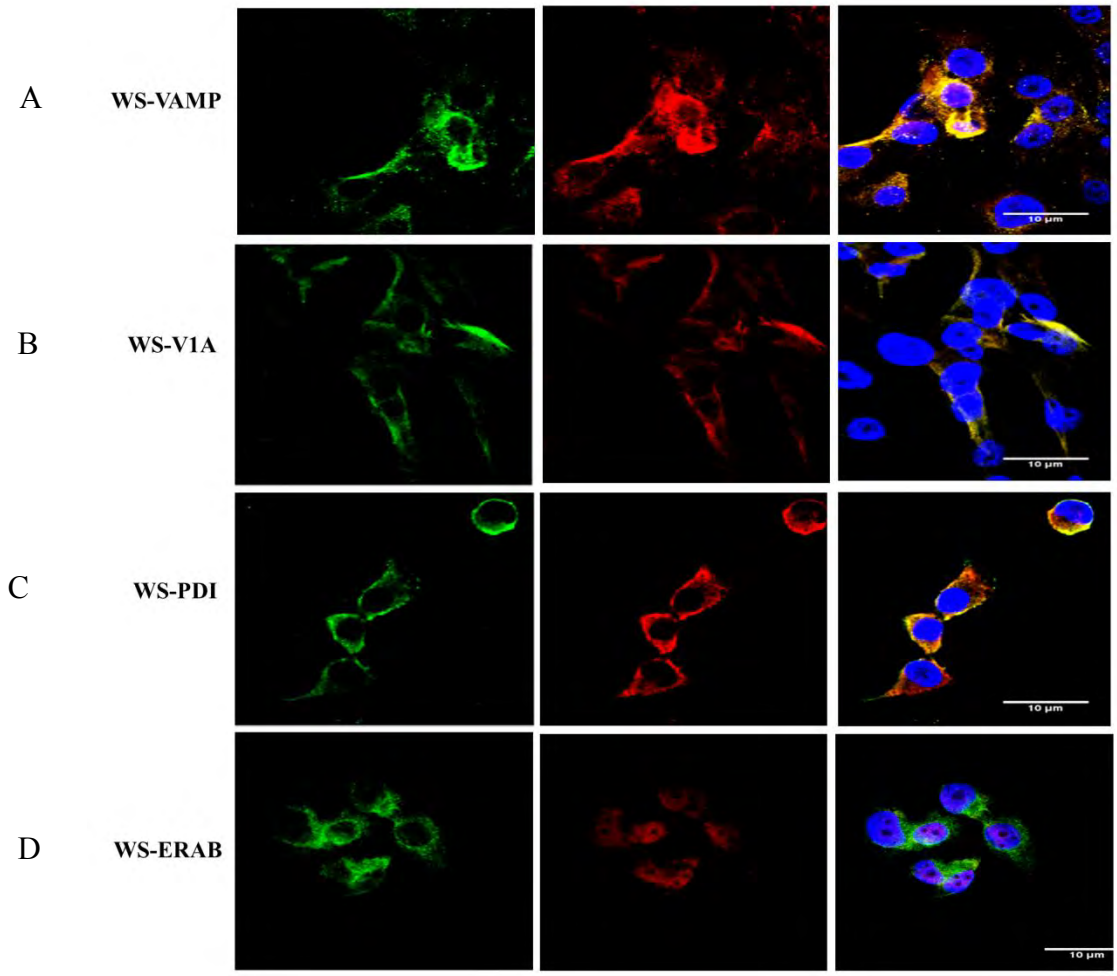

Figure 4.9: WFS1 localisation in wild type human neuroblastoma cell line by confocal microscopy

A: Co-localisation of WFS1 with VAMP (secretory vesicles) Immunofluorescence analysis using antibody to WFS1 (green) and VAMP (red), B: Co-localisation of WFS1 with V1A subunit of ATP6V1A (secretory vesicles) Immunofluorescence analysis using antibody to WFS1 (green) and V1A subunit of ATP6V1A (red), C: Co-localisation of WFS1 with PDI (ER) Immunofluorescence analysis using antibody to WFS1 (green) and PDI (red), D: Lack of co-localisation of WFS1 with ERAB (mitochondrial marker) - Immunofluorescence analysis using antibody to WFS1 (green) and ERAB (red). Scale bars represent 10µm. Images were taken by Ms Fenton.

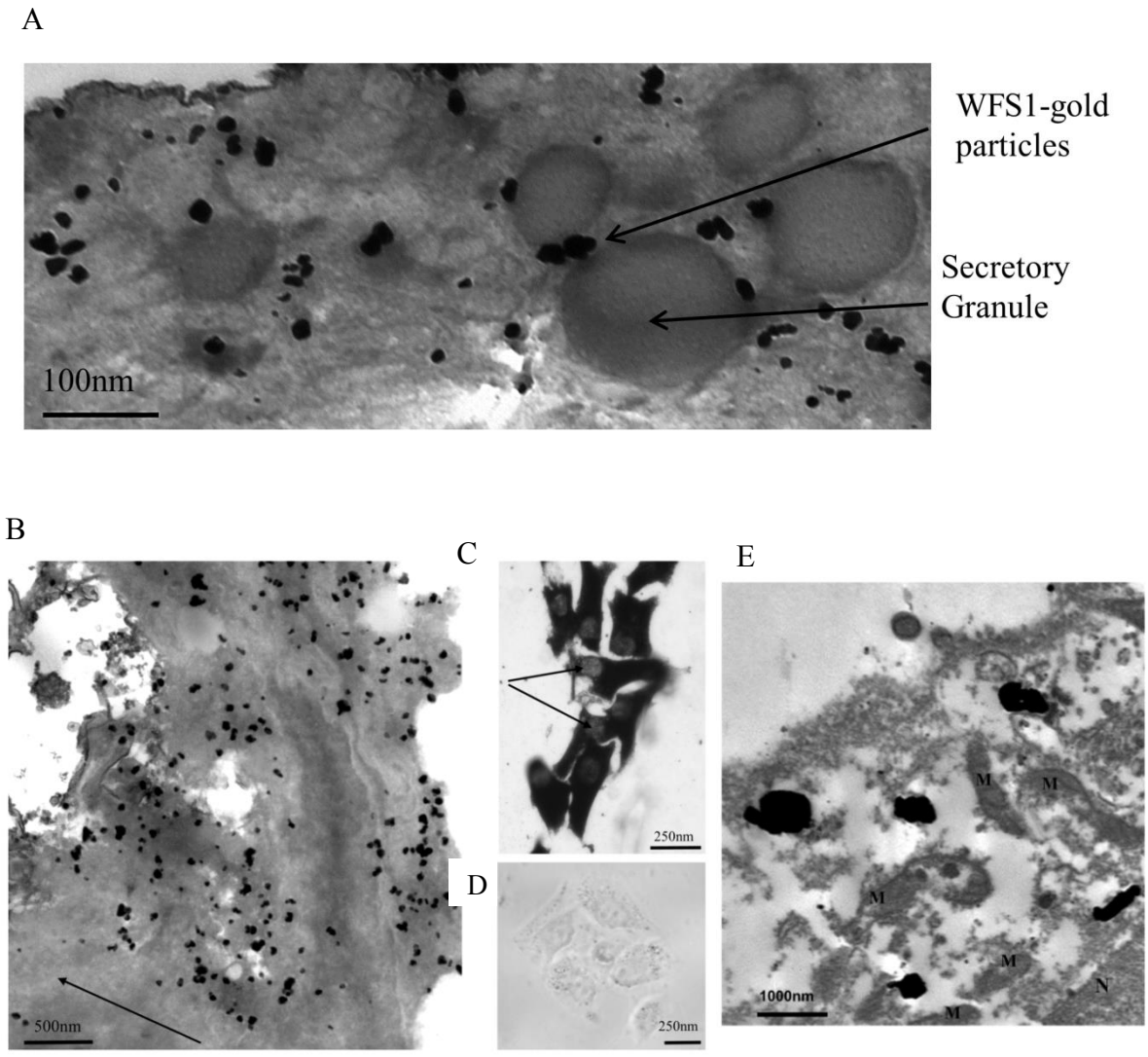

Figure 4.10: Subcellular distribution of WFS1 by electron-microscopy

A: Representative electron micrograph showing subcellular distribution of WFS1 in neuroblastoma cells and strong association with secretory granules by pre- embedding immunogold staining. Scale bar represents 100nm. B: Enlarged field in the EM. Arrow points to the immuno-negative nucleus visible in the bottom left corner. Scale bar 500 nm. C: Light microscope picture of immunogold stained cells, arrows point to nuclei (lighter) lacking immuno-signal. Scale bar 250nm. D:Negative control (primary antibody omitted). Scale bar 250nm. E: Enlarged field. Letters signify mitochondria (M), nucleus (N). Scale bar 1000nm. In collaboration with Prof Sik's Team

After finding co-localisation of WFS1 with ATP6V1A by immunofluorescence microscopy and demonstration of WFS1 association with secretory vesicles by electron-microscopy; the possibility that the two proteins interact was investigated by co-immunoprecipitation (Co-IP) assays in HEK293 and SK-N-AS cells. The co-IP experiments were performed in collaboration with Dr Astuti. The expression constructs of full length hWFS1 cDNA (amino acids 1-890), truncated WFS1 N-terminus (amino acids 1-321) and truncated WFS1 C-terminus (amino acids 652-890) in pCMV-Myc vector were previously described (Zatyka et al., 2008). The pFLAG-CMV-ATP6V1A construct was generated by cloning by Dr Astuti.

First of all, the association between WFS1 and ATP6V1A was investigated in over-expression system in both directions. HEK293 cells were co-transfected with pCMV-Myc-WFS1 / pFLAG-CMV-ATP6V1A. WFS1 was precipitated and ATP6V1A was detected by immunoblotting. The data presented in Figure 4.11A showed that Myc-WFS1 interacts with FLAG-ATP6V1A. A 70kDa protein was co-immunoprecipitated together with WFS1 (lane 3) using anti-WFS1 antibody, and the identity of this protein was confirmed as ATP6V1A by re-probing with specific anti-ATPV1A antibody. In reverse direction, the precipitation was carried out with FLAG antibody (ATP6V1A) and immunoblotting with c-myc antibody (WFS1). Thus, in the reverse experiment a 100kDa protein was co-immunoprecipitated together with ATPV1A (Fig 4.11B, lane 3) using anti-FLAG antibody, and was identified as Wolfram protein by reprobing with specific anti-WFS1 antibody. No co-immunoprecipitation was observed in control extracts co-transfected with either FLAG-empty/Myc-WFS1 or FLAG-V1A/Myc-empty plasmids (Fig 4.11A lanes 1, 2; 4.11B, lanes 1, 2). This interaction seems to be specific between WFS1 and

ATP6V1A as the study by (Zatyka et al., 2008) detected no co-immunoprecipitation between Myc-WFS1 and FLAG-RASSF1A or GFP.

To further evaluate whether this interaction occurs with endogenously expressed proteins in human neuroblastoma SK-N-AS cells, endogenous ATP6V1A protein was co-precipitated with WFS1 using anti-WFS1 antibody (Figure 4.11C lane 2). No co-immunoprecipitation was detected when anti-FLAG antibody was used under the same conditions (Figure 4.12C lane 1), indicating that ATP6V1A interaction with WFS1 is specific. This data suggests that these two proteins may associate *in vivo*.

Further to elucidate where in the cell this interaction occurs, the interaction of ATP6V1A was investigated with the C and N terminal domains of the WFS1 protein. The C-terminal domain of the WFS1 protein is located in the ER lumen and the N-terminus is located in the cytoplasm (Ishihara et al., 2004). HEK293 cells were co-transfected with plasmids expressing either Myc-tagged N-terminus of Wolfram protein (amino acids 1-321) or Myc-C-terminal domain of Wolfram protein (amino acids 652-890) and FLAG-tagged ATP6V1A. For positive control, HEK293 cells were co-transfected with plasmids expressing Myc-tagged full length WFS1 and FLAG-tagged ATP6VIA. An interaction was found between the ATP6V1A and the cytoplasmic N-terminal domain of WFS1 (Figure 4.12 lane 3). There was no interaction observed with the C-terminal domain of WFS1 (located in the ER lumen, Figure 4.13, lane 3). This data suggests that the interaction between Wolfram protein and the V1A subunit of proton pump occurs in the cytoplasm.

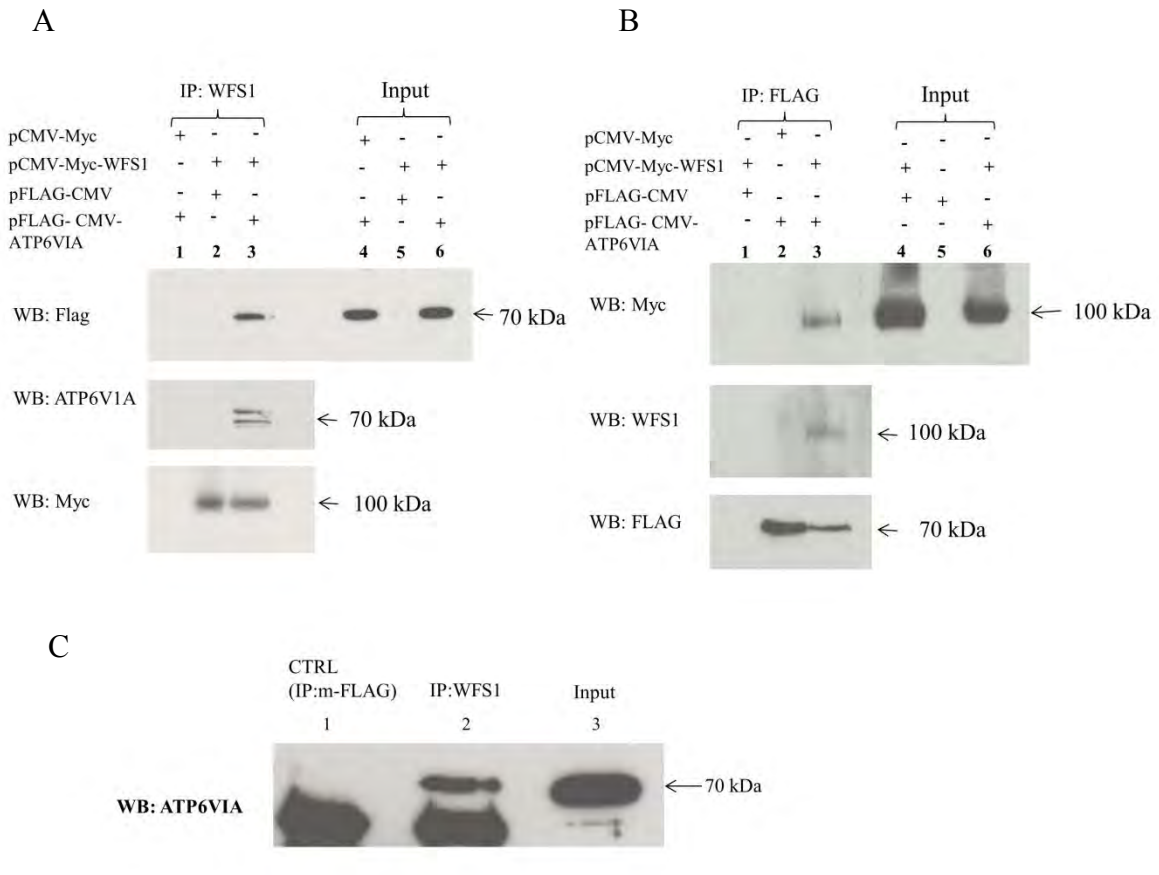

Figure 4.11: Protein interaction of WFS1 with ATP6V1A by co- immunoprecipitation

A) Co-IP of full length c-myc tagged -WFS1 with the FLAG tagged ATP6V1A co-transfected to HEK293 cells, using rabbit polyclonal WFS1 antibody (lanes 1- 3). Mouse monoclonal FLAG antibody was used for detection. The identity of detected protein was confirmed by reprobing with specific antibody to anti ATP6V1A (mouse monoclonal). Bottom panel: re-probing with c-myc antibody (mouse monoclonal) shows the presence of WFS1 in the relevant extracts (lanes 2,3); Input (4% of total extracts used for IP).
B) Co-IP of full length c-myc tagged WFS1 and FLAG tagged ATP6V1A with mouse monoclonal FLAG antibody (lanes 1- 3). Detection with polyclonal, rabbit c-myc antibody, Below: reprobing with anti WFS1 antibody (rabbit polyclonal) to confirm the identity of co-precipitated protein. Bottom panel: reprobing with polyclonal rabbit FLAG antibodies to demonstrate the presence of V1A in relevant extracts (lanes 2,3). Input (4% of total lysates used for IP). C) Interaction between endogenous proteins (WFS1 and V1A) in human neuroblastoma cells. Rabbit polyclonal anti-WFS1 antibody was used for co-precipitation and mouse monoclonal anti V1A antibodies were used for immunoblotting (lane 2). Negative control: pull down with FLAG antibody (mouse monoclonal, lane1). Input (lane 3, 2% of total lysates used for IP). In collaboration with Dr Astuti

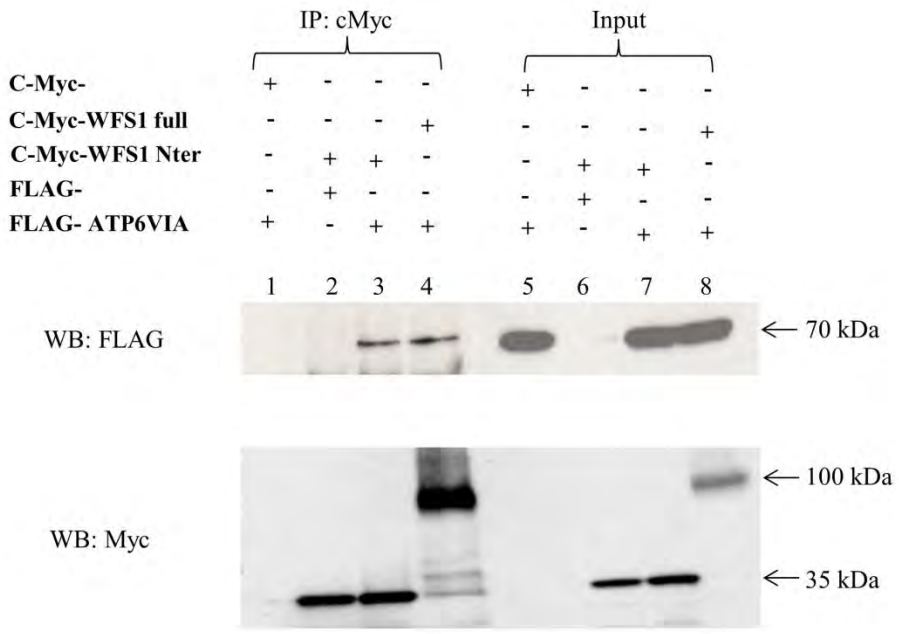

Figure 4.12: Protein interaction between ATP6V1A and the N-terminal domain of WFS1

The N-terminal domain of WFS1 interacts with ATP6V1A. Co-IP of c-myc tagged N-terminal domain of WFS1 (aa 1-321) with FLAG tagged ATP6V1A with c-myc rabbit polyclonal antibody in HEK293 cells (lanes 1-3). Detection: with mouse monoclonal FLAG antibodies. Full length myc-WFS1 was used as a positive control for interaction (lane 4). Bottom panel: reprobing with c-myc (mouse monoclonal antibody) to demonstrate the presence of either truncated (lane 2,3) or full length (lane 4) WFS1. Input (4% of total lysates used for IP). In collaboration with Dr. Astuti

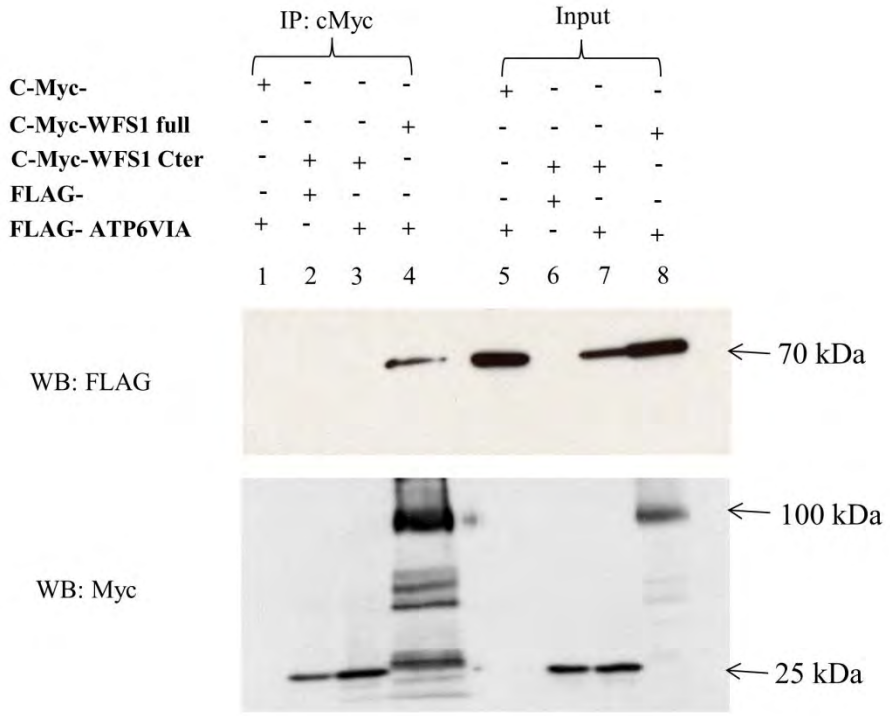

Figure 4.13: No interaction between ATP6V1A and the C-terminal domain of WFS1

The C-terminal domain of WFS1 does not interact with ATP6V1A. There is no co-immunoprecipitation of c-myc tagged C-terminal domain (aa 652-890) of WFS1 with FLAG tagged ATP6V1A with c-myc rabbit polyclonal antibody in HEK 293 cells (lanes 1-3). Immunoblotting: with mouse monoclonal FLAG antibodies. Full length c-myc-WFS1 was used as positive control for interaction (lane 4). Bottom panel: reprobing with c-myc (mouse monoclonal,) to demonstrate the presence of either full length (lane 4) or truncated (lane 2,3) WFS1. Input (4% of total lysate used for IP). In collaboration with Dr Astuti

4.4 Discussion

This study was centred around the role of WFS1 in regulation of expression and stability of the ion pumps (Na^+/K^+-ATPase and H^+-VATPase) subunits and a novel interaction between WFS1 and the V1A subunit of the V-ATPase. WFS1 depleted neuronal cells showed reduced expression of the beta1 subunit of the sodium pump (ATP1B1) and V1A subunit of the H^+ proton pump (ATP6V1A). These findings were confirmed in four cell models. The effect of WFS1 depletion was shown to be specific to these two subunits since the expression of the other subunits of both pumps was not reduced by reduced WFS1 expression. Furthermore, WFS1 was shown to be necessary for the stability of ATP1B1 and ATP6V1A by demonstrating a rapid degradation of both proteins in WFS1 depleted cells after CX treatment in comparison to the control. The V1A subunit of the H^+ proton pump was shown to be co-localised with WFS1 by immunofluorescence microscopy and an association was shown between WFS1 and the vesicular granules by electron-microscopy. The V1A subunit of the H^+ V-ATPase was shown to interact with the full length WFS1 and its N-terminal domain by co-immunoprecipitation in both endogenous and over-expression systems.

WFS1 stably and transiently depleted human neuroblastoma cells, along with WFS1 transiently depleted human NT2 cells and WFS1 stably depleted mouse neuronal (neuro2A) cell lines all showed significant reduction in the expression of both the V1A subunit of V-type H^+-ATPase and the beta1 subunit of sodium potassium-ATPase. WFS1 depletion affected the expression levels of these two proteins in similar fashion which was neither cell type nor species specific. Furthermore, the effects of WFS1 protein depletion were shown to be specific for the beta1

subunit of the sodium pump and the V1A subunit of the H^+ proton pump, since no significant decrease was observed in the expression levels of alpha1 subunit of the sodium pump and the V1C1 and V0D2 subunits of the vacuolar proton pump. These findings suggest that WFS1 regulates the expression of ATP1B1 and ATP6V1A specifically through some unknown mechanisms.

As mentioned before, V1A and V1B subunits of the proton pump exist as triplicates forming a hexameric ring which is the catalytic site of the V-ATPase; and mediate the hydrolysis of ATP (Tabares and Betz, 2010, Beyenbach and Wieczorek, 2006, Wieczorek et al., 2009). Therefore, the reduced levels of V1A subunit are likely to have functional consequences for the whole pump. Similarly, the study by Ferea and Bown (1996) showed that knockout of the V1A gene has vital effects for the cells. The non-homologous region of the V1A subunit is shown to be important for the reversible dissociation of the V-ATPase complex (Toei et al., 2010).

The results of the degradation assays showed that both ATP1B1 and the ATP6V1A subunits were degraded more rapidly in the WFS1 depleted cells in comparison to the controls; these observations suggest that WFS1 is necessary for their stability. This has many consequences for the two ion pumps; it has been reported that when the beta subunit of the sodium pump is not available for the alpha subunit to couple with, the excess of alpha subunits is degraded rapidly in the ER. Therefore, the presence of the beta-subunit of the sodium pump is crucial for the expression of the sodium pump (Geering et al., 1996). In addition, the degradation of the beta1 subunit of sodium pump was shown in MDCK cells using CX, and the findings suggested that

the assembly and correct folding of alpha1 and beta1subunits are required for their exit from the ER (Tokhtaeva et al., 2009). Similarly, when the V1A subunit of the V-ATPase is degraded this can affect the formation of the hexameric ring for generation of the catalytic site of the pump for ATP hydrolysis to take place. Degradation of the V1A subunit therefore has structural and functional consequences for the proton pump (Forgac, 2007). These findings, together with the previously reported interaction between WFS1 and the beta1 subunit of the sodium pump (Zatyka et al., 2008) suggest a role for WFS1 in the expression and/or stability of ATP1B1 and ATP6V1A proteins.

The degradation of ATP1B1 and ATP6V1A was shown not to be associated with the proteasomal pathway, as no accumulation of ATP1B1 and ATP6V1A proteins was observed after inhibition of the proteasome in WFS1 depleted and control cells (Gharanei et al., 2012). These findings suggest that WFS1 protein may protect these pump subunits from degradation by lysosomes or other, as yet unspecified cellular proteases. The proteasome is the site of degradation for short lived proteins such as cytosolic proteins and misfolded proteins. The lysosomes are involved in degradation of long lived and transmembrane proteins. Furthermore Na^+/K^+ ATPase is shown to be degraded via both proteasomal and lysosomal pathways in kidney proximal tubule cells (Thévenod et al., 2000). Therefore, it could be speculated that the pump subunits investigated in this project are targeted to the lysosomes for degradation and that WFS1 protein may have a role in protecting these subunits from lysosomal degradation.

WFS1 protein was primarily thought to localise exclusively to the ER (Inoue et al., 1998, Takeda et al., 2001). Recently, WFS1 was reported to localise to the secretory granules in pancreatic beta cells, and WFS1 depletion was shown to affect intra-vesicular acidification (Hatanaka et al., 2011). In the present study, immunofluorescence microscopy showed co-localisation of WFS1 with the V1A subunit of V-ATPase. Similarly, immuno-gold particles against WFS1 were detected associated with neurosecretory vesicles. Intragranular acidification depends on the operation of V-type H^+-ATPase to generate the optimal pH.

In this study an interaction was identified between WFS1 protein and the V1A subunit of V-type H^+-ATPase in transiently transfected HEK293 cells as well as in SK-N-AS cells between endogenous proteins. The data demonstrated that the WFS1/V1A subunit interaction occurs with the WFS1 protein N-terminal domain (amino acids 1-321). WFS1 is an ER membrane protein with the C-terminal domain located in the ER lumen and the N-terminal domain in the cytoplasm (Ishihara et al., 2004). It is likely that the WFS1 protein assumes the same orientation across secretory vacuole membranes. The mature V-type H^+ V-ATPase is located in the secretory vacuole membrane with the V1A subunit projecting into the cytoplasm. Therefore it is hypothesised that the WFS1 protein/V1A interaction is likely to occur in the cytoplasm. V-type H^+-ATPase has a 'ball and stalk' structure, with the V1 sector (including the V1A subunit) containing catalytic domains, and the V0 sector constituting the proton pathway. The data presented in this chapter and Gharanei et al. (2012) in conjunction with those of Hatanaka et al. (2011) raise the intriguing possibility that WFS1 is required for the proper functioning of the

vesicular proton pump in acidification of vesicles; and that reduced acidification in the absence of WFS1 may affect the release of neurotransmitters from neurosecretory vesicles.

Previously, Zatyka et al. (2008) showed that the WFS1/beta 1 subunit interaction most likely occurs in the ER lumen. WFS1 may be involved in its proper folding and assembly of the pump. However, the WFS1/V1A subunit interaction appears to be mediated by the WFS1 N-terminal domain, which suggests the interaction does not happen in the ER lumen, but in the cytoplasm. It may occur on the surface of secretory vesicles, contributing to stability of the proton pump and facilitating its function. However it may also take place on the surface of the ER where it could facilitate the transport of the nascent peptide into the ER or later on the transport of mature pump from the ER to its final destination in the membrane of secretory vesicles.

In summary, the data presented in this chapter showed that WFS1 is necessary for the expression and stability of the beta1 subunit of the sodium pump and the V1A subunit of the vacuolar proton pump. WFS1 protein is a molecular partner of V1A subunit of vacuolar H^+ATPase, and co-localises with it in secretory granules in neuroblastoma cells. The disruption of this interaction in Wolfram syndrome provides a plausible link between the neurological and endocrine disorders seen in the syndrome.

Chapter Five: Adenoviral over-expression of BiP/GRP78 alleviates ER stress

5.1 Introduction

In eukaryotic cells the endoplasmic reticulum (ER) is an important compartment where protein and lipid synthesis takes place. This multifunctional organelle is responsible for processing and properly folding of the secreted and transmembrane proteins. Disruption of ER functions by environmental and genetic factors results in the accumulation of misfolded and unfolded proteins in the ER lumen, a phenomenon known as ER stress. ER stress activates a signalling cascade called the Unfolded Protein Response (UPR) to resolve ER stress (Oslowski et al., 2011). Within the ER reside molecular chaperones which play important roles in protein folding and synthesis. One of the best characterised ER chaperone proteins is the glucose regulated protein (GRP78), which is a member of the ER stress protein family, that is also known as immunoglobulin binding protein (BiP) and HSPA5 (Lee, 2005).

This protein was originally discovered to be upregulated in response to glucose deprivation in cultured cells (Shiu et al., 1977). Subsequent studies showed that this upregulation was to protect the ER against the harmful effects of accumulated damaged proteins in the ER (Munro and Pelham, 1986). The study conducted by Brostrom and colleagues (1990) further advanced the role of GRP78 as a molecular chaperone in the ER. They reported that removal of Ca^{2+} from the culture media resulted in halting of the synthesis of all new proteins until the expression of GRP78 was increased (Brostrom et al., 1990). Elevated levels of GRP78 expression were shown to be sufficient for protein translation to proceed, implying that cells require GRP78 to continue processing existing proteins, as well as those proteins that might be damaged from a cytotoxic

insult (Brostrom et al., 1990). Similar results were observed when other chemical insults, such as tunicamycin which blocks N-linked protein glycosylation; thapsigargin, which inhibits the ER calcium ATPase pump and the calcium ionophore A23187 were added to the culture (Drummond et al., 1987, Dorner et al., 1992). Later studies determined that GRP78 is an ER resident protein which is synthesised in response to a variety of stress conditions that perturb ER function and homeostasis (Lee, 2001). Studies have shown that GRP78 has high capacity for Ca^{2+} binding which was shown to be very important in protecting cells against cell damage and apoptosis (Koch et al., 1986).

It is well established that GRP78 protects cells against apoptosis caused by disturbances of ER homeostasis, and its over-expression limits the damage in normal tissues and organs exposed to ER stress (Jamora et al., 1996, Liu et al., 1997, Morris et al., 1997). However, natural induction of GRP78 in neoplastic cells is shown to be associated with cancer progression and drug resistance (Lee, 2001). The induction of GRP78 has been commonly used as an indicator for the UPR (Lee, 2001). This molecular chaperone functions as an ER stress signalling regulator and has the ability to block the apoptotic pathways (Kaufman, 1999, Reddy et al., 2002). A summary of its functions is given in Figure 5.1. As described in the main introduction, GRP78 plays an important role in the ER stress signalling pathways. Several ER resident trans-membrane proteins (IRE1, PERK and ATF6) act as transducers in this signalling network (Rutkowski and Kaufman, 2004, Kaufman, 1999, Sommer and Jarosch, 2002). In non-stressed cells, GRP78 binds to all three transducers which are maintained in an inactive state. Upon ER stress, all three sensors are released from GRP78 and become activated to resolve ER stress. IRE1 and PERK homodimerise

through their luminal domains, autophosphorylate their respective cytoplasmic domains, and become activated (Bertolotti et al., 2000). ATF6 translocates from the ER to the Golgi complex, where it is cleaved by the proteases S1P and S2P. The cleaved form of ATF6 enters the nucleus and acts as an active transcription factor to upregulate UPR target genes such as GRP78 (Shen et al., 2002, Hong et al., 2004b). Therefore, GRP78 is a key regulator of ER stress transducers since their activation upon ER stress is dependent on their release from GRP78.

A plethora of studies have shown that adenoviral over-expression of GRP78 could result in alleviation of ER stress (Zhang et al., 2009, Fu et al., 2007, Dorner et al., 1992, Fu et al., 2008, Lai et al., 2008, Yamada et al., 2006). The study by Lai and colleagues (2008) used adenoviral over-expression of GRP78 in INS-1 cells to attenuate ER stress conditions. They showed that 3-5 fold increase in GRP78 levels provided some protection against ER stress caused by thapsigargin. They demonstrated significant reduction in IRE1 pathway activation but only modest reduction in the activation of the PERK pathway. This study also established that INS-1 cells over-expressing GRP78 have higher steady-state pro-insulin levels, indicating that GRP78 may be important for insulin biosynthesis (Lai et al., 2008). The study by Zhang and colleagues (2009) demonstrated improved glucose-stimulated insulin secretion and partial rescue of high glucose-induced suppression of pro-insulin levels in INS-1 pancreatic beta cells with adenoviral over-expression of GRP78. However, they observed little effect of GRP78 over-expression on the levels of ER stress markers (Zhang et al., 2009).

The study by Leborgne-Castel et al. (1999) demonstrated that over-expression of BiP leads to downregulation of the basal transcript levels of endogenous BiP genes and greatly reduces UPR. Although over-expression of BiP in mammalian cells has been shown to reduce the rate of protein secretion Dorner et al. (1992) other reports have shown only an effect on cell viability during ER stress, with no effect on the transport rate of secretory proteins (Morris et al., 1997). In yeast, lower BiP levels caused reduced protein secretion, whereas over-expression of BiP did not result in any noticeable effect on the protein secretion rate (Robinson et al., 1996). Similarly the study by Yamada et al. (2006) showed that over-expression of GRP78 results in normalisation of PERK phosphorylation level in WFS1 deficient MIN6 cells.

As the cell models used in this project showed that WFS1 depletion results in enhanced ER stress, apoptosis and impaired cell cycle kinetics (Chapter 3). In this chapter, it was attempted to rescue ER stress in WFS1 stably depleted human neuroblastoma cells by infecting them with adenovirus over-expressing hamster BiP and GFP. It was hypothesised the over-expression of GRP78 will reduce ER stress, apoptosis and normalise cell cycle kinetics and the level of ion pumps subunits in WFS1 depleted cells.

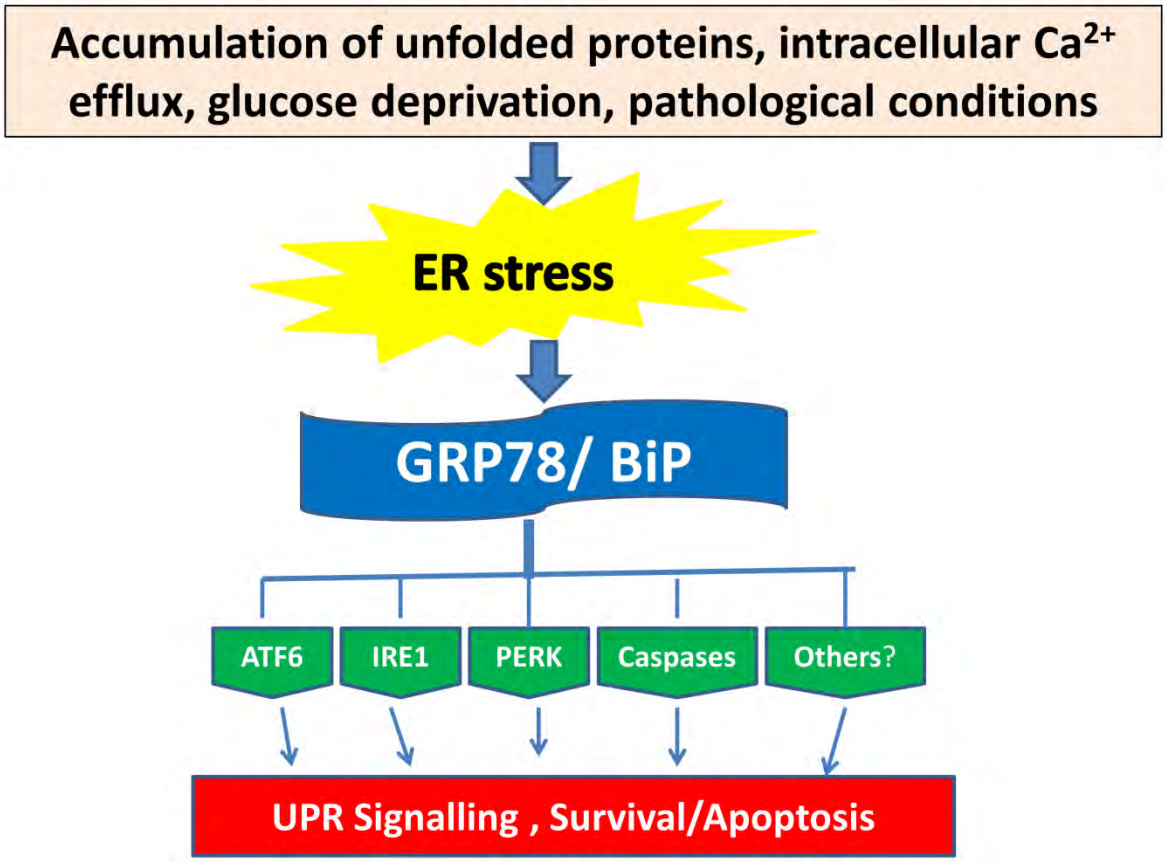

Figure 5.1: GRP78 the master regulator of ER stress and survival

In non-stressed cells, ER-stress transducers ATF6, IRE1, and PERK are maintained in an inactive state through interaction with GRP78. Upon ER stress and formation of misfolded protein in the ER, GRP78 is released from these sensors which become activated, triggering the UPR. GRP78 is also known to complex with procaspases such as caspase-7 and caspase-12 that associate with the ER membrane. Through these interactions, GRP78 regulates the balance between cell survival and apoptosis in ER-stressed cells. Image taken from Lee (2005).

5.2 Aims

The aims of this chapter were four fold

1. To over-express BiP/GRP78 on adenoviral vector in WFS1 depleted cells and optimise the viral multiplicity of infection (MOI).
2. To investigate the effect of adenoviral over-expression of BiP/GRP78 on ER stress
3. To investigate whether BiP/GRP78 over-expression has an effect on apoptosis and cell cycle kinetics
4. To assess whether the Wolfram protein has an ER stress independent function in the pathology of WS and whether its effects on sodium and proton pumps are independent of its effects on ER stress regulation

5.3 Results

Over-expression of BiP/GRP78 in WFS1 depleted cells; optimisation of viral MOI

As described in the introduction, adenoviral over-expression of the ER stress chaperone BiP/GRP78 has been used in many studies to reduce ER stress. Therefore, this study attempts to rescue ER stress in WFS1 stably depleted neuroblastoma cells by infecting them with adenovirus over-expressing hamster BiP (ad-BiP) or a negative control expressing Green Fluorescent Protein, GFP (ad-GFP). Samples of adenoviruses expressing either GFP (ad-GFP) or BiP/GRP78 (ad-BidP) (Fu et al., 2007) were a kind gift from Professor Guy Rutter, Imperial College, London and were amplified and purified by Dr Zatyka. The titer of the virus was also established by Dr Zatyka as 1.7 $x10^{10}$ ifu/mL for both ad-GFP and ad-BiP.

The multiplicity of infection (MOI) of the virus is the number of viral particles (ifu=infectious units) per cell. As mentioned in the Material and Methods chapter, in viral treatment experiments $4.0x10^5$ cells were seeded per 6 well plate. Several optimisation experiments were performed in order to find the optimal MOI of the virus that could affect ER stress in WFS1 stably depleted neuroblastoma cells without affecting cells' viability. In the first experiment, 2µL of the undiluted virus was used for infection giving a MOI of 85 (2x ($1.7x10^7$ ifu/µL) / 4.0 $x10^5$ = 0.85 x 10^2 =85). The cells were incubated for approximately 16 hours with the virus; afterwards the media was changed and the ad-GFP treated cells were monitored under a fluorescent microscope. The majority of the cells were expressing the Green Fluorescent Protein (emitting green light) suggesting that the infection was successful. The data presented in Figure 5.2 shows the levels of hamster BiP measured by WB (Figure 5.2A), which indicates a good level of BiP over-

expression by showing a strong band in ad-BiP infected samples and indicates no band in ad-GFP infected and untreated samples. The expression of hamster BiP was confirmed by QPCR by using specific primers to hamster BiP. (The expressions of hamster BiP and endogenous BiP were distinguished by using sets of primers specific species, see methods chapter). The data presented in figure 5.2B shows that the expression of hamster BiP was increased by 3 to 5 fold in the ad-BiP infected cells in comparison to the ad-GFP infected cells, consistent with the protein data.

In the next step, the levels of ER stress markers: endogenous BiP; CHOP and spliced XBP1 were measured in ad.BiP infected cells relative to ad.GFP treatment by QPCR (The expression of each of the markers in the ad-GFP infected clones was assigned as 100%) and presented in Figure 5.2C. The levels of endogenous BiP were decreased about 5 fold in ad-BiP samples in comparison to ad-GFP infected samples. However the expression levels of CHOP and spliced XBP1 were increased considerably in ad-BiP infected samples (2 to 3 fold CHOP and 8- 3 fold in spliced XBP1). This data suggested that perhaps the viral load used for the infection was too large and may have caused an even higher stress instead of relieving it. It was decided to repeat the experiment with reduced MOI of the virus. In the next step, the virus was diluted two-four times based on the study by Dorner et al. (1992) who demonstrated that BiP over-expression reduces the expression of GRPs (GRP94 and GRP78), therefore it was decided to include GRP94 into the experiments. The data with 2x viral dilution (MOI 43) is presented in Figure 5.2D indicating that the expression of endogenous BiP and GRP94 are decreased at MOI 43; however the levels of CHOP and sp-XBP1 remain high. The results obtained with 4x diluted virus which gave an MOI of 21 are presented in Figure 5.2E. These show that the expression levels of all

markers in comparison to previous transfection (MOI 43) decreased by about 50%. For example: CHOP fold increase at MOI 43 was 270 and at MOI 21 it is 180, also the levels of GRP94 and BiP levels were further decreased. Nevertheless, the levels of CHOP and spliced XBP1 remained higher than in ad.GFP infected cells. In the light of these results and the literature it was decided to dilute the virus further.

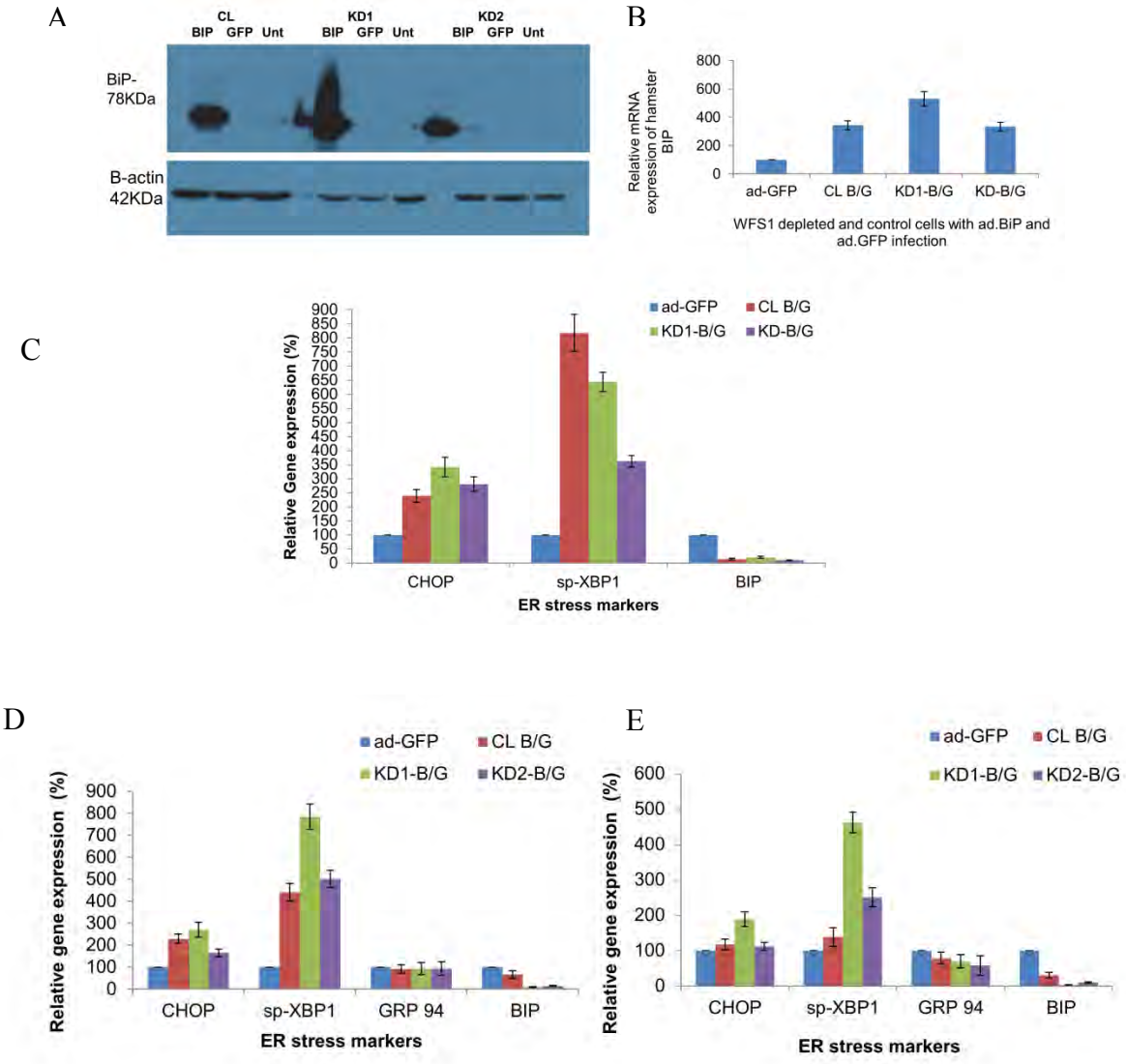

Figure 5.2: Optimisation of viral MOI

(A): Immunoblot analysis of BiP protein using lysates from WFS1 depleted human SK-N-AS cells with adenovirus over-expression of GRP78, GFP or untreated (MOI 85). The amount of actin is shown in the lower panel. (B): Quantitative real-time PCR of hamster BiP, (MOI 85) (C) Quantitative real-time PCR of CHOP, sp-XBP1 and endogenous BiP in stable clones with WFS1 depletion in human SK-N-AS cell line with over-expression of GRP78 (MOI 85). (C): Quantitative real-time PCR of CHOP, sp-XBP1, GRP94 and BiP in stable clones with WFS1 depletion in human SK-N-AS cell line over-expressing BiP- 2x diluted virus (MOI 43). (D): Quantitative real-time PCR of CHOP, sp-XBP1, GRP94 and BiP in stable clones with WFS1 depletion in human SK-N-AS cell line with over-expression of BiP- 4x diluted virus (MOI 21). CL=control, KD1, KD2, KD3=WFS1 depleted clones. Unt = untreated. The expression of each of the markers in the ad-GFP infected clones was assigned as 100%). B/G= BiP/GFP, BiP infection is compared to GFP infection in each clone

5.3.1 Alleviation of ER stress by adenoviral over-expression of BiP/GRP78

The study by Zhang et al. (2009) used adenoviral over-expression of BiP/GRP78 with an MOI of 3 and only 2 hour incubation of the virus with cells; they washed the cells with PBS after removing the virus containing media. Based on this study and my previous observations, it was decided to dilute the virus 10x to achieve an MOI of 8.5. Also, it was decided to wash the cells once with PBS after removing the virus containing media. After washing the cells, fresh media was added and the cells were incubated for another 24 hours. Accordingly, the expression of hamster BiP was measured by QPCR and immunoblotting. The data is presented in figure 5.3. BiP expression measured by QPCR was approximately 2 fold higher in ad-BiP infected cells in comparison to ad-GFP infected cells (Fig 5.3A and Table 5.1) with the fold-changes: 169±20%, 241±8%, 197±20%, 204±30% in: CL, KD1-3 respectively , ($n=3$, $p<0.05$, Mean±SEM). Figure 5.3B shows the expression of hamster BiP on protein level; the immunoblot shows strong bands in ad-BiP infected and no bands in ad-GFP infected samples. The beta actin immunoblot shows equal loading of the samples. Significant increases in BiP protein levels were demonstrated in ad-BiP infected cells in comparison to GFP infection: 1569±459, 1292±296, 1430±664 and 960±107 in CL, KD1-3 respectively ($n>3$, $p<0.05$).

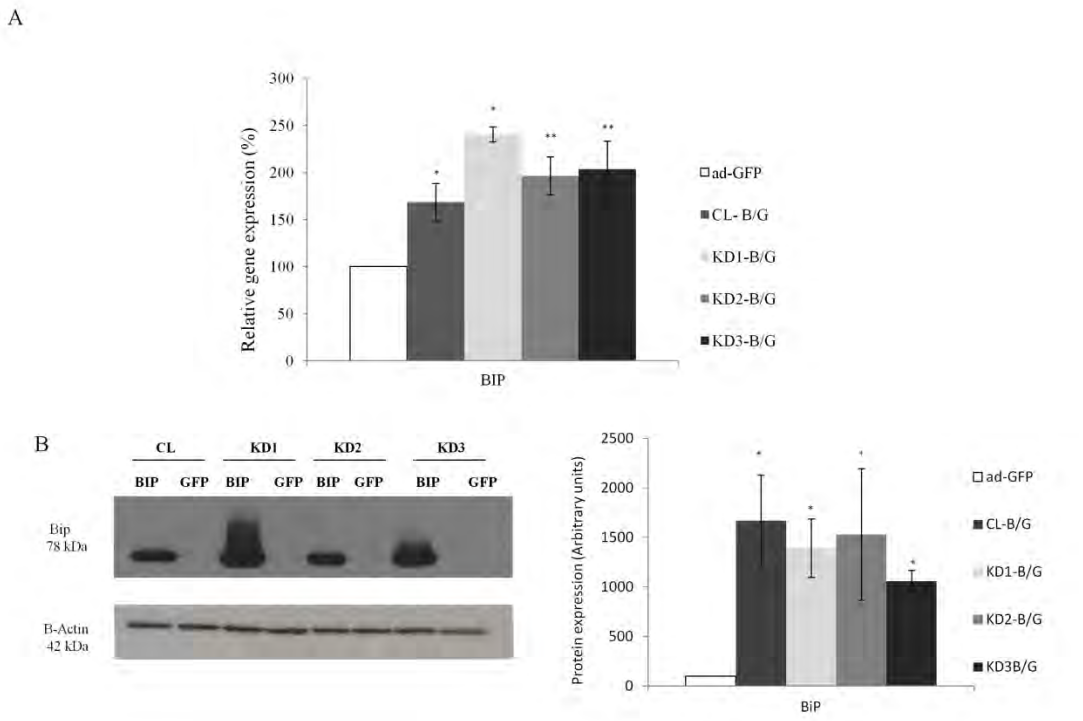

Figure 5.3: Adenoviral over-expression of BiP mRNA and protein

(A): Quantitative real-time PCR of (Hamster) BiP in stable clones with WFS1 depletion in human SK-N-AS cell line with over-expression of BiP/GRP78 (MOI 8.5). (B)Immunoblot analysis of BiP protein using lysates from WFS depleted human SK-N-AS cells with adenovirus over-expression of BiP and GFP. The amount of actin is shown in the lower panel. Protein quantification of the immune-blot is shown with the bar charts. CL=control, KD1, KD2, KD3=WFS1 depleted clones, (n>3) T-test ad-BiP/ad-GFP for all clones. *p<0.05, **p<0.01, and ***p<0.001. The expression of BiP is presented in arbitrary units. All ad-GFP infected clones (CL and KD1-3) are illustrated by one white bar on the chart. B/G= BiP/GFP , BiP infection is compared to GFP infection in each clone

Table 5.1: Expression of ER stress markers in ad-BiP and ad-GFP infected samples

N>3	**CL-BiP/GFP**		**KD1-BiP/GFP**		**KD2-BiP/GFP**		**KD3-BiP/GFP**	
Ad-GFP=100	Expression (%)	p-value	Expression (%)	p-value	Expression (%)	p-value	Expression (%)	p-value
CHOP	87±4	$3.70x10^{-02}$	71±17	$2.69x10^{-02}$	89±7	$3.93x10^{-02}$	83±4.6	$1.87x10^{-02}$
Sp-XBP1	68±8	$3.65x10^{-02}$	64±19	$3.89x10^{-02}$	47±5	$1.50x10^{-03}$	70±8	$2.65x10^{-02}$
GRP 94	65±17	$2.93x10^{-02}$	48±15	$1.19x10^{-05}$	73±2	$2.74x10^{-02}$	70±15	$1.19x10^{-02}$
BiP	19±18	$1.55x10^{-02}$	10±8	$1.42x10^{-08}$	35±16	$5.04x10^{-04}$	26±11	$9.47x10^{-06}$
Hamster BiP	169±2	$4.02x10^{-02}$	241±8	$1.19x10^{-02}$	197±20	$3.56x10^{-03}$	204±30	$5.14x10^{-03}$

Quantitative real-time PCR measurements of CHOP, Spliced XBP1, GRP94, endogenous BiP and (Hamster) BiP in stable clones with WFS1 depletion in human SK-N-AS cell line with over-expression of BiP/GRP78 (MOI 8.5). CL=control, KD1, KD2, KD3=WFS1 depleted clones, n= number of experiments (n>3). P-values are calculated using student T-test comparing means. The expression of each of the markers in the ad-GFP infected clones was assigned as 100%.

In the next step the expression of ER stress markers was measured in ad-BiP infected cells relative to ad-GFP infected cells by quantitative real time PCR (the expression of each of the markers in the ad-GFP infected clones was assigned as 100%). As shown in Figure 5.4A and Table 5.1, CHOP mRNA was decreased to 87±4%, 71±17%, 89±7% and 83±5% in CL and KD1-3 respectively in ad-BiP infected cells in comparison to ad-GFP infected cells ($n=3$, $p<0.05$). The expression of spliced XBP1 was decreased to 68±8%, 64±19%, 47±5%, and 70±8% in CL, KD1 and KD3 respectively in ad-BiP infected samples in comparison to the ad-GFP infected cells ($n=3$, $p<0.05$). GRP94 mRNA levels in ad-BiP treated cells were decreased to 65±17%, 48±15%, 73±2% and 70±15% in CL and KD1-3 respectively ($n=3$, $p<0.05$). The biggest decrease was measured for endogenous BiP with a decrease to 19±18%, 10±8%, 35±16% and 26±11% in ad-BiP versus ad-GFP infected CL and KD1-3 respectively ($n=3$, $p<0.05$).

In addition, the expression of GRP94 was measured by immunoblotting (Figure 5.4B). (The protein levels in ad-GFP infected cells were assigned as 100%) GRP94 expression was decreased in ad-BiP infected cells to 56±10%, 70±13%, 64±10% and 80±3% in CL and KD1-3 respectively relative to ad-GFP infected ($n=3$, $p<0.05$). In summary, the data presented in this chapter shows that the enhanced UPR was abolished and demonstrated a reduction in the levels of ER stress markers by adenoviral over-expression of BiP/GRP78.

A

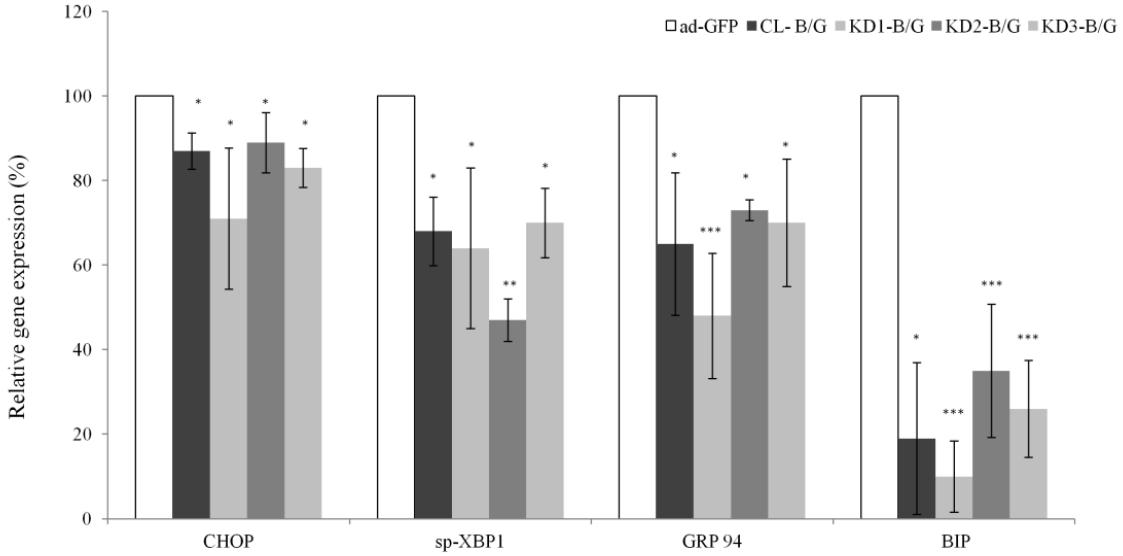

B

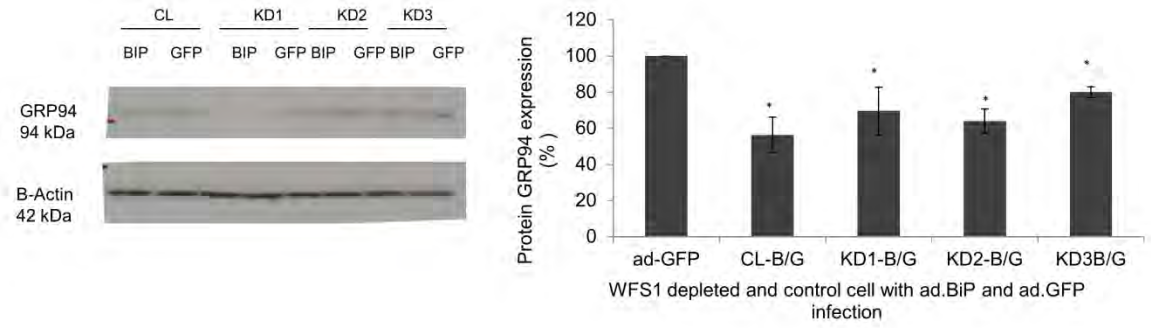

Figure 5.4: Expression of ER stress markers in ad-BiP infected samples

A: Q PCR analysis of ER stress markers; CHOP, sp-XBP1, GRP94 and endogenous BiP in stably depleted WFS1 clones infected with ad-BiP in comparison to corresponding controls infected with ad-GFP (MOI 8.5). The expression of each marker was assumed equal to 100% for each ad-GFP infected clone (CL, KD1-3) and is illustrated by one white bar on the chart. CL=control, KD1, KD2, KD3=WFS1 depleted clones, (n>3) *p<0.05, **p<0.01, and ***p<0.001. B: Representative immunoblot with antibodies to GRP94 and beta actin and immunoblot quantification in stably WFS depleted clones infected with ad-BiP in comparison to corresponding controls infected with ad-GFP. The expression of each protein was assumed equal to 100% for each ad-GFP infected clone (CL, KD1-3) and is illustrated by one white bar on the chart. T-test: GRP94: ad-BiP/ad-GFP p<0.05, n=3 for all clones. B/G= BiP/GFP, BiP infection is compared to GFP infection in each clone

5.3.2 Over-expression of BiP/GRP78 reduces apoptosis and normalises cell cycle kinetics

Studies have shown that over-expression of BiP results in reduction of apoptosis (Reddy et al., 2003). After observing significant alleviation of CHOP mRNA (a pro-apoptotic marker) in ad-BiP infected cells (Figure 3.8, Chapter 3), it was decided to evaluate the percentage of apoptotic cells in ad-BiP and ad-GFP infected cells. This experiment was carried out by High Content Cytometry (HCC), where the cells were grown in culture, and infected with the virus according to the protocol described in Material and Methods chapter. The plate was then fixed, stained and scanned by the High Content Cytometer eX3 Acumen operated by Dr Nagy's Lab.

The data presented in Figure 5.5A and Table 5.2 show that all ad-BiP infected cells have significantly reduced levels of apoptotic cells in comparison to ad-GFP infected cells. This means that expression of BiP/GRP78 reduces the apoptosis levels in these cells. Interestingly, it also shows that the percentage of apoptotic cells in ad-GFP infected control is higher than in ad-GFP infected KD2 and KD3, which is different than in untreated cells (Figure 3.11C, Table 3.1-Chapter 3). The apoptosis noted in the control ad-GFP infected cells is likely to be the apoptosis induced by the experimental procedure (infection with adenovirus) rather than the 'baseline' rate of apoptosis in these cells. In summary, the enhanced ER stress response was abolished and a reduction in the levels of ER stress markers and apoptotic cells was demonstrated by adenoviral over-expression of BiP/GRP78.

The data presented in Chapter 3 showed that the WFS1 depleted cells have persistently abnormal cell cycle kinetics. According to many studies, cell cycle abnormalities or cell cycle arrest could be caused by elevated ER stress (Brewer and Diehl, 2000). The study of Brewer and Diehl (2000) reported a link between cell cycle arrest and UPR by down regulation of cyclin D1, as the UPR causes cell cycle arrest by inhibition of general translation, which also affects the levels of cyclin D1, necessary for the cell cycle progression. Based on the observations in this project and on literature, it was hypothesised that alleviation of ER stress by adenoviral over-expression of BiP might result in normalisation of the cell cycle abnormalities in WFS1 depleted neuroblastoma cells. Therefore, the cell cycle kinetics experiment was undertaken using HCC. The data presented in Figure 5.5B, C and Table 5.2 show the number of cells in G1 and G2 phases of the cell cycle after ad-BiP and ad-GFP infection. These figures demonstrate that ad-BiP infection significantly reduced the number of cells in G1 phase, which could be explained by the fact that BiP over-expression reduces ER stress and allows the cells to pass through the G1 phase. KD1 cells originally showed a persistent cell cycle arrest in G1 phase. This data shows that BiP over-expression removed the G1 block in KD1 resulting in normalisation of the cell cycle. Consistent with this finding, in ad-BiP infected cells the percentage of cells in G2 phase was increased. The highest increase in percentage of G2 phase cells was observed in ad-BiP infected KD1.

Table 5.2: Percentage of apoptotic, G1 and G2 phase cells in ad-BiP and ad-GFP infected cells

	CL	KD1	KD2	KD3
Ad-BiP-apoptotic cells	6±1.7	6±1.6	3±1	3±1
Ad-GFP-apoptotic cells	11±1.6	19±3.9	7±1	5±1
Ad-BiP-G1 cells	16±6.2	9±2.6	12±4	11±3
Ad-GFP-G1-cells	41±2.6	52±3.5	25±2	22±3
Ad-BiP-G2 cells	49±5.6	62±5	53±4	59±8
Ad-GFP-G2-cells	28±3	27±3	41±3	45±3

The values are Mean ±SEM (%). p-values within ad-GFP treated cells: CL v KD1=0.0001, CL v KD2=10^{-05}, CLvKD3=10^{-05}, p-values ad-BiP v GFP treatment = CL, KD1 and KD2 p=10^{-05}, KD3 p=10^{-03}

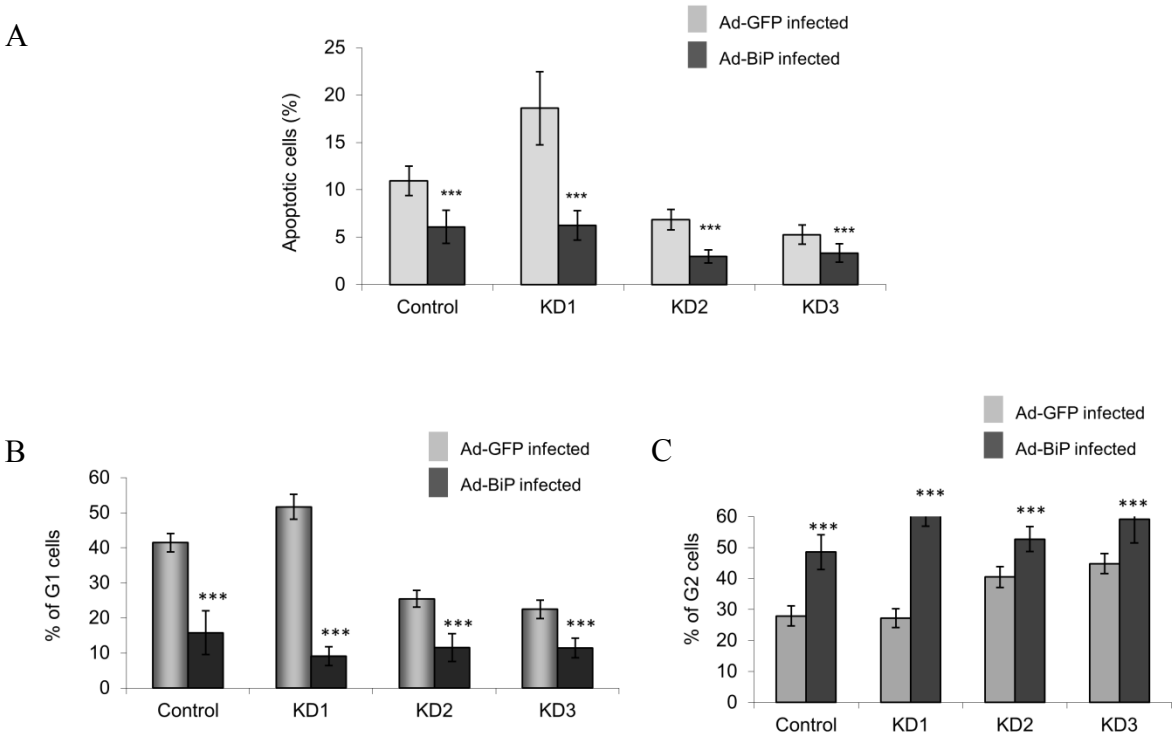

Figure 5.5: Over-expression of BiP reduces apoptosis and normalises cell cycle kinetics

WFS1 stably depleted and control SK-N-AS cells were grown for 24h, infected with adenovirus BiP or GFP (MOI 8.5) for 16 hours, washed with PBS and grown for 24h. Cells were reseeded in 96 well plates and grown for another 24 hours; afterwards cells were fixed with 85% cold ethanol and stained with PI as indicated in Materials and Methods before being scanned with the Acumen eX3 cytometer. (A) percentage of apoptotic cells in ad-BiP and ad-GFP infected WFS1 depleted and control neuroblastoma cells. (B and C) Percentage of G1 and G2 cells in ad-BiP and ad-GFP infected WFS1 depleted and control neuroblastoma cells. CL= control, KD1, KD2 and KD3 stably WFS1 depleted clones. *p<0.05, **p<0.01, and ***p<0.001. B/G= BiP/GFP, BiP infection is compared to GFP infection in each clone

5.3.3 ER stress independent WFS1 role in the expression of the ion pump subunits ATP1B1 and ATP6V1A

After observing significant alleviation in the levels of the main ER stress marker by adenoviral over-expression of BiP/GRP78, it was speculated whether the pathology underlying Wolfram Syndrome is a result of abnormal ER stress only. If the answer was positive then the observed decreased levels of the beta1 subunit of the sodium pump and the V1A subunit of the proton pump in WFS1 depleted cells (Figures 4.3-4.5, Chapter 4) might normalise with adenovirus over-expression of BiP/GRP78. In that case, treatment with molecular chaperones might be the potential treatment for Wolfram syndrome. Therefore it was decided to evaluate whether over-expression of BiP affects the expression levels of ATP1B1 and ATP6V1A proteins. The results presented in Figure 5.6 show no significant difference in the expression of both proteins in ad-BiP infected cells relative to ad-GFP infected: ATP1B1 expression was measured as 93±15%, 111±11%, 120±21% and 106±19% in CL and KD1-3 (n=3, p=NS). Similarly the ATP6V1A expression in ad-BiP infected versus ad-GFP infected samples showed 93±17%, 101±13%, 105±9% and 103±11% in CL and KD1-3 (n=3, p=NS). The obtained data suggest that alleviation of ER stress does not affect expression levels of the beta1 subunit of sodium pump and the V1A subunit of the proton pump.

To investigate further whether the expressions of the ion pumps subunits was ER stress independent, chemical induction of ER stress was undertaken using thapsigargin. A chemical compound that inhibits the ER calcium ATPase pump . Wild type SK-N-AS cells were treated with 1μM thapsigargin for 24 hours and the expressions of ATP1B1, ATP6V1A, as well as ER

stress markers BiP and CHOP were measured by immunoblotting. As shown in Figure 5.7 thapsigargin treatment resulted in the expected elevation of BiP and CHOP expression by 753±134%, and 1936±471% respectively (n=3, $p<0.05$). On the contrary, both ATP1B1 and ATP6V1A were expressed at similar levels in thapsigargin treated cells and DMSO treated controls. ATP1B1 expression was measured as 102±10% and ATP6V1A expression 100.33±10% in thapsigargin treated samples vs DMSO treated cells (n=4, p=NS).

Overall, these results show that ER stress, measured as elevated levels of CHOP, BiP, spliced XBP1 and GRP94 in WFS1 depleted neuroblastoma cells was reduced by over-expression of hamster BiP/GRP78 resulting in abolition of the previously observed enhanced ER stress response. Over-expression of hamster BiP did not affect the expression of ATP1B1 or ATP6V1A, and the experiment with thapsigargin did not show any dependence of ATP1B1 and ATP6V1A expression on ER stress levels.

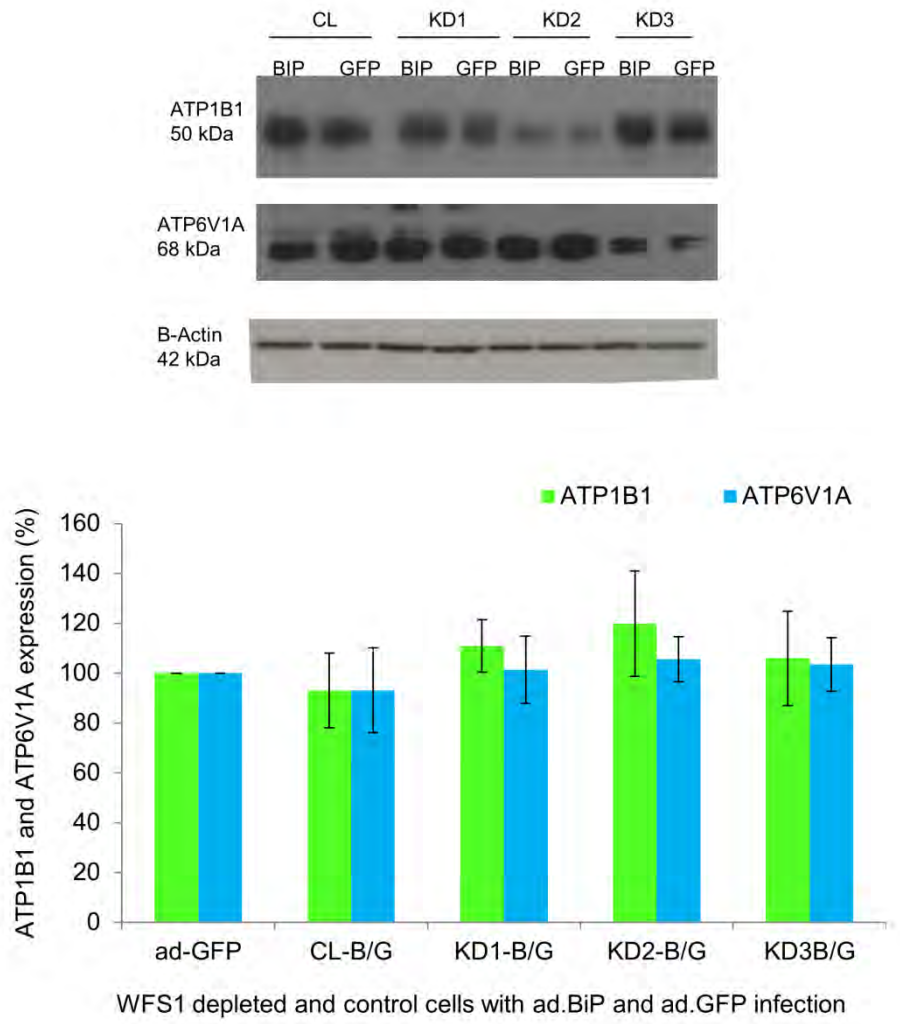

Figure 5.6: Expression of ATP1B1 and ATP6V1A in ad.BiP and ad.GFP infected cells

Representative immunoblot with antibodies to ATP1B1, ATP6V1A and beta actin and immunoblot quantification in stably WFS1 depleted clones infected with ad-BiP in comparison to corresponding controls infected with ad-GFP. The expression of each protein was assumed equal to 100% for each ad-GFP infected clone (CL, KD1-3) and is illustrated by one white bar on the chart. T-test for ATP1B1 and ATP6V1A: p=NS for all clones, (n=3). B/G= BiP/GFP, BiP infection is compared to GFP infection in each clone

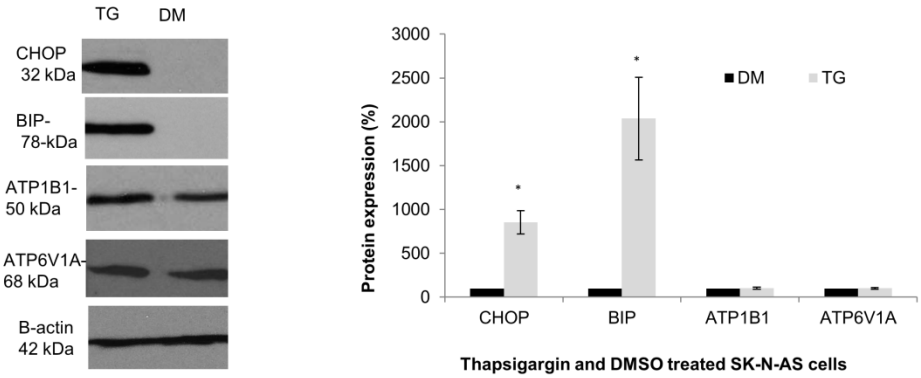

Figure 5.7: Chemical ER stress induction by thapsigargin treatment

Chemical induction of ER stress in wild type SK-N-AS cells-representative immunoblot with antibodies to CHOP, BiP, ATP1B1, ATP6V1A and beta actin. Neuroblastoma cells were treated with 1μM thapsigargin for 24 hours before harvesting in RIPA buffer. The expression in DMSO treated cells was assumed as equal to 100%. (TG–thapsigargin, DM-DMSO) Immunoblot quantification: t-test: CHOP and BIP: $p<0.05$ and ATP1B1, ATP6V1A p=NS.

5.4 Discussion

The study presented in this chapter was focused on alleviation of ER stress in WFS1 depleted and control SK-N-AS cells by adenovirus over-expression of BiP/GRP78. Significant suppression was shown in the mRNA levels of the four main ER stress markers: BiP, GRP94, CHOP and spliced XBP1 (sp-XBP1), along with a reduction in GRP94 protein levels in ad-BiP infected samples in comparison to the ad-GFP infected cells. These results suggest that ER stress can be relieved by over-expression of GRP78 by adenovirus in human neuronal cells. However, an excessive amount of the virus for infection resulted in increase in ER stress. Over production of BiP in the cells resulted in reduction of apoptosis and normalisation of cell cycle kinetics. The data in this chapter also demonstrated that the expression levels of the beta one the subunit of the sodium pump and the V1A subunit of the proton pump in WFS1 depleted neuroblastoma cells were ER stress independent.

Treatment of ER stress has been the focus of intensive research over the last decade where the majority of studies have been conducted in animal models. Adenoviral over-expression of GRP78 was used in several studies to reduce ER stress (Dorner et al., 1992, Fu et al., 2008), however none of these studies showed reduction of ER stress as extensively as this study, where the reduction of the expression of four main ER stress markers (BiP, CHOP, SP-XBP1 and GRP94) was demonstrated. An earlier study by Dorner and colleagues (1992) used over-expression of GRP78 by adenovirus in Chinese Hamster Ovary (CHO) cells and showed that over-expression of GRP78 greatly reduced induction of endogenous BiP and GRP94 in response to stress. The authors suggested that GRP78 over-expression either alleviates the stress or is directly involved

in signalling stress-induced expression of GRPs (GRP78 and GRP94). The study conducted by Fu and colleagues (2008) used adenoviral over-expression of GRP78 in the rat cardiomyocytes and showed that BiP over-expression attenuated CHOP expression and rescued cardiomyocyte death by proteasome inhibition. These authors suggested that cell survival by GRP78 over-expression is predominantly through attenuation of a CHOP dependent pathway. However, the study by Zhang and colleagues (2009) used adenoviral over-expression of GRP78 in pancreatic beta cells, they did not show any reduction in CHOP mRNA level induced by prolonged exposure to high glucose and were unable to detect any differences in XBP-1 splicing. Therefore they concluded that GRP78 over-expression is not sufficient to completely relieve ER stress (Zhang et al., 2009).

The data presented in this chapter also demonstrated significant reduction in the percentage of apoptotic cells in ad-BiP infected samples in comparison to ad-GFP infection. Apoptosis occurs when cells fail to maintain ER homeostasis. When adenoviral over-expression results in a decreased level of apoptotic cells, this implies that the survival chances of the cells will be increased which is an important point to consider in treatment of a disease. A study by Reddy and colleagues (2003) reported that over-expression of GRP78 in CHO cells, human leukaemia, and bladder carcinoma cell lines directly inhibit cytotoxic drug-induced apoptosis which was correlated with a higher survival rate in clonogenic assays (a microbiology technique for studying the effectiveness of specific agents on the survival and proliferation of cell). The mechanism of this suppression was shown to be associated with blocking the activity of caspase7 by over-expression of GRP78 (Reddy et al., 2003). Caspase 7 is one of the members of the apoptotic

executing group which is structurally and functionally most similar to caspase 3 (Wolf and Green, 1999). Active caspase 7 has been shown to be associated with the mitochondria and the ER membranes, whereas caspase 3 remains cytosolic (Rao et al., 2001). Similarly the study by Laybutt et al. (2007) reported that attenuation of ER stress by overproduction of BiP/GRP78 in MIN6 cells significantly protected against lipid induced apoptosis. However, the study by Lai et al. (2008) used a similar protocol of adenoviral over-expression of GRP78 in MIN6 cells in an attempt to rescue palmitate induced apoptosis, but they did not find significant reduction of apoptosis in ad-BiP infected samples. The failure of the experiment might have been due any differences in the experimental procedures as some techniques are very sensitive and altering any parameter could affect the outcome of the experiment.

The data demonstrated in this chapter also showed that attenuation of ER stress by over-expression of BiP would potentially result in normalisation of cell cycle kinetics in WFS1 depleted and control neuroblastoma cell lines. The link between UPR and cell cycle arrest in G1 phase is well known to be mediated by downregulation of cyclin D1 due to general translational suppression via eIF2a phosphorylation (Brewer and Diehl, 2000). Based on the reported observations that increased ER stress causes cell cycle arrest in G1 phase Mihailidou et al. (2010), it was hypothesised that reducing ER stress might cause normalisation of the cell cycle. The finding in this chapter demonstrated the G1 block was removed by showing significantly reduced number of G1 cells in ad.BiP infected cells relative to GFP treatment in KD 1 cell line, which was shown to have a cell cycle arrest in G1 phase (Chapter 3, secetion 3.3.4). This finding

suggest that, alleviation of ER stress has great potential in normalising cell cycle kinetics in WFS1 depleted cells.

The data presented in chapter four demonstrated that WFS1 depleted cells displayed reduced expression of the beta1 subunit of the sodium pump and the V1A subunit of the proton pump (Figure 4.3). It was also demonstrated that WFS1 is necessary for the stability of both pump subunits (Figure 4.8). As WFS1 depletion is associated with increased ER stress (Fonseca et al., 2005, Philbrook et al., 2005, Riggs et al., 2005), it was decided to evaluate whether the reduced expression of these pump subunits was triggered by increased ER stress. The data presented in this chapter demonstrated that there was no significant difference in the expression of ATP1B1 and ATP6V1A in ad-BiP treated samples in comparison to ad-GFP treated samples (Figure 5.6). These findings suggest that expression levels of the ion pump subunits were not affected by alleviation of ER stress by ad.BiP infection. Similarly, chemically induction of ER stress by thapsigargin didn't affect the expression of ATP6V1A and ATP1B1 (Figure 5.7). Collectively, this data suggest that WFS1 might be regulating the expression of ATP1B1 and ATP6V1A in an ER stress independent manner.

Previously, WFS1 is shown to be a mediator of the ER stress signalling pathways (Fonseca et al., 2005, Fonseca et al., 2010) and its function have been identified in relation to ER stress. The findings in this project are pointing to the existence of an additional ER stress independent function of WFS1. A proposed mechanism of the current understanding of Wolframin function is summarised in Figure 5.8, in WFS1 positive cells Wolframin maintains cellular homeostasis as

an important component of the ER stress response. In addition, it controls expression and stability of certain proteins such as the beta1 subunit of sodium pump and V1A subunit of the proton pump, ensuring proper folding and maturation of the pumps necessary for their function. In Wolfram syndrome, defective or absent WFS1 does not properly control ER homeostasis leading to increased ER stress in the cells. In addition, WFS1 does not perform its function in beta1 and V1A subunit stability/folding/assembly. This in turn leads to reduced amounts of mature pumps in the relevant cell's organelles, impairing their function and leading to impaired ion transport across the membranes. Changes in membrane potential could result in disturbances in regulation of cell volume and osmolarity and possible lead to impaired stability and tightness of intercellular junctions (sodium pump) (Köksoy, 2002). Reduced levels of V1A subunit of the proton pump results in defective acidification and priming of secretory granules preceding exocytosis (proton pump) (Nishi and Forgac, 2002b, Hatanaka et al., 2011). It is likely that depletion of these subunits provides an alternative mechanism of pathology in Wolfram syndrome in addition to ER stress.

Overall, this chapter demonstrated that adenoviral over-expression of BiP/GRP78 in WFS1 depleted neuroblastoma cell lines resulted in alleviation of ER stress, reduction of apoptotic cells and normalisation of cell cycle kinetics. This data also revealed an ER stress independent role of WFS1 in the expression of beta1 subunit of sodium pump and V1A subunit of proton pump; further experiments in primary cells and animal models are needed to confirm these observations.

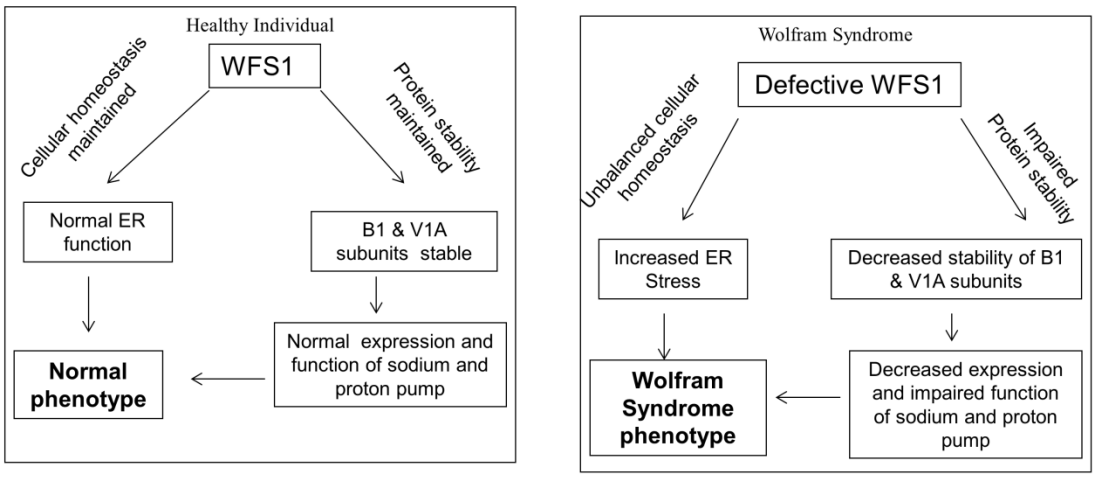

Figure 5.8: Contribution of Na^+/K^+ ATPase and VATPase to the pathology of WS

Normal conditions: cellular homeostasis is maintained and the pumps are functioning normally. In Wolfram syndrome, defective WFS1 causes enhanced ER stress, decreased levels of ATP1B1 and ATP6V1A subunit of Na^+/K^+ ATPase and proton pumps respectively, affects stability of the subunits, affecting their expression and function. No relationship was observed between ER stress and expression of the pump subunits.

Chapter Six: Investigation of the effect of SodiumValproate on WFS1 depleted cells

6.1 Introduction

Valproate (Sodium valproate, Valproic acid, 2-propylpentanoic acid, divalproex sodium; VPA) is a saturated short chain branched fatty acid with good central nervous system (CNS) penetration (Porsteinsson et al., 2001). Figure 6.1 shows the chemical structure of valproate containing 8 carbons and two fatty acid side chains. This drug has been widely used as an anticonvulsant or antiepileptic and mood stabiliser (Grimes and Jope, 1999). The anticonvulsant activity of VPA is thought to be mediated through its effect on the levels of the inhibitory neurotransmitter gamma-amino butyric acid (GABA) in the brain. GABA has acute inhibitory effects on neuronal transmission and excitation in the central nervous system (Wei et al., 2011). It was shown that VPA increases the levels of GABA in the brain and prolongs the recovery of inactivated sodium channels. These properties are proposed to be responsible for the action of VPA as a CNS depressant.

One of the many proposed mechanisms of actions for VPA is that it has been shown to block the voltage gated sodium channel and T-type calcium channel; these mechanisms make VPA a broad spectrum anticonvulsant drug. VPA interacts directly with the sodium channels and inhibits the repetitive firing of neurons (Large et al., 2009). *In vitro* studies have shown that VPA increases GABA levels by increasing the activity of glutamic acid decarboxylase and by inhibiting GABA transaminase (Jakutiene et al., 2007). Thus, the biosynthetic enzymes of GABA are stimulated by

VPA and enzymes involved in its degradation are inhibited by VPA treatment (Phiel et al., 2001, Johannessen, 2000).

VPA has shown efficacy in treatment of several neuropsychiatric conditions such as schizophrenia, bipolar disease, and acute mania; it has also been used in numerous non-psychiatric disorders, including neuropathic pain and prophylaxis of migraine (Rosenberg, 2007). VPA is shown to have beneficial effects in cellular and animal models of many neurodegenerative diseases such as stroke, Alzheimer's disease (AD), Parkinson's disease (PD), Huntington's disease (HD), spinal cord injury, spinal muscular atrophy, retinal degeneration, and human immunodeficiency virus-1 infection (Tariot et al., 2002, Chuang and Priller, 2006). In these studies, VPA is shown to have the ability to protect against apoptotic insults *in vivo* and *in vitro* (Chuang, 2004), for example, pre-treatment with VPA protected cultured brain neurons from glutamate-induced apoptosis (Shimizu et al., 2003, Chen et al., 2006).

The exact mechanism of action for VPA in the treatment of bipolar disease is not clear. Studies have shown that valproate induces the expression of neuroprotective genes such as BCL-2 by increasing their transcription. VPA increases the transcriptional activity of transcription factor AP1 by increasing its binding to DNA, leading to enhancement of the transcription of the AP1 target genes. AP1 is a hetero-dimeric protein which is composed of the c-Fos, c-Jun and ATF protein families that function in transcriptional upregulation of genes involved in proliferation, differentiation and defence mechanisms in neurons (Chen et al., 1999).

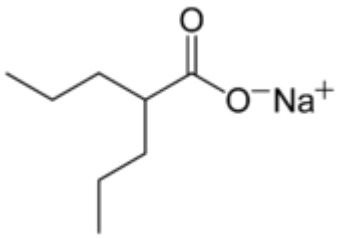

Figure 6.1: Chemical structure of Sodium Valproate

(ChemicalBook, 2008)

VPA belongs to the class I Histone Deacetylase (HDACs) inhibitors, which regulate gene expression through epigenetic mechanisms (Phiel et al., 2001, Gottlicher et al., 2001). Histones are highly conserved proteins that are involved in the formation of the structural unit of chromatin. Covalent modification of histone proteins, in particular acetylation and deacetylation of the lysine residues, are important for gene transcription in normal and malignant cells (Luo and Dean, 1999). The equilibrium of histone acetylation is controlled by histone acetyl transferase and histone deacetylase (HAT and HDAC). Their balance seems to be essential for normal cell growth and their imbalance is associated with cancer progression (Waterborg, 2002). Studies have shown that VPA may affect the concentration of HDACs by inducing its proteasomal degradation (Gottlicher et al., 2001, Kramer et al., 2003). Inhibition of HDACs results in hyperacetylation of histones, which is followed by relaxation of DNA conformation and finally by transcriptional activation of different genes (Hrzenjak et al., 2006). HDAC inhibitors, including VPA, phenyl butyrate (PB), sodium butyrate (SB), and trichostatin A (TSA), cause chromatin remodelling through histone

hyperacetylation to regulate expression of neuroprotective/neurotrophic proteins and pro-apoptotic/pro-inflammatory proteins (Brett et al., 2005).

VPA is an approved drug by the Food and Drug Administration for the treatment of epilepsy and bipolar disorder all over the world (Chen et al., 1999). VPA has also useful phamaco-kinetic properties with a significantly longer biological half-life than other HDAC inhibitors (Catalano et al., 2005). This drug is rapidly absorbed from the gastro-intestinal tract. It produces mild adverse effects in patients even when the serum levels exceed the normal therapeutic range. The therapeutic ranges for patients are between 50-100µg/mL, higher concentrations of VPA around 1000µg/mL might be toxic and cause metabolic acidosis (Anderson et al., 2003, Wallace, 1998).

Studies have also shown that VPA inhibits a major signalling enzyme, glycogen synthase kinase-3 beta (GSK3β) (Chen et al., 1999). GSK3β is a regulator of axonal remodelling, cellular proliferation, embryonic patterning and organogenesis (Morin, 1999, Dickinson et al., 1994). GSK3β phosphorylates one of its substrates, β-catenin, resulting in its rapid degradation. Therefore β-catenin protein will be accumulated upon inhibition of GSK3β by VPA (Hedgepeth et al., 1997, Stambolic et al., 1996). Similarly, treatment of human neuroblastoma SH-SY5Ycells with VPA increased the stability and protein levels of β-catenin (Chen et al., 1999). This notion is further supported by another study showing that chronic valproate treatment in rodents results in increased cortical β-catenin levels (Zhou et al., 2008). Increased availability of β-catenin may improve the function of synapses and influence cell proliferation, and cell survival, through its binding with cadherin, presenilin, and several transcription factors. It is not yet known if VPA inhibits GSK3β directly or at some point upstream in one of the pathways that regulates its activity (Imahori and Uchida, 1997).

VPA appears to have complex effects on various molecular signalling pathways and a number of studies have demonstrated its neuroprotective potentials (Dou et al., 2003, Jeong et al., 2003, Morland et al., 2004). Specifically, in the treatment of AD, many of the time-dependent, cellular actions of valproate could be considered as neuroprotective. Mark and colleagues (1995) for the first time demonstrated in an *in vitro* study that VPA treatment results in reduction of neuronal injury and the disease progression rate in AD. Subsequent studies supported this hypothesis by showing that VPA demonstrates neuroprotective effects in a variety of model systems (Mark et al., 1995, Loy and Tariot, 2002). The neuroprotective mechanism of VPA is thought to be achieved through the following (Figure 6.2); VPA activates BCL-2 which leads to enhancing cell survival by blocking the apoptotic caspase cascade. Inhibition of HDAC by VPA increased the synthesis of β-catenin followed by stabilisation of synapses, leading both to derepression and transcriptional activation of specific antiapoptotic genes and VPA inhibits the activity of GSK3β (Loy and Tariot, 2002).

Previous studies have shown that valproate provides protection against cell death by regulating ER stress proteins and anti-apoptotic genes (Bown et al., 2002). The study by Bown and colleagues (2002) showed that VPA treatment increased the expression of GRP78 without inducing ER stress; glioma cells were treated with VPA for 7 days and after the treatment the drug was removed and GRP78 levels monitored for 48 hours. Their data showed that the GRP78 mRNA returned to normal levels within 6 hours, suggesting that VPA increased the expression of GRP78 temporarily without damaging ER homeostasis. In hepatoblastoma cells, VPA treatment increased expressions of

GRP78/94 without increasing the expression of CHOP. The authors showed that VPA treatment increased the transcription rate of the ER proteins; they speculated that VPA regulates intracellular Ca^{2+} levels (Bown et al., 2002).

A study conducted by Kakiuchi et al. (2009) showed that VPA modulates the unfolded protein response (UPR) through the regulation of WFS1 expression, by showing elevation of WFS1 protein and mRNA levels in neuro2a cells with VPA treatment without any effect on the levels of ER stress markers. The authors speculated that VPA specifically regulates WFS1 without activating other components of the ER stress signalling pathway. Their findings suggested that the likely action of VPA in bipolar disorder might be linked to changes in gene expression and modulation of UPR. These authors also showed that under normal conditions WFS1 forms a complex with GRP94, and VPA treatment enhances its dissociation from GRP94 and increases its transcription (Kakiuchi et al., 2009). Similarly, a recent study by Terasmaa et al. (2011) used VPA in a WFS1 knockout mouse model and in a streptozocin induced diabetic mice and showed that VPA treatment normalises the glucose intolerance in WFS1 knockout mice. The authors also showed that acute VPA administration lowered blood glucose levels in the diabetic mouse model.

The aim of the present study was to use sodium valproate as a therapeutic agent to investigate its efficacy in WFS1 depleted human neuroblastoma cells; to assess whether VPA treatment could provide protection against the irresolvable ER stress and apoptosis. The hypothesis of this study was that VPA treatment would cause induction of WFS1 expression resulting in minimising or

normalising the characteristics of WFS1 depleted cells identified in this project: ER stress, apoptosis, cell cycle kinetics and the ion pump subunits.

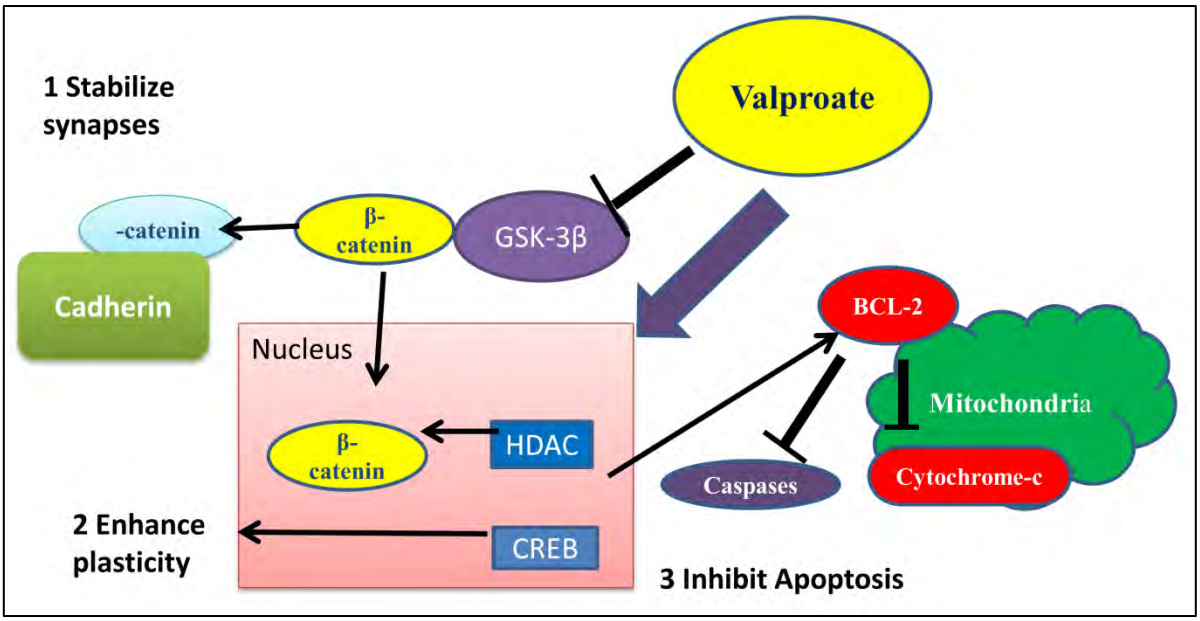

Figure 6.2 Schematic diagram of possible neuroprotective effects of valproate.

(1) Significant benefit may be anticipated through inhibition of GSK3β, likely through inhibition of β-catenin phosphorylation or increased synthesis of β-catenin through inhibition of HDAC leading to stabilisation of synapses. (2) Activation of CREB, another substrate of GSK-3β, may lead to enhanced plasticity-dependent pathways promoting memory. (3) Derepression of specific genes by HDAC inhibition, or activation of β-catenin acting as a transcription factor, may lead to cell survival and inhibition of apoptosis.

Abbreviations: Bcl-2: B-cell lymphoma protein-2; CREB: cyclic AMP-responsive element-binding protein; GSK3β: glycogen synthase kinase 3β (tau kinase I); HDAC: histone deacetylase. Figure taken from Loy and Tariot (2002).

6.2 Aims

Sodium valproate is a histone deacytelase inhibitor that has been shown in previous studies to induce the expression of WFS1 without altering the expression of other ER stress markers. The aims of this study were four fold:

1. To assess changes in WFS1 expression in VPA treated WFS1 depleted cells on protein and RNA level
2. To assess the effects of VPA treatment on the expression of ER stress and apoptosis markers
3. To assess the effects of VPA on the expression of beta1 subunit of sodium pump and V1A subunit of proton pump
4. To assess the effect of VPA on cell cycle kinetics and the expression of WFS1 in cell cycle phases.

6.3 Results

6.3.1 Effect of VPA treatment on the expression of WFS1 in human neuroblastoma cell lines by High Content Cytometry

A study conducted by Kakiuchi et al. (2009) demonstrated induction of the WFS1 expression in rodent neuronal cell lines after treatment with sodium valproate at the following concentrations: 50, 100 and 200μg/mL. In the light of their observation, in the current study the toxicity of VPA was assessed by HCC using a wider range of concentrations (10, 50, 100, 200, 400 and 600μg/mL), with 24 hours treatment, to evaluate whether higher VPA concentrations are tolerable to human neuroblastoma cells. The data showed no significant effect of the increasing drug concentration on cell viability measured as ongoing apoptosis (percentage of apoptotic cells) and on total cell number, suggesting that the drug was not toxic to the cells at these concentrations (Figures 6.3A and B). Figure 6.3A shows the percentage of apoptotic cells does not seem to significantly rise at any of the VPA concentrations. These data suggest that there was very little cell death in the cultures and VPA administration did not induce an increase in apoptosis. Figure 6.3B shows that the total cell number did not change significantly with VPA treatment. There was a slight decline with the highest dose, which was probably caused by alteration in the cell cycle as at this dose the percentage of apoptotic cells did not significantly increase.

A

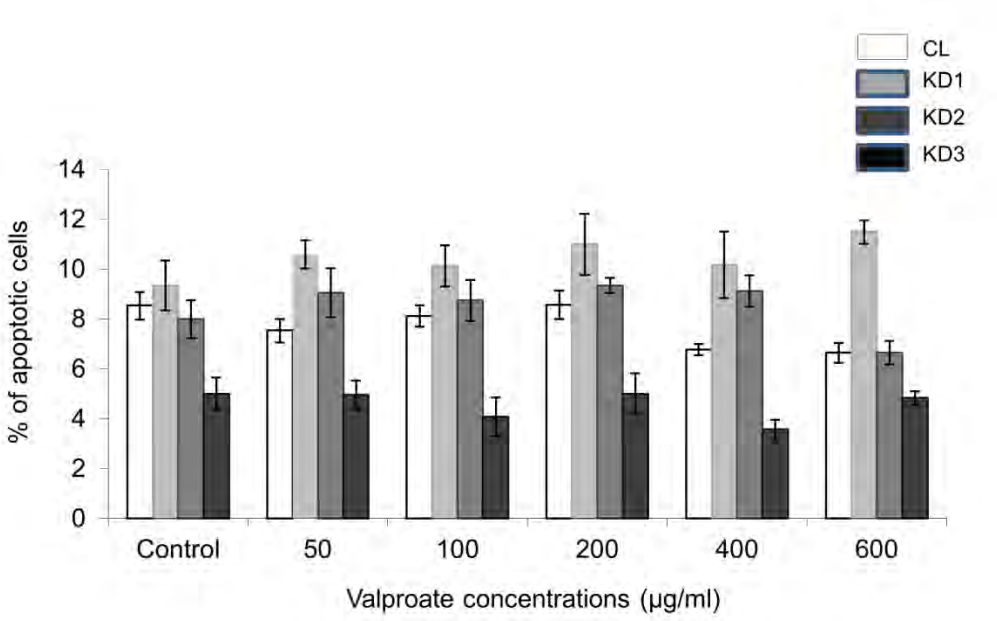

B

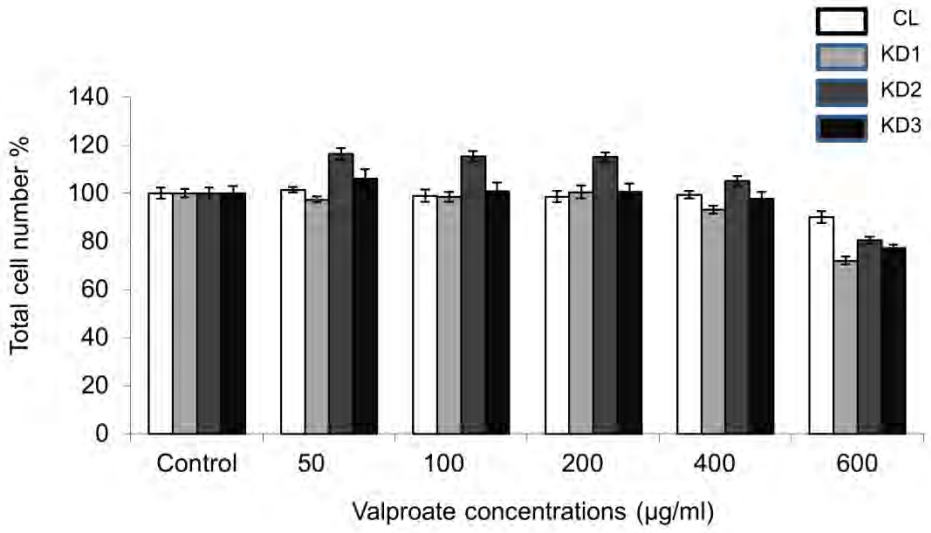

Figure 6.3: Toxicity assessment of valproate to human neuroblastoma cells

WFS1 stably depleted and control SK-N-AS cells were grown for 24h and incubated with various concentrations of valproate for another 24 hours. At the end of incubation, cells were fixed with 85% ethanol and stained with PI as indicated in Materials and Methods before being scanned with the Acumen eX3 cytometer.(A) The percentage of apoptotic cells in WFS1 depleted and control SK-N-AS cells after VPA treatment. (B) Total cell number against different concentrations of valproate. N=8 and p=NS

To assess the effectiveness of VPA in human neuroblastoma cell lines with reduced WFS1 expression and to determine its optimal dose, the expression of WFS1 was measured in VPA treated samples by HCC. The data is presented as protein per cell in Figure 6.4. This Figure shows that the expression of WFS1 was increased at most chosen concentrations in the control and in the three knockdown cell lines. In the control cell line, the expression of WFS1 was significantly increased at 50, 100 and 200µg/mL and there were no changes observed at 400 and 600µg/mL in comparison to untreated cells. In the KD1 cell line, the expression of WFS1 was not changed up to 200µg/mL and significantly increased at 400 and 600 µg/mL. In the KD2 cell line, there was a significant increase in WFS1 expression in at all VPA concentrations used. In the KD3 lines, the expression of WFS1 was significantly increased only at the highest VPA dose. These findings suggest that VPA treatment has a dose dependent but variable effect in WFS1 depleted neuroblastoma cell lines. However, 600µg/mL VPA treatment induced the expression of WFS1 in the three knockdowns but not in the control.

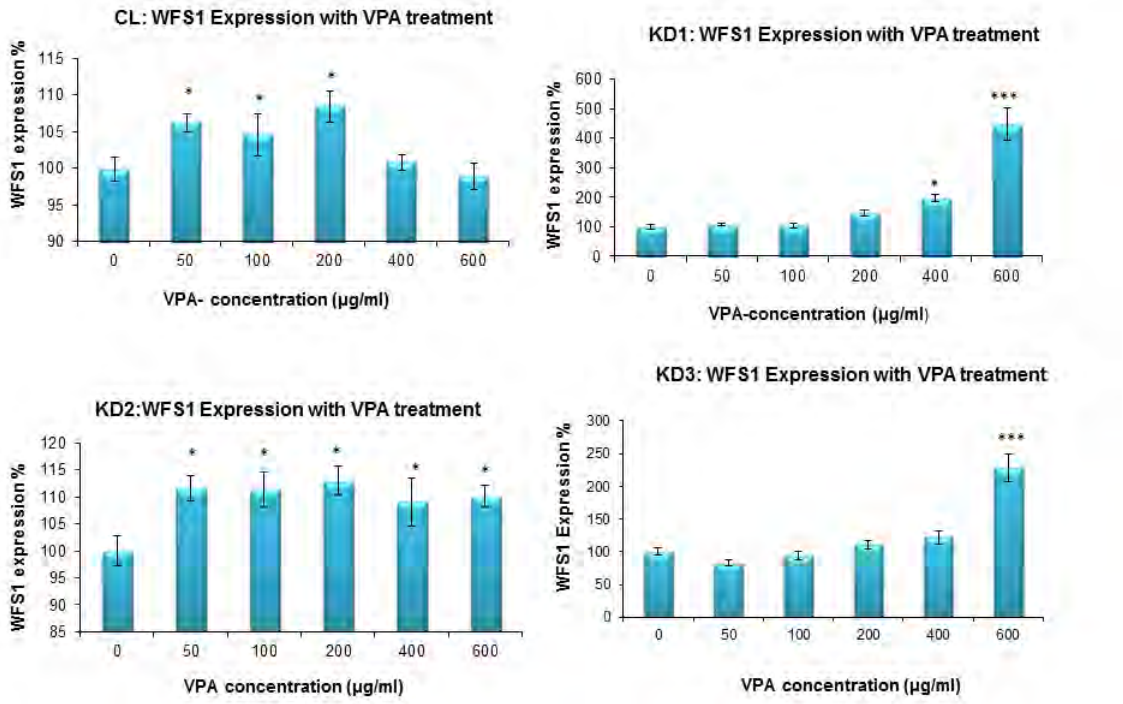

Figure 6.4: Expression of WFS1 with VPA treatment measured by HCC

WFS1 stably depleted and control SK-N-AS cells were grown for 24h and incubated with various concentrations of valproate for another 24 hours. Afterwards, cells were fixed with glyo-fixx and 85% ethanol and stained O/N with primary antibody and for 2 hours with secondary FITS antibody the following day. The plate was then stained with PI as indicated in Materials and Methods before being scanned with the Acumen eX3 cytometer. The expression of WFS1 in untreated samples was assumed to be equal to 100% and drug treated samples were compared to untreated cells. N=8, T-test: *p<0.05, **p<0.01, and ***p<0.001

6.3.2 VPA treatment increases WFS1 expression on mRNA and protein levels

Based on the toxicity data obtained by HCC, the effects of VPA treatment were investigated on mRNA and on protein levels at three concentrations (50, 100 and 200µg/mL) for 24 hours in two WFS1 depleted cell lines and the control cell line. The reason for choosing these concentrations was as they are within the recommended therapeutic ranges for humans. Also the data presented in Figure 6.4 was not analysed yet, which shows that 600µg/mL is the ideal concentration to take forward. The data presented in Figure 6.5 shows the mRNA expression of *WFS1* in VPA treated samples by QPCR. The drug treated samples were measured and compared to untreated sample of the same clone. The expression of *WFS1* was significantly increased in VPA treated samples in comparison to untreated. There was a higher elevation of the *WFS1* mRNA observed in the control cells in comparison to the WFS1 depleted cell lines. However in all three cell lines the expression was the highest at 100µg/mL (Figure 6.5B). Two to 6 fold increases were observed in *WFS1* mRNA expression in the control samples, 2 to 3 fold increases in KD2 and 2 to 4 fold increases in KD3 with VPA treatment.

The expression of Wolfram protein (Wolframin) measured in VPA treated cells is presented in Figure 6.6. This figure shows significant elevations of WFS1 expression in VPA treated samples versus untreated. The data showed an obvious elevation of the expression of WFS1 in the two knockdowns at every concentration of VPA studied, in comparison to the control. In the control cell line, increase of the WFS1 protein levels was observed only at 200µg/mL which was not statistically significant. In KD2, there was a 60% increase in the WFS1 protein expression at 50µg/mL, 180% increase at 100µg/mL and about 3 fold increases at 200µg/mL. In the KD3 cell

line, there was approximately 2 fold increase in the expression of WFS1 at the three concentrations of VPA in the cells. Overall, the obtained data indicates that VPA is capable of increasing the expression of WFS1 in human neuroblastoma cell lines.

A

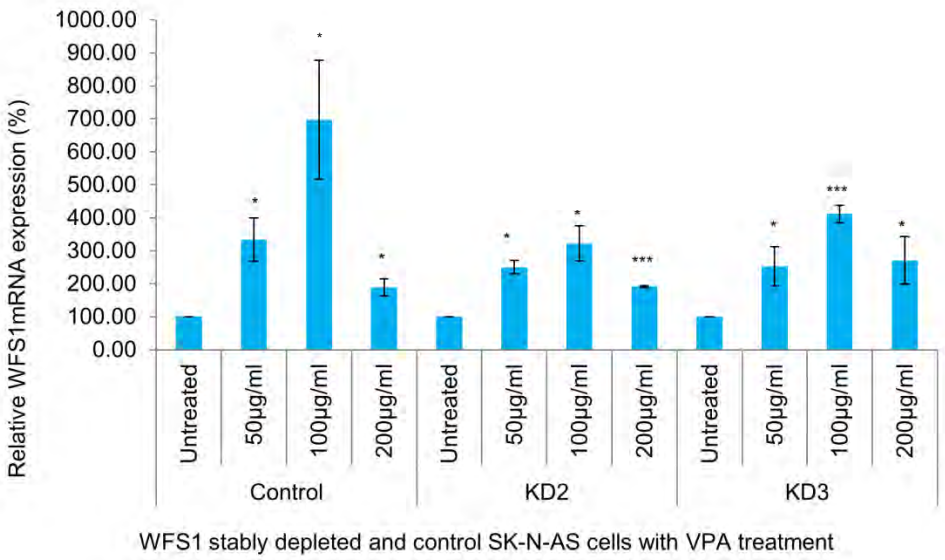

B

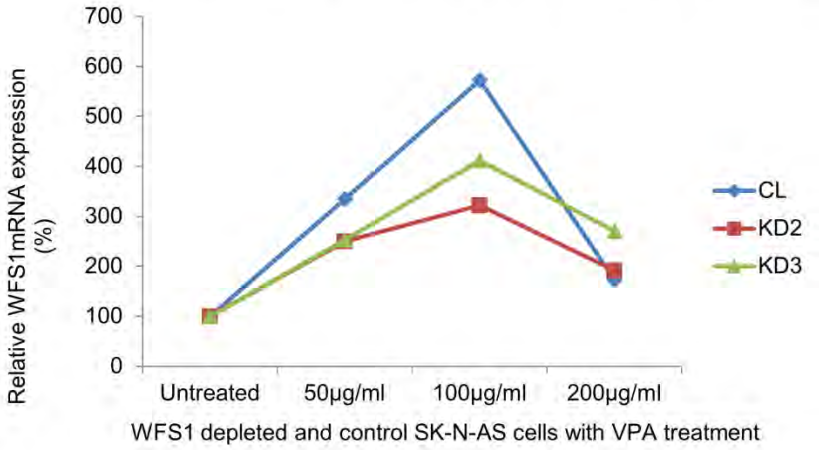

Figure 6.5: VPA treatment increased *WFS1* mRNA expression

(A). Quantitative real-time PCR of WFS1 in stable clones with WFS1 depletion in human SK-N-AS cell line with VPA 24 h treatment. CL=control, KD2 and KD3=WFS1 depleted clones, (n>3) T-test, *p<0.05, **p<0.01, and ***p<0.001. (B) Same data presented as line graphs. The expression in untreated cells was assumed as 100% and the drug treated samples were compared to untreated samples.

A

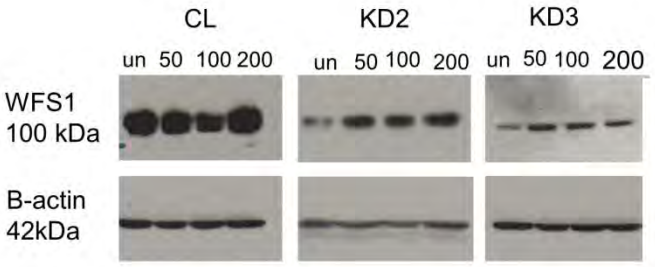

B

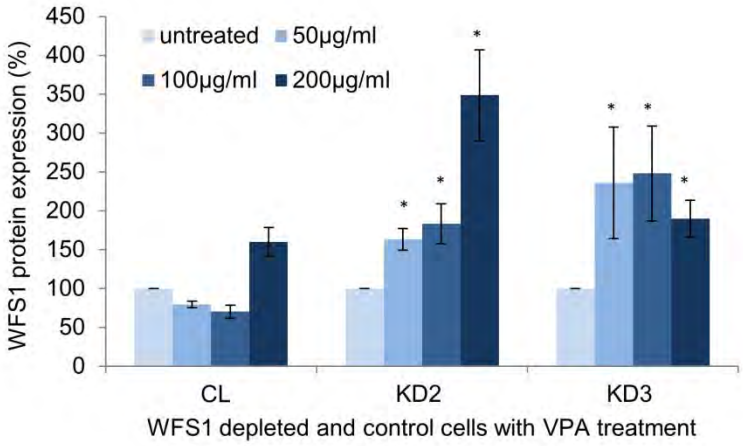

Figure 6.6: Elevation of WFS1 protein by valproate treatment

A: Immunoblot analysis of WFS1 protein using lysates from WFS1 stably depleted human SK-N-AS cells with 24h VPA treatment (50, 100 and 200µg/mL). The amount of beta actin is shown in the lower panel. B: Protein quantification of the immunoblot. CL=control, KD2 and KD3=WFS1 depleted clones, n>3, T-test: *p<0.05, **p<0.01, and ***p<0.001). The expression in untreated cells was assumed as 100% and the drug treated samples were compared to untreated samples

6.3.3 Valproate treatment has no effect on the expression of ER stress markers

After observing an obvious increase in the mRNA and the protein expression of WFS1, it was decided to investigate the expression of ER stress markers in VPA treated samples. The mRNA expressions of BiP, CHOP and spliced XBP1 were measured by real time PCR in cells with 24h VPA treatment in comparison to the untreated cells. The data presented in Figure 6.7 shows that VPA treatment at these conditions had no significant effect on the mRNA expression of ER stress markers BiP, CHOP and spliced XBP1. The expression of BiP and GRP94 were also measured on protein level by immunoblotting in VPA treated samples (Figure 6.8). The obtained data showed no significant changes in BiP or GRP94 expression in VPA treated samples in comparison to untreated. Overall, 24 hours treatment of WFS1 depleted and control cells with sodium valproate at 50, 100 and 200µg/mL had no significant effect on the mRNA and protein expression of ER stress markers BiP, CHOP, SP-XBP1 and GRP94.

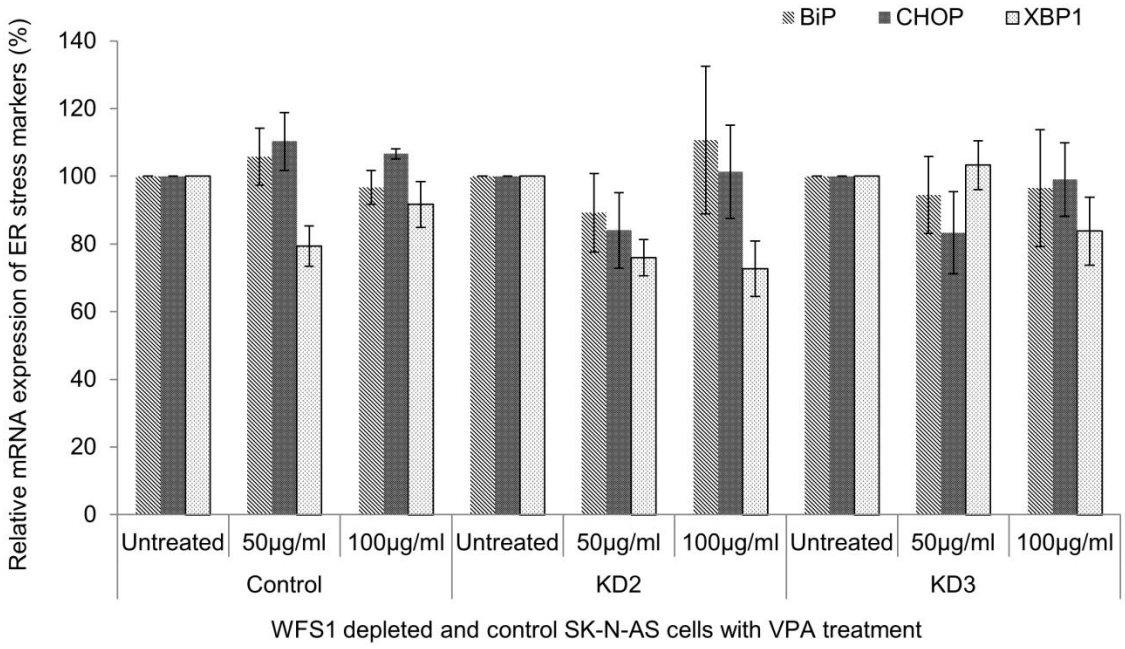

Figure 6.7: mRNA expression of ER stress markers after VPA treatment

Quantitative real-time PCR analysis of BiP, CHOP and Spliced XBP1 in stable clones with WFS1 depletion in human SK-N-AS cell line with VPA 24h treatment CL=control, KD2 and KD3=WFS1 depleted clones, (n>3), T-test: p=NS. mRNA expression in untreated cells was assumed 100% and the drug treated samples were compared to untreated samples

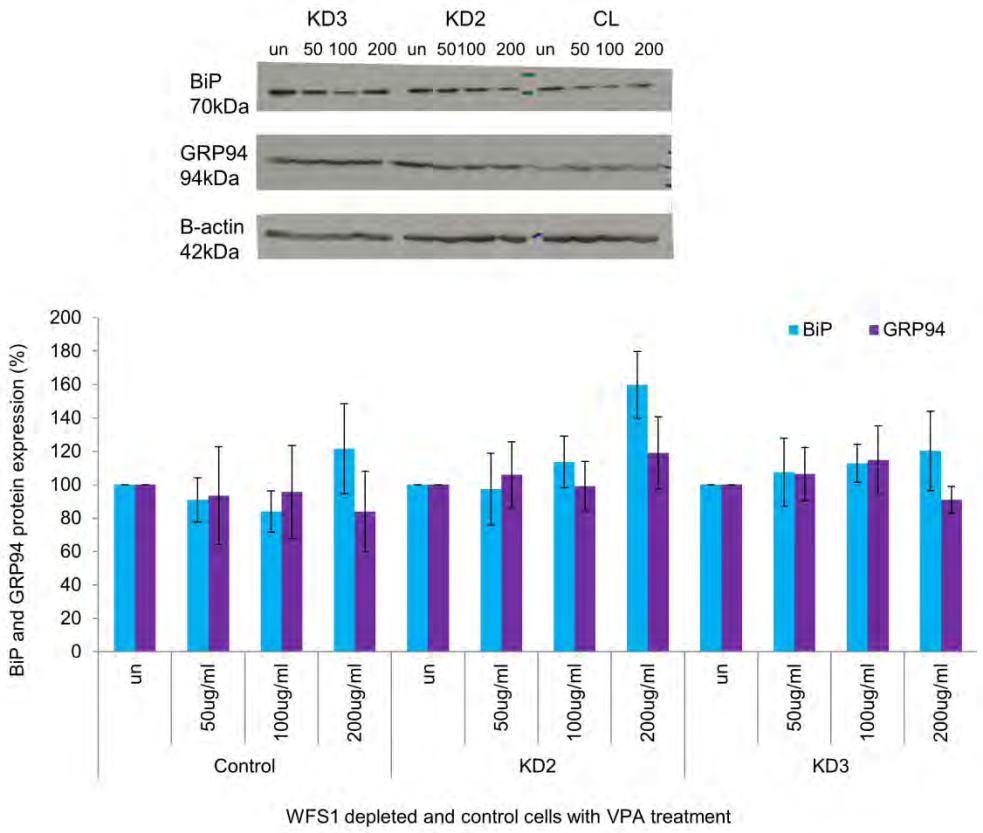

Figure 6.8: Protein expression of ER stress markers with VPA treatment

Immunoblot analysis of BiP and GRP94 protein using lysates from WFS1 depleted human SK-N-AS cells with 24 h VPA treatment (50, 100 and 200µg/mL). The amount of beta actin is shown in the lower panel. Quantification of the immunoblot, CL=control, KD2 and KD3=WFS1 depleted clones, (n>3) T-test: p=NS. Protein expression in untreated cells was assumed as 100% and the drug treated samples were compared to untreated samples

6.3.4 The effect of Valproate treatment on the levels of apoptotic markers in WFS1 depleted cells

Several studies have shown the neuroprotective effect of VPA in *in vitro* and *in vivo* disease models of neurodegenerative diseases (Chen et al., 1999, Chen et al., 2006). Therefore, the expression levels of the pro-apoptotic marker BAX and anti-apoptotic marker BCL-2 were measured in VPA treated samples by real time PCR. BCL-2 and BAX are members of the BCL-2 family of proteins which are central regulators of the mitochondrial pathway of apoptosis. The BCL-2 family is composed of pro- and anti-apoptotic proteins. Anti-apoptotic members such as BCL-2 promote cell survival by inhibiting the functions of the pro-apoptotic proteins. The data presented in Figure 6.9 shows that the expression of BCL-2 was significantly increased by 2 fold in VPA treated control and WFS1 depleted cells in comparison to the untreated cells. The expression of BAX was slightly increased by 10 to 40% in VPA treated samples in comparison to the untreated cells; however this increase was not statistically significant.

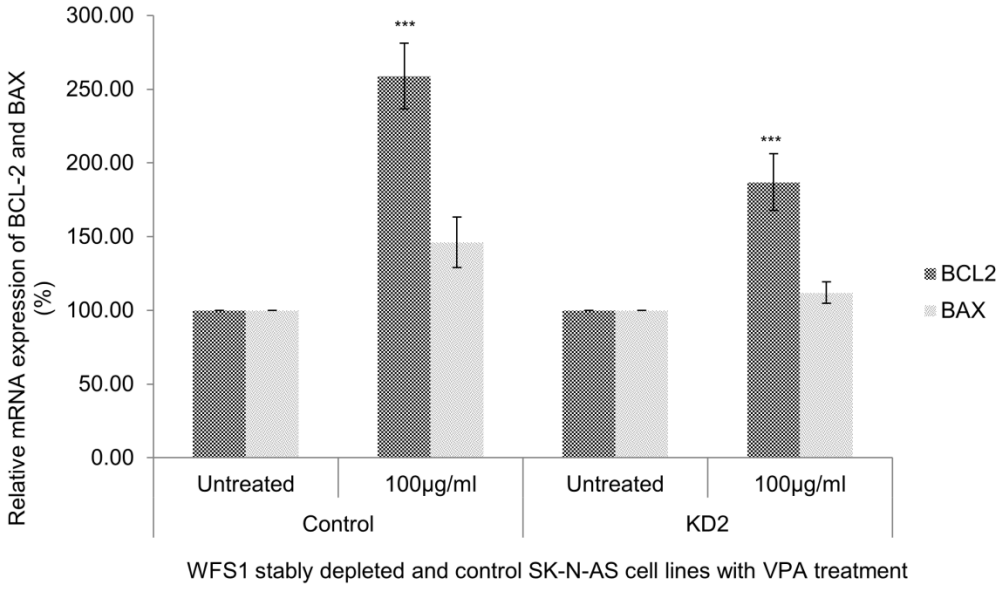

Figure 6.9: mRNA expression of apoptotic markers after VPA treatment

Quantitative real-time PCR of BCL-2 and BAX in stable clones with WFS1 depletion in human SK-N-AS cell lines after treatment with VPA (100µg/mL) for 24h, CL=control, KD2=WFS1 depleted clone, (n>3), T-test: BCL-2 p=0.001, BAX-p=NS **(***p<0.05, **p<0.01, and ***p<0.001), the expression in untreated cells was assumed 100% and the drug treated samples were compared to untreated samples.

6.3.5 Valproate treatment normalises the expression of the beta1 subunit of sodium pump and the V1A subunit of proton pump

The data presented in chapter 4 demonstrated that WFS1 depleted cells harbour reduced expression of the beta1 subunit of sodium pump and the V1A subunit of the vacuolar proton pump. As VPA treatment resulted in an increase of WFS1 expression, it was hypothesised that VPA treatment might also cause elevation of the expression of these two ion pump subunits. Therefore, the expression levels of the beta1 subunit of sodium pump and the V1A subunit of vacuolar proton pump were measured by immunoblotting in VPA treated samples. The immunoblot data is presented in Figure 6.10 and showed that the expression of both ATP1B1 and ATP6V1A in the knockdowns with VPA treatment was significantly increased in comparison to untreated samples. The expression of beta1 subunit of sodium pump in control cells was increased by 20%, 5% and 10% at 50, 100 and 200µg/mL VPA treatment respectively in comparison to untreated samples, which was not statistically significant. In the KD2 cell line, the ATP1B1 expression was significantly increased by 3 fold at 50µg/mL VPA, by 120% at 100µg/mL and by 80% at 200µg/mL VPA treatment in comparison to untreated samples ($n>3$, $p<0.05$). In the KD3 cell line, the ATP1B1 expression was significantly increased by 51%, 52% and 35% at 50, 100 and 200µg/mL respectively ($n>3$, $p<0.05$).

The expression of the V1A subunit of the vacuolar proton pump measured in the control cells after 24 hour VPA treatment was slightly decreased by 7%, 24%, and 10% at 50, 100 and 200 µg/mL in comparison to untreated sample (100%); however these changes were not statistically significant. In KD2 cell line, V1A expression was significantly increased by 54%, 61% and 42%

at 50, 100 and 200µg/mL ($p<0.05$). In the KD3 cell line, the expression of V1A was significantly increased by 58%, 125% and 106% at 50, 100 and 200µg/mL ($p<0.05$). The data is taken from more than three experiments using three different drug treated protein lysates. In the control samples, the expression of ATP1B1 and ATP6V1A after valproate treatment was not significantly changed. This could be explained as these samples have normal expression levels of both proteins and perhaps other mechanisms prevent over-expression. WFS1 depleted cells show decreased expressions of ATP1B1 and ATP6V1A and therefore VPA treatment could upregulate the expression of these two proteins in these cells.

A

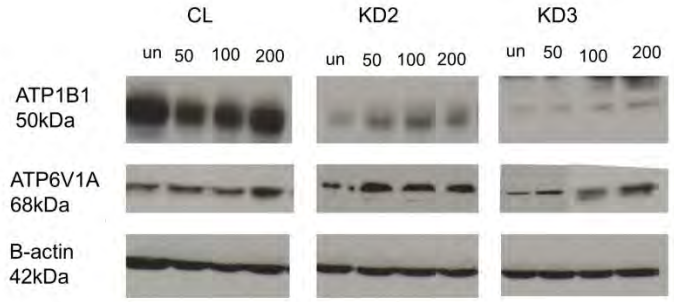

B

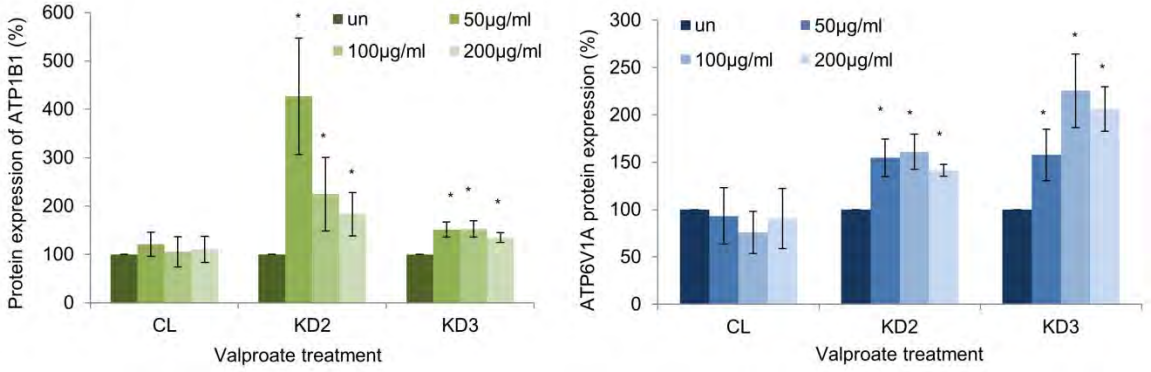

Figure 6.10: Protein expression of ATP1B1 and ATP6V1A after VPA treatment

A: Immunoblot analysis of ATP1B1 and ATP6V1A proteins using lysates from control and WFS1 depleted human SK-N-AS cells with 24h VPA treatment (50, 100 and 200µg/mL). The amount of beta actin is shown in the lower panel. B: Quantification of immunoblot CL=control, KD2 and KD3=WFS1 depleted clones, (n>3), T-test: $p<0.05$, (*$p<0.05$, **$p<0.01$, and ***$p<0.001$). The expression in untreated samples was assumed as 100% and the drug treated samples were compared

6.3.6 The effect of VPA on cell cycle kinetics and expression of WFS1 in G1 and G2 phases

The effect of VPA treatment was investigated on cell cycle kinetics in the three WFS1 depleted and control cell lines by assessing the fractions of cells in G1 and G2 phases by HCC. The KD1 cell line was included in these experiments as this cell line was shown to have a cell cycle arrest in the G1 phase (Chapter 3). Consequently it was thought that the effect of the drug treatment would be more obvious in this cell line. The data is expressed as the percentage of G1 and G2 cells after VPA treatment and presented in Figure 6.11. Figure 6.11A shows the effect of various concentrations of VPA in the control cell line; the percentage of G1 cells was significantly increased at 200, 400 and 600µg/mL in comparison to untreated cells. The percentage of G2 cells did not show any significant changes with VPA treatment. Figure 6.11B shows the effect of VPA on cell cycle kinetics and apoptosis in KD1 cell line. The percentage of G1 cells was unaffected up to 400µg/mL and significantly increased at 600µg/mL. Similarly, the percentage of G2 cells was unchanged up 400µg/mL and significantly decreased at 600µg/mL in comparison to untreated cells (Figure 6.11B, 2nd chart). In the KD2 cell line, the effect of VPA on the percentage of G1 cells was not significant and the percentage of G2 cells with VPA treatment was reduced significantly at 50, 100 and 200µg/mL in comparison to untreated cells (Figure 6.11C, 2nd graph). In the KD3 cell line, the percentage of G1 cells increased only at 600µg/mL VPA treatment in comparison to untreated cells. Similarly, the percentage of G2 cells decreased significantly at 600µg/mL. Overall, this is preliminary data and inconclusive at this stage. More experiments are needed to expand and confirm the findings to draw any conclusion.

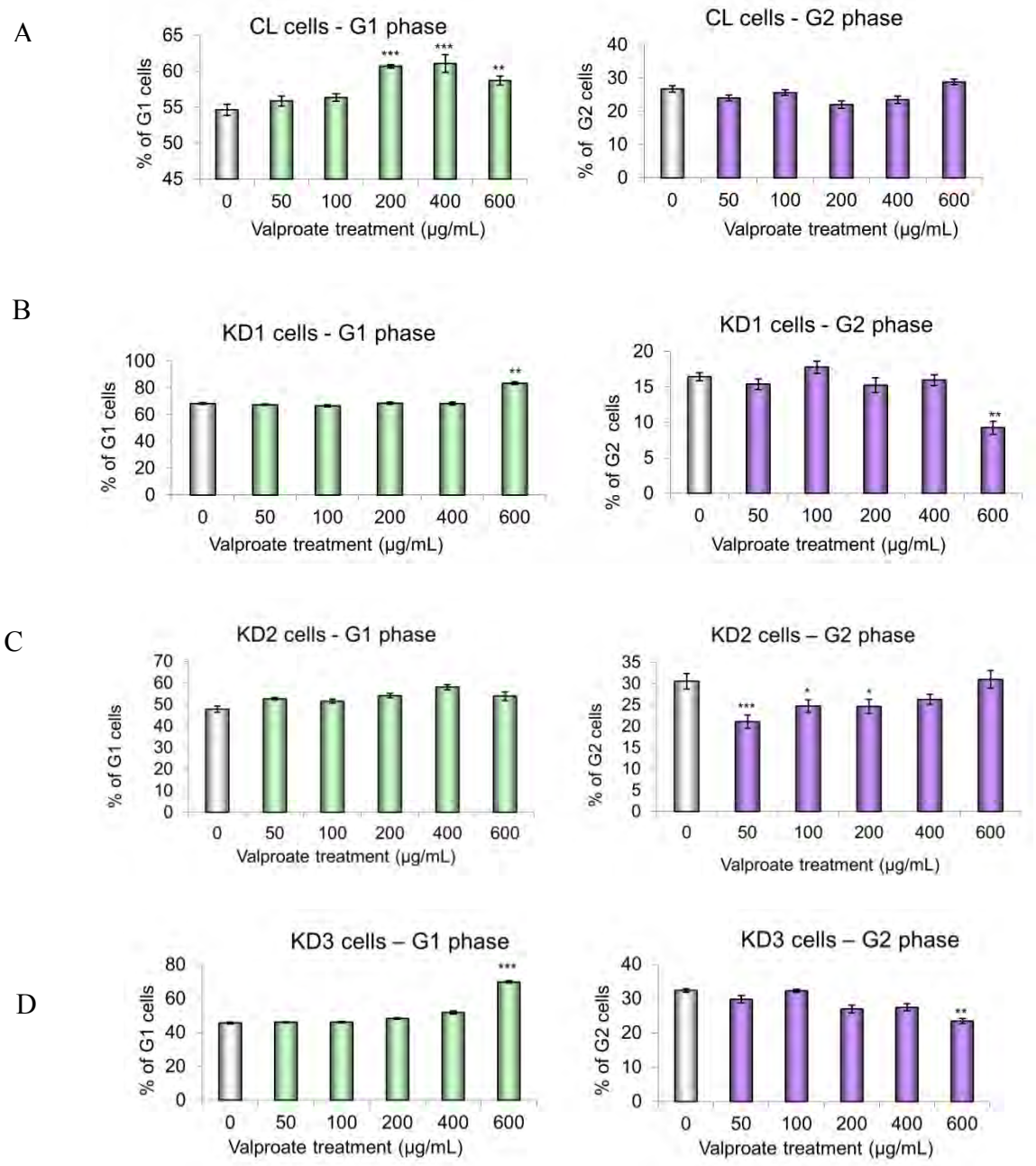

Figure 6.11: Effect of VPA on cell cycle kinetics and apoptosis in WFS1 depleted cells

WFS1 stably depleted and control SK-N-AS cells were grown for 24h and incubated with various concentrations of valproate for 24 hours. At the end of incubation, cells were fixed and stained with PI and scanned with the Acumen eX3 cytometer. (A) The percentage of G1 and G2 cells assessed against various concentrations of VPA in control cell line. (B-D) percentage of G1and G2 cells in KD1, KD2 and KD3 respectively after VPA treatment. N=8**,** T-test: *p<0.05, **p<0.01, and ***p<0.001

The expression of the WFS1 protein; (Wolframin) was assessed in the G1 and G2 phases of the cell cycle using HCC. Changes in protein expression can be expressed in different ways: changes in cell numbers that express WFS1, changes in total WFS1 protein and the amount of WFS1 protein per cell. Data presented in Figure 6.12 shows that the WFS1 protein expression is cell cycle dependent. The first graph shows changes in total WFS1 protein in G1 and G2 phases of the cell cycle, (measured as total fluorescence); the second graph shows the percentage of WFS1 positive cells (cells expressing WFS1) in the G1 and G2 phases of the cell cycle and the third graph shows the WFS1 protein content calculated as protein per cell (total fluorescence divided by a number of cells) in different phases of the cell cycle.

Generally, WFS1 expression was more frequent in G2 cells than in G1 cells. In the control cell line, the first graph shows that the total WFS1 protein expression in G1 cells was decreased in all concentrations of VPA in comparison to untreated cells, where maximum decrease was observed at 400µg/mL followed by an increase at 600µg/mL VPA treatment. Similarly in G2 phase, the total WFS1 protein significantly increased at 600µg/mL VPA treatments. The second graph shows that there were more WFS1 positive G2 cells at each concentration of VPA than WFS1 positive G1 cells. The percentage of G1 cells expressing WFS1 did not change significantly with VPA treatment, while the percentage of G2 cells expressing WFS1 increased significantly at 600µg/mL. The third graph shows that there were no significant changes in WFS1 protein per cell in either G1 or G2 phases with VPA treatment.

The effect of VPA treatment was similar in All three WFS1 depleted cell lines, therefore a representative set of data of one cell line (KD3) is presented in figure 6.12 B; In WFS1 depleted cells, the first graph shows that VPA treatment significantly increased the WFS1 protein expression in both populations (G1 and G2) only at the highest dose. The second graph shows that the proportion of WFS1 positive G1 cells increased only at the highest VPA concentration, but in the G2 population it increased also at lower doses. The third graph shows that the WFS1 protein per cell was higher in G1 cells than in G2 cells, where in G2 cells it did not change with VPA treatment and the protein per G1 cells significantly decreased at the highest dose of VPA.

Overall, this data shows that in WFS1 depleted neuroblastoma cells the elevation of WFS1 protein expression by VPA was cell cycle dependent. In the control cell line, the total WFS1 protein in G1 phase was decreasing with VPA treatment and in G2 cells the protein levels were decreasing at lower concentrations but significantly increased at the highest dose. However in WFS1 depleted cells, the total WFS1 protein was increased very gradually but significantly at the highest dose. This increase was most probably caused by the increase of the percentage of WFS1 positive cells in G1 and G2 phases after VPA treatment, where the expression of WFS1 was more frequent in G2 than in G1 cells. These findings are preliminary and inconclusive at this stage, more experiments are needed to confirm the finding and draw any conclusion about the effect of VPA on the expression of WFS1 in cell cycle phases.

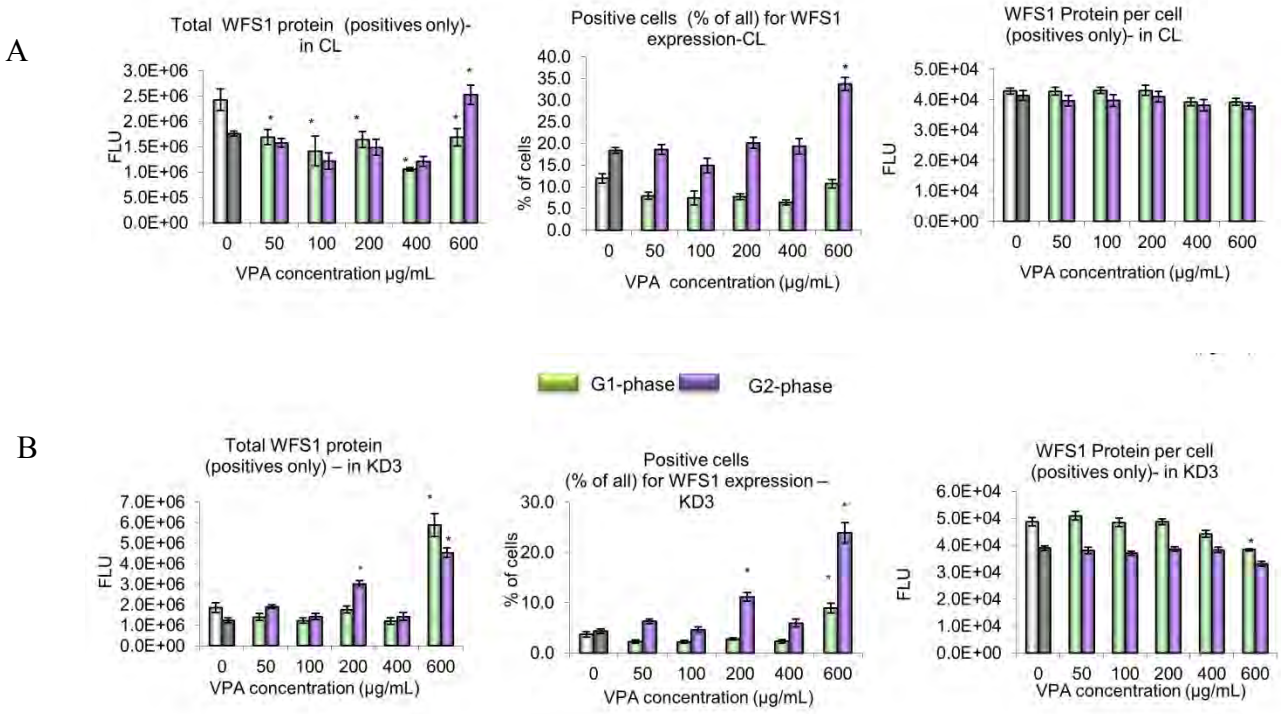

Figure 6.12 Expression of WFS1 protein in G1 and G2 phases measured by HCC

WFS1 stably depleted and control SK-N-AS cells were grown for 24h and incubated with various concentrations of VPA for 24 hours. At the end of incubation, cells were fixed and stained with PI and scanned with the Acumen eX3 cytometer. Left graph: total WFS1 protein expression, middle graph: percentage of WFS1 positive cells, right graph: WFS1protein per cell. A: CL and B: KD3. N=8, T-test: *p<0.05, **p<0.01, and ***p<0.001

6.4 Discussion

This study demonstrates that sodium valproate has potential to be used as a therapeutic agent in the treatment of Wolfram syndrome. The data presented in this chapter showed that 24 hour VPA treatment caused significant induction in the expression of WFS1 on mRNA and protein levels in human neuroblastoma cells with reduced expression of WFS1. This 24 hour treatment with VPA did not have a significant effect on the expression of ER stress markers BiP, CHOP, GRP94 and spliced XBP1 on mRNA and/or on protein levels. VPA treatment caused significant elevation of the expression of the neuroprotective protein BCL-2 and did not cause significant effects on the expression of the pro-apoptotic marker BAX in WFS1 depleted and control SK-N-AS cells. Furthermore, 24h VPA treatment resulted in significant elevation of the expression of ATP1B1 and ATP6V1A in WFS1 depleted SK-N-AS cells on protein level.

The findings in this chapter are consistent with previous findings showing induced expression of WFS1 by VPA treatment in rodent neuronal cells. A study by Kakiuchi et al. (2009) showed that VPA treatment modulates ER stress by activating the promoter region of the *WFS1* gene. The authors showed an association between WFS1 and GRP94 protein under normal conditions and VPA treatment decreased the ratio between immunoprecipitated WFS1 and GRP94 in a dose-dependent manner. Their results indicated that VPA caused dissociation of WFS1 from the complex with GRP94 and that GRP94-free WFS1 levels are increased with valproate treatment (Kakiuchi et al., 2009).

The obtained data also demonstrates that 24h VPA treatment did not significantly change the expression of ER stress markers: BiP, CHOP, spliced XBP1 and GRP94. This data suggest that the upregulation of WFS1 by VPA could be attributed to some specific mechanism of VPA, because under the same conditions, the expression of ER stress markers was not affected. This specific upregulation of WFS1 expression could be due to activation of the promoter sequence of WFS1 by VPA and/or WFS1 release from the complex with GRP94 as reported by Kakiuchi et al. (2009) and Kakiuchi et al. (2006).

Previous studies in rodent neuronal cells have shown that chronic VPA treatment regulates ER stress proteins (Wang et al., 1999, Chen et al., 2000). The study conducted by Bown et al. (2000) showed that chronic VPA treatment protects the cells by reversibly inducing the expression of ER stress proteins (BiP, GRP94) to alert the cell to switch on the UPR. A very recent study by Zhang et al. (2011) showed that VPA treatment protects ischemic retinae from ER stress induced apoptosis by promoting the expression of ER chaperones. They demonstrated a significant increase in the expression of BiP in rat brain and C6 glioma cells resulting in prevention of apoptosis mediated by CHOP (Zhang et al., 2011).

In the present study, 24 hours treatment with VPA (100µg/mL) significantly increased the expression of the neuroprotective protein BCL-2. However, no significant changes were observed in the expression of the pro-apoptotic protein BAX. These findings are supported by previous studies showing increased expression of BCL-2 in response to VPA treatment. The study conducted by Chen and colleagues (1999) demonstrated that chronic VPA treatment provides

protection against cell death possibly through regulation of anti-apoptotic genes; they showed increased expression of the anti-apoptotic protein BCL-2 in the frontal cortex of rats following chronic VPA treatment. BCL-2 has been shown to protect a variety of cells including neurons against both necrotic and apoptotic cell death. Their findings implied that VPA could be the potential treatment for various neurodegenerative disorders (Chen et al., 1999).

A wide range of studies have investigated the role of VPA in cancer treatment (Catalano et al., 2005, Wei et al., 2011). Wei and colleagues (2011) showed that 48h treatment with VPA inhibited cell proliferation and induced apoptosis in HepG2 cells in a dose dependent manner. They showed that VPA treatment decreased the expression of BCL-2 and had no effect on the expression of BAX. They also showed morphological changes caused by VPA treatment; however reducing the membrane potential of mitochondria, condensation and fragmentation of chromatins and activation of Caspase 3 and 9, all signs of apoptosis. Similarly, the study conducted by Catalano et al. (2005) showed that VPA treatment induced apoptosis in poorly differentiated thyroid carcinoma suggesting that VPA is a promising anticancer drug. Thus VPA has different mechanisms of actions depending on the cell type, drug concentration and the length of treatment (Loy and Tariot, 2002).

Furthermore, this chapter showed that VPA treatment significantly increased the expression of ATP1B1 and ATP6V1A in WFS1 depleted neuroblastoma cells (Figure 6.10). The data presented in Chapter four focused on the role of WFS1 in the stability and regulation of these two ion pump subunits, showing reduced expression of ATP1B1 and ATP6V1A in WFS1 depleted cells

(Figures 4.3-4.5 and 4.8). This data suggests that the observed induction in the expression of ATP1B1 and ATP6V1A in WFS1 depleted cells could be either a direct consequence of VPA treatment or a secondary effect of the WFS1 upregulation by VPA. Since the expression of these two proteins was not significantly increased in the control cells, it could be speculated that this effect is most probably due to WFS1 induction by VPA in WFS1 depleted cells.

Studies have shown that VPA treatment affects the G1-S transition and causes cell cycle arrest in the G1 phase of the cell cycle resulting in activation of differentiation processes by increasing the expression of p21 in human ESS-1 cell lines (endometrial stromal sarcomas) (Hrzenjak et al., 2006). The study by Catalano et al. (2005) showed that VPA treatment induces cell cycle arrest in the G1 phase in association with increased expression of p21 and cyclin A in cancer cells. The data obtained on cell cycle events in this chapter is preliminary and needs to be confirmed in other cell lines and cell models to understand the mechanism of action of VPA in regulation of WFS1 and cell cycle events. Further studies are required to investigate the effect of VPA treatment over a longer period of time on the expression of WFS1 in cell cycle phases to understand the mechanism of VPA in treatment of WS and other neurodegenerative disorders. This could be achieved by studying the effect of VPA in several cell lines including primary cells, using wider range of the drug concentrations and different assays. To understand the effect on cell cycle, the regulators of the cell cycle checkpoints should be assessed in VPA treated samples such as p21 and the proteins of the cyclin family.

To distinguish the neuroprotective and anti-tumour functions of VPA, a broad range of experiments are required. The main experiments could be to establish when VPA functions to inhibit apoptosis and when it induces apoptosis like in cancer cells. A series of *in vitro* and *in vivo* experiments could be carried out with different concentrations of VPA within the therapeutic ranges, experimenting on different cell types and different time courses of VPA treatment. The effect of these treatments could be tested by luciferase assay, annexin binding assay or measuring the levels of apoptotic markers such as the BCL-2 and the caspases families. Morphological changes could be also investigated such as shrinkage of the mitochondrial membrane. It may be possible that after confirmation of these findings in primary cells and *in vivo* models, VPA could be translated in clinical trials for treatment of Wolfram syndrome, at least for patients with missense mutations, who make up a large number (±50%) of patients in the Wolfram database (EURO-WABB, 2012). The data in this chapter clearly demonstrated that VPA significantly increased the expression of ATP1B1 and ATP6V1A only in the cells with reduced expression of WFS1. Therefore, treatment of Wolfram patients with missense mutations with sodium valproate could potentially slow down the progression of this neurodegenerative disease.

Chapter Seven: TUDCA alleviates ER stress and apoptosis

7.1 Introduction

TaurineConjugatedUrsodeoxyCholicAcid (TUDCA) is a hydrophilic bile acid which is endogenously produced in low levels in the liver by conjugation of taurine to urosodeoxy cholic acid. TUDCA is approved as a drug by the Food and Drug Administration (FDA) for the treatment of several liver diseases and has a well characterised safety profile in humans (Ozcan et al., 2009, Rodrigues et al., 2000, Xie et al., 2002). TUDCA has shown clinical efficacy for the treatment of hepatobiliary, biliary cirrhosis and cholestasis (Rodrigues et al., 2001, Rodrigues and Steer, 2001, Rodrigues et al., 2003). The chemical structure of TUDCA is presented in Figure 7.1.

TUDCA plays a unique role in modulating the apoptotic threshold in both hepatic and non-hepatic cells, acting as an anti-apoptotic agent. The anti-apoptotic mechanisms of ursodeoxycholic acid (UDCA) and TUDCA are attributed to their ability to directly inhibit the production of reactive oxygen species and prevent the disturbance of the outer layer of the mitochondrial membrane (Castro et al., 2004, Rodrigues and Steer, 2001, Rodrigues et al., 2003). These bile acids have anti-apoptotic and cytoprotective effects on hepatocytes by increasing bile flow and biliary acid secretion and hepatocellular vesicular exocytosis.

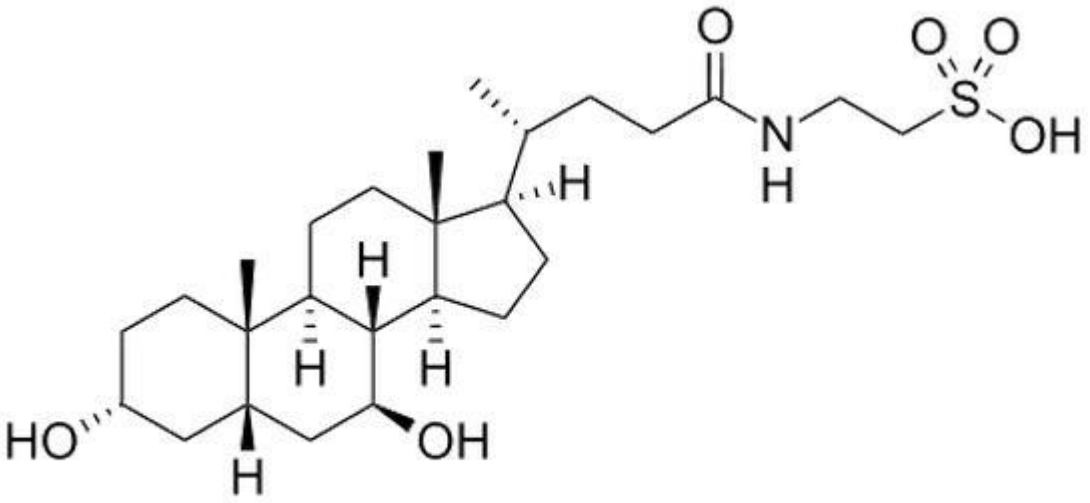

Figure 7.1: TUDCA; a hydrophilic bile acid
(ChemicalBook, 2008)

TUDCA is known to inhibit apoptosis via many pathways such as antagonising BAX translocation from the cytosol to the mitochondria and caspase activation in hepatocytes and in brain. TUDCA is also known to inhibit mitochondrial permeability transition and cytochrome c release (Rodrigues and Steer, 2001, Rodrigues et al., 2003). Recent reports have shown that TUDCA acts as a chemical chaperone (Ozcan et al., 2009). Chemical chaperones are groups of low molecular weight compounds that have been shown to increase functions of the Endoplasmic Reticulum (ER) and reduce ER stress (Perlmutter, 2002). As mentioned before, the ER is a crucial organelle functioning in proper synthesis, initial post-translational modification, proper folding and maturation of newly synthesised transmembrane and secretory proteins. It also serves as a regulator of calcium homeostasis (Shiraishi et al., 2006). Various stresses interfere with ER function resulting in the generation of mutant proteins leading to the accumulation of unfolded proteins in the ER lumen (Kaneko and Nomura, 2003). ER stress induced apoptosis is a crucial factor contributing to the pathophysiological conditions seen in many neurological disorders such as Alzheimer's diseases (AD), Parkinson's disease (PD), Huntington's disease (HD) and cardiovascular diseases (Szegezdi et al., 2006).

In many studies TUDCA is used in cell models where ER stress and apoptosis are chemically induced by thapsigargin or tunicamycin. Thapsigargin induces apoptosis through activation of caspase-12 as a result of increased cytosolic calcium. The study by Xie et al. (2002) demonstrated that TUDCA protects cells from thapsigargin induced apoptosis by blocking a calcium mediated apoptotic pathway with inhibition of caspase 12 activation. The study by Ozcan and colleagues (2009) demonstrated that TUDCA treatment alleviate tunicamycin induced ER stress in liver and

adipose tissue; enhance insulin sensitivity, and maintain euglycemia in a mouse model of severe obesity and type 2 diabetes.

The protective role of TUDCA has been extended to several experimental models of different neurodegenerative disorders demonstrating that, in neuronal cells, TUDCA inhibits apoptosis induced by several stimuli (Rodrigues et al., 2000, Rodrigues et al., 2003, Xie et al., 2002). For example, studies have shown that TUDCA is capable of significantly reducing mitochondrial perturbations associated with apoptosis induction in cultured neuronal cells incubated with 3-nitropropionic acid (Rodrigues et al., 2000). Similarly, TUDCA administration was shown to reduce the morphologic striatal lesions in the 3-nitropropionic acid rat model of HD (Keene et al., 2001). Moreover, behavioural studies showed the neuroprotective effect of TUDCA resulting in reduction of hyperactive behaviour in a transgenic mouse model of HD (Keene et al., 2002).

In a rat model of PD, TUDCA treatment was shown to improve the survival and function of nigral transplants (Duan et al., 2002). In this study, TUDCA significantly reduced apoptosis in ventral mesencephalic tissue cultures and within the transplants, implying that this bile acid inhibits apoptosis, aiding the survival of the dopamine neurons. Similarly, TUDCA treatment was shown to partially rescue a PD model of *Caenorhabditis elegans* from mitochondrial dysfunction (Ved et al., 2005). The anti-apoptotic effects of TUDCA were also shown in more acute conditions using rat models of transient focal cerebral ischemia (Rodrigues et al., 2002). In addition, intravenous administration of TUDCA was shown to reduce the infarct volume by 50%, modulating the levels of apoptosis and inhibiting the neurobehavioral impairment.

Moreover, in a collagenase-induced haemorrhagic model of stroke, TUDCA treatment resulted in reducing the degree of brain injury, and improved neurologic performance. This was caused by the actions of TUDCA in inhibiting caspase activation and preserving mitochondrial membrane stability (Rodrigues et al., 2003). A study by Colak and colleagues (2008) showed that intra-peritoneal injections of TUDCA had neuroprotective effects in a murine model of spinal cord injury. They demonstrated that TUDCA reduced the number of necrotic and apoptotic cells by mitochondrial stabilisation. Interestingly, pretreatment with TUDCA also significantly reduced glutamate-induced apoptosis of rat cortical neurons (Çolak et al., 2008). TUDCA was capable of modulating glutamate-induced caspase activation and cytochrome c release, reducing the apoptotic threshold (Castro et al., 2004).

To investigate whether TUDCA might be effective in the treatment of WS, the present study was focussed on assessing the effect of TUDCA in human neuroblastoma cell lines with WFS1 depletion. The expression levels of the ER stress and apoptosis markers BiP, CHOP, GRP94, BCL-2 and BAX and the role of TUDCA treatment in cell cycle kinetics were investigated in this chapter. The reason for choosing TUDCA was based on the literature, as TUDCA is known for reduction of ER stress and apoptosis. The hypothesis of this study was that TUDCA treatment would result in reduction of ER stress, apoptosis and normalisation of cell cycle impairment.

7.2 Aims

TUDCA has been shown to reduce ER stress and apoptosis in *in vitro* and *in vivo* animal models. In this chapter, the anti-apoptotic effects of TUDCA were investigated in human neuroblastoma cell models with reduced expression of WFS1.

The aims were as follows:

1. To assess the effect of TUDCA on BiP expression in neuroblastoma cells by High Content Cytometry.
2. To assess the effect of TUDCA treatment on the expression of ER stress and apoptosis markers by real time PCR.
3. To assess the effect of TUDCA treatment on cell cycle kinetics.

7.3 Results

7.3.1 Assessments of TUDCA toxicity and effectiveness in human neuronal cells

TUDCA is a small chemical chaperone that is known to reduce the levels of ER stress in diabetic and neurodegenerative disease models by enhancing the proper folding of the proteins. Studies have shown that TUDCA at 200 and 400μM reduces ER stress and apoptosis (Ozcan et al., 2006). Therefore the toxicity of this drug was assessed at a wider concentration range (100-900 μM) by High Content Cytometry. The data presented in Figure 7.2A shows the percentage of apoptotic cells in culture with 24h TUDCA treatment. The data showed no significant increase in the percentage of apoptotic cells with TUDCA treatment. There was a very low level of apoptosis in the cell culture (±10%) at all concentrations. Also the total cell number (Figure 7.2B) did not reduce significantly with TUDCA treatment, suggesting this drug was not toxic to human neuroblastoma cells at the chosen concentrations.

A

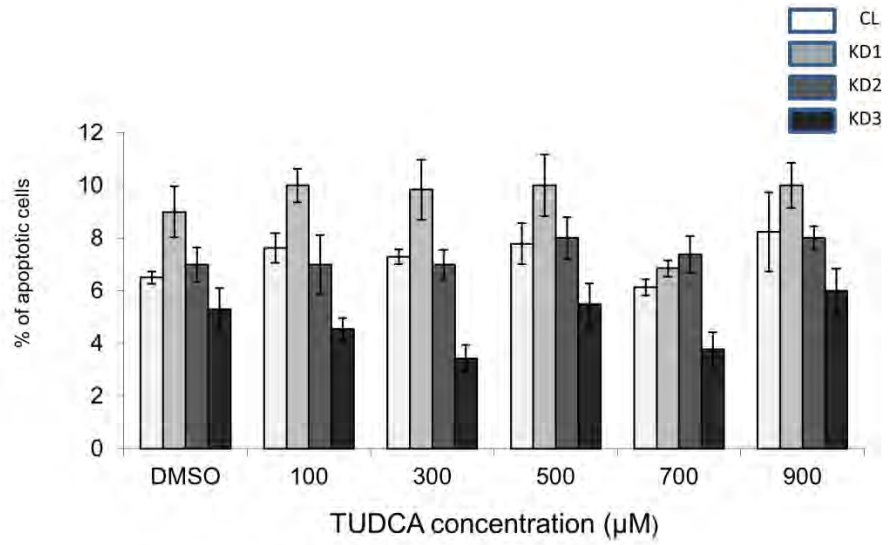

B

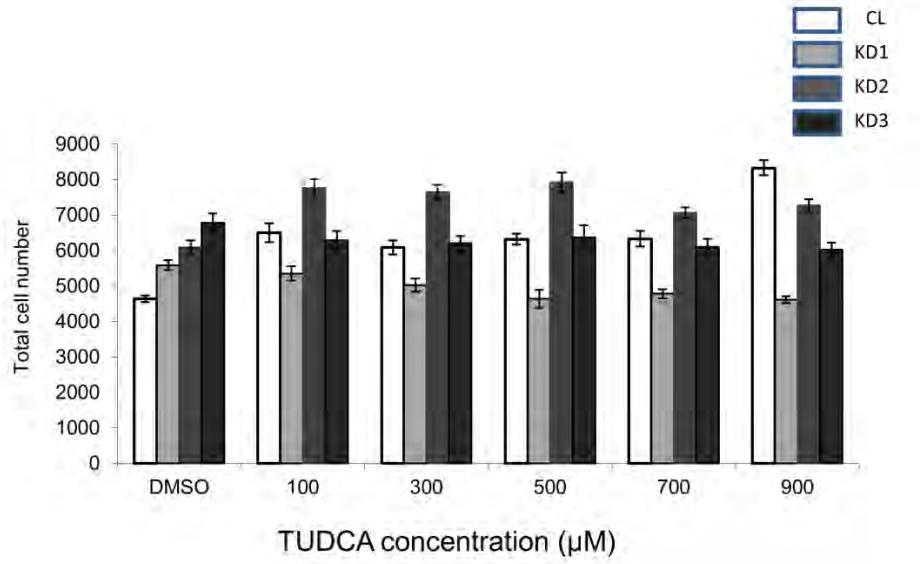

Figure 7.2: Toxicity assessment of TUDCA to human neuroblastoma cells

WFS1 stably depleted and control SK-N-AS cells were grown for 24h and incubated with various concentrations of TUDCA for 24 hours. At the end of incubation, cells were fixed and stained with PI before being scanned with the Acumen eX3 cytometer. (A) Percentage of apoptotic cells in WFS1 depleted and control SK-N-AS cells after TUDCA treatment. (B) Total cells number at various concentrations (100-900µM) of TUDCA. N=8 and p=NS

The effect of TUDCA is often shown by fluctuations in the expression of BiP/GRP78, which is a master regulator of ER stress. The expression of BiP increases in the presence of ER stress caused by accumulation of unfolded proteins, calcium and glucose deprivation and several cytotoxic insults (Brostrom and Brostrom, 1997). Studies have shown that cells require BiP to continue processing existing proteins and properly process damaged proteins (Bown et al., 2002). Therefore, in this study the effectiveness of TUDCA was determined by measuring the expression levels of BiP in samples with 24h TUDCA treatment by HCC. As studies have shown that TUDCA attenuates ER stress, it was hypothesised that the expression of BiP may be reduced in TUDCA treated samples in comparison to untreated.

Figure 7.3 shows that the expression of BiP was reduced at several concentrations of TUDCA. In the control cells, BiP expression was significantly reduced at 300, 500 and 700µM TUDCA treatment in comparison to the untreated samples. In KD1, a significant decrease in BiP expression was observed at 100µM and 300µM TUDCA treatment. In KD2 cells significant decreases in BiP expression were observed at 100µM TUDCA and in KD3 cells, significant decreases in BiP expression was observed at 100µM and 500µM TUDCA treatment in comparison to the untreated cells.

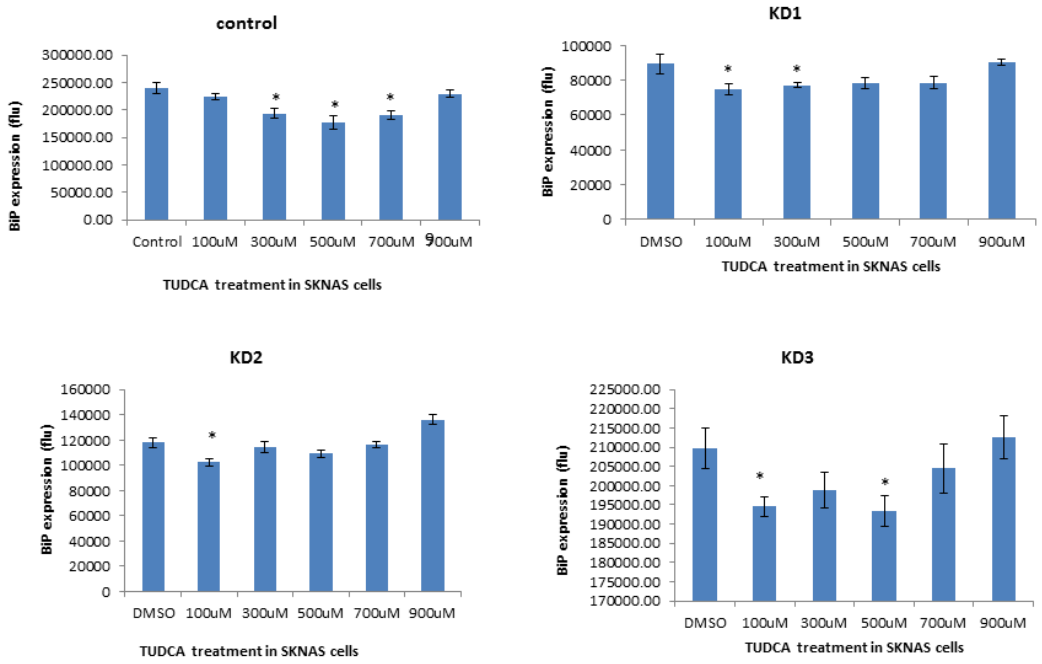

Figure 7.3: Expression of BiP measured by HCC in TUDCA treated cells

WFS1 stably depleted and control SK-N-AS cells were grown for 24h and incubated with various concentrations of TUDCA for 24 hours. At the end of incubation, cells were fixed and incubated with BiP antibody O/N, stained with PI and scanned with the Acumen eX3 cytometer. CL=control, KD1-3=WFS1 depleted clones, T-test * $p<0.05$, n=8**.** Drug treated samples were compared to untreated samples

7.3.2 Effect of TUDCA treatment on the expressions of ER stress and apoptosis marker

Based on the HCC data of BiP expression with 24h TUDCA treatment, it was decided to take two concentrations of TUDCA 100µM and 500µM, and measure expression of several ER stress markers at the mRNA level. These two concentrations were taken forward because 3 out of 4 cell lines showed reduced BiP expression at 100µM and 2 out of 4 cell lines showed reduction in BiP expression at 500µM. WFS1 depleted and control human neuroblastoma cells were grown in 6 well plates for 24 hours to reach about 80% confluency. The next day cells were treated with TUDCA; each concentration was used in quadruplicates and after 24h harvested in TRIzol.

The expression of ER stress markers BiP, CHOP, sp-XBP1 and GRP94 were measured by real time PCR. The data presented in Figure 7.4 shows that 24h hours treatment of cells in culture was not sufficient to decrease the level of ER stress markers. In fact, cells treated with TUDCA for 24h showed increased expression of all four ER stress makers in comparison to untreated cells. This raised the possibility that 24h TUDCA treatment at the chosen concentration might be causing more stress on the cells rather than relieving it.

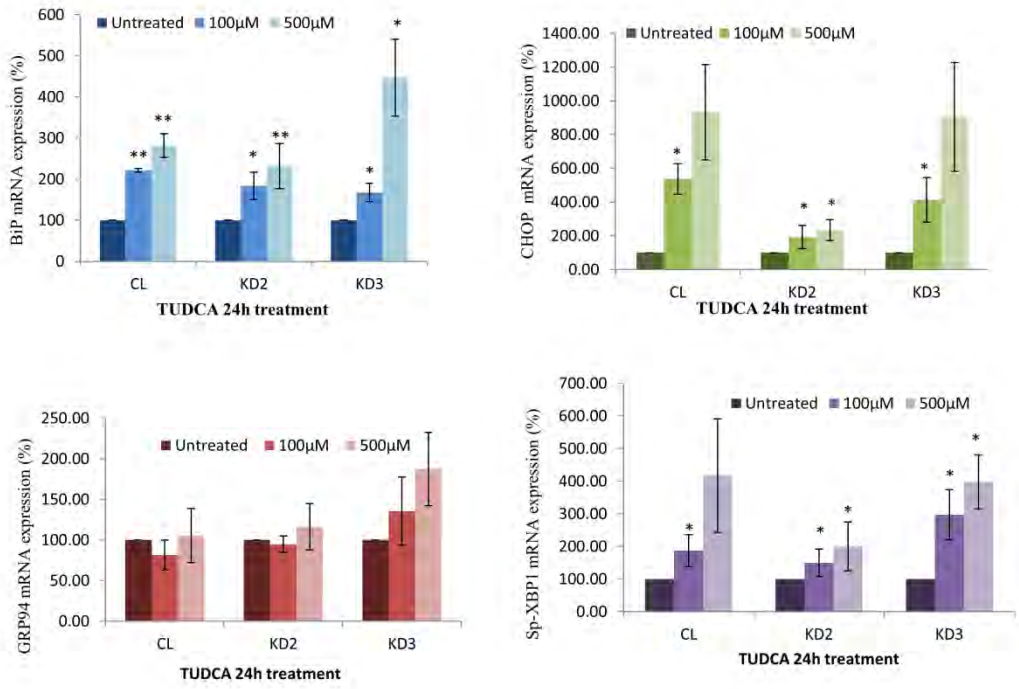

Figure 7.4: mRNA expression of ER stress markers with TUDCA treatment

Quantitative real-time PCR analysis of BiP, CHOP, GRP94 and sp- XBP1 in stable clones with WFS1 depletion in human SK-N-AS cell line with 24h TUDCA treatment (100 and 500µM), CL=control, KD2, KD3=WFS1 depleted clones, (n>3) T-test: *p<0.05, **p<0.01, and ***p<0.001). The expression in untreated cells was assumed as 100% and the drug treated samples were compared to untreated samples

Accordingly, it was decided to extend the treatment time as TUDCA has previously been shown to attenuate ER stress mediated cell death by interrupting the apoptosis pathways at longer administration times than 24 hours (Rodrigues et al., 2003). *In vivo* animal models have shown an effect on apoptosis by regular treatment from 2 to 3 weeks (Ceylan-Isik et al., 2011), whereas *in vitro* studies have shown the effect of TUDCA on ER stress and apoptosis after culturing cells for 6 days with TUDCA (Kim et al., 2011). Amin and colleagues (2012) used TUDCA (150mg/Kg/day) for four weeks in a mouse model of type 2 diabetes; they found that blood glucose, insulin and body weight were significantly reduced with TUDCA treatment. Similarly, TUDCA was recently shown to alleviate ER stress after 5 weeks of treatment in obesity induced myocardial mouse models (Ceylan-Isik et al., 2011). In addition, Yang et al. (2010) showed reduction of ER stress after 3 weeks TUDCA treatment in ob/ob mice.

In the light of these studies it was decided to extend the treatment of TUDCA to 3 days with the same concentrations. The study by Kim et al. (2011) showed that the optimum concentration of TUDCA was 200μM for 6 days treatment, and there were no significant differences in their observations at 100μM and 200μM TUDCA treatment. Therefore, one WFS1 depleted cell line (KD2) and the control cell line were grown for 24 hours and treated with 100μM and 500μM TUDCA for 3 days, with media change each day, and adding fresh drug. Cells were harvested as protein and RNA lysates and the expression of ER stress and apoptosis markers was measured by real-time PCR and western blotting. These experiments were performed with one WFS1 depleted cell line to reduce the complexity and costs of the experiments.

The obtained data showed that the mRNA expression of the two ER stress markers BiP and CHOP were suppressed with 3 days of TUDCA (100μM) treatment. The expression of BiP in KD2 was significantly decreased by 35±12% with TUDCA treatment; however the decrease of BiP in the control samples with TUDCA treatment was not statistically significant. CHOP mRNA expression was significantly decreased by 15±6% to 38±7% in WFS1 depleted and control cells with TUDCA treatment. Three days TUDCA treatment resulted in significantly increased expression of the neuroprotective protein BCL-2 in control and WFS1 depleted SK-N-AS cells (control=51±29% and KD2=95±17%). In addition, the expression of the pro-apoptotic protein BAX was significantly decreased in WFS1 depleted and control cells with 3 days TUDCA treatment by (28±10% to 38±11%) (Figure 7.5).

Similarly, the expression of BiP and GRP94 proteins were significantly decreased after 100 μM and 500μM TUDCA treatment for three days (Figure 7.6). BiP protein expression in control cells was decreased by 20±4% to 50±14% at 100μM and 500μM TUDCA treatments and BiP protein suppression in KD2 was by 54±19% to 39±15% with 100μM and 500μM TUDCA. In the same experiment, the protein expression of GRP94 was evaluated. The data showed 47±17% to 53±13% decrease in control samples with TUDCA treatment in comparison to the untreated samples and there was about 50±17% decrease in the expression of GRP94 protein in TUDCA treated WFS1 depleted cell line (KD2) in comparison to its untreated control (Table 7.1 and Figure 7.6).

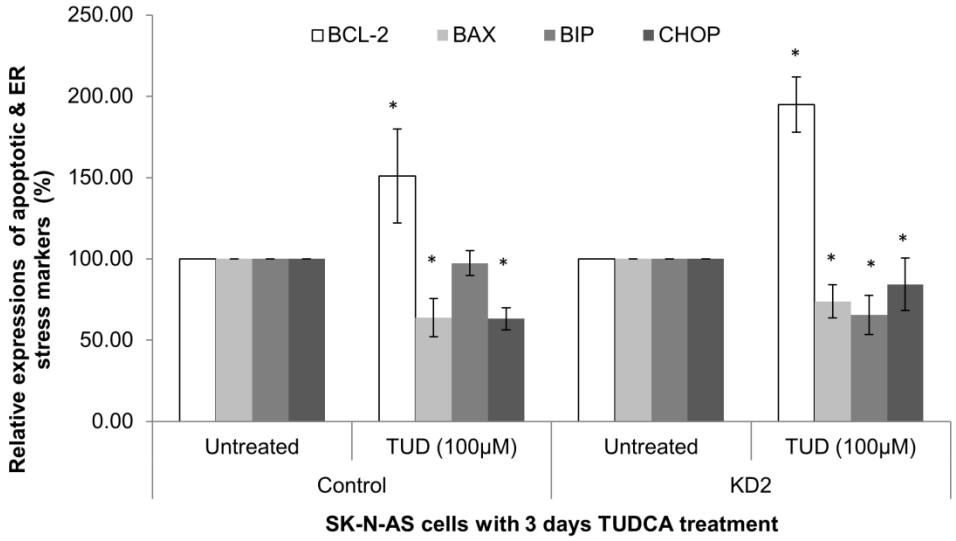

Figure 7.5: mRNA expression of ER stress and apoptosis markers with 3 days TUDCA

Quantitative real-time PCR analysis of BiP, CHOP, BCL-2 and BAX in stable clones with WFS1 depletion in human SK-N-AS cell line with 3days TUDCA treatment (100 μM), CL=control, KD2=WFS1 depleted clones, (n>3), T-test: *p<0.05, **p<0.01, and ***p<0.001). The expression in untreated cells was assumed as 100% and the drug treated samples were compared to untreated samples

Table 7.1 Expression of BiP and GRP94 proteins in TUDCA treated samples

N=3	CL-Un	CL-100	CL-500	KD2-Un	KD2-100	KD2-500
BiP	100	81±4	49±14	100	46±19	61±15
GRP94	100	53±17	47±13	100	46±17	48±17

Expression levels are expressed as mean±SEM. Un= untreated, KD2= WFS1 depleted cell line, CL= control.

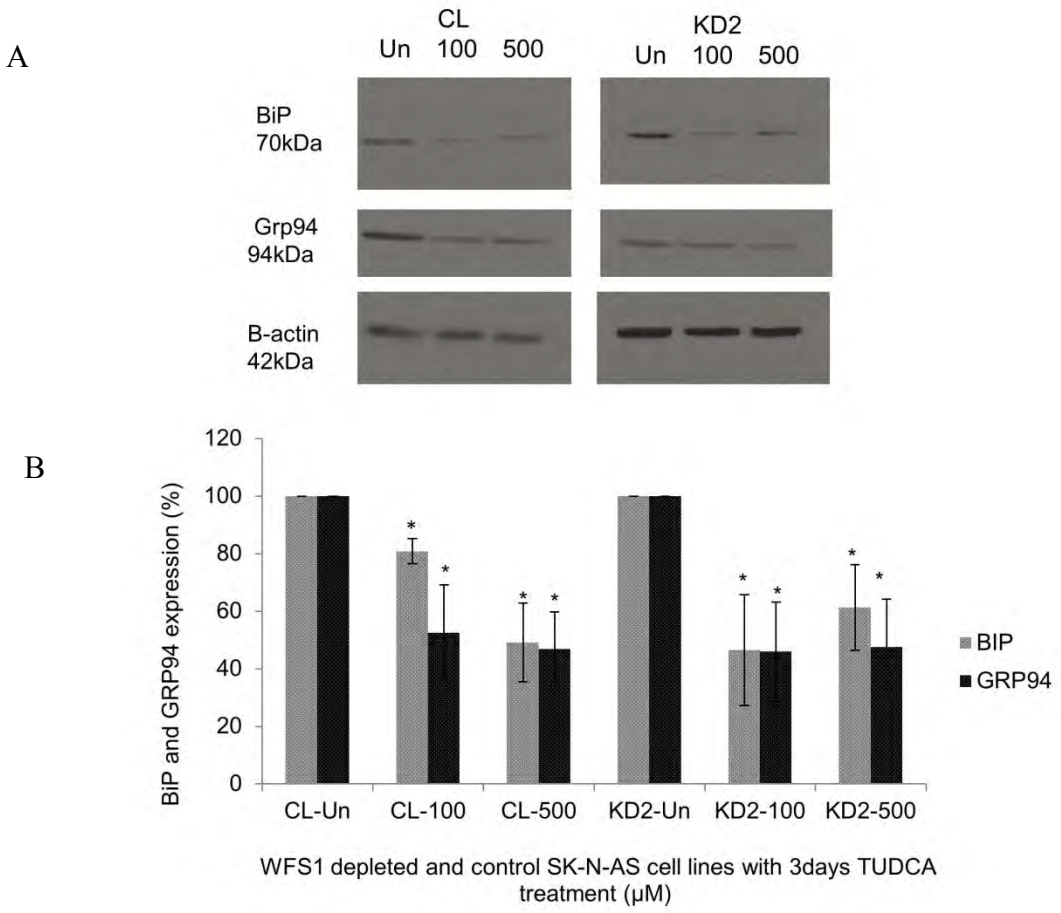

Figure 7.6: Protein expression of ER stress markers with 3 days TUDCA treatment

A: Immunoblot analysis of BiP and GRP94 proteins using lysates from WFS1 depleted human SK-N-AS cells after 3 days TUDCA treatment (100 and 500μM). The amount of beta actin is shown in the lowest panel. B: Protein quantification of the immunoblot. CL=control, KD2=WFS1 depleted clones, (n>3) T-test: *p<0.05, **p<0.01, and ***p<0.001). The expression in untreated cells was assumed at 100% and the drug treated samples were compared to untreated samples.

7.3.3 Effect of TUDCA treatment on cell cycle kinetics

The effect of TUDCA on the cell cycle kinetics was investigated by HCC and expressed as changes in the fractions of cells in the G1 and G2 phases of the cell cycle. The data presented in Figure 7.7 shows the percentage of G1 and G2 cells in control cells and in the three WFS1 depleted cells (KD1-3) with TUDCA treatment. The KD1 cell line was included in these experiments as this cell line displayed a cell cycle arrest in the G1 phase of the cell cycle (Chapter 3, section 3.3.4); therefore, it was hypothesised that the effect of the drug in this cell line would be more obvious.

Figure 7.7A shows the effect of various concentrations of TUDCA treatment on the percentage of cells in G1 and G2 phases of the cell cycle in the control cell line. The data shows a dose dependent increase in the percentage of G1 cells, which was significant at the highest dose. The dose curve is linear with a R^2 value of 0.73; for a drug dose response a R^2 value of above 0.6 is considered as good linear correlation (Geva-Zatorsky et al., 2010). TUDCA treatment did not affect the percentage of G2 cells in this cell line. In KD1 cell line, TUCDA treatment caused a dose dependent significant reduction in the percentage of G1 cells (Figure 7.7B). The dose curve is linear with an R^2 value of 0.84. As this cell line was shown to develop tetraploidy and cell cycle arrest in the G1 phase (chapter 3 section 3.3.4), decreasing the percentage of G1 cells by TUDCA would potentially mean rescuing the cells from the G1 arrest. No significant effect was seen in the percentage of G2 cells with TUDCA treatment. In the KD2 cell line, TUDCA treatment significantly increased the percentage of cells in G1 phase at all chosen concentrations. The percentage of cells in G2 phase was decreased significantly at 100, 300 and 500μM TUDCA

treatment (Figure 7.7C). In the KD3 cell line, TUDCA treatment did not seem to cause any significant changes to the percentage of cells in G1 or G2 phases of the cell cycle (Figure 7.7D).

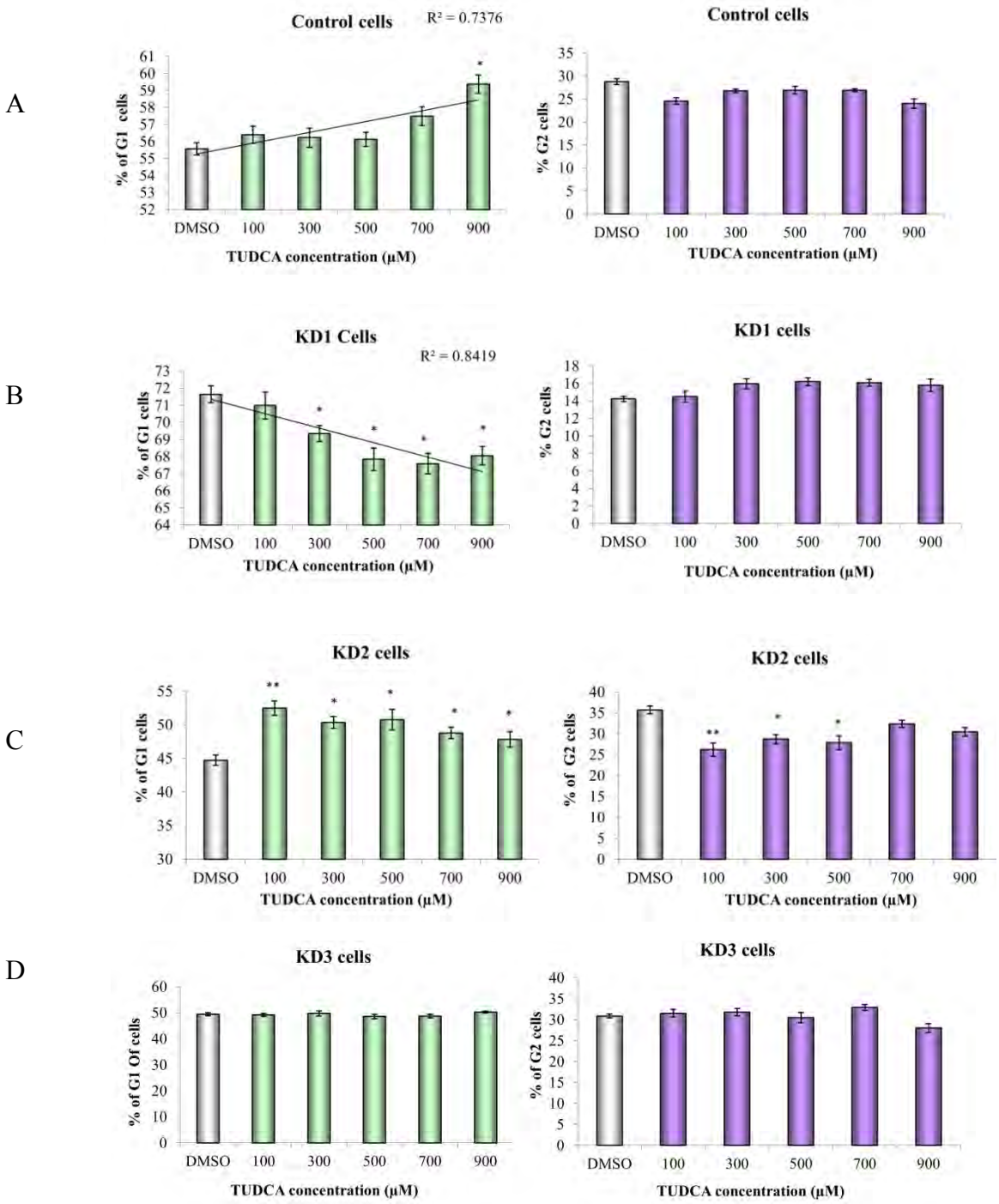

Figure 7.7: Effect of TUDCA treatment on cell cycle kinetics and apoptosis

WFS1 stably depleted and control SK-N-AS cells were grown for 24h and incubated with various concentrations of TUDCA for 24 hours. At the end of incubation, cells were fixed and stained with PI and scanned with the Acumen eX3 cytometer. (A) The percentage of G1and G2 cells in CL, B=KD1, C=KD2 and D=KD3, n=8, T-test: *p<0.05, **p<0.01, and ***p<0.001

7.4 Discussion

The data presented in this chapter demonstrated that treatment of the human neuroblastoma (SK-N-AS) cell lines with the chemical chaperone TUDCA resulted in decreasing the levels of ER stress and apoptotic markers. Furthermore, the observed preliminary data showed that TUDCA has some potential in modulation of cell cycle kinetics in WFS1 depleted cells. TUDCA is an endogenous bile acid that is produced in human liver and is widely used for treatment of different liver diseases. Recently, the focus of intensive research has been on the use of TUDCA as a chemical chaperone in the treatment of ER stress related disorders such as diabetes, cardiovascular complications and neurodegenerative diseases such as AD and HD (Amaral et al., 2009, Ozcan et al., 2009). Studies have shown that bile acids are important regulatory molecules that function much like hormones (Studer et al., 2012) and they are known to have immunoregulatory properties (Wang et al., 2011).

In this experimental model, 24 hours TUDCA treatment did not reduce the expression levels of ER stress markers on protein and mRNA levels. However, 24h TUDCA treatment decreased the expression of BiP measured by HCC. This discrepancy could be due to the differences in the experimental approaches between HCC and Western blotting (WB) or QPCR; HCC is a very sensitive technique that is capable of measuring the expression of proteins per single cell whereas the QPCR and WB measure the expression in a heterogeneous total cell population. Therefore the effect of a drug with a shorter exposure time is detectable by HCC but a longer exposure time may be required to become measurable by WB and QPCR.

Based on an intensive literature search on the studies of *in vivo* and *in vitro* TUDCA treatment (Ceylan-Isik et al., 2011, Kim et al., 2011, Yang et al., 2010), it was decided to extend the time of drug treatment to 3 days. The obtained data showed that 3 days of TUDCA treatment resulted in significant reduction of the expression of ER stress markers BiP, CHOP, and GRP94. Also the expression of the pro-apoptotic protein BAX was significantly reduced with TUDCA treatment whereas the expression of the neuroprotective protein BCL-2 was significantly elevated with 3 days TUDCA treatment in comparison to the untreated samples. These findings were supported by many studies that have shown that TUDCA attenuates ER stress mediated cell death by interrupting the classic pathway of apoptosis (Rodrigues et al., 2001).

The study by Kim and colleagues (2011) examined the anti-apoptotic effect of TUDCA on ER stress induced apoptosis in pre-implantation pig embryos; they found that 6 days treatment of pig embryos in culture with 200μM TUDCA significantly induced the expression BCL-XL and reduced the expression of pro-apoptotic protein BAX. Similarly, TUDCA treatment in obesity induced myocardial dysfunction mouse model lowered systolic blood pressure and lessened glucose intolerance by reducing ER stress. The authors demonstrated significant reductions in the expression of the ER stress markers: BiP, phosphorylated PERK and phosphorylated EIF2a after 5 weeks of chronic TUDCA treatment (Ceylan-Isik et al., 2011).

On the other hand, the study conducted by Yang et al. (2010) investigated the effect of oral TUDCA treatment on hepatic steatosis and gene expression in obese mice. Their data showed improvement in fatty liver disease, but showed no reduction in the expression of ER stress

markers. However the authors showed that the expression of the oxidative stress markers (Gsta1, Gsta2, Gsta4 and Gstm1-4) were significantly downregulated after TUDCA treatment, implying that oral TUDCA treatment is able to decrease oxidative stress in the liver cells (Yang et al., 2010). The study by Ozcan et al. (2009) investigated whether TUDCA could reverse ER stress in the hypothalamus of obese mice. They demonstrated significant reduction in the expression of ER stress markers (Ozcan et al., 2009). Rodrigues and colleagues reported that TUDCA treatment resulted in a marked reduction in neuronal cell death, elevating the levels of Bcl-2 leading to improvement in the neurological functions of the experimental rats (Rodrigues et al., 2003). The mechanism of action of TUDCA in preventing ER stress mediated apoptosis (Figure 7.8) is thought to be through blocking a calcium mediated apoptotic pathway by reducing calcium efflux as well as activation of caspase 12 (Xie et al., 2002, Nakagawa et al., 2000). Studies have shown that TUDCA inhibits cells growth in cancer cells by inducing apoptosis (Fimognari et al., 2009).

In addition, studies on the role of TUDCA in cell cycle regulation so far have shown that this bile acid downregulates the expression of cyclin D1 and induces cell cycle arrest (Castro et al., 2007). However, the data presented in this chapter suggest that TUDCA treatment may have the ability to normalise cell cycle kinetics, as TUDCA treatment showed a trend of reducing cells in G1 phase with increasing dose of TUDCA in the KD1 cell line (Figure 7.7B). This cell line was shown to have cell cycle arrest in G1 phase (Chapter3, section 3.3.4). TUDCA treatment also reduced the percentage of cells in G2 phase of cell cycle in KD2 cell line and elevated the percentage of cells in G1 phase (Fig 7.7C), which was shown to have a cell cycle arrest in G2

phase of the cell cycle (Chapter3, section 3.3.4) These findings suggest that TUDCA might also have the ability to rescue cells from G2 arrest. TUDCA treatment in KD3 cell line did not show any effect, this cell line was shown not to suffer from any cell cycle disturbances (Chapter3, section 3.3.4). This data seems contradictory as the three WFS1 depleted cell line have variable cell cycle kinetics, therefore the effect of treatment is also variable in these three cell line. These are preliminary findings that need to be continued and expanded in this and different cell models.

Overall, the data presented in this chapter implies that TUDCA significantly reduces ER stress, prevents ER stress mediated apoptosis and shows potential in modulation/normalisation of cell cycle kinetics; this chemical chaperone could be the potential treatment for many ER stress related disorders such as Wolfram syndrome.

Future studies are needed to investigate the functions of TUDCA in cell cycle regulation in Wolfram syndrome. Examples of experimental approaches that could be considered are: using different TUDCA concentration, various incubation times, different cell lines and animal models. The effect of TUDCA could be evaluated by measuring the expression levels of cell cycle regulatory proteins e.g. p21, p53, and the members of the cyclin family. More *In vitro* and *in vivo* studies are needed to confirm the efficacy of TUDCA in reduction of neuronal cell death and ER stress in Wolfram syndrome. After confirming and expanding these findings in primary cells and *in vivo* animal models could be taking TUDCA to clinical trials for treatment of Wolfram syndrome.

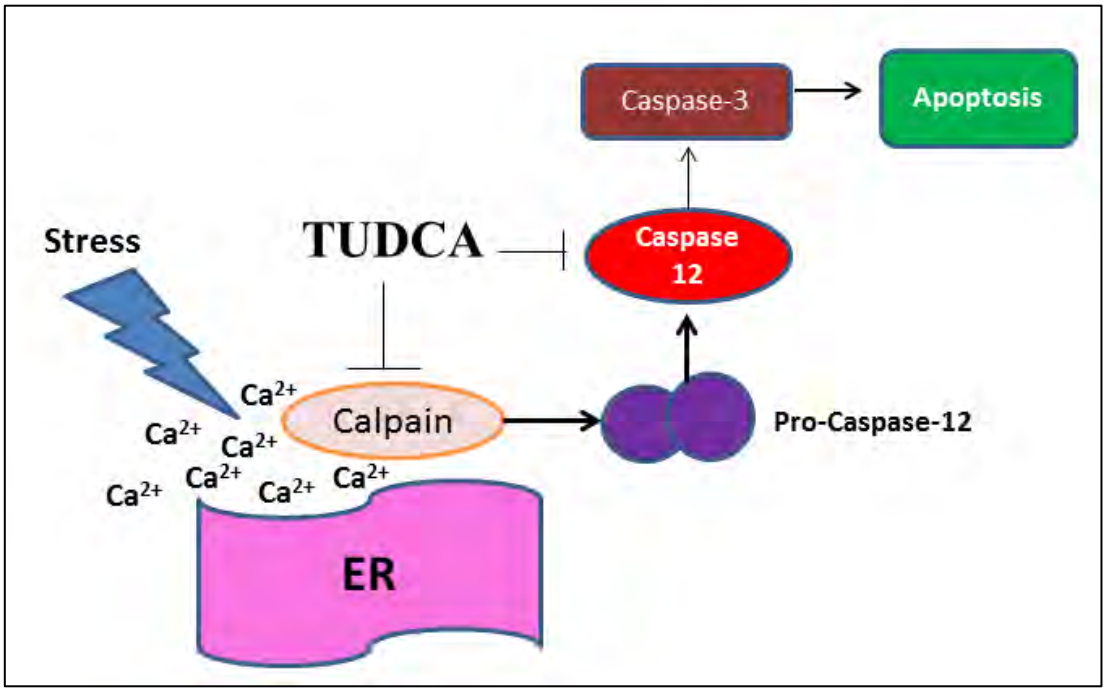

Figure 7.8 Proposed mechanism for inhibition of ER stress induced apoptosis by TUDCA

TUDCA inhibits apoptosis associated with ER stress by modulating intracellular calcium levels and inhibiting calpain and caspase-12 activation. Figure adapted from Amaral et al. (2009)

Chapter Eight: Discussion and Future Perspectives

8.1 Discussion

ER stress and protein misfolding are implicated in a variety of neurodegenerative diseases such as Alzheimer's, Parkinson's, and amyotrophic lateral sclerosis; endocrine diseases such as Type 1 and Type 2 diabetes; and cardiovascular diseases such as heart disease and atherosclerosis (Kim et al., 2008). The world is currently facing an epidemic of neurodegenerative disorders because people are living longer due to better quality of life and medical progress (Nieoullon, 2011). The life span has more than doubled since the1840s in Western societies. Studies suggest that more than 32 million people in the US are expected to be over the age of 80 years by 2050 and half of them will have Alzheimer's disease. The risk of Alzheimer's and Parkinson's diseases are exponentially increasing for ages 65 years plus (Dye et al., 2012). Neurodegenerative disorders represent a substantial financial burden on the society. Per year, brain disorders cost up to 386 billion euros in Europe (Andlin-Sobocki et al., 2005) and over 317 billion US dollars in the USA (Brain-Research, 2012). Similarly, the cases of cardiovascular diseases and diabetes are exponentially increasing every year. In the UK, the number of people diagnosed with diabetes has increased from 1.4 to 2.9 million over the last 15 years and this number is expected to increase to 5 million by 2025 (Diabetes-UK, 2012). The majority of these cases are Type 2 diabetes, which develops due to excess calorie intake, lack of exercise, and with aging. For these reasons it is critical to understand ER stress pathways, UPR and protein misfolding disorders.

8.1.1 Importance of studying Wolfram syndrome

Neurodegenerative disorders are usually polygenic, have multifactorial etiology and involve complex biological pathways. Due to this complexity, it is difficult in the research context to identify targeted therapeutic interventions (Hershey et al., 2012). Therefore, research into monogenic diseases such as Wolfram syndrome is an attractive way to understand more complex disorders. Wolfram syndrome is a good model of both diabetes and neurodegeneration. It is a monogenic disease with multi-symptom manifestations, which are caused by the deficiency of a single protein, Wolframin (Hershey et al., 2012). Wolframin is a multifunctional protein that is involved in a variety of processes such as ER stress, apoptosis and cell cycle regulation (Fonseca et al., 2005, Yamada et al., 2006). Wolfram syndrome involves selective loss of neuronal and pancreatic beta cells leading to neurodegeneration and diabetes. Heterozygous mutations in Wolfram syndrome cause susceptibility to T2D and psychiatric illnesses (Swift et al., 1990, Ishihara et al., 2004). Studying this heterogeneous disorder will greatly enhance the knowledge about the pathways and mechanisms of more complex disorders such as neurodegenerative diseases and diabetes. Successful treatments for Wolfram syndrome could provide the proof of principle for treatment of more common and complex forms of ER stress related disorders. Wolfram syndrome therefore, could provide a very useful model for studying the impact of ER stress on the brain and neuro-development (Lin and Popko, 2009, Hershey et al., 2012).

8.1.2 The purpose of this study

The majority of the research in Wolfram syndrome has been concentrated on diabetes. The current knowledge in this field is mainly from experimental findings in mice pancreatic beta cells (Fonseca et al., 2005, Ishihara et al., 2004, Riggs et al., 2005, Ueda et al., 2005, Yamada et al., 2006, Zatyka et al., 2008). Since DM is the first manifestation of the disease and pancreatic beta cell loss is the underling mechanism, more attention has been dedicated to this area. This thesis aims to investigate the neurological aspects of Wolfram syndrome, to identify potential therapeutic agents for treatment, and attempt to relate Wolfram syndrome to the common forms of neurodegeneration involving protein misfolding and ER stress. The main aims of this study were: to prepare and characterise Wolfram syndrome cell models in human and mouse neuronal cells; to investigate the effects of WFS1 deficiency; to extend our knowledge of WFS1 function; and to identify therapeutic targets for this disease.

The hypothesis for this project was that WFS1 depleted neuronal cells would exhibit increased levels of ER stress, apoptosis and cell cycle impairment. Adenoviral over-expression of GRP78 and treatment with TUDCA and VPA would result in attenuation of ER stress, apoptosis and normalisation of cell cycle kinetics. In addition it was hypothesised that Wolframin might have more interacting than demonstrated so far.

Collectively, the main finding of this thesis was that in four distinct neuronal cell models (stably and transiently WFS1 depleted human SK-N-AS cell line, WFS1 transiently depleted human NT2 cell lines and WFS1 stably depleted mouse neuro2A cell lines) WFS1 depletion resulted in

enhanced ER stress, apoptosis and impaired cell cycle kinetics. WFS1 depleted cells showed significantly decreased levels of the CDK inhibitor p21. P21 levels were shown to be inversely associated with apoptosis and cell cycle disturbances. Immunofluorescence and electron-microscopy analyses showed that in addition to the ER, WFS1 also localises to secretory granules in human neuroblastoma cells. A novel interaction was demonstrated between WFS1 and the V1A subunit of the vacuolar-type H^+ V-ATPase (proton pump) by co-immunoprecipitation of overexpressed proteins in HEK293 cells, and with endogenous proteins in human neuroblastoma cells. The interaction was mapped to the WFS1-N terminal domain, but not the C-terminus. WFS1 depleted cells showed reduced levels of ATP1B1 (beta1 subunit of sodium pump) and ATP6V1A (V1A subunit of the H^+ proton pump) and WFS1 was shown to be necessary for the stability of these two ion pump subunits.

Adenoviral over-expression of GRP78 resulted in significant alleviation of the ER stress, apoptosis and normalisation of cell cycle kinetics in WFS1 depleted neuronal cells. However, alleviation of ER stress by GRP78 over-expression or chemically induction of ER stress by thapsigargin had no effect on the expressions of the beta1 subunit of sodium pump and the V1A subunit of the proton pump, pointing to an ER stress independent function of WFS1 in the regulation of expression of the ion pump subunits. TUDCA (Tauroursodeoxycholic acid) treatment significantly reduced ER stress and apoptosis in WFS1 depleted cells. VPA (Sodium Valproate) treatment significantly increased the expression of WFS1 resulting in significant elevation of the neuroprotective protein BCL-2 and normalisation of the levels of beta1 subunit of sodium pump and the V1A subunit of the proton pump.

8.1.3 Neuroblastoma cell lines are good neuronal models for studying WS

The four neuronal cell models generated in this project displayed the characteristic previously described in cell and animal models of Wolfram syndrome as wells in fibroblasts from Wolfram patients. Therefore they seem to be good models of Wolfram syndrome for further research such as functional studies and drug testing. These cells show increased levels of BiP, CHOP, sp-XBP1, GRP94, ATF6 and HRD1 on protein and/or on mRNA levels, which results in increased apoptosis and abnormal cell cycle kinetics as discussed in detail in section 3.4 of Chapter 3. Previous studies have shown that WFS1 regulates a negative feedback loop in the ER stress signalling pathway by interacting with ATF6 through HRD1 (Fonseca et al., 2010). The data presented in Chapter 3 confirms this function of WFS1 by showing increased levels of the ER stress sensor ATF6 in human neuronal cells with WFS1 depletion (Figure 3.9). However, the levels of HRD1 were shown to be upregulated in the cells with WFS1 depletion, in contrast to the findings by Fonseca et al. (2010). HRD1 is an ER resident E3 ligase involved in removal of unfolded proteins by degradation via the ubiquitin-proteasome system ERAD. Previous studies have shown that, in the presence of ER stress, HRD1 expression levels were upregulated through the IRE-XBP1 pathway. HRD1 expression was also shown to increase in the presence of overexpressed XBP1 and ATF6 (Kaneko et al., 2007). Since both of these transcription factors are upregulated in the cell models used in the present study, it is not surprising that the levels of HRD1 are also elevated.

Furthermore, the present study indicates that all three apoptotic pathways induced by ER stress (Caspases, BCL-2 and CHOP) are triggered in Wolfram syndrome contributing to degeneration of neurones (Figure 3.11, Chapter 3). These phenotypes could be useful for future functional and therapeutic experiments, since apoptosis mediated neuronal cell death is the underlying mechanism of many neurodegenerative diseases. Therapeutic interventions capable of reducing or normalising the levels of the apoptotic markers mentioned in Chapter 3 could be the potential treatment for Wolfram Syndrome and other neurodegenerative diseases.

The involvement of WFS1 in the regulation of the cell cycle kinetics was one of the fascinating observations in this project. Three WFS1 depleted cell lines showed different cell cycle kinetics to the control. Furthermore, the preliminary data showed that the cell cycle regulatory protein p21 was significantly down regulated in WFS1 depleted neuronal cells and WFS1 depleted neuronal cells that retained their $p21^{(CIP1/WAF1)}$ expression were protected from neuronal apoptosis and cell cycle disturbance caused by the WFS1 depletion (Figure 3.15). These findings suggest that increasing the levels of $p21^{(CIP1/WAF1)}$ could protect cells from apoptosis and could potentially open new avenues of research and therapy into Wolfram syndrome and ER stress related disorders. This data suggests that it should be possible to find an intervention that is capable of inducing the expression of this protein could prove a potential treatment for Wolfram syndrome and for other neurodegenerative disorders.

8.1.4 WFS1 is necessary for the stability and expression of the ion pump subunits (ATP1B1 and ATP6V1A)

It is well established that WFS1 is a regulator of ER stress and is involved in ER stress pathways (Fonseca et al., 2005, Fonseca et al., 2010). This study was undertaken to investigate additional functions of WFS1 and it was hypothesised that apart from regulating the ER stress pathway this protein may have additional functions. This was very challenging as WFS1 has no homology with other known proteins. Therefore, it was decided to look at novel interacting partners. The data presented in Chapter 4 of this thesis and in Gharanei et al. (2012) identified the V1A subunit of the proton pump as a novel interacting partner for WFS1. This interaction was shown between over-expressed and endogenous proteins. Most importantly this interaction was identified with the N-terminal domain of WFS1. The N-terminus of WFS1 is located in the cytoplasm, which means that WFS1 may have a function outside the ER lumen. The study conducted by Hatanaka et al. (2011) showed that WFS1 is located to the vesicular granules in pancreatic beta cells and is involved in their acidification. The data presented in this thesis showed that in neuronal cells WFS1 also localises to the secretory granules (Figure 4.8 and 4.9 Chapter 4), which suggests that WFS1 may also be involved in acidification of secretory granules in neuronal cells, a crucial process for secretion of neurotransmitters.

One of the interesting findings of this study was that WFS1 regulates the expression of both, the beta1 subunit of the sodium pump and the V1A subunit of the proton pump. The present study demonstrated significantly reduced levels of ATP1B1 and ATP6V1A in WFS1 depleted neuronal cells and these two subunits were shown to be rapidly degraded in the absence of WFS1. These findings suggest that WFS1 is necessary for their stability which will most likely have

consequences for the stability and proper functioning of the two ion pumps (the V-ATPase and Na^+/ K^+ ATPase). It is well known that the sodium and proton pump carry out crucial functions within the neurones. Examples of these vital roles are the control of osmolality, excitability and action potential of neurons by the sodium pump and the regulation of pH, protein transport and acidification by the proton pump (Tokhtaeva et al., 2011, Xu, 2011, Short, 2010, Tabares and Betz, 2010).

8.1.5 ER stress independent role of WFS1 in the regulation of the ion pump subunits

When it was found that WFS1 had a role in the ER stress response pathway and was involved in the regulation of the sodium pump and proton pump, further experiments were undertaken to investigate whether the regulation of the two pumps by WFS1 was an ER stress dependent process. To answer this question, therapeutic approaches were considered to resolve ER stress. First of all over-expression of the molecular chaperone BiP/GRP78 was used in WFS1 depleted neuronal cells. The data presented in chapter 5 demonstrated that BiP over-expression significantly alleviated the levels of four main ER stress markers (BiP, CHOP, GRP94 and sp-XBP1) (Figure 5.4). Furthermore, BiP over-expression significantly reduced the levels of apoptosis and normalised cell cycle kinetics (Figure 5.5). However, BiP over-expression had no effect on the expression of ATP1B1 and ATP6V1A (Figure 5.6). To clarify if ER stress had an effect on expression of subunits of the ion pumps, ER stress was chemically induced in WFS1 depleted cells by thapsigargin treatment. Even these elevated levels of ER stress had no effect on the expressions of the two ion pump subunits (Figure 5.7). Collectively this data suggests that

WFS1 has an ER stress independent function in regulation of the two ion pump subunits ATP1B1 and ATP6V1A. It is possible that WFS1 plays a chaperone like role in folding and assembly of these two ion pump subunits, which is a crucial process for the proper functioning of the sodium and the vacuolar proton pumps.

8.1.6 Therapeutic approaches to reduce ER stress and apoptosis

The second therapeutic approach used in this project was the histone deacetylase inhibitor (HDAC) sodium valproate (VPA) treatment of WFS1 depleted neuronal cells. VPA treatment resulted in significant upregulation of WFS1 expression on protein and mRNA levels. Although VPA treatment had no significant effect on the levels of ER stress markers, this drug was capable of significantly inducing the expression of ATP1B1 and ATP6V1A. VPA treatment may affect the expression of WFS1 through mechanisms previously described by Kakiuchi et al. (2009); VPA induces the expression of WFS1 by activating its promoter region and by releasing WFS1 from the WFS1-GRP94 complex. The increased expression of the ion pump subunits could be either a direct effect of VPA treatment or a secondary effect via increased levels of WFS1. Since the expression of both ion pump subunits (ATP1B1 and ATP6V1A) was significantly increased in WFS1 depleted cells and not in the control cells, this effect might be a result of WFS1 induction in these cells. These preliminary results seem promising for the treatment of Wolfram syndrome; further experiments are needed to identify the mechanisms of action of VPA in the treatment of Wolfram syndrome. Since VPA increases the expression of WFS1, this could be useful for treatment of patients with missense mutations, where WFS1 function is partially retained. According to the Euro-WABB database (www.euro-wabb.org) missense mutations

make 106 out of 225 total mutations, which is close to 50% of the mutations registered (EURO-WABB, 2012). Further studies are required to confirm the effectiveness of VPA in primary cells and in *in vivo* models of Wolfram syndrome.

Finally, the chemical chaperone TUDCA was used to resolve ER stress in WFS1 depleted neuronal cells. The data in chapter seven demonstrated that TUDCA treatment resulted in alleviation of ER stress and apoptosis markers in these cell lines. TUDCA is known for its role in the treatment of liver disorders and it is currently being investigated for the treatment of ER stress related disorders such as AD and PD and endocrine disorders such as diabetes (Duan et al., 2002, Engin and Hotamisligil, 2010, Keene et al., 2001, Ozcan et al., 2009, Ramalho et al., 2006, Rodrigues et al., 2003). Overall, this data suggests that TUDCA treatment is capable of resolving ER stress and ER stress induced apoptosis in cell models of Wolfram syndrome. Further studies are required to confirm these findings in primary cells or *in vivo* models of Wolfram syndrome.

Overall, studying a rare disease such Wolfram syndrome is an attractive approach to understand the pathological mechanisms of more complex ER stress related disorders and to provide therapeutic proof of principle for their better management. Increasing evidence suggests that these factors are also involved in pathogenesis of cancer, since the anti-apoptotic branch of UPR is shown to be elevated in cancer cells (Schönthal, 2009). The elevated levels of BiP in tumour cells are thought to be a defensive strategy for their survival (Lee and Hendershot, 2006). Based on the evidence presented in this thesis, the combination of chemical and molecular chaperones could enhance neuronal function, and survival. However, excessive upregulation of molecular

and chemical chaperones or high levels of VPA might lead to undesirable side effects such as causing cancer or alteration in cell cycle regulation. Therefore a delicate balance of these therapeutics is required for beneficial neuroprotective effects.

8.2 Conclusions

The data presented in this thesis contributes significantly to the current knowledge of Wolfram syndrome and neurodegenerative disorders. The mechanisms of neuronal cell death seen in Wolfram Syndrome might be in common with other protein misfolding neurodegenerative diseases including AD, PD and HD. The data demonstrated that WFS1 depleted neuronal cells exhibit high levels of ER stress, apoptosis and cell cycle disturbances. WFS1 specifically interacts with the V1A subunit of H^+ V-ATPase; this interaction may be important both for pump assembly in the ER, and for vesicular acidification. In addition, the presence of WFS1 is necessary for the expression and stability of the V1A subunit of the vacuolar proton pump and the beta1 subunit of the sodium pump (H^+-VATPase and Na^+/K^+-ATPase). These findings suggest a new ER stress independent function for WFS1. Treatment of WFS1 depleted cells with chemical and molecular chaperones TUDCA and GRP78 showed promising results in providing protection against ER stress induced apoptosis. VPA treatment may be useful for patients with *WFS1* missense mutations, where increasing the expression of partially effective WFS1 may compensate for its impaired function. The preliminary data showed that cell cycle regulatory protein p21 may be a potential therapeutic target in Wolfram syndrome. The work in this thesis has potentially opened several therapeutic doors for Wolfram syndrome and other ER stress related or protein misfolding diseases.

One of the main limitations of this work was that the experimental work was performed on immortal cell lines. Therefore, the study should be extended to primary cells and *in vivo* models.

8.3 Future work and prospects

This has been a very interesting project which could be followed from different angles. Currently this project is continued by Dr Astuti in Prof Barrett's research group. Dr Astuti is using these WFS1 depleted cell models for the continuations of the drug treatment studies. One of the interesting findings in this project was that WFS1 depleted cells show reduced expression of p21 and that p21 levels were inversely associated with apoptosis and cell cycle disturbances, need to be confirmed and expanded. However, p21 may be an interesting target in drug testing project. Dr Astuti will be testing several drugs including TUDCA and VPA to evaluate their effects on p21 expression. Any drug that is capable of activating p21 protein or inducing its expression will be further investigated. Rapamycin is an example of a drug that is known to induce the expression of p21 in a variety of cell types including glioblastoma and neuroblastoma cells (Anandharaj et al., 2011). The drug treatment findings from this project will require confirmation by a variety of methods in primary cells and in animal models. The ultimate goal will be to find a drug suitable for testing in clinical trials for treatment of Wolfram syndrome and other ER stress related disorders.

Another important observation in this thesis was the reduced expression levels and stability of the beta1 subunit of the sodium pump and the V1A subunit of the proton pump in WFS1 depleted cells. The role of WFS1 in the expression and function of these ion pumps and the involvement of the two pumps in the pathogenesis of Wolfram syndrome should be further investigated. WFS1 does not seem to protect these subunits from proteasomal degradation (Gharanei et al., 2012); it will be interesting to investigate how WFS1 stabilises these proteins. One possibility is that it protects them from degradation by the lysosome or by other proteases. In addition, to better understand the pathogenesis of Wolfram syndrome, studies could be carried out to investigate the effects of impaired ion pump functions on the functions of neuronal cells. Examples could be: evaluation of acidification of secretory granules by proton pump and excitability of the neuronal cells by the sodium pump. Potentially, these experiments could be further taken into *in vivo* models such as knockout mice of *WFS1*. Currently, there is a possibility of obtaining more universal models by de-differentiation of patient fibroblasts to iPS (Induced Pluripotent Stem) cells and subsequent differentiation of iPS cells to the required tissue e.g. neurons. These types of projects are attempted in many research centres. Prof Barrett collected skin samples from several patients and his research group is participating in such project. This approach may help to overcome difficulties and limitations related to using cell lines, primary cells and animal models.

Chapter Nine: References

ADA 2012. Diagnosis and Classification of Diabetes Mellitus. *Diabetes Care,* 35**,** S64-S71.

ADACHI, Y., YAMAMOTO, K., OKADA, T., YOSHIDA, H., HARADA, A. & MORI, K. 2008. ATF6 Is a Transcription Factor Specializing in the Regulation of Quality Control Proteins in the Endoplasmic Reticulum. *Cell Structure and Function,* 33**,** 75-89.

AMARAL, J. D., VIANA, R. J. S., RAMALHO, R. M., STEER, C. J. & RODRIGUES, C. M. P. 2009. Bile acids: regulation of apoptosis by ursodeoxycholic acid. *Journal of Lipid Research,* 50**,** 1721-1734.

AMR, S., HEISEY, C., ZHANG, M., XIA, X.-J., SHOWS, K. H., AJLOUNI, K., PANDYA, A., SATIN, L. S., EL-SHANTI, H. & SHIANG, R. 2007. A Homozygous Mutation in a Novel Zinc-Finger Protein, ERIS, Is Responsible for Wolfram Syndrome 2. *American Journal of Human Genetics,* 81**,** 673-683.

ANANDHARAJ, A., CINGHU, S. & PARK, W.-Y. 2011. Rapamycin-mediated mTOR inhibition attenuates survivin and sensitizes glioblastoma cells to radiation therapy. *Acta Biochimica et Biophysica Sinica,* 43**,** 292-300.

ANDERSON, G. D., TEMKIN, N. R., CHANDLER, W. L. & WINN, H. R. 2003. Effect of valproate on hemostatic function in patients with traumatic brain injury. *Epilepsy research,* 57**,** 111-119.

ANDLIN-SOBOCKI, P., JÖNSSON, B., WITTCHEN, H.-U. & OLESEN, J. 2005. Costs of Disorders of the Brain in Europe. *European journal of neurology* 12.

ARENDT, T. 2001. Alzheimer's disease as a disorder of mechanisms underlying structural brain self-organization. *Neuroscience,* 102**,** 723-765.

BANDO, Y., KATAYAMA, T., ALESHIN, A. N., MANABE, T. & TOHYAMA, M. 2004. GRP94 reduces cell death in SH-SY5Y cells perturbated calcium homeostasis. *Apoptosis,* 9**,** 501-508.

BAO, Q. & SHI, Y. 2007. Apoptosome: a platform for the activation of initiator caspases. *Cell Death and Differentiation,* 14**,** 56-65.

BARRAL, J. M., BROADLEY, S. A., SCHAFFAR, G. & HARTL, F. U. 2004. Roles of molecular chaperones in protein misfolding diseases. *Seminars in Cell & Developmental Biology,* 15**,** 17-29.

BARRETT, T. G. & BUNDEY 1997. Wolfram (DIDMOAD) syndrome. *Journal of Medical Genetics,* 34**,** 838-841.

BARRETT, T. G., BUNDEY, S. E. & MACLEOD, A. F. 1995. Neurodegeneration and Diabetes - Uk Nationwide Study of Wolfram (Didmoad) Syndrome. *Lancet,* 346**,** 1458-1463.

BEGGAH, A., MATHEWS, P., BEGUIN, P. & GEERING, K. 1996. Degradation and Endoplasmic Reticulum Retention of Unassembled α- and β-Subunits of Na,K-ATPase Correlate with Interaction of BiP. *Journal of Biological Chemistry,* 271**,** 20895-20902.

BERTOLOTTI, A., ZHANG, Y., HENDERSHOT, L. M., HARDING, H. P. & RON, D. 2000. Dynamic interaction of BiP and ER stress transducers in the unfolded-protein response. *Nature Cell Biology,* 2**,** 326-332.

BEYENBACH, K. W. & WIECZOREK, H. 2006. The V-type H+ ATPase: molecular structure and function, physiological roles and regulation. *Journal of Experimental Biology,* 209**,** 577-589.

BOWN, C. D., WANG, J.-F., CHEN, B. & YOUNG, L. T. 2002. Regulation of ER stress proteins by valproate: therapeutic implications. *Bipolar Disorders,* 4**,** 145-151.

BRAIN-RESEARCH. 2012. *Brain Disorders: By the Numbers* [Online]. Cambridge. Available: http://mcgovern.mit.edu/brain-disorders/by-the-numbers [Accessed 25-11-2012 2012].

BRETT, L., JOANN, M. G., BEAL, M. F. & RAJIV, R. R. 2005. Remodeling Chromatin and Stress Resistance in the Central Nervous System: Histone Deacetylase Inhibitors as Novel and Broadly Effective Neuroprotective Agents. *Current Drug Targets - CNS & Neurological Disorders,* 4**,** 41-50.

BREWER, J. W. & DIEHL, J. A. 2000. PERK mediates cell-cycle exit during the mammalian unfolded protein response. *Proceedings of the National Academy of Sciences of the United States of America,* 97**,** 12625-12630.

BROSTROM, C. O. & BROSTROM, M. A. 1997. Regulation of Translational Initiation during Cellular Responses to Stress. *In:* KIVIE, M. (ed.) *Progress in Nucleic Acid Research and Molecular Biology.* Academic Press.

BROSTROM, M. A., CADE, C., PROSTKO, C. R., GMITTER-YELLEN, D. & BROSTROM, C. O. 1990. Accommodation of protein synthesis to chronic deprivation of intracellular sequestered calcium. A putative role for GRP78. *Journal of Biological Chemistry,* 265**,** 20539-46.

CALFON, M., ZENG, H., URANO, F. & RON, D. 2002. IRE1 couples endoplasmic reticulum load to secretory capacity by processing the XBP-1 mRNA. *Nature,* 415**,** 92-96.

CASTRO, R. E., AMARAL, J. D., SOLÁ, S., KREN, B. T., STEER, C. J. & RODRIGUES, C. M. P. 2007. Differential regulation of cyclin D1 and cell death by bile acids in primary rat hepatocytes. *American Journal of Physiology - Gastrointestinal and Liver Physiology,* 293**,** G327-G334.

CASTRO, R. E., SOLÁ, S., RAMALHO, R. M., STEER, C. J. & RODRIGUES, C. M. P. 2004. The Bile Acid Tauroursodeoxycholic Acid Modulates Phosphorylation and Translocation of Bad via Phosphatidylinositol 3-Kinase in Glutamate-Induced Apoptosis of Rat Cortical Neurons. *Journal of Pharmacology and Experimental Therapeutics,* 311**,** 845-852.

CATALANO, M. G., FORTUNATI, N., PUGLIESE, M., COSTANTINO, L., POLI, R., BOSCO, O. & BOCCUZZI, G. 2005. Valproic Acid Induces Apoptosis and Cell Cycle Arrest in Poorly Differentiated Thyroid Cancer Cells. *Journal of Clinical Endocrinology & Metabolism,* 90**,** 1383-1389.

CEYLAN-ISIK, A. F., SREEJAYAN, N. & REN, J. 2011. Endoplasmic reticulum chaperon tauroursodeoxycholic acid alleviates obesity-induced myocardial contractile dysfunction. *Journal of Molecular and Cellular Cardiology,* 50**,** 107-116.

CHANG, B.-D., WATANABE, K., BROUDE, E. V., FANG, J., POOLE, J. C., KALINICHENKO, T. V. & RONINSON, I. B. 2000. Effects of p21Waf1/Cip1/Sdi1 on cellular gene expression: Implications for carcinogenesis, senescence, and age-related diseases. *Proceedings of the National Academy of Sciences,* 97**,** 4291-4296.

CHAUSSENOT, A., BANNWARTH, S., ROUZIER, C., VIALETTES, B., MKADEM, S. A. E., CHABROL, B., CANO, A., LABAUGE, P. & PAQUIS-FLUCKLINGER, V. 2011. Neurologic features and genotype-phenotype correlation in Wolfram syndrome. *Annals of Neurology,* 69**,** 501-508.

CHEMICALBOOK. 2008. *Chemical Search Engine* [Online]. TIANJIN: TIANJIN PHARMACN MEDICAL TECHNOLOGY CO.,LTD. Available: http://www.chemicalbook.com/ChemWebSiteList_EN.aspx [Accessed 10.05.2012 2012].

CHEN, B., WANG, J. F. & YOUNG, L. T. 2000. Chronic valproate treatment increases expression of endoplasmic reticulum stress proteins in the rat cerebral cortex and hippocampus. *Biological Psychiatry,* 48**,** 658-664.

CHEN, G., ZENG, W.-Z., YUAN, P.-X., HUANG, L.-D., JIANG, Y.-M., ZHAO, Z.-H. & MANJI, H. K. 1999. The Mood-Stabilizing Agents Lithium and Valproate RobustlIncrease the Levels of the Neuroprotective Protein bcl-2 in the CNS. *Journal of Neurochemistry,* 72**,** 879-882.

CHEN, P. S., PENG, G. S., LI, G., YANG, S., WU, X., WANG, C. C., WILSON, B., LU, R. B., GEAN, P. W., CHUANG, D. M. & HONG, J. S. 2006. Valproate protects dopaminergic neurons in midbrain neuron//glia cultures by stimulating the release of neurotrophic factors from astrocytes. *Molecular Psychiatry,* 11**,** 1116-1125.

CHIPUK, J. E., MOLDOVEANU, T., LLAMBI, F., PARSONS, M. J. & GREEN, D. R. 2010. The BCL-2 Family Reunion. *Molecular Cell,* 37**,** 299-310.

CHUANG, D.-M. & PRILLER, J. 2006. Potential use of lithium in neurodegenerative disorders. *Lithium in Neuropsychiatry.*

CHUANG, D. M. 2004. Neuroprotective and neurotrophic actions of the mood stabilizer lithium: can it be used to treat neurodegenerative diseases? *Critical reviews in neurobiology,* 16**,** 83-90.

ÇOLAK, A., KELTEN, B., SAĞMANLIGIL, A., AKDEMIR, O., KARAOĞLAN, A., ŞAHAN, E., ÇELIK, Ö. & BARUT, Ş. 2008. Tauroursodeoxycholic acid and secondary damage after spinal cord injury in rats. *Journal of Clinical Neuroscience,* 15**,** 665-671.

COPANI, A., CONDORELLI, F., CARUSO, A., VANCHERI, C., SALA, A., GIUFFRIDA STELLA, A. M., CANONICO, P. L., NICOLETTI, F. & SORTINO, M. A. 1999. Mitotic signaling by β-amyloid causes neuronal death. *The FASEB Journal,* 13**,** 2225-2234.

COQUERET, O. 2003. New roles for p21 and p27 cell-cycle inhibitors: a function for each cell compartment? *Trends in cell biology,* 13**,** 65-70.

COTTER, T. G. 2009. Apoptosis and cancer: the genesis of a research field. *Nature Publishing Group,* 9**,** 501.

CREDLE, J. J., FINER-MOORE, J. S., PAPA, F. R., STROUD, R. M. & WALTER, P. 2005. On the mechanism of sensing unfolded protein in the endoplasmic reticulum. *Proceedings of the National Academy of Sciences of the United States of America,* 102**,** 18773-18784.

CRYNS, K., SIVAKUMARAN, T. A., VAN DEN OUWELAND, J. M. W., PENNINGS, R. J. E., CREMERS, C., FLOTHMANN, K., YOUNG, T. L., SMITH, R. J. H., LESPERANCE, M. M. & VAN CAMP, G. 2003. Mutational spectrum of the WFS1 gene in Wolfram syndrome, nonsyndromic hearing impairment, diabetes mellitus, and psychiatric disease. *Human Mutation,* 22**,** 275-287.

DASH, B. C. & EL-DEIRY, W. S. 2005. Phosphorylation of p21 in G2/M Promotes Cyclin B-Cdc2 Kinase Activity. *Molecular and Cellular Biology,* 25**,** 3364-3387.

DEHAY, C. & KENNEDY, H. 2007. Cell-cycle control and cortical development. *Nature Reviews of Neuroscience,* 8**,** 438-450.

DIABETES-UK. 2012. *Diabetes in the UK 2012 (April 2012) Key statistics on diabetes* [Online]. Available: http://www.diabetes.org.uk/Professionals/Publications-reports-and-resources/Reports-statistics-and-case-studies/Reports/Diabetes-in-the-UK-2012/ [Accessed 2012].

DICKINSON, M. E., KRUMLAUF, R. & MCMAHON, A. P. 1994. Evidence for a mitogenic effect of Wnt-1 in the developing mammalian central nervous system. *Development,* 120**,** 1453-1471.

DORNER, A. J., WASLEY, L. C. & KAUFMAN, R. J. 1992. Overexpression of GRP78 mitigates stress induction of glucose regulated proteins and blocks secretion of selective proteins in Chinese hamster ovary cells. *The EMBO journal,* 11**,** 1563-71.

DOU, H., BIRUSINGH, K., FARACI, J., GORANTLA, S., POLUEKTOVA, L. Y., MAGGIRWAR, S. B., DEWHURST, S., GELBARD, H. A. & GENDELMAN, H. E. 2003. Neuroprotective Activities of Sodium Valproate in a Murine Model of Human Immunodeficiency Virus-1 Encephalitis. *The Journal of Neuroscience,* 23**,** 9162-9170.

DOYLE, K. M., KENNEDY, D., GORMAN, A. M., GUPTA, S., HEALY, S. J. M. & SAMALI, A. 2011. Unfolded proteins and Endoplasmic Reticulum stress in neurodegenerative disorders. *Journal of Cellular and Molecular Medicine,* 5.

DRUMMOND, I., LEE, A., RESENDEZ, E., JR & STEINHARDT, R. 1987. Depletion of intracellular calcium stores by calcium ionophore A23187 induces the genes for glucose-regulated proteins in hamster fibroblasts. *Journal of Biological Chemistry,* 262**,** 12801-12805.

DUAN, W. M., RODRIGURES, C. M. P., ZHAO, L. R., STEER, C. J. & LOW, W. C. 2002. Tauroursodeoxycholic Acid Improves the Survival and Function of Nigral Transplants in a Rat Model of Parkinsons Disease. *Cell Transplantation,* 11**,** 195-205.

DULIĆ, V., STEIN, G. H., FAR, D. F. & REED, S. I. 1998. Nuclear Accumulation of p21Cip1 at the Onset of Mitosis: a Role at the G2/M-Phase Transition. *Molecular and Cellular Biology,* 18**,** 546-557.

DYE, R. V., MILLER, K. J., SINGER, E. J. & LEVINE, A. J. 2012. Hormone Replacement Therapy and Risk for Neurodegenerative Diseases. *International Journal of Alzheimer's Disease,* 2012**,** 18.

EL-BADRY, O. M., HELMAN, L. J., CHATTEN, J., STEINBERG, S. M., EVANS, A. E. & ISRAEL, M. A. 1991. Insulin-like growth factor II-mediated proliferation of human neuroblastoma. *The Journal of Clinical Investigation,* 87**,** 648-657.

ELMORE, S. 2007. Apoptosis: A Review of Programmed Cell Death. *Toxicologic Pathology,* 35**,** 495-516.

ENGIN, F. & HOTAMISLIGIL, G. S. 2010. Restoring endoplasmic reticulum function by chemical chaperones: an emerging therapeutic approach for metabolic diseases. *Diabetes, Obesity and Metabolism,* 12**,** 108-115.

EURO-WABB, T. 2012. *The EURO-WABB Project* [Online]. Available: http://www.euro-wabb.org/en/lovd-genetic-variation-database [Accessed 04/12/2012 2012].

FAN, T.-J., HAN, L.-H., CONG, R.-S. & LIANG, J. 2005. Caspase Family Proteases and Apoptosis. *Acta Biochimica et Biophysica Sinica,* 37**,** 719-727.

FIMOGNARI, C., LENZI, M., CANTELLI-FORTI, G. & HRELIA, P. 2009. Apoptosis and Modulation of Cell Cycle Control by Bile Acids in Human Leukemia T Cells. *Annals of the New York Academy of Sciences,* 1171**,** 264-269.

FONSECA, S. G., FUKUMA, M., LIPSON, K. L., NGUYEN, L. X., ALLEN, J. R., OKA, Y. & URANO, F. 2005. WFS1 is a novel component of the unfolded protein response and maintains homeostasis of the endoplasmic reticulum in pancreatic beta-cells. *Journal of Biological Chemistry,* 280**,** 39609-39615.

FONSECA, S. G., GROMADA, J. & URANO, F. 2011. Endoplasmic reticulum stress and pancreatic β-cell death. *Trends in Endocrinology & Metabolism,* 22**,** 266-274.

FONSECA, S. G., ISHIGAKI, S., OSLOWSKI, C. M., LU, S., LIPSON, K. L., GHOSH, R., HAYASHI, E., ISHIHARA, H., OKA, Y., PERMUTT, M. A. & URANO, F. 2010. Wolfram syndrome 1 gene negatively regulates ER stress signaling in rodent and human cells. *The Journal of Clinical Investigation,* 120**,** 744-755.

FONSECA, S. G., URANO, F. & WEIR, G. C. 2012. Wolfram syndrome 1 and adenylyl cyclase 8 interact at the plasma membrane to regulate insulin production and *Nature Cell Biology,* 14**,** 1105-1112.

FORGAC, M. 2007. Vacuolar ATPases: rotary proton pumps in physiology and pathophysiology. *Nature Review of Molecular Cell Biology,* 8**,** 917-929.

FRADEJAS, N., PASTOR, M. D., BURGOS, M., BEYAERT, R., TRANQUE, P. & CALVO, S. 2010. Caspase-11 mediates ischemia-induced astrocyte death: Involvement of endoplasmic reticulum stress and C/EBP homologous protein. *Journal of Neuroscience Research,* 88**,** 1094-1105.

FRIBLEY, A., ZHANG, K. & KAUFMAN, R. J. 2009. Regulation of Apoptosis by the Unfolded Protein Response

Apoptosis. *In:* ERHARDT, P. & TOTH, A. (eds.). Humana Press.

FU, H. Y., MINAMINO, T., TSUKAMOTO, O., SAWADA, T., ASAI, M., KATO, H., ASANO, Y., FUJITA, M., TAKASHIMA, S., HORI, M. & KITAKAZE, M. 2008. Overexpression of endoplasmic reticulum-resident chaperone attenuates cardiomyocyte death induced by proteasome inhibition. *Cardiovasc Res*

FU, Y., LI, J. & LEE, A. S. 2007. GRP78/BiP Inhibits Endoplasmic Reticulum BIK and Protects Human Breast Cancer Cells against Estrogen Starvation-Induced Apoptosis. *Cancer Research.*

FUQUA, J. S. 2000. Wolfram syndrome: Clinical and genetic aspects. *Endocrinologist,* 10**,** 51-59.

GABREËLS, B. A. T. F., SWAAB, D. F., DE KLEIJN, D. P. V., DEAN, A., SEIDAH, N. G., VAN DE LOO, J.-W., VAN DE VEN, W. J. M., MARTENS, G. J. M. & VAN LEEUWEN, F. W. 1998. The Vasopressin Precursor Is Not Processed in the Hypothalamus of Wolfram Syndrome Patients with Diabetes Insipidus: Evidence for the Involvement of PC2 and 7B2. *Journal of Clinical Endocrinology & Metabolism,* 83**,** 4026-4033.

GALLUZZI, P., FILOSOMI, G., VALLONE, I. M., BARDELLI, A. M. & VENTURI, C. 1999. MRI of Wolfram syndrome (DIDMOAD). *Neuroradiology,* 41**,** 729-731.

GAO, H.-M. & HONG, J.-S. 2008. Why neurodegenerative diseases are progressive: uncontrolled inflammation drives disease progression. *Trends in immunology,* 29**,** 357-365.

GEERING, K., BEGGAH, A., GOOD, P., GIRARDET, S., ROY, S., SCHAER, D. & JAUNIN, P. 1996. Oligomerization and maturation of Na,K-ATPase: functional interaction of the cytoplasmic NH2 terminus of the beta subunit with the alpha subunit. *The Journal of Cell Biology,* 133**,** 1193-1204.

GENIS, D., DAVALOS, A., MOLINS, A. & FERRER, I. 1997. Wolfram syndrome: A neuropathological study. *Acta Neuropathologica,* 93**,** 426-429.

GEVA-ZATORSKY, N., DEKEL, E., COHEN, A. A., DANON, T., COHEN, L. & ALON, U. 2010. Protein Dynamics in Drug Combinations: a Linear Superposition of Individual-Drug Responses. *Cell,* 140**,** 643-651.

GHARANEI, S., ZATYKA, M., ASTUTI, D., FENTON, J., SIK, A., NAGY, Z. & BARRETT, T. G. 2012. Vacuolar-type H+-ATPase V1A subunit is a molecular partner of Wolfram

syndrome 1 (WFS1) protein, which regulates its expression and stability. *Human Molecular Genetics*.

GOLDSTEIN, M. N. 1968. Neuroblastoma Cells In Tissue Culture. *Journal of Pediatric Surgery,* 3**,** 166-169.

GOMEZ-ZAERA, M., STROM, T. M., RODRIGUEZ, B., ESTIVILL, X., MEITINGER, T. & NUNES, V. 2001. Presence of a major WFS1 mutation in Spanish wolfram syndrome pedigrees. *Molecular Genetics and Metabolism,* 72**,** 72-81.

GORMAN, A. M. 2008. Neuronal cell death in neurodegenerative diseases: recurring themes around protein handling. *Journal of Cellular and Molecular Medicine,* 12**,** 2263-2280.

GOTTLICHER, M., MINUCCI, S., ZHU, P., KRAMER, O. H., SCHIMPF, A., GIAVARA, S., SLEEMAN, J. P., LO COCO, F., NERVI, C., PELICCI, P. G. & HEINZEL, T. 2001. Valproic acid defines a novel class of HDAC inhibitors inducing differentiation of transformed cells. *EMBO J,* 20**,** 6969-6978.

GOW, A. & WRABETZ, L. 2009. CHOP and the endoplasmic reticulum stress response in myelinating glia. *Current Opinion in Neurobiology,* 19**,** 505-510.

GRIMES, C. A. & JOPE, R. S. 1999. Cholinergic Stimulation of Early Growth Response-1 DNA Binding Activity Requires Protein Kinase C and Mitogen-Activated Protein KInase Kinase Activation and Is Inhibited by Sodium Valporate in SH-SY5y Cells. *Journal of Neurochemistry,* 73**,** 1384-1392.

GUPTA, S., CUFFE, L., SZEGEZDI, E., LOGUE, S. E., NEARY, C., HEALY, S. & SAMALI, A. 2010. Mechanisms of ER Stress-Mediated Mitochondrial Membrane Permeabilization. *International Journal of Cell Biology,* 2010.

HAMANAKA, R. B., BENNETT, B. S., CULLINAN, S. B. & DIEHL, J. A. 2005. PERK and GCN2 Contribute to eIF2{alpha} Phosphorylation and Cell Cycle Arrest after Activation of the Unfolded Protein Response Pathway.

HAN, C., JIN, L., MEI, Y. & WU, M. 2012. Endoplasmic reticulum stress inhibits cell cycle progression via induction of p27 in melanoma cells. *Cellular Signalling*.

HANNON, G. J. & BEACH, D. 1994. pl5INK4B is a potentia| effector of TGF-[beta]-induced cell cycle arrest. *Nature,* 371**,** 257-261.

HARDING, H. P., CALFON, M., URANO, F., NOVOA, I. & RON, D. 2002. TRANSCRIPTIONAL AND TRANSLATIONAL CONTROL IN THE MAMMALIAN UNFOLDED PROTEIN RESPONSE. *Annual Review of Cell and Developmental Biology,* 18**,** 575-599.

HARDING, H. P., NOVOA, I., ZHANG, Y., ZENG, H., WEK, R., SCHAPIRA, M. & RON, D. 2000a. Regulated Translation Initiation Controls Stress-Induced Gene Expression in Mammalian Cells. *Molecular Cell,* 6**,** 1099-1108.

HARDING, H. P., ZHANG, Y., BERTOLOTTI, A., ZENG, H. & RON, D. 2000b. Perk Is Essential for Translational Regulation and Cell Survival during the Unfolded Protein Response. *Molecular Cell,* 5**,** 897-904.

HARDY, C., KHANIM, F., TORRES, R., SCOTT-BROWN, M., SELLER, A., POULTON, J., COLLIER, D., KIRK, J., POLYMEROPOULOS, M., LATIF, F. & BARRETT, T. 1999. Clinical and molecular genetic analysis of 19 Wolfram syndrome kindreds demonstrating

a wide spectrum of mutations in WFS1. *American Journal of Human Genetics,* 65**,** 1279-1290.

HATANAKA, M., TANABE, K., YANAI, A., OHTA, Y., KONDO, M., AKIYAMA, M., SHINODA, K., OKA, Y. & TANIZAWA, Y. 2011. Wolfram syndrome 1 gene (WFS1) product localizes to secretory granules and determines granule acidification in pancreatic β-cells. *Human Molecular Genetics,* 20**,** 1274-1284.

HEDGEPETH, C. M., CONRAD, L. J., ZHANG, J., HUANG, H.-C., LEE, V. M. Y. & KLEIN, P. S. 1997. Activation of the Wnt Signaling Pathway: A Molecular Mechanism for Lithium Action. *Developmental Biology,* 185**,** 82-91.

HERSHEY, T., LUGAR, H. M., SHIMONY, J. S., RUTLIN, J., KOLLER, J. M., PERANTIE, D. C., PACIORKOWSKI, A. R., EISENSTEIN, S. A., PERMUTT, M. A. & THE WASHINGTON UNIVERSITY WOLFRAM STUDY, G. 2012. Early Brain Vulnerability in Wolfram Syndrome. *PLoS ONE,* 7**,** e40604.

HINTON, A., SENNOUNE, S. R., BOND, S., FANG, M., REUVENI, M., SAHAGIAN, G. G., JAY, D., MARTINEZ-ZAGUILAN, R. & FORGAC, M. 2009. Function of a Subunit Isoforms of the V-ATPase in pH Homeostasis and in Vitro Invasion of MDA-MB231 Human Breast Cancer Cells. *Journal of Biological Chemistry,* 284**,** 16400-16408.

HOFMANN, S. & BAUER, M. F. 2006. Wolfram syndrome-associated mutations lead to instability and proteasomal degradation of wolframin. *Febs Letters,* 580**,** 4000-4004.

HOFMANN, S., PHILBROOK, C., GERBITZ, K.-D. & BAUER, M. F. 2003. Wolfram syndrome: structural and functional analyses of mutant and wild-type wolframin, the WFS1 gene product. *Human Molecular Genetics,* 12**,** 2003-2012.

HONG, M., LI, M. Q., MAO, C. H. & LEE, A. S. 2004a. Endoplasmic reticulum stress triggers an acute proteasome-dependent degradation of ATF6. *Journal of Cellular Biochemistry,* 92**,** 723-732.

HONG, M., LUO, S., BAUMEISTER, P., HUANG, J.-M., GOGIA, R. K., LI, M. & LEE, A. S. 2004b. Underglycosylation of ATF6 as a Novel Sensing Mechanism for Activation of the Unfolded Protein Response. *Journal of Biological Chemistry,* 279**,** 11354-11363.

HOOZEMANS, J. J. M., BRUCKNER, M. K., ROZEMULLER, A. J. M., VEERHUIS, R., EIKELENBOOM, P. & ARENDT, T. 2002. Cyclin D1 and cyclin E are co-localized with cyclo-oxygenase 2 (COX-2) in pyramidal neurons in Alzheimer disease temporal cortex. *Journal of Neuropathology and Experimental Neurology,* 61**,** 678-688.

HOOZEMANS, J. J. M., STIELER, J., VAN HAASTERT, E. S., VEERHUIS, R., ROZEMULLER, A. J. M., BAAS, F., EIKELENBOOM, P., ARENDT, T. & SCHEPER, W. 2006. The unfolded protein response affects neuronal cell cycle protein expression: Implications for Alzheimer's disease pathogenesis. *Experimental Gerontology,* 41**,** 380-386.

HOOZEMANS, J. J. M., VEERHUIS, R., ROZEMULLER, A. J. M., ARENDT, T. & EIKELENBOOM, P. 2004. Neuronal COX-2 expression and phosphorylation of pRb precede p38 MAPK activation and neurofibrillary changes in AD temporal cortex. *Neurobiology of Disease,* 15**,** 492-499.

HORISBERGER, J.-D. 2004. Recent Insights into the Structure and Mechanism of the Sodium Pump. *Physiology,* 19**,** 377-387.

HRZENJAK, A., MOINFAR, F., KREMSER, M.-L., STROHMEIER, B., STABER, P. B., ZATLOUKAL, K. & DENK, H. 2006. Valproate inhibition of histone deacetylase 2 affects differentiation and decreases proliferation of endometrial stromal sarcoma cells. *Molecular Cancer Therapeutics,* 5**,** 2203-2210.

IMAHORI, K. & UCHIDA, T. 1997. Physiology and Pathology of Tau Protein Kinases in Relation to Alzheimer's Disease. *The Journal of Biochemistry,* 121**,** 179-188.

INOUE, Y.TANIZAWA, J.WASSON & P.BEHN 1998. A gene encoding a transmembrane protein is mutatd in patients with diabetes mellitus and optic atrophy (Wolfram syndrome). *Nature Genetics,* 20**,** 143-147.

ISHIHARA, H., TAKEDA, S., TAMURA, A., TAKAHASHI, R., YAMAGUCHI, S., TAKEI, D., YAMADA, T., INOUE, H., SOGA, H., KATAGIRI, H., TANIZAWA, Y. & OKA, Y. 2004. Disruption of the WFS1 gene in mice causes progressive beta-cell loss and impaired stimulus-secretion coupling in insulin secretion. *Human Molecular Genetics,* 13**,** 1159-1170.

JAISSER, F., JAUNIN, P., GEERING, K., ROSSIER, B. C. & HORISBERGER, J. D. 1994. Modulation of the Na,K-pump function by beta subunit isoforms. *The Journal of General Physiology,* 103**,** 605-623.

JAKUTIENE, E., GRIKINIENE, J., VAITKEVICIUS, A. & STAKISAITIS, D. 2007. Sodium valproate stimulates potassium and chloride urinary
excretion in rats: gender differences. *BMC Pharmacology,* 7.

JAMORA, C., DENNERT, G. & LEE, A. S. 1996. Inhibition of tumor progression by suppression of stress protein GRP78/BiP induction in fibrosarcoma B/C10ME. *Proceedings of the National Academy of Sciences,* 93**,** 7690-7694.

JAUNIN, P., JAISSER, F., BEGGAH, A. T., TAKEYASU, K., MANGEAT, P., ROSSIER, B. C., HORISBERGER, J. D. & GEERING, K. 1993. Role of the transmembrane and extracytoplasmic domain of beta subunits in subunit assembly, intracellular transport, and functional expression of Na,K-pumps. *The Journal of Cell Biology,* 123**,** 1751-1759.

JEONG, M. R., HASHIMOTO, R., SENATOROV, V. V., FUJIMAKI, K., REN, M., LEE, M. S. & CHUANG, D.-M. 2003. Valproic acid, a mood stabilizer and anticonvulsant, protects rat cerebral cortical neurons from spontaneous cell death: a role of histone deacetylase inhibition. *FEBS Letters,* 542**,** 74-78.

JOHANNESSEN, C. U. 2000. Mechanisms of action of valproate: a commentatory. *Neurochemistry International,* 37**,** 103-110.

JONIKAS, M. C., COLLINS, S. R., DENIC, V., OH, E., QUAN, E. M., SCHMID, V., WEIBEZAHN, J., SCHWAPPACH, B., WALTER, P., WEISSMAN, J. S. & SCHULDINER, M. 2009. Comprehensive Characterization of Genes Required for Protein Folding in the Endoplasmic Reticulum. *Science,* 323**,** 1693-1697.

KAKIUCHI, C., ISHIGAKI, S., OSLOWSKI, C. M., FONSECA, S. G., KATO, T. & URANO, F. 2009. Valproate, a Mood Stabilizer, Induces WFS1 Expression and Modulates Its Interaction with ER Stress Protein GRP94. *PLoS ONE,* 4**,** e4134.

KAKIUCHI, C., ISHIWATA, M., HAYASHI, A. & KATO, T. 2006. XBP1 induces WFS1 through an endoplasmic reticulum stress response element-like motif in SH-SY5Y cells. *Journal of Neurochemistry,* 97**,** 545-555.

KALAI, M., LAMKANFI, M., DENECKER, G., BOOGMANS, M., LIPPENS, S., MEEUS, A., DECLERCQ, W. & VANDENABEELE, P. 2003. Regulation of the expression and processing of caspase-12. *Journal of Cell Biology,* 162**,** 457-467.

KANE, P. M. 2006. The Where, When, and How of Organelle Acidification by the Yeast Vacuolar H+-ATPase. *Microbiology and Molecular Biology Reviews,* 70**,** 177-191.

KANEKO, M., ISHIGURO, M., NIINUMA, Y., UESUGI, M. & NOMURA, Y. 2002. Human HRD1 protects against ER stress-induced apoptosis through ER-associated degradation. *Febs Letters,* 532**,** 147-152.

KANEKO, M. & NOMURA, Y. 2003. ER signaling in unfolded protein response. *Life Sciences,* 74**,** 199-205.

KANEKO, M., YASUI, S., NIINUMA, Y., ARAI, K., OMURA, T., OKUMA, Y. & NOMURA, Y. 2007. A different pathway in the endoplasmic reticulum stress-induced expression of human HRD1 and SEL1 genes. *FEBS Letters,* 581**,** 5355-5360.

KARASKOV, E., SCOTT, C., ZHANG, L., TEODORO, T., RAVAZZOLA, M. & VOLCHUK, A. 2006. Chronic Palmitate But Not Oleate Exposure Induces Endoplasmic Reticulum Stress, Which May Contribute to INS-1 Pancreatic β-Cell Apoptosis. *Endocrinology,* 147**,** 3398-3407.

KATO, T., ISHIWATA, M., YAMADA, K., KASAHARA, T., KAKIUCHI, C., IWAMOTO, K., KAWAMURA, K., ISHIHARA, H. & OKA, Y. 2008. Behavioral and gene expression analyses of Wfs1 knockout mice as a possible animal model of mood disorder. *Neuroscience Research,* 61**,** 143-158.

KAUFMAN, R. J. 1999. Stress signaling from the lumen of the endoplasmic reticulum: coordination of gene transcriptional and translational controls. *Genes & Development,* 13**,** 1211-1233.

KAWANO, J., FUJINAGA, R., YAMAMOTO-HANADA, K., OKA, Y., TANIZAWA, Y. & SHINODA, K. 2009. Wolfram syndrome 1 (Wfs1) mRNA expression in the normal mouse brain during postnatal development. *Neuroscience Research,* 64**,** 213-230.

KEENE, C. D., RODRIGUES, C. M. P., EICH, T., CHHABRA, M. S., STEER, C. J. & LOW, W. C. 2002. Tauroursodeoxycholic acid, a bile acid, is neuroprotective in a transgenic animal model of Huntington's disease. *Proceedings of the National Academy of Sciences,* 99**,** 10671-10676.

KEENE, C. D., RODRIGUES, C. M. P., EICH, T., LINEHAN-STIEERS, C., ABT, A., KREN, B. T., STEER, C. J. & LOW, W. C. 2001. A Bile Acid Protects against Motor and Cognitive Deficits and Reduces Striatal Degeneration in the 3-Nitropropionic Acid Model of Huntington's Disease. *Experimental Neurology,* 171**,** 351-360.

KHANIM, F., KIRK, J., LATIF, F. & BARRETT, T. G. 2001. WFS1/Wolframin mutations, Wolfram syndrome, and associated diseases. *Human Mutation,* 17**,** 357-367.

KIM, I., XU, W. & REED, J. C. 2008. Cell death and endoplasmic reticulum stress: disease relevance and therapeutic opportunities. *Nature Review of Drug Discovery,* 7**,** 1013-1030.

KIM, J. S., SONG, B. S., LEE, K. S., KIM, D. H., KIM, S. U., CHOO, Y. K., CHANG, K. T. & KOO, D. B. 2011. Tauroursodeoxycholic Acid Enhances the Pre-Implantation Embryo Development by Reducing Apoptosis in Pigs. *Reproduction in Domestic Animals***,** no-no.

KINSLEY, B. T. & FIRTH, R. G. F. 1992. The Wolfram Syndrome - a Primary Neurodegenerative Disorder with Lethal Potential. *Irish Medical Journal,* 85**,** 34-36.

KINSLEY, B. T., SWIFT, M., DUMONT, R. H. & SWIFT, R. G. 1995. Morbidity and Mortality in the Wolfram-Syndrome. *Diabetes Care,* 18**,** 1566-1570.

KOCH, G., SMITH, M., MACER, D., WEBSTER, P. & MORTARA, R. 1986. Endoplasmic reticulum contains a common, abundant calcium-binding glycoprotein, endoplasmin. *Journal of Cell Science,* 86**,** 217-232.

KÕKS, S., PLANKEN, A., LUUK, H. & VASAR, E. 2002. Cat odour exposure increases the expression of wolframin gene in the amygdaloid area of rat. *Neuroscience Letters,* 322**,** 116-120.

KÖKSOY, A. A. 2002. Na+, K+–ATPASE: a review. *Journal of Ankara medical school* 24.

KRAMER, O. H., ZHU, P., OSTENDORFF, H. P., GOLEBIEWSKI, M., TIEFENBACH, J., PETERS, M. A., BRILL, B., GRONER, B., BACH, I., HEINZEL, T. & GOTTLICHER, M. 2003. The histone deacetylase inhibitor valproic acid selectively induces proteasomal degradation of HDAC2. *EMBO J,* 22**,** 3411-3420.

LAI, E., BIKOPOULOS, G., WHEELER, M. B., ROZAKIS-ADCOCK, M. & VOLCHUK, A. 2008. Differential activation of ER stress and apoptosis in response to chronically elevated free fatty acids in pancreatic β-cells. *American Journal of Physiology - Endocrinology And Metabolism,* 294**,** E540-E550.

LARGE, C. H., KALINICHEV, M., LUCAS, A., CARIGNANI, C., BRADFORD, A., GARBATI, N., SARTORI, I., AUSTIN, N. E., RUFFO, A., JONES, D. N. C., ALVARO, G. & READ, K. D. 2009. The relationship between sodium channel inhibition and anticonvulsant activity in a model of generalised seizure in the rat. *Epilepsy research,* 85**,** 96-106.

LASSUS, P., OPITZ-ARAYA, X. & LAZEBNIK, Y. 2002. Requirement for Caspase-2 in Stress-Induced Apoptosis Before Mitochondrial Permeabilization. *Science,* 297**,** 1352-1354.

LAYBUTT, D., PRESTON, A., ÅKERFELDT, M., KENCH, J., BUSCH, A., BIANKIN, A. & BIDEN, T. 2007. Endoplasmic reticulum stress contributes to beta cell apoptosis in type 2 diabetes. *Diabetologia,* 50**,** 752-763.

LEE, A. S. 2001. The glucose-regulated proteins: stress induction and clinical applications. *Trends in Biochemical Sciences,* 26**,** 504-510.

LEE, A. S. 2005. The ER chaperone and signaling regulator GRP78/BiP as a monitor of endoplasmic reticulum stress. *Methods,* 35**,** 373-381.

LEE, A. S. & HENDERSHOT, L. M. 2006. ER stress and cancer. *Cancer Biology & Therapy,* 5**,** 721-722.

LEE, H. O., DAVIDSON, J. M. & DURONIO, R. J. 2009. Endoreplication: polyploidy with purpose. *Genes & Development,* 23**,** 2461-2477.

LIN, W. & POPKO, B. 2009. Endoplasmic reticulum stress in disorders of myelinating cells. *Nature Neurosciences,* 12**,** 379-385.

LIPSON, K. L., FONSECA, S. G., ISHIGAKI, S., NGUYEN, L. X., FOSS, E., BORTELL, R., ROSSINI, A. A. & URANO, F. 2006. Regulation of insulin biosynthesis in pancreatic beta cells by an endoplasmic reticulum-resident protein kinase IRE1. *Cell Metabolism,* 4**,** 245-254.

LIU, H., BOWES, R. C., VAN DE WATER, B., SILLENCE, C., NAGELKERKE, J. F. & STEVENS, J. L. 1997. Endoplasmic Reticulum Chaperones GRP78 and Calreticulin Prevent Oxidative Stress, Ca2+ Disturbances, and Cell Death in Renal Epithelial Cells. *Journal of Biological Chemistry,* 272**,** 21751-21759.

LIVAK, K. J. & SCHMITTGEN, T. D. 2001. Analysis of Relative Gene Expression Data Using Real-Time Quantitative PCR and the 2−ΔΔCT Method. *Methods,* 25**,** 402-408.

LOY, R. & TARIOT, P. 2002. Neuroprotective properties of valproate. *Journal of Molecular Neuroscience,* 19**,** 301-307.

LUO, R. X. & DEAN, D. C. 1999. Chromatin Remodeling and Transcriptional Regulation. *Journal of the National Cancer Institute,* 91**,** 1288-1294.

LUUK, H., KOKS, S., PLAAS, M., HANNIBAL, J., REHFELD, J. F. & VASAR, E. 2008. Distribution of Wfs1 protein in the central nervous system of the mouse and its relation to clinical symptoms of the Wolfram syndrome. *Journal of Comparative Neurology,* 509**,** 642-660.

LUUK, H., PLAAS, M., RAUD, S., INNOS, J., SUTT, S., LASNER, H., ABRAMOV, U., KURRIKOFF, K., KOKS, S. & VASAR, E. 2009. Wfs1-deficient mice display impaired behavioural adaptation in stressful environment. *Behavioural Brain Research,* 198**,** 334-345.

MARCINIAK, S. J., GARCIA-BONILLA, L., HU, J., HARDING, H. P. & RON, D. 2006. Activation-dependent substrate recruitment by the eukaryotic translation initiation factor 2 kinase PERK. *The Journal of Cell Biology,* 172**,** 201-209.

MARK, R. J., WESSON ASHFORD, J., GOODMAN, Y. & MATTSON, M. P. 1995. Anticonvulsants attenuate amyloid β-peptide neurotoxicity, Ca2+ deregulation, and cytoskeletal pathology. *Neurobiology of Aging,* 16**,** 187-198.

MATSUMOTO, M., MINAMI, M., TAKEDA, K., SAKAO, Y. & AKIRA, S. 1996. Ectopic expression of CHOP (GADD153) induces apoptosis in M1 myeloblastic leukemia cells. *FEBS Letters,* 395**,** 143-147.

MATTSSON, G., JANSSON, L. & CARLSSON, P.-O. 2002. Decreased Vascular Density in Mouse Pancreatic Islets After Transplantation. *Diabetes,* 51**,** 1362-1366.

MCBAIN, S. C. & MORGAN, N. G. 2003. Functional effects of expression of wolframin-antisense transcripts in BRIN-BD11 beta-cells. *Biochemical and Biophysical Research Communications,* 307**,** 684-688.

MCCULLOUGH, K. D., MARTINDALE, J. L., KLOTZ, L.-O., AW, T.-Y. & HOLBROOK, N. J. 2001. Gadd153 Sensitizes Cells to Endoplasmic Reticulum Stress by Down-Regulating Bcl2 and Perturbing the Cellular Redox State. *Molecular and Cellular Biology,* 21**,** 1249-1259.

MIHAILIDOU, C., PAPAZIAN, I., PAPAVASSILIOU, A. G. & KIARIS, H. 2010. CHOP-dependent Regulation of p21/waf1 During ER Stress. *Cellular Physiology and Biochemistry,* 25**,** 761-766.

MINTON, J. A. L., HATTERSLEY, A. T., OWEN, K., MCCARTHY, M. I., WALKER, M., LATIF, F., BARRETT, T. & FRAYLING, T. M. 2002. Association studies of genetic variation in the WFS1 gene and type 2 diabetes in UK populations. *Diabetes,* 51**,** 1287-1290.

MORIN, P. J. 1999. β-catenin signaling and cancer. *Biological Essays,* 21**,** 1021-1030.
MORISHIMA, N., NAKANISHI, K., TAKENOUCHI, H., SHIBATA, T. & YASUHIKO, Y. 2002. An endoplasmic reticulum stress-specific caspase cascade in apoptosis - Cytochrome c-independent activation of caspase-9 by caspase-12. *Journal of Biological Chemistry,* 277**,** 34287-34294.
MORLAND, C., BOLDINGH, K. A., IVERSEN, E. G. & HASSEL, B. 2004. Valproate is Neuroprotective Against Malonate Toxicity in Rat Striatum[colon] An Association With Augmentation of High-Affinity Glutamate Uptake. *Journal of Cerebral Blood Flow Metabolisim,* 24**,** 1226-1234.
MORRIS, J. A., DORNER, A. J., EDWARDS, C. A., HENDERSHOT, L. M. & KAUFMAN, R. J. 1997. Immunoglobulin Binding Protein (BiP) Function Is Required to Protect Cells from Endoplasmic Reticulum Stress but Is Not Required for the Secretion of Selective Proteins. *Journal of Biological Chemistry,* 272**,** 4327-4334.
MU, T.-W., ONG, D. S. T., WANG, Y.-J., BALCH, W. E., YATES, J. R., SEGATORI, L. & KELLY, J. W. 2008. Chemical and Biological Approaches Synergize to Ameliorate Protein-Folding Diseases. *Cell,* 134**,** 769-781.
MUNRO, S. & PELHAM, H. R. B. 1986. An hsp70-like protein in the ER: Identity with the 78 kd glucose-regulated protein and immunoglobulin heavy chain binding protein. *Cell,* 46**,** 291-300.
MURRAY, M. & STOUT, A. P. 1947. DISTINCTIVE CHARACTERISTICS OF THE SYMPATHICOBLASTOMA
CULTIVATED IN VITRO; method for prompt diagnosis
American. Journal of Pathology, 23**,** 429-441.
NAGY, Z., ESIRI, M. M. & SMITH, A. D. 1997. Expression of cell division markers in the hippocampus in Alzheimer's disease and other neurodegenerative conditions. *Acta Neuropathologica,* 93**,** 294-300.
NAKAGAWA, T., ZHU, H., MORISHIMA, N., LI, E., XU, J., YANKNER, B. A. & YUAN, J. 2000. Caspase-12 mediates endoplasmic-reticulum-specific apoptosis and cytotoxicity by amyloid-[beta]. *Nature,* 403**,** 98-103.
NELSON, N. 1991. Structure and pharmacology of the proton-ATPases. *Trends in Pharmacological Sciences,* 12**,** 71-75.
NELSON, N. 2003. A journey from mammals to yeast with the vacuolar H+-ATPase. *Journal of Bioenergetic. Biomembranes.,* 35**,** 281-289.
NIEOULLON, A. 2011. Neurodegenerative diseases and neuroprotection: current views and prospects. *Journal of Applied Biomedicine,* 9**,** 173-183.
NISHI, T. & FORGAC, M. 2002a. The vacuolar (H+)-ATPases â€" nature's most versatile proton pumps. *Nat Rev Mol Cell Biol,* 3**,** 94-103.
NISHI, T. & FORGAC, M. 2002b. The vacuolar (H+)-ATPases: Nature's most versatile proton pumps. *Nature Review of Molecular Cell Biology,* 3**,** 94-103.
NOGUCHI, Y., YASHIMA, T., HATANAKA, A., UZAWA, M., YASUNAMI, M., KIMURA, A. & KITAMURA, K. Year. A mutation in Wolfram syndrome type 1 gene in a Japanese family with autosomal dominant low-frequency sensorineural hearing loss. *In:* 27th

Annual Midwinter Research Meeting of the Association-for-Research-in-Otolaryngology*, Feb 21-26 2004 Daytona Beach, FL. 1189-1194.
NORBURY, C. J. & HICKSON, I. D. 2001. CELLULAR RESPONSES TO DNA DAMAGE. *Annual Review of Pharmacology and Toxicology,* 41**,** 367-401.
NOVOA, I., ZENG, H., HARDING, H. P. & RON, D. 2001. Feedback Inhibition of the Unfolded Protein Response by GADD34-Mediated Dephosphorylation of eIF2α. *The Journal of Cell Biology,* 153**,** 1011-1022.
OGATA, M., HINO, S.-I., SAITO, A., MORIKAWA, K., KONDO, S., KANEMOTO, S., MURAKAMI, T., TANIGUCHI, M., TANII, I., YOSHINAGA, K., SHIOSAKA, S., HAMMARBACK, J. A., URANO, F. & IMAIZUMI, K. 2006. Autophagy Is Activated for Cell Survival after Endoplasmic Reticulum Stress. *Molecular and Cellular Biology,* 26**,** 9220-9231.
OIKAWA, D., KIMATA, Y., KOHNO, K. & IWAWAKI, T. 2009. Activation of mammalian IRE1α upon ER stress depends on dissociation of BiP rather than on direct interaction with unfolded proteins. *Experimental Cell Research,* 315**,** 2496-2504.
OKADA, T., YOSHIDA, H., AKAZAWA, R., NEGISHI, M. & MORI, K. 2002. Distinct roles of activating transcription factor 6 (ATF6) and double-stranded RNA-activated protein kinase-like endoplasmic reticulum kinase (PERK) in transcription during the mammalian unfolded protein response. *Biochemical Journal,* 366**,** 585-594.
OSLOWSKI, C. M., URANO, F. & CONN, P. M. 2011. Measuring ER Stress and the Unfolded Protein Response Using Mammalian Tissue Culture System. *Methods in Enzymology*. Academic Press.
OSMAN, A. A., SAITO, M., MAKEPEACE, C., PERMUTT, M. A., SCHLESINGER, P. & MUECKLER, M. 2003. Wolframin expression induces novel ion channel activity in endoplasmic reticulum membranes and increases intracellular calcium. *Journal of Biological Chemistry,* 278**,** 52755-52762.
OZCAN, L., ERGIN, A. S., LU, A., CHUNG, J., SARKAR, S., NIE, D., MYERS JR, M. G. & OZCAN, U. 2009. Endoplasmic Reticulum Stress Plays a Central Role in Development of Leptin Resistance. *Cell Metabolism,* 9**,** 35-51.
OZCAN, U., YILMAZ, E., OZCAN, L., FURUHASHI, M., VAILLANCOURT, E., SMITH, R. O., GORGUN, C. Z. & HOTAMISLIGIL, G. S. 2006. Chemical chaperones reduce ER stress and restore glucose homeostasis in a mouse model of type 2 diabetes. *Science,* 313**,** 1137-1140.
PARENTI, G. 2009. Treating lysosomal storage diseases with pharmacological chaperones: from concept to clinics. *Embo Molecular Medicine,* 1**,** 268-279.
PAYNE, W. P. B. A. S. L. 2005. .High-content screening in oncology using fluorescence microplate cytometry. *Nature Methods*
PERLMUTTER, D. H. 2002. Chemical Chaperones: A Pharmacological Strategy for Disorders of Protein Folding and Trafficking. *Pediatric Research,* 52**,** 832-836.
PHIEL, C. J., ZHANG, F., HUANG, E. Y., GUENTHER, M. G., LAZAR, M. A. & KLEIN, P. S. 2001. Histone Deacetylase Is a Direct Target of Valproic Acid, a Potent Anticonvulsant, Mood Stabilizer, and Teratogen. *Journal of Biological Chemistry,* 276**,** 36734-36741.

PHILBROOK, C., FRITZ, E. & WEIHER, H. 2005. Expressional and functional studies of Wolframin, the gene function deficient in Wolfram syndrome, in mice and patient cells. *Experimental Gerontology,* 40**,** 671-678.

PICKETT, K. A., DUNCAN, R. P., PACIORKOWSKI, A. R., PERMUTT, M. A., MARSHALL, B., HERSHEY, T. & EARHART, G. M. 2012. Balance impairment in individuals with Wolfram syndrome. *Gait & posture,* 36**,** 619-624.

PORSTEINSSON, A., PN, T., R, E., CJ, H. & C, I. 2001. Placebo-controlled study of divalproex sodium for agitation in dementia. *American Journal Geriatric Psychiatry,* 9**,** 58-66.

RAJAN, S. S., V.SRINIVASAN, M.BALASUBRAMANYAM & U.TATU 2007. Endoplasmic reticulum (ER) stress & diabetes. *Indian Journal of Medical Research,* 125**,** 411-424.

RAMALHO, R. M., BORRALHO, P. M., CASTRO, R. E., SOLÁ, S., STEER, C. J. & RODRIGUES, C. M. P. 2006. Tauroursodeoxycholic acid modulates p53-mediated apoptosis in Alzheimer's disease mutant neuroblastoma cells. *Journal of Neurochemistry,* 98**,** 1610-1618.

RANSOM, M., DENNEHEY, B. K. & TYLER, J. K. 2010. Chaperoning Histones during DNA Replication and Repair. *Cell,* 140**,** 183-195.

RAO, R. V., HERMEL, E., CASTRO-OBREGON, S., DEL RIO, G., ELLERBY, L. M., ELLERBY, H. M. & BREDESEN, D. E. 2001. Coupling Endoplasmic Reticulum Stress to the Cell Death Program. *Journal of Biological Chemistry,* 276**,** 33869-33874.

RAUD, S., SUTT, S., LUUK, H., PLAAS, M., INNOS, J., KOKS, S. & VASAR, E. 2009. Relation between increased anxiety and reduced expression of alpha1 and alpha2 subunits of GABA(A) receptors in Wfs1-deficient mice. *Neuroscience Letters,* 460**,** 138-142.

REDDY, R. K., DUBEAU, L., KLEINER, H., PARR, T., NICHOLS, P., KO, B., DONG, D., KO, H., MAO, C., DIGIOVANNI, J. & LEE, A. S. 2002. Cancer-inducible Transgene Expression by the Grp94 Promoter. *Cancer Research,* 62**,** 7207-7212.

REDDY, R. K., MAO, C., BAUMEISTER, P., AUSTIN, R. C., KAUFMAN, R. J. & LEE, A. S. 2003. Endoplasmic Reticulum Chaperone Protein GRP78 Protects Cells from Apoptosis Induced by Topoisomerase Inhibitors. *Journal of Biological Chemistry,* 278**,** 20915-20924.

RIGGS, A. C., BERNAL-MIZRACHI, E., OHSUGI, M., WASSON, J., FATRAI, S., WELLING, C., MURRAY, J., SCHMIDT, R. E., HERRERA, P. L. & PERMUTT, M. A. 2005. Mice conditionally lacking the Wolfram gene in pancreatic islet beta cells exhibit diabetes as a result of enhanced endoplasmic reticulum stress and apoptosis. *Diabetologia,* 48**,** 2313-2321.

RIGOLI, L., LOMBARDO, F. & DI BELLA, C. 2010. Wolfram syndrome and WFS1 gene. *Clinical Genetics,* 79**,** 103-117.

ROBINSON, A. S., BOCKHAUS, J. A., VOEGLER, A. C. & WITTRUP, K. D. 1996. Reduction of BiP Levels Decreases Heterologous Protein Secretion in Saccharomyces cerevisiae. *Journal of Biological Chemistry,* 271**,** 10017-10022.

RODRIGUES, C., AMP, X, LIA, M. P., SOLÁ, S., BRITO, M. A., BRONDINO, C. D., BRITES, D. & MOURA, J. J. G. 2001. Amyloid β-Peptide Disrupts Mitochondrial Membrane Lipid and Protein Structure: Protective Role of Tauroursodeoxycholate. *Biochemical and Biophysical Research Communications,* 281**,** 468-474.

RODRIGUES, C. M. & STEER, C. J. 2001. The therapeutic effects of ursodeoxycholic acid as an anti-apoptotic agent. *Expert Opinion on Investigational Drugs,* 10**,** 1243-1253.

RODRIGUES, C. M. P., SOLÁ, S., NAN, Z., CASTRO, R. E., RIBEIRO, P. S., LOW, W. C. & STEER, C. J. 2003. Tauroursodeoxycholic acid reduces apoptosis and protects against neurological injury after acute hemorrhagic stroke in rats. *Proceedings of the National Academy of Sciences,* 100**,** 6087-6092.

RODRIGUES, C. M. P., SPELLMAN, S. R., SOLA, S., GRANDE, A. W., LINEHAN-STIEERS, C., LOW, W. C. & STEER, C. J. 2002. Neuroprotection by a Bile Acid in an Acute Stroke Model in the Rat. *Journal of Cereberal Blood Flow Metabolisim,* 22**,** 463-471.

RODRIGUES, C. M. P., STIEERS, C. L., KEENE, C. D., MA, X., KREN, B. T., LOW, W. C. & STEER, C. J. 2000. Tauroursodeoxycholic Acid Partially Prevents Apoptosis Induced by 3-Nitropropionic Acid. *Journal of Neurochemistry,* 75**,** 2368-2379.

ROHAYEM, J., EHLERS, C., WIEDEMANN, B., HOLL, R., OEXLE, K., KORDONOURI, O., SALZANO, G., MEISSNER, T., BURGER, W., SCHOBER, E., HUEBNER, A., LEE-KIRSCH, M. A. & GROUP, T. W. S. D. W. 2011. Diabetes and Neurodegeneration in Wolfram Syndrome. *Diabetes Care,* 34**,** 1503-1510.

ROSENBERG, G. 2007. The mechanisms of action of valproate in neuropsychiatric disorders: can we see the forest for the trees? *Cellular and Molecular Life Sciences,* 64**,** 2090-2103.

RUTKOWSKI, D. T. & KAUFMAN, R. J. 2004. A trip to the ER: coping with stress. *Trends in cell biology,* 14**,** 20-28.

RUTKOWSKI, D. T. & KAUFMAN, R. J. 2007. That which does not kill me makes me stronger: adapting to chronic ER stress. *Trends in Biochemical Sciences,* 32**,** 469-476.

SANDHU, M. S., WEEDON, M. N., WASSON, J., DALY, A., PERMUTT, M. A. & BARROSO, I. 2007. Common variants in WFS1 confer risk of type 2 diabetes. *Nature Genetics,* 39**,** 951-953.

SCHEINER-BOBIS, G. 2002. The sodium pump. *European Journal of Biochemistry,* 269**,** 2424-2433.

SCHEUNER, D., MIERDE, D. V., SONG, B., FLAMEZ., D., CREEMERS4, J. W. M., TSUKAMOTO, K., RIBICK, M., SCHUIT., F. C. & KAUFMAN, R. J. 2005. Control of mRNA translation preserves endoplasmic reticulum function in beta cells and maintains glucose homeostasis. *Nature Medicine,* 11**,** 757-764.

SCHÖNTHAL, A. H. 2009. Endoplasmic reticulum stress and autophagy as targets for cancer therapy. *Cancer letters,* 275**,** 163-169.

SCHRODER, M. & KAUFMAN, R. J. 2005. The mammalian unfolded protein response. *Annual Review of Biochemistry,* 74**,** 739-789.

SEOANE, J., HONG-VAN, L. & JOAN, M. 2002. Myc suppression of the p21Cip1 Cdk inhibitor influences the outcome of the p53 response to DNA damage. *Nature,* 419**,** 729-734.

SHADRINA, M. I. & SLOMINSKY, P. A. 2006. Molecular genetics of Parkinson's disease. *Russian Journal of Genetics,* 42**,** 858-871.

SHANNON, P., BECKER, L. & DECK, J. 1999. Evidence of widespread axonal pathology in Wolfram syndrome. *Acta Neuropathologica,* 98**,** 304-308.

SHAO, E., NISHI, T., KAWASAKI-NISHI, S. & FORGAC, M. 2003. Mutational Analysis of the Non-homologous Region of Subunit A of the Yeast V-ATPase. *Journal of Biological Chemistry,* 278**,** 12985-12991.

SHEN, J., CHEN, X., HENDERSHOT, L. & PRYWES, R. 2002. ER Stress Regulation of ATF6 Localization by Dissociation of BiP/GRP78 Binding and Unmasking of Golgi Localization Signals. *Developmental cell,* 3**,** 99-111.

SHERR, C. J. 1993. Mammalian G1 cyclins. *Cell,* 73**,** 1059-1065.

SHERR, C. J. & ROBERTS, J. M. 1995. Inhibitors of mammalian G1 cyclin-dependent kinases. *Genes & Development,* 9**,** 1149-1163.

SHIMIZU, E., HASHIMOTO, K., OKAMURA, N., KOIKE, K., KOMATSU, N., KUMAKIRI, C., NAKAZATO, M., WATANABE, H., SHINODA, N., OKADA, S.-I. & IYO, M. 2003. Alterations of serum levels of brain-derived neurotrophic factor (BDNF) in depressed patients with or without antidepressants. *Biological Psychiatry,* 54**,** 70-75.

SHIRAISHI, H., OKAMOTO, H., YOSHIMURA, A. & YOSHIDA, H. 2006. ER stress-induced apoptosis and caspase-12 activation occurs downstream of mitochondrial apoptosis involving Apaf-1. *Journal of Cell Science,* 119**,** 3958-3966.

SHIU, R. P., POUYSSEGUR, J. & PASTAN, I. 1977. Glucose depletion accounts for the induction of two transformation-sensitive membrane proteinsin Rous sarcoma virus-transformed chick embryo fibroblasts. *Proceedings of the National Academy of Sciences of the United States of America,* 74**,** 3840-4.

SHORT, B. 2010. The acid test of v-ATPase function. *The Journal of Cell Biology,* 189**,** 773.

SOMMER, T. & JAROSCH, E. 2002. BiP Binding Keeps ATF6 at Bay. *Developmental cell,* 3**,** 1-2.

SONG, B., SCHEUNER, D., RON, D., PENNATHUR, S. & KAUFMAN, R. J. 2008. Chop deletion reduces oxidative stress, improves β cell function, and promotes cell survival in multiple mouse models of diabetes. *The Journal of Clinical Investigation,* 118**,** 3378-3389.

SOTO, C. 2003. Unfolding the role of protein misfolding in neurodegenerative diseases. *Nature Review of Neuroscience,* 4**,** 49-60.

STAMBOLIC, V., RUEL, L. & WOODGETT, J. R. 1996. Lithium inhibits glycogen synthase kinase-3 activity and mimics Wingless signalling in intact cells. *Current biology : CB,* 6**,** 1664-1669.

STEFANI, M. 2004. Protein misfolding and aggregation: new examples in medicine and biology of the dark side of the protein world. *Biochimica et Biophysica Acta (BBA) - Molecular Basis of Disease,* 1739**,** 5-25.

STOPPINI, M., ANDREOLA, A., FORESTI, G. & BELLOTTI, V. 2004. Neurodegenerative diseases caused by protein aggregation: a phenomenon at the borderline between molecular evolution and ageing. *Pharmacological Research,* 50**,** 419-431.

STROM, T. M., HORTNAGEL, K., HOFMANN, S., GEKELER, F., SCHARFE, C., RABL, W., GERBITZ, K. D. & MEITINGER, T. 1998. Diabetes insipidus, diabetes mellitus, optic atrophy and deafness (DIDMOAD) caused by mutations in a novel gene (wolframin) coding for a predicted transmembrane protein. *Human Molecular Genetics,* 7**,** 2021-2028.

STUDER, E., ZHOU, X., ZHAO, R., WANG, Y., TAKABE, K., NAGAHASHI, M., PANDAK, W. M., DENT, P., SPIEGEL, S., SHI, R., XU, W., LIU, X., BOHDAN, P., ZHANG, L., ZHOU, H. & HYLEMON, P. B. 2012. Conjugated bile acids activate the sphingosine-1-phosphate receptor 2 in primary rodent hepatocytes. *Hepatology,* 55**,** 267-276.

SUN-WADA, G.-H., TOYOMURA, T., MURATA, Y., YAMAMOTO, A., FUTAI, M. & WADA, Y. 2006. The a3 isoform of V-ATPase regulates insulin secretion from pancreatic β-cells. *Journal of Cell Science,* 119**,** 4531-4540.

SWIFT, R. G., SADLER, D. B. & SWIFT, M. 1990. Psychiatric Findings in Wolfram Syndrome Homozygotes. *Lancet,* 336**,** 667-669.

SZEGEZDI, E., LOGUE, S. E., GORMAN, A. M. & SAMALI, A. 2006. Mediators of endoplasmic reticulum stress-induced apoptosis. *EMBO Reproduction,* 7**,** 880-885.

SZEGEZDI, E., MACDONALD, D. C., NÍ CHONGHAILE, T., GUPTA, S. & SAMALI, A. 2009. Bcl-2 family on guard at the ER. *American Journal of Physiology - Cell Physiology,* 296**,** C941-C953.

TABARES, L. & BETZ, B. 2010. Multiple Functions of the Vesicular Proton Pump in Nerve Terminals. *Neuron,* 68**,** 1020-1022.

TAKEDA, K., INOUE, H., TANIZAWA, Y., MATSUZAKI, Y., OBA, J., WATANABE, Y., SHINODA, K. & OKA, Y. 2001. WFS1 (Wolfram syndrome 1) gene product: predominant subcellular localization to endoplasmic reticulum in cultured cells and neuronal expression in rat brain. *Human Molecular Genetics,* 10**,** 477-484.

TAKEI, D., ISHIHARA, H., YAMAGUCHI, S., YAMADA, T., TAMURA, A., KATAGIRI, H., MARUYAMA, Y. & OKA, Y. 2006. WFS1 protein modulates the free Ca2+ concentration in the endoplasmic reticulum. *FEBS Letters,* 580**,** 5635-5640.

TARIOT, P. N., LOY, R., RYAN, J. M., PORSTEINSSON, A. & ISMAIL, S. 2002. Mood stabilizers in Alzheimer's disease: symptomatic and neuroprotective rationales. *Advanced Drug Delivery Reviews,* 54**,** 1567-1577.

TERASMAA, A., SOOMETS, U., OFLIJAN, J., PUNAPART, M., HANSEN, M., MATTO, V., EHRLICH, K., MUST, A., KÕKS, S. & VASAR, E. 2011. Wfs1 mutation makes mice sensitive to insulin-like effect of acute valproic acid and resistant to streptozocin. *Journal of Physiology and Biochemistry,* 67**,** 381-390.

THÉVENOD, F., FRIEDMANN, J. M., KATSEN, A. D. & HAUSER, I. A. 2000. Up-regulation of Multidrug Resistance P-glycoprotein via Nuclear Factor-κB Activation Protects Kidney Proximal Tubule Cells from Cadmium- and Reactive Oxygen Species-induced Apoptosis. *Journal of Biological Chemistry,* 275**,** 1887-1896.

THIELE, C. J. 1998. Neuroblastoma Cell Lines. *Journal of Human Cell Culture. Lancaster, UK,* 1**,** 21-53.

THIELE, C. J., MCKEON, C., TRICHE, T. J., ROSS, R. A., REYNOLDS, C. P. & ISRAEL, M. A. 1987. Differential protooncogene expression characterizes histopathologically indistinguishable tumors of the peripheral nervous system. *The Journal of Clinical Investigation,* 80**,** 804-811.

TOEI, M., SAUM, R. & FORGAC, M. 2010. Regulation and Isoform Function of the V-ATPases. *Biochemistry,* 49**,** 4715-4723.

TOKHTAEVA, E., SACHS, G., SOUDA, P., BASSILIAN, S., WHITELEGGE, J. P., SHOSHANI, L. & VAGIN, O. 2011. Epithelial Junctions Depend on Intercellular Trans-interactions between the Na,K-ATPase β1 Subunits. *Journal of Biological Chemistry,* 286**,** 25801-25812.

TOKHTAEVA, E., SACHS, G. & VAGIN, O. 2009. Assembly with the Na,K-ATPase1 Subunit Is Required for Export of Î²1 and Î²2 Subunits from the Endoplasmic Reticulum. *Biochemistry,* 48**,** 11421-11431.

TTPLABTECH. 2012. *Laser scanning imaging with acumen eX3* [Online]. Melbourn: Studio 24. Available: http://www.ttplabtech.com/ [Accessed 2012].

UEDA, K., KAWANO, J., TAKEDA, K., YUJIRI, T., TANABE, K., ANNO, T., AKIYAMA, M., NOZAKI, J., YOSHINAGA, T., KOIZUMI, A., SHINODA, K., OKA, Y. & TANIZAWA, Y. 2005. Endoplasmic reticulum stress induces Wfs1 gene expression in pancreatic β-cells via transcriptional activation. *European Journal of Endocrinology,* 153**,** 167-176.

UEMURA, A., OKU, M., MORI, K. & YOSHIDA, H. 2009. Unconventional splicing of XBP1 mRNA occurs in the cytoplasm during the mammalian unfolded protein response. *Journal of Cell Science,* 122**,** 2877-2886.

UPTON, J.-P., AUSTGEN, K., NISHINO, M., COAKLEY, K. M., HAGEN, A., HAN, D., PAPA, F. R. & OAKES, S. A. 2008. Caspase-2 Cleavage of BID Is a Critical Apoptotic Signal Downstream of Endoplasmic Reticulum Stress. *Molecular and Cellular Biology,* 28**,** 3943-3951.

URANO, F., BERTOLOTTI, A. & RON, D. 2000. IRE1 and efferent signaling from the endoplasmic reticulum. *Journal of Cell Science,* 113**,** 3697-3702.

VAN DEN OUWELAND, J. M. W., CRYNS, K., PENNINGS, R. J. E., WALRAVEN, I., JANSSEN, G. M. C., MAASSEN, J. A., VELDHUIJZEN, B. F. E., ARNTZENIUS, A. B., LINDHOUT, D., CREMERS, C., VAN CAMP, G. & DIKKESCHEI, L. D. 2003. Molecular characterization of WFS1 in patients with Wolfram syndrome. *Journal of Molecular Diagnostics,* 5**,** 88-95.

VED, R., SAHA, S., WESTLUND, B., PERIER, C., BURNAM, L., SLUDER, A., HOENER, M., RODRIGUES, C. M. P., ALFONSO, A., STEER, C., LIU, L., PRZEDBORSKI, S. & WOLOZIN, B. 2005. Similar Patterns of Mitochondrial Vulnerability and Rescue Induced by Genetic Modification of α-Synuclein, Parkin, and DJ-1 in Caenorhabditis elegans. *Journal of Biological Chemistry,* 280**,** 42655-42668.

VINCENT, I., ROSADO, M. & DAVIES, P. 1996. Mitotic mechanisms in Alzheimer's disease? *The Journal of Cell Biology,* 132**,** 413-425.

WALLACE, S. J. 1998. Myoclonus and epilepsy in childhood: A review of treatment with valproate, ethosuximide, lamotrigine and zonisamide. *Epilepsy research,* 29**,** 147-154.

WANG, J.-F., BOWN, C. & YOUNG, L. T. 1999. Differential Display PCR Reveals Novel Targets for the Mood-Stabilizing Drug Valproate Including the Molecular Chaperone GRP78. *Molecular Pharmacology,* 55**,** 521-527.

WANG, Y.-D., CHEN, W.-D., YU, D., FORMAN, B. M. & HUANG, W. 2011. The G-Protein-coupled bile acid receptor, Gpbar1 (TGR5), negatively regulates hepatic inflammatory

response through antagonizing nuclear factor kappa light-chain enhancer of activated B cells (NF-κB) in mice. *Hepatology,* 54**,** 1421-1432.

WARFEL, A, N., EL-DEIRY & S, W. 2013. p21WAF1 and tumourigenesis: 20 years after. *Current Opinion in Oncology,* 25**,** 52-58.

WASSON, J. & PERMUTT, M. A. 2008. Candidate gene studies reveal that the WFS1 gene joins the expanding list of novel type 2 diabetes genes. *Diabetologia,* 51**,** 391-393.

WATERBORG, J. H. 2002. Dynamics of histone acetylation in vivo. A function for acetylation turnover? *Biochemistry and Cell Biology,* 80**,** 363-378.

WEI, H., KIM, S. J., ZHANG, Z., TSAI, P. C., WISNIEWSKI, K. E. & MUKHERJEE, A. B. 2008. ER and oxidative stresses are common mediators of apoptosis in both neurodegenerative and non-neurodegenerative lysosomal storage disorders and are alleviated by chemical chaperones. *Human Molecular Genetics,* 17**,** 469-477.

WEI, W., LIAO XIAO-LI, JING-HONG, C., DAN-DAN, L. & JIAN-WEI, J. 2011. Sodium valproate induces mitochondria-dependent apoptosis in
human hepatoblastoma cells. *Chinese Medical Journal,* 124**,** 2167-2172.

WELCH, W. J. & BROWN, C. R. 1996. Influence of molecular and chemical chaperones on protein folding. *Cell Stress & Chaperones,* 1**,** 109-115.

WIECZOREK, H., BEYENBACH, K. W., HUSS, M. & VITAVSKA, O. 2009. Vacuolar-type proton pumps in insect epithelia. *Journal of Experimental Biology,* 212**,** 1611-1619.

WILKENS, S., VASILYEVA, E. & FORGAC, M. 1999. Structure of the Vacuolar ATPase by Electron Microscopy. *Journal of Biological Chemistry,* 274**,** 31804-31810.

WOLF, B. B. & GREEN, D. R. 1999. Suicidal Tendencies: Apoptotic Cell Death by Caspase Family Proteinases. *Journal of Biological Chemistry,* 274**,** 20049-20052.

WOLFRAM, D. & WAGENER, H. 1938. Diabetes mellitus and simple optic atrophy among siblings: report of four cases. *mayo clinic proceedings,* 13**,** 715-718.

XIE, Q., KHAOUSTOV, V. I., CHUNG, C. C., SOHN, J., KRISHNAN, B., LEWIS, D. E. & YOFFE, B. 2002. Effect of tauroursodeoxycholic acid on endoplasmic reticulum stress–induced caspase-12 activation. *Hepatology,* 36**,** 592-601.

XU, K. Y. 2011. Allosteric property of the (Na++K+)-ATPase β1 subunit. *Biochemical and Biophysical Research Communications,* 415**,** 479-484.

YAMADA, T., ISHIHARA, H., TAMURA, A., TAKAHASHI, R., YAMAGUCHI, S., TAKEI, D., TOKITA, A., SATAKE, C., TASHIRO, F., KATAGIRI, H., ABURATANI, H., MIYAZAKI, J. & OKA, Y. 2006. WFS1-deficiency increases endoplasmic reticulum stress, impairs cell cycle progression and triggers the apoptotic pathway specifically in pancreatic beta-cells. *Human Molecular Genetics,* 15**,** 1600-1609.

YAMAGUCHI, S., ISHIHARA, H., TAMURA, A., YAMADA, T., TAKAHASHI, R., TAKEI, D., KATAGIRI, H. & OKA, Y. 2004. Endoplasmic reticulum stress and N-glycosylation modulate expression of WFS1 protein. *Biochemical and Biophysical Research Communications,* 325**,** 250-256.

YAMAMOTO, K., SATO, T., MATSUI, T., SATO, M., OKADA, T., YOSHIDA, H., HARADA, A. & MORI, K. 2007. Transcriptional Induction of Mammalian ER Quality Control Proteins Is Mediated by Single or Combined Action of ATF6± and XBP1. *Developmental cell,* 13**,** 365-376.

YAMAMOTO, K., SUZUKI, N., WADA, T., OKADA, T., YOSHIDA, H., KAUFMAN, R. J. & MORI, K. 2008. Human HRD1 Promoter Carries a Functional Unfolded Protein Response Element to Which XBP1 but not ATF6 Directly Binds. *The Journal of Biochemistry,* 144**,** 477-486.

YANG, J.-S., KIM, J. T., JEON, J., PARK, H. S., KANG, G. H., PARK, K. S., LEE, H. K., KIM, S. & CHO, Y. M. 2010. Changes in Hepatic Gene Expression upon Oral Administration of Taurine-Conjugated Ursodeoxycholic Acid in ob/ob Mice. *PLoS ONE,* 5**,** e13858.

YANG, Y., MUFSON, E. J. & HERRUP, K. 2003. Neuronal Cell Death Is Preceded by Cell Cycle Events at All Stages of Alzheimer's Disease. *The Journal of Neuroscience,* 23**,** 2557-2563.

YOSHIDA, H. 2004. Molecular biology of the ER stress response. *Seikagaku,* 76**,** 617-630.

YOSHIDA, K. & MIKI, Y. 2010. The cell death machinery governed by the p53 tumor suppressor in response to DNA damage. *Cancer Science,* 101**,** 831-835.

YUAN, J., LIPINSKI, M. & DEGTEREV, A. 2003. Diversity in the Mechanisms of Neuronal Cell Death. *Neuron,* 40**,** 401-413.

YURIMOTO, S., HATANO, N., TSUCHIYA, M., KATO, K., FUJIMOTO, T., MASAKI, T., KOBAYASHI, R. & TOKUMITSU, H. 2009. Identification and Characterization of Wolframin, the Product of the Wolfram Syndrome Gene (WFS1), as a Novel Calmodulin-Binding Protein. *Biochemistry,* 48**,** 3946-3955.

ZALSMAN, G., MANN, M. J., HUANG, Y.-Y., OQUENDO, M. A., BRENT, D. A., BURKE, A. K., ELLIS, S. P. & MANN, J. J. 2009. Wolframin gene H611R polymorphism: No direct association with suicidal behavior but possible link to mood disorders. *Progress in Neuro-Psychopharmacology and Biological Psychiatry,* 33**,** 707-710.

ZATYKA, M., RICKETTS, C., XAVIER, G. D., MINTON, J., FENTON, S., HOFMANN-THIEL, S., RUTTER, G. A. & BARRETT, T. G. 2008. Sodium-potassium ATPase beta 1 subunit is a molecular partner of Wolframin, an endoplasmic reticulum protein involved in ER stress. *Human Molecular Genetics,* 17**,** 190-200.

ZENTENO, J. C., RUIZ, G., PEREZ-CANO, H. J. & CAMARGO, M. 2008. Familial Wolfram syndrome due to compound heterozygosity for two novel WFS1 mutations. *Molecular Vision,* 14**,** 1353-1357.

ZHANG, L., LAI, E., TEODORO, T. & VOLCHUK, A. 2009. GRP78, but Not Protein-disulfide Isomerase, Partially Reverses Hyperglycemia-induced Inhibition of Insulin Synthesis and Secretion in Pancreatic beta-Cells. *Journal of Biological Chemistry,* 284**,** 5289-5298.

ZHANG, W., FENG, D., LI, Y., IIDA, K., MCGRATH, B. & CAVENER, D. R. 2006. PERK EIF2AK3 control of pancreatic ² cell differentiation and proliferation is required for postnatal glucose homeostasis. *Cell Metabolism,* 4**,** 491-497.

ZHANG, Z., TONG, N., GONG, Y., QIU, Q., YIN, L., LV, X. & WU, X. 2011. Valproate protects the retina from endoplasmic reticulum stress-induced apoptosis after ischemia–reperfusion injury. *Neuroscience Letters,* 504**,** 88-92.

ZHOU, R., YUAN, P., WANG, Y., HUNSBERGER, J. G., ELKAHLOUN, A., WEI, Y., DAMSCHRODER-WILLIAMS, P., DU, J., CHEN, G. & MANJI, H. K. 2008. Evidence for Selective microRNAs and Their Effectors as Common Long-Term Targets for the Actions of Mood Stabilizers. *Neuropsychopharmacology,* 34**,** 1395-1405.

ZIMMET 2001. Global and societal implications of the diabetes epidemic. *Nature,* 414**,** 782-787.
ZINSZNER, H., KURODA, M., WANG, X., BATCHVAROVA, N., LIGHTFOOT, R. T., REMOTTI, H., STEVENS, J. L. & RON, D. 1998. CHOP is implicated in programmed cell death in response to impaired function of the endoplasmic reticulum. *Genes & Development,* 12**,** 982-995.

Chapter Ten: Peer reviewed publication